The Role of Dlk1 in the Gene Regulatory Network Underlying Motor Neuron Diversification

Von der Fakultät für Mathematik, Informatik und Naturwissenschaften der RWTH Aachen University zur Erlangung des akademischen Grades einer Doktorin der Naturwissenschaften genehmigte Dissertation

vorgelegt von

Yasmine Wasser

Master of Science, Biologie.

aus

Bergisch Gladbach

Berichter*:* *Prof. Dr. Till Marquardt*

Prof. Dr. Geraldine Zimmer-Bensch

Tag der mündlichen Prüfung*:* *16.08.2022*

Prof. Dr. Till Marquardt
Interfaculty Chair for Neurobiological Research
University hospital RWTH Aachen, Clinic for Neurology &
Institute of Zoology (Biology II),
RWTH Aachen University

Prof. Dr. Geraldine Zimmer-Bensch
Department of Functional Epigenetics
Institute of Zoology (Biology II)
RWTH Aachen University

Prof. Dr. Frank Müller
Molecular and Cellular Physiology
Institute of Structural Biology and Biophysics 1 (IBI-1)
Jülich Research Centre

External supervisor:
Dr. Phillip Grote
Institute of Cardiovascular Regeneration
Centre for Molecular Medicine
Goethe University

Date of the oral examination: 16.08.2022

Affidavit

I, Yasmine Wasser, hereby declare that my doctoral thesis entitled "The Role of Dlk1 in the Gene Regulatory Network Underlying Motor Neuron Diversification" has been written independently, with no additional sources or aids other than those stated.

Aachen, June 2022

Yasmine Wasser

Table of Contents

Acknowledgements

I would like to thank my thesis committee, **Prof. Dr. Till Marquardt**, **Prof. Dr. Geraldine Zimmer-Bensch,** and **Dr. Philipp Grote** for undertaking the responsibility of the thesis committee. I would like to thank all of you, for accompanying me in the three years of my doctoral research period, giving me critical observations and for the helpful advice which guided this thesis and also during the TAC meetings. Furthermore, I would like to thank **Prof. Dr. Frank Müller** who undertook the third chair of my defence. Thank you, for your spontaneous consent and support.

Beside the member ship of my thesis committee, I would like to thank **Prof. Dr. Till Marquardt,** for the opportunity to join his working group with all those inspiring researchers. Thank you for your support of this thesis, your enthusiasm for my projects, your critical observations and helpful remarks.

Then I would like to thank the **RTG2461 research group** of the RWTH Aachen, especially the chair, **Prof. Dr. Marc Spehr** and the coordinators **Dr. Jenny Spehr** and **Oke Nommensen**, for giving me possibility to be a part of this remarkable group, to get in contact with amazing researchers in the field and to get know new and inspiring people. Moreover, I would like to thank you, for your support in difficult time, without questioning my academic career in the RTG group. Thank you, for having always an open ear in the difficult times for me.

This thesis could not be possible, without the help and guidance of **Dr. Dr. Pardes Habib**. Thank you, for taking over part of the supervision in difficult times and offering me a guidance for my thesis. Further, I want to thank you, for giving me an introduction to stroke research and in brain slice culture. A big thank goes to his great working group, especially **Eren Arik, Ole Hanisch** and **Jonas Pes** for your introduction and help with the hypoxia chamber and every upcoming question in regard to hypoxia.

A special thanks goes to the group leader of our working group, **Dr. Daniel Müller**. Thank you, for introducing me to the Dlk1 project, your passionate participation, the guidance of the thesis, the weekly discussion and support in science, motivation and organisation.

A massive thanks go to my direct supervisor **Dr. Matthias Marks** for undertaking the supervision in the lab, for the support, beginning with my master study, the introduction to ESC culture and their differentiation, the teaching about genetic modifications, and embryonic development. Your enthusiasm about our work is catching and I am so glad to learn from your expertise. You inspire me and my work. Thank you for being a friend to me.

Thanks to both of you, **Daniel and Matthias** for the scientific discussions, the advice and critical reading of my thesis and the help to complete the project successfully.

Furthermore, this thesis would be not possible without the uninterrupted support in the lab by **Anna Michely**. I am so happy, that you came into our lab and became part of our great ESC Crew and a friend to me. Your helping hand in every minute was more than imaginable. Additional thanks go to all current and former ESC Crew members, for being such an adorable and supportive team.

Thanks as well to the technicians of the laboratory **Louisa Neumann, Sandra Brill, Irmi Diepolder** and **Sabine Hamm** for your support in the lab. Especially to **Louisa** for taking over the mouse preparations and the brain slice staining. I want to thank all staff members of the **Marquardt research group** and also all other lab members of the **neurology department** in the UK Aachen for their constant helpfulness and friendly working atmosphere.

I would like to thank **Prof. Dr. Schulz** to give me possibility to study in his laboratory. Also, I would like to thank **Dr. Aaron Voigt**, to open me the door to the neurological research six years ago. You were the first one, to give me the possibility to work in a neurological laboratory and to study on neurodegenerative diseases. You supported me during my bachelor thesis, which even not changed during the master thesis and this doctoral thesis and for this, I am very grateful. Thank you for your support, your critical thinking and helpful advises throughout the whole time, which I could spent in this lab.

I would also like to thank my friends and the family. Being supported throughout one's life to follow the dreams is not something that can be taken for granted. Therefore, I am profoundly grateful, happy and proud to have the best family in the world. To **my parents**, my brother, **Joscha** and my sister-in-law, **Emily**, I would like to thank for your support, your help, your motivation, your encouragement and your love throughout my years of study and the process of research and writing.

And last, but by no means least, to the most important person, my love and future husband **Jens** for his unbelievable support and belief in me from day one, when we met. You were the first one, who introduced me into the world of scientific work and cell culture. And as my passion for neuroscience was growing, my love to you was growing. I am so happy to have you beside me and I would like to thank you, for everything you have done for me during this thesis; the scientific discussion, the help, the encouragement, the support with food, breaks, hugs and your love. It’s not only a phrase, but quite honestly, this thesis would not have been possible without all of you.

List of figures:

List of supplement figures:

List of tables:

Abstract

Delta-like homologue 1 (Dlk1) has been established as molecular determinant of motor neuron (MN) functional diversification. Previous studies in mouse and chicken embryo revealed Dlk1-dependent gene expression during MN development, which promotes fast alpha MN subtype properties. However, previous experiments to identify Dlk1 interaction partners and components of the Dlk1 pathway were not sufficient to fully resolve the pathway.

This thesis addresses the mechanism through which Dlk1 promotes the fast alpha MN properties. Based on previous observations, the major focus of the thesis was hypoxia-dependent Dlk1 regulation and its contribution to MN diversification during embryogenesis. Prior, E12.5 embryos were analysed with regards to Dlk1 protein expression and the evidence of lower oxygen conditions, as different oxygen levels could have an influence during neurogenesis. Dlk1 is influenced by lower oxygen levels in cancer-dependent gene regulations. Therefore, Dlk1 might also be influenced by low oxygen levels during neurogenesis. However, since no meaningful differences in hypoxia could be observed in the spinal cord of the embryo, the focus was shifted to MN development *in vitro*. Therefore, mouse embryonic stem cells were differentiated into MNs and analysed. With this approach, a decrease in the amount of full-length Dlk1 protein could be observed, triggered by hypoxic stimulation. Next, Dlk1 regulation was also investigated *in situ* in murine brain slices. Here, it was possible to verify the effects obtained in embryonic stem cell-derived MNs. It has been shown, that full-length Dlk1 protein levels decrease after a hypoxic stimulus, regardless of the age and gender of the mice. To further investigate the decrease of Dlk1 protein after hypoxia, a genetically modified embryonic stem cell line was used to investigate Dlk1 processing. It was found that Dlk1 undergoes cleavage after hypoxic stimulation. Furthermore, it could be shown that the cleavage is likely dependent on the TACE/Adam17 protease. Evidence was found for the nuclear translocation of the cleaved Dlk1 intracellular fragment upon hypoxia-mediated cleavage. Taken together, Dlk1 is cleaved by Adam17 in an extracellular and intracellular fragment, triggered by an external hypoxic stimulation. The Dlk1 intracellular fragment in part translocated to the nucleus, where it could function as a transcriptional co-factor and mediate the gene expression signature implemented by Dlk1. Further, the thesis analyses if *Mmp9* gene regulation is might be associated with the hypoxic-stimulated Dlk1-dependent process. Dlk1 processing in cancer-dependent cell regulation could indicate an influence on the extracellular matrix reorganisation. Hereafter, Dlk1 might be involved in the Mmp9 secretion mediated by hypoxic induction.

Zusammenfassung

Delta-like homologue 1 (Dlk1) wurde als molekularer Determinant in der Funktionsvielfalt der Motoneuronen etabliert. Vorrangegangene elektrophysiologische Studien an Maus- und Hühnerembryonen zeigten eine Dlk1-abhängige Genexpression während der Motoneuronenentwicklung für einen funktionellen Motorneuron Subtypen. Diese Dlk1-abhängige Genexpression führt zu einem zellulären Phänotyp, der die Eigenschaften von schnellen Alpha Motoneuronen aufweist. Vorangegangene Experimente zu Dlk1-Interaktionspartnern und zur Stimulation des Dlk1-Signalwegs reichten nicht aus, um den Signalweg aufzuklären.

Diese Arbeit untersucht den Dlk1-abhängigen Mechanismus, der dazu führt, dass Motorneuronen die Eigenschaften der schnellen Alpha Motoneuron aufweisen. Daher wurde die Hypoxie-abhängige Dlk1-Regulation in Bezug auf die Diversifizierung von Motoneuronen während der Embryogenese untersucht. Zunächst wurden 12.5 Tage alte Embryonen (E12.5) im Hinblick auf die Expression von Dlk1 im Zusammenhang mit geringeren Sauerstoffbedingungen analysiert. Unterschiedliche Sauerstoffkonzentrationen können einen großen Einfluss auf die Embryogenese haben. Daher lag die Vermutung nahe, dass die Wechselwirkungen zu Interaktionspartnern durch eine niedrige Sauerstoffkonzentration beeinflusst werden kann. Da jedoch keine aussagekräftigen Unterschiede in der Hypoxie-abhängigen Proteinantwort im Rückenmark des Embryos festgestellt werden konnten, wurde der Fokus auf die Entwicklung der Motoneuronen *in vitro* beschränkt. Um die Entwicklung von Motorneuronen zu analysieren wurden embryonale Stammzellen bis zu einem Zustand von ausgewachsenen Motoneuronen differenziert und anschließend analysiert. Bei diesem Ansatz konnte, durch einen hypoxischen Stimulus, die Abnahme der Proteinmenge von Dlk1 beobachtet werden. Um jedoch auszuschließen, dass es sich bei diesem Effekt um ein Artefakt der Zellkultur handelt, wurde die Prozessierung des Dlk1 Proteins ebenfalls in murinen Hirnschnitten untersucht. Mit diesem zusätzlichen Ansatz war es möglich, die Hypoxie-abhängigen Proteinänderungen im Vergleich zu vorangegangenen Experimenten in Motoneuronen zu verifizieren. Zusätzlich konnte gezeigt werden, dass die Abnahme der Proteinmenge von Dlk1 nach einem hypoxischen Stimulus unabhängig vom Alter und Geschlecht der Mäuse ist. Um die Abnahme der Proteinmenge von Dlk1 nach Hypoxie zu klären, wurde eine modifizierte embryonale Stammzelllinie genutzt. Diese hat den Vorteil, einen zusätzlichen HA-Tag am C-terminalen Ende zu haben. Dlk1 wird nach hypoxischer Stimulation in eine extrazelluläre Domaine und ein intrazelluläres Fragment gespalten. Basierend auf dieser Tatsache, konnte gezeigt werde, dass eine der Spaltungen durch die TACE/Adam17-Protease vermittelt wird. Ausgehend von der Spaltung konnte auch das intrazelluläre Fragment und seine Translokation in den Zellkern beobachtet werden.

Insgesamt konnte gezeigt werden, dass ein externe hypoxische Stimulation zu einer Spaltung von Dlk1 in ein extrazelluläres und intrazelluläres Fragment führt. Das intrazelluläre Fragment wurde weiter in den Zellkern transloziert, wo es möglicherweise transkriptionelle Co-Faktor-ähnliche Aktivitäten hat. Ausgehend von diesen Daten wird weiter untersucht, ob die *Mmp9* Gene Regulierung mit dem Dlk1-abhängigen Prozess der Krebszellregulierung, wie z. B. der Reorganisation der extrazellulären Matrix, in Zusammenhang stehen könnte. Demnach könnte Dlk1 an der durch hypoxische Stimulus vermittelten Mmp9-Sekretion beteiligt sein.

1. Introduction

1.1. Murine embryogenesis

Mammalian embryonic development starts with the fertilisation of a mature oocyte by a sperm in the oviduct, the prerequisite for embryogenesis in mammalians. The process of embryogenesis entails the development from a single-cell zygote to a multicellular embryo (Hogan *et al.*, 1986; Kaufmann, 2005; Wolpert *et al.*, 2007). Embryogenesis is divided into four distinct stages, depicted as cleavage, blastula stage, gastrulation and organogenesis (Wolpert *et al.*, 2007). During the cleavage stage, the developing single-cell zygote is progressing into small blastomeres by cleavage divisions. Those cells are forming a hollow sphere, also called the blastocyst, within the first three and a half days (embryonic day 3.5 (E3.5)) of murine development (Watson *et al.*, 2004). During this blastocyst formation, cells undergo two defined cell fate decisions (Hiiragi and Solter, 2004; Yamanaka *et al.*, 2006). The first cell fate decision leads to the development of the embryo, whereas the second cell fate decision leads to the future foetus (Hiiragi and Solter, 2004; Wolpert *et al.*, 2007; Wennekamp *et al.*, 2013).

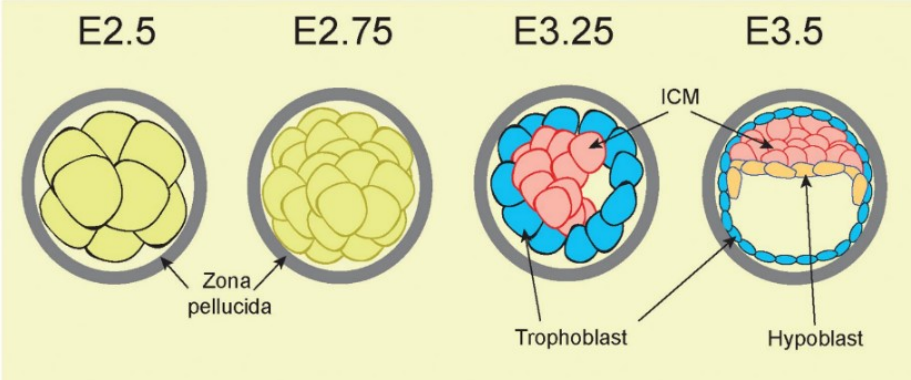

Figure 1-1: *Generation of the blastocyst during murine embryogenesis. At E2.5 cells are surrounded by the zona pellucida. The cell cleavage divisions give rise up to 32-to 64-cell transitions. Followed by the generation of the blastocyst, with the cell discrimination into the ICM and the surrounding trophoblast. The ICM will be then separated into the hypoblast and ICM by E3.5. Image modified after (Kafer and Cesare, 2020). E, embryonic day; ICM, inner cell mass.*

The trophoblast is formed by cells outside the blastocyst (figure 1-1) (Gao *et al.*, 2011; Morris *et al.* 2012; Kafer and Cesare, 2020). The cells of the trophoblast have different cell fates, cellular properties, and positions within the embryo (Gao *et al.*, 2011; Krupa *et al.*, 2014). The trophoblast will generate the extra-embryonic ectoderm and the ectoplacental cone, from which the placenta later develops. The inner cell mass divides into the epiblast and hypoblast. Later the epiblast will generate the primitive ectoderm, whereas the hypoblast will give rise to the primitive endoderm (Evans and Kaufman, 1981; Kaufmann, 2005; Wolpert *et al.*, 2007). The ectoderm in turn then forms the embryo (Tam and Loebel, 2007; Bedzhov *et al.*, 2014).

After four and a half days, the blastocyst is released from the zona pellucida, penetrates into the maternal tissue and proliferates (Yamanaka *et al.*, 2006; Wolpert *et al.*, 2007).

From E5.5 onwards, the pro-amniotic cavity is formed and is creating a cup-shaped cylindric structure (Wolpert *et al.*, 2007; Kafer and Cesare, 2020). The next step of the embryogenesis is the gastrulation, the process of the formation of the three germ layers and the subsequent diversification into organ identities during organogenesis (Kondoh and Takemoto, 2012; Williams *et al.*, 2012; Attardi *et al.*, 2018). The whole process of gastrulation takes three days (until E7.5) and includes three different events. The first one is the anterior posterior (AP) axis patterning, the second event is the transition from the pluripotency stage to the specification of three germ layers and the third is the diversification of the germ layers into the organ identities (Perea-Gomez *et al.*, 2004; Wolpert *et al.*, 2007; Bardot and Hadjantonakis, 2020). The detailed process is described in the following paragraph.

At E5.5, the epiblast has a radial symmetrical and a maternally oriented proximal-distal axis, which allow spatial information. At this stage, the AP axis is generated (Smith *et al.*, 1994; Robertson *et al.*, 2003; Perea-Gomez *et al.*, 2004). At the anterior side of the embryo, an accumulation of cells secretes signals to induce the second event, which is termed the transition (Rodriguez *et al.*, 2005). For the induction of the transition of the epiblast, the expression of a combination of distinct signal molecules, like Wingless and Int-1 (Wnt), bone morphogenic proteins (BMP), Nodal, and Fibroblast growth factors (Fgf) are acquire (Acloque *et al.*, 2009; Kalluri, 2009; Williams *et al.*, 2012; Lamouille, Xu and Derynck, 2014).

At E8.5, organogenesis starts with the transformation of the yolk sack (Rodriguez *et al.*, 2005; Kafer and Cesare, 2020). With the turnover of the embryo, the envelopment completes at the 8 to 13 somite stage of development (Kaufmann, 2005). In the following days, the embryo starts to develop all organs. With the developing organs the whole embryo is growing in size beyond the birth (Kaufmann, 2005; Wolpert *et al.*, 2007).

1.2. Development of the nervous system

The process of nervous system generation includes the formation of the spinal cord during embryogenesis, which can be divided in several steps (Jessell, 2000; Bianchi, 2018). The first step is the neurulation, which starts by formation of the neural ectoderm at embryonic day E7.5 until formation of the neural tube at E10.5 (Karfunkel, 1974; Briscoe and Ericson, 2001; Rogers, Moody and Casey, 2009). After this, axon patterning and neural cell fate decisions are induced to promote the formation of the central nervous system (Dasen, Liu and Jessell, 2003; Jessell, Sürmeli and Kelly, 2011).

1.2.1. Neurulation and spinal cord formation

Prior to neurogenesis, the precursor of the spinal cord is formed. This process starts with the formation of the neural plate shortly after induction of the neural ectoderm (Hines and Marx, 1996; Chang and Hemmati-Brivanlou, 1998; Copp, Greene and Murdoch, 2003). The neural plate is a flattened structure, which starts to curl up during development to create the neural folds. On the opposing side of the neural folds, the neural groove is formed. Following this, the neural folds continue to curve upwards until the lateral edges of the neuronal plate are folded around to finally connect to each other (Copp, Greene and Murdoch, 2003; Greene and Copp, 2009; Pyrgaki *et al.*, 2010). Initiation of neural tube closure is different in various vertebrates. In mammalian species, the closure occurs in the mid-anterior region and progressively extends more anterior (rostral) and posterior (caudal) starting around E8.0 (Copp, Greene and Murdoch, 2003; Greene and Copp, 2009; Harrington, Chalasani and Brewster, 2010). The dorsal region, where the neural folds are connected, has an accumulation of specialised glial and neuroepithelial cells and is termed roof plate. Among other functions, the roof plate is necessary to secrete morphogenic signals to induce neuronal progenitor domains (Kondrychyn *et al.*, 2013; Shinozuka *et al.*, 2019). On the opposite side, the former median region of the neural plate is the ventral surface of the neural tube, which has an accumulation of glial cells, the floor plate (Jessell, 2000; Chesnutt *et al.*, 2004). Upon closure of the neural tube, the neural crest cells arise and the remaining ectoderm is forming the epidermis overlaying the neural tube (Mauch and Schoenwolf, 2001). The cells, which are located along the lumen of the spinal cord give rise to new spinal neuronal progenitor domains (Hines and Marx, 1996; Wolpert *et al.*, 2007).

1.2.2. Rostrocaudal axis formation and ventral patterning for neuron formation

Gastrulation is starting at E5.5 and includes the generation of the rostrocaudal (RC) axis of the whole embryo including the spinal cord (Morris *et al.*, 2012), mainly influenced by different morphogens, especially the Fibroblasts growth factor (Fgf), Wingless and Int-1 (Wnt), and retinoic acid (RA) signalling (Chesnutt *et al.*, 2004; Ishihara and Fukuda, 2016). Those signals facilitate the establishment of the different central nervous system structures (brain vesicles of the forebrain, midbrain, and hindbrain) and the spinal cord (Ishihara and Fukuda, 2016). Fgf signalling is increasing progressively towards the posterior end as a concentration gradient. RA counteracts Fgf, the levels of which are higher anteriorly and progressively lower posteriorly (figure 1-2, A).

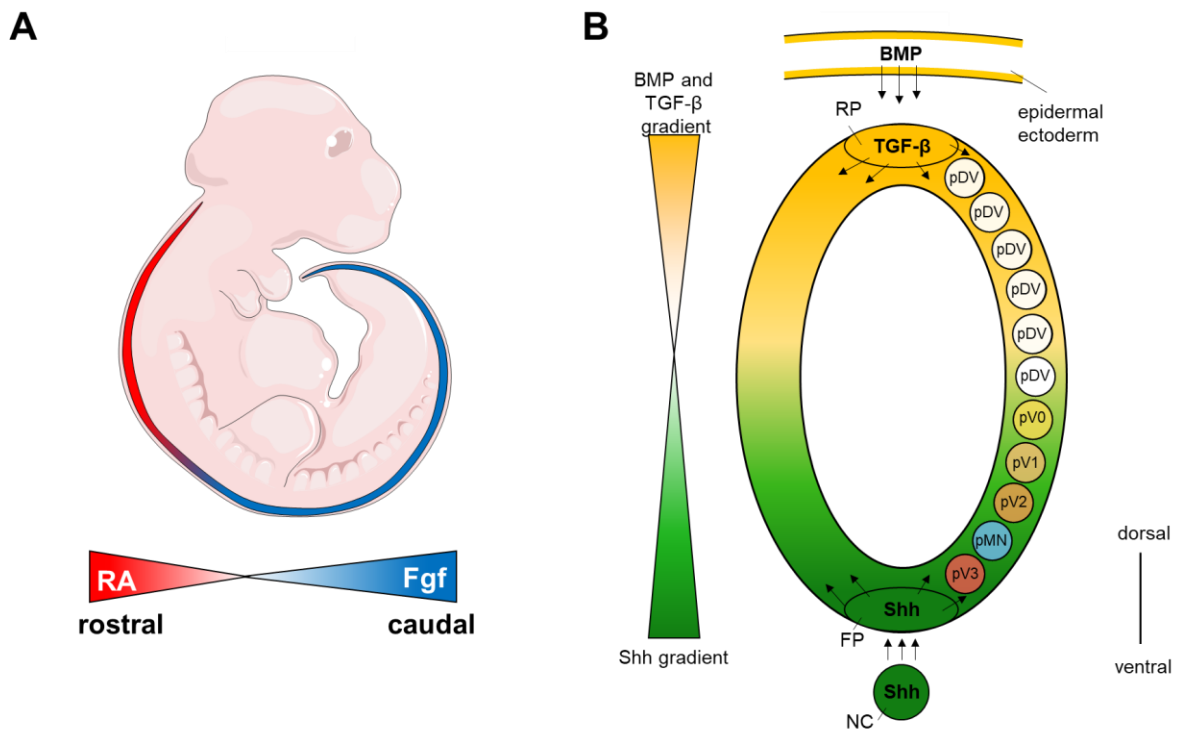

Figure 1-2: *Rostrocaudal and ventral patterning of the spinal cord.* ***A:*** *Formation of the rostrocaudal axis is dependent on the signalling of Fgf (blue) and RA (red), creating gradients to determine the forebrain, midbrain, hindbrain vesicles and the spinal cord. Fgf is progressively reduced from the caudal end towards the rostral end.* ***B:*** *Dorsoventral patterning is dependent on BMP and TGF-β secreted from the roof plate form a dorsoventral gradient (yellow) counteracting the ventrodorsal gradient (green) of Sonic hedgehog secreted by the floor plate and notochord to determine the interneuron progenitor (pV0, pV1, pV2, and pV3) domains and the motor neuron progenitor (pMN) domain in the ventral half of the spinal cord. BMP and TGF-β signalling inducing the formation of the dorsal interneuron progenitor (pDV). Shh, sonic hedgehog; NC, notochord; FP, floor plate; RF, roof plate; BMP, bone morphogenetic proteins; TGF-β, transforming growth factor beta. Figure modified after (Morris et al., 2012).*

In parallel to the RC axis the dorsoventral (DV) axis is created in the spinal cord by morphogenic signals from the roof plate, the floor plate and the notochord (Jessell, 2000; Ille *et al.*, 2007; Catela, 2020). The epidermal ectoderm, which is surrounding the roof plate is providing morphogens of the transforming growth factor-beta (TGF-β) family, while the morphogens BMP-4, BMP-7, and Wnt, to induce the roof plate formation (Ille *et al.*, 2007). Hereafter, non-neuronal cells of the roof plate produce signals for patterning the dorsal half of the spinal cord by creating a gradient (BMPs and TGF-β) (Hines and Marx, 1996; Stifani, 2014b). This dorsal to ventral decreasing gradient of morphogens from the TGF-β family, as well as the BMPs and Wnt signalling induce sensory interneuron progenitor domain formation (figure 1-2, B, pDV) (Wilson *et al.*, 2001; Ille *et al.*, 2007; Liu, Peng and Jing, 2018; Shinozuka *et al.*, 2019).

The morphogenic signal in the ventral half of the spinal cord for the formation of neural cell type fates is the sonic hedgehog (Shh) gradient. Shh is secreted by the notochord to initially

induce the floor plate formation. Subsequently, Shh is secreted by the notochord and the floor plate resulting in a concentration gradient with high levels of Shh in the ventral region of the neural tube and continuously declining levels in more dorsal regions. Together with the opposing gradient of BMPs and Wnt signalling, both are inducing the progenitor domains in a concentration dependent manner (Ericson *et al.*, 1996; Jessell, 2000). This emerging gradient induces the formation of different ventral interneuron progenitor domains (pV0, pV1, pV2, and pV3) and the motor neuron progenitor (pMN) domain. The ventral interneuron progenitor subtypes are eventually modifying the activity of MNs during movement generation (Briscoe *et al.*, 2000; Catela, 2020).

1.2.3. Motor neuron formation

MNs innervate the muscle fibres via a specialised kind of synapse, the neuromuscular junction, in order to control muscle fibre contraction. MN generation during embryogenesis starts around day E10.5 and proceeds until E12.5 (Wolpert *et al.*, 2007). Nevertheless, half of the MNs are dying after these days, because MNs whose axon termini failed to generate stable contact with muscle are eliminated. The elimination was induced by apoptosis due to insufficient supply of target-derived neurotrophic factors (Oppenheim, 1991; Lotto *et al.*, 2001). Further functional motor unit formation relies on the reduction of polyinnervations. Polyinnervation persists after MN death and is eventually resolved by synapse competition in the first two postnatal weeks (Morgana, Giuseppe and Alberto, 2012; Yamaguchi and Miura, 2015). MNs are the first post-mitotic cells developing from the pMN domain (Lee and Pfaff, 2001). Sequentially, the pMN domain switches and produces oligodendrocytes (Soula *et al.*, 2001; Zhou, Choi and Anderson, 2001). One of the most crucial factors for MN formation is Shh, the counterpart to BMP signalling (Roelink *et al.*, 1995; Ericson *et al.*, 1996; Briscoe and Thérond, 2013). Shh activates or represses gene expression via the transmembrane receptor complex of the Shh signalling pathway (Hines and Marx, 1996; Catela, 2020). Those genes are expressed by the different pMN and interneuron progenitor cells (pV) in the ventral half of the neural tube (Dessaud, McMahon and Briscoe, 2008; Catela, 2020). This complex consists of the receptor protein Patched (Ptc) and the signal-transducing subunit, Smoothened (Smo) (Hynes *et al.*, 2000; Wijgerde *et al.*, 2002). In this pathway, the extracellular Shh gradient is converted into either an intracellular glioma-associated oncogene (GLI) activator or repressor signal (Pachikara *et al.*, 2007). With binding of Shh to Ptc, the inhibition of Smo is abolished and thereafter Smo can activate downstream factors, like several protein kinases, transport proteins, and the GLI proteins (Jacob and Briscoe, 2003; Vokes *et al.*, 2007, 2008). The cleavage of GLI leads to its activation, which results in the expression of Shh downstream genes, like *Olig2*, *Nkx2.2*, and *Ptch1* (Cohen *et al.*, 2015). On the opposite, in absence of Shh, the GLI proteins proteolytically proceed into repressors inhibiting Shh target expression

(Pachikara *et al.*, 2007; Catela, 2020). The combination of the GLI repressor and activator proteins at different positions along the DV axis determine the activated Shh target genes and their expression levels (Persson *et al.*, 2002; Meyer and Roelink, 2003). Those genes are classified into two classes (class I and class II). The transcription factors of the class I are expressed in a Shh-dependent manner and including homeodomain proteins of the *Dbx*, *Irx*, and *Pax* family. Whereas, class II transcription factors including Nkx proteins and the basic helix-loop-helix (bHLH) protein Olig2 (figure 1-3) (Marquardt and Pfaff, 2001; Lee *et al.*, 2005; Sagner *et al.*, 2018).

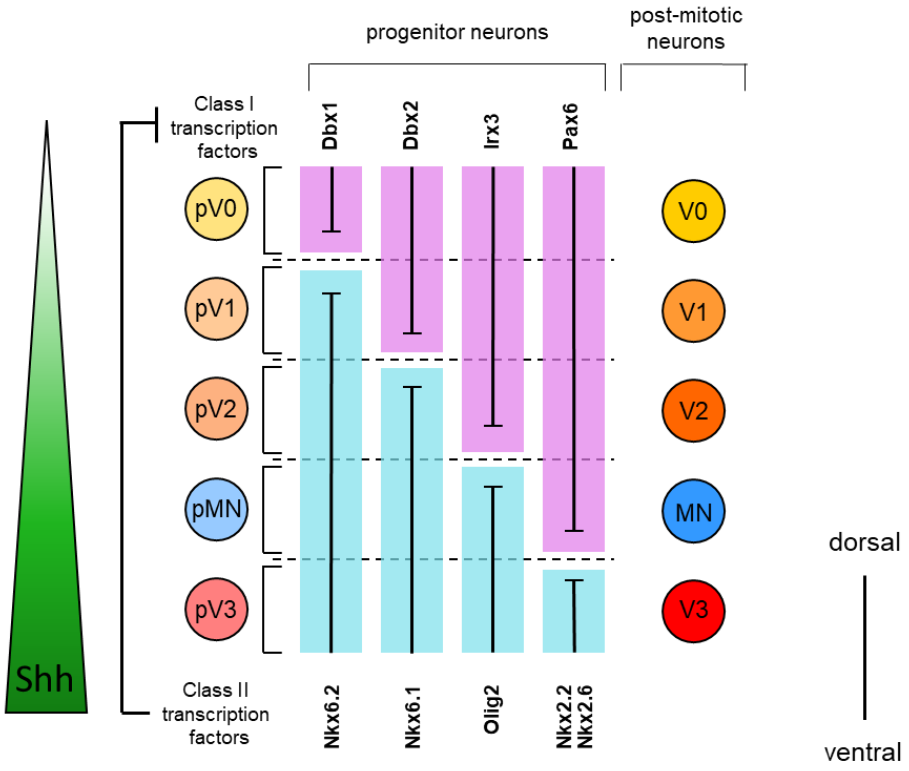

Figure 1-3: *Induction of ventral progenitor domains. The Shh concentration (green gradient) leads to the expression of different transcription factors of class I, (Dbx1,2; Irx3; and Pax6; above the bars, violet bars) and class II (Nkx6.2,1; Olig2; and Nkx2.6,6; below the bars, blue bars). Class I and II transcription factors are inhibiting each other resulting in a cross-repression interplay. Progenitor domains are expressing the respective code to induce the post-mitotic neuron development. Shh, sonic hedgehog; pV0,1, 2, and 3, progenitor interneuron domain pV0, pV1, pV2, and pV3; pMN, motor neuron progenitor domain; V0, V1, V2, and V3, interneuron type 0, 1, 2, and 3, MN, motor neuron. Figure modified after (Marquardt and Pfaff, 2001).*

A distinct cross-repressive interplay exists between the two classes of transcription factors (Ericson *et al.*, 1997; Briscoe *et al.*, 2000). Thus, the possible imbalance in the initiated Shh gradient results in stably expressed transcription factors and sharped boundaries of progenitor domains. The boundary between the pV0 and pV1 domain is based on the cross-repression of the class I transcription factor Dbx1 and the class II transcription factor Nkx6.2. Whereas the class II transcription factor Nkx6.1 is the counterpart of the class I transcription factor Dbx2

at the boundary of the pV1 and the pV2 domains (Vallstedt *et al.*, 2001). For the ventral boundary between the pV2 and the pMN domain, the class I transcription factor Irx3 and the class II transcription factor Olig2 are inhibiting each other. The most ventral boundary is mainly dependent on the inhibition between the class I transcription factor Pax6 and the class II transcription factors Nkx2.2 and Nkx2.6 (Toch *et al.*, 2020). Thus, the Shh gradient is responsible for the eventual generation of the different ventral neuronal subtypes (V3, MN, V2, V1, and V0) by setting up distinct ventral progenitor domains, each defined by a unique combination of class I and II transcription factors (Jessell, 2000; Lee *et al.*, 2005; Catela, 2020). Thereafter, these distinct transcription factors are sufficient to induce the formation of the ventral progenitor subtypes (Hines and Marx, 1996; Catela, 2020).

For the generation of post-mitotic MNs, the transcription factors Olig2, Nkx6.1, Nkx6.2, and Pax6 are required. Olig2 activates the expression of the bHLH transcription factor Neurogenin 2 (Ngn2) (Novitch, Chen and Jessell, 2001; Lee *et al.*, 2005). As soon as the Ngn2 protein concentration exceeds the protein concentration of Olig2, the cells exit the cell cycle and differentiate terminally (Scardigli *et al.*, 2001; Lee *et al.*, 2005). The combination of the proteins, Ngn2, LIM homeobox protein 3 (Lhx3), and LIM homeodomain transcription factor Islet1 (Isl1) activates the expression of Isl2. Isl1 is forming a complex together with Lhx3 and the LIM only protein NLI. Together, they are forming a hexamer of 2Isl1:2Lhx3:2NL1 to activate the expression of *Mnx1* (also known as *homeobox gene 9*; *Hb9*) (Liang *et al.*, 2011). *Mnx1* is specific for post-mitotic MNs and it is crucial for the consolidation of MN identity through active suppression of the interneuron programme (Arber *et al.*, 1999; Thaler *et al.*, 2002; Liang *et al.*, 2011; Catela, 2020). MNs express the two V2 interneuron repressors, the LIM only protein LMO4 and Mnx1. LMO4 is required to suppress the interneuron generation by blocking the tetramer assembly of V2 interneurons, while Mnx1 directly binds the tetramer and suppresses their activation (Liang *et al.*, 2011). Therefore, the expression of Mnx1 is considered as the determinant of MN identity.

1.3. Motor neuron specification

1.3.1. Upper and lower motor neurons

To precisely control movements and muscle contractions, a variety of MN subtypes with distinct properties is required. This is essential to control the subtle nuances of movements. MNs can be classified into two main categories: upper and lower MNs. The two categories can be grouped according to their cell soma location, neurotransmitter, and targets. Upper MNs are restricted to the central nervous system, as their cell somata are located in the pre-motor and primary motor cortex (Genc, Gozutok and Ozdinler, 2019). In mice, they are connected

indirectly to lower MNs. Glutamatergic upper MNs connecting to interneurons, which further connecting to lower spinal MNs (Genc, Gozutok and Ozdinler, 2019; Zayia and Tadi, 2022). The somas of the lower MNs are located in the brainstem, as well as in the ventral horn of the spinal cord. Further, lower MNs are cholinergic and are receiving inputs from somatosensory neurons and interneurons (Zayia and Tadi, 2022). Lower motor neurons acquire stereotypic positions within the spinal cord according to the individual muscles and muscle groups they are innervating. The three main classes of lower MNs are brachial, visceral and somatic MNs.

1.3.2. Specification of motor column

MNs have a columnar identity, as they can be assigned to specific motor columns based on their axon trajectories, their pattern of muscle innervation and their stereotypic positions within the ventral horn of the spinal cord (Jessell, 2000; Landmesser, 2001). The spinal cord can be subdivided into five different segments along the rostral to caudal axis (Briscoe *et al.*, 2000; Jessell, 2000; Dasen and Jessell, 2009). From rostral to caudal, the first section is the cervical part, which marks the transition from the hindbrain to the spinal cord. The cervical part is followed by the thicker brachial segment. More caudal, the thoracic and lumbar segments follow. The most caudal segment is named sacral segment (Agalliu *et al.*, 2009; Jung *et al.*, 2014).

Visceral MNs are regulating the contraction of smooth muscles and are mainly found in the thoracic segment, organised in the preganglionic column (PGC) (Francius and Clotman, 2014). The visceral MNs project to the sympathetic ventral chain by forming synapses with the noradrenergic neurons of the paravertebral ganglia (Francius, 2013; Francius and Clotman, 2014). The visceral MNs, are regulating cardiac and smooth muscle contractions and exocrine/endocrine gland activity (Francius and Clotman, 2014).

Spinal somatic MNs are innervating skeletal muscle fibres. MNs of the lateral motor columns (LMC) are innervating limb muscles and few muscles of the back. Therefore, the LMCs are found in the brachial (forelimb) and lumbar (hindlimb) segment (Kania, Johnson and Jessell, 2000; Dasen, Liu and Jessell, 2003). The LMC is further divided in the lateral and medial motor column (LMC_l and LMC_m respectively). MNs of the LMC_l innervate the dorsal portion of the limb buds, mainly extensor muscles, while the MNs of the LMC_m are connecting to muscles of the ventral portion of the developing limb anlagen (Kania, Johnson and Jessell, 2000; Kania and Jessell, 2003). The same is known for MNs of the hypaxial motor column (HMC), which are projecting to hypaxial muscles of the ventral body and therefore also found only in the thoracic segment (Nagashima *et al.*, 2020). The last group of MNs is the medial motor column (MMC), innervating trunk musculature and therefore extend along the entirety spinal cord (Agalliu *et al.*, 2009; Nagashima *et al.*, 2020).

The outgrow of motor axons out of the spinal cord, towards the muscle fibres lead to the formation of the nerve-muscle connection (De Marco Garcia and Jessell, 2008). For MNs located in the LMC, motor axons enter the limb mesenchyme and form several main nerve trunks (Tosney and Landmesser, 1985; Lieberam *et al.*, 2005). Along those main nerve trunks, small groups of motor axons split up to form finer nerve branches, directed towards their target muscles (Swanson and Lewis, 1982; English, Wolf and Segal, 1993). The cell bodies of those MNs, which are innervating an individual target muscle are found in discrete clusters, termed motor pools (Romanes, 1951; De Marco Garcia and Jessell, 2008). With the establishment and specification of motor pool identity MNs acquire the ability to form precise axonal trajectories and innervate individual muscle targets (Dasen *et al.*, 2005).

Axon targeting specificity by MNs is thought to be mediated by combinations of the Homeobox (Hox) family of transcription factors and LIM transcription factors, which specify different columnar and pool identities and activate or repress the expression of receptors for axon guidance molecules present in the peripheral mesenchyme (Philippidou and Dasen, 2013; Catela *et al.*, 2016). Initially, the motor column identity is determined by the activity of the Hox transcription factors, arrayed along the RC axis of the spinal cord (Dasen *et al.*, 2005; Dasen and Jessell, 2009). In the spinal cord, the expression of *Hox* genes are spatially and temporally dynamic (Philippidou and Dasen, 2013). The morphogenic gradient of Fgf originates from the caudal region, further it has high concentration in the sacral and lumbar regions, while the RA morphogenic gradient comes from the rostral region and therefore has a higher concentration in the brachial region. Those gradients induce the expression of the Hox transcription factors. In the mouse genome, there are in total 39 different *Hox* genes organised in four genetic clusters, *Hoxa*, *Hoxb*, *Hoxc* and *Hoxd* (Goodman and Scambler, 2001). In the hindbrain, the *Hox* genes *Hox1*-*Hox4* are expressed, whereas in the spinal cord, the *Hox* genes *Hox5*-*Hox11* are expressed and encoding their respecify proteins (Philippidou and Dasen, 2013). The ordering of Hox genes in the genome mirrors their expression along the RC axis, which is known as spatial collinearity. Next to the spatial collinearity, there is also a temporal and quantity collinearity (Papageorgiou, 2015). The combinatory co-expression of different *Hox* genes and the respective cross-repressive effects of other *Hox* genes are define the subsets of motor columns. The Hox6 and Hox9 protein is expressed in the LMC, which results in the conversion of the brachial MNs into the thoracic MNs (Bel-Vialar, Itasaki and Krumlauf, 2002; Dasen, Liu and Jessell, 2003). The decreasing Fgf concentration in the thoracic region leads in turn to the expression of other *Hox* genes, such as *Hoxc9* (Dasen and Rosenfeld, 2001). In the lumbar region, *Hoxc10* is highly expressed and represses *Hoxc6* and *Hoxc9* to induce LMC identity (Philippidou and Dasen, 2013).

Within the LMC, one of the target effectors of Hox proteins is the gene encoding the protein Forkhead box P1 (FoxP1) (Dasen *et al.*, 2008). Hox proteins (Hox6 paralogues and Hox10 paralogues) at the limb level are inducing high levels of *FoxP1* to determine the LMC identity, whereas at thoracic levels, Hoxc9 leads to the expression of lower level of *FoxP1,* determining the PGC identity (Dasen *et al.*, 2008). Thus, the specific combinatorial expression of the different Hox transcription factors play an important part in establishing the diversity of MNs in the segments of the spinal cord (Philippidou and Dasen, 2013; Catela, 2020).

1.3.3. Somatic motor units

1.3.3.1. Skeletal muscle physiology

The muscular system in the body is composed of two main types of muscles: (I) the smooth, and (II) the striated muscles. Those striated muscles are further grouped in (I) skeletal and (II) cardiac muscles. The cardiac muscles are responsible for the rhythmic contractions of the heart, while the smooth muscles are involved in the control of the vascular tone and the internal digestive and secretion organs (Cuevas, 2015). Both types of muscles are innervated by the autonomic nervous system. The skeletal muscles, are the only group which comprises voluntary muscles. The muscles fibres composing the skeletal muscles are innervated by the somatic MNs. This group of muscles is in focus of this research aiming at understanding spinal MN functional diversification. The skeletal muscle fibres are necessary to generate movements, mediated by the correct MN execution of movements and posture (Close, 1972; Schiaffino and Reggiani, 2011). Skeletal muscles arise from the somites, where initially myoblasts are generated, which subsequently fuse to syncytia thereby forming the skeletal muscle fibres (Buckingham *et al.*, 2003; McDermott *et al.*, 2005; Musumeci *et al.*, 2015). Two general types of muscle fibres can be distinguished, the intrafusal and the extrafusal muscle fibres. While the extrafusal fibres are responsible for the generation of muscle force, the intrafusal fibres are part of the muscle spindles, specialised sensory organs relaying information regarding muscle tension to the central nervous system.

The muscle spindle is a small encapsulated sensory receptor organ, which detects changes in the length of the muscle in which it is located (Schiaffino and Reggiani, 2011; Kandell *et al.*, 2013). The muscle spindle has three main components: (I) specialised intrafusal muscle fibres, with noncontractile central regions, (II) sensory fibres, which are terminated at the noncontractile regions of the intrafusal muscle fibres, and (III) motor axons, that terminate at the contractile regions of the intrafusal muscle fibres (Kandell *et al.*, 2013). The intrafusal muscle fibres can be classified in the three different types: (I) dynamic nuclear bag fibre (B1), (II) static nuclear bag fibres (B2), and (III) the nuclear chain fibres. Corresponding to the classification of intrafusal fibres, the extrafusal muscle fibres can be further classified into the types I, IIA, IIB, and IIX according to their molecular and functional characteristics, and their

myosin heavy chain isoform expression (Schiaffino and Reggiani, 2011; Talbot and Maves, 2016).

1.3.3.2. Functional diversity of motor neurons mirrors the diversity of muscle fibres

The majority of somatic MNs is located in the Rexed lamina IX of the brain stem and the spinal cord. From there the MNs extend their axons via the ventral roots towards their muscular targets (Schiaffino and Reggiani, 2011). After reaching the target muscle, the motor axons branch out and form synapses on their respective muscle fibre targets. In addition to motor pool and column identities, somatic MNs can also be divided based on their innervating muscle fibre types. Thus, they are classify in alpha (α), beta (β), and gamma (γ) MNs (Kanning, Kaplan and Henderson, 2010).

Individual muscles usually consist of different types of muscle fibres. Hence, individual motor pools contain different functional MN subtypes. The most basic functional unit in the skeletal neuromuscular system is the motor unit, which consists of a single MN as well as the entirety of the skeletal muscles fibres it innervates. A key characteristic of a motor units is that they contain only a single type of muscle fibre in the mature organism (Liddell and Sherrington, 1925; Manuel, 2011).

Muscle contractions are induced by the αMNs, which innervate extrafusal muscles fibres, whereas, γMNs exclusively innervate the intrafusal fibres of the muscle spindles (Schiaffino and Reggiani, 2011). Therefore, γMNs control the sensitivity of the muscle spindles and are involved in the monitoring and adjustment of muscles contraction (Proske and Gandevia, 2012; Akay *et al.*, 2014; Takeoka *et al.*, 2014; Kiehn, 2016). The ratio between the αMNs and γMNs is reported as 2 to 1 (Leksell, 1945; Hunt and Kuffler, 1951; Granit and Henatsch, 1956). The βMNs are innervating extrafusal as well as the intrafusal fibres (Bessou, Emonet-Dénand and Laporte, 1965; Manuel, 2011). Beside the functional observations of βMNs, they are poorly characterised to date.

Morphologically, MNs can be differentiated in regards to their soma size and axon diameter (Manuel, 2011). The soma size of γMNs is approximately half the size of αMNs and also their axon calibre is smaller than that of axons of αMNs (Burke *et al.*, 1977; Westbury, 1982; Moschovakis, Burke and Fyffe, 1991; Shneider *et al.*, 2009). The larger αMNs axon conduct the action potential faster than the smaller γMNs or βMNs. αMNs show more dendritic branches compared to γMNs and there is also a difference in the presynaptic inputs and postsynaptic targets (Kanning, Kaplan and Henderson, 2010). Based on the morphological parameters described before, the βMNs are grouped between the αMNs and γMNs. Their soma size and axon diameter is in between the average of αMN and γMNs (Manuel, 2011). Those morphological differences are also represented in their electrophysiological properties.

1.3.4. Subclassification of alpha, beta, and gamma motor neurons

In the past, the three subtypes of somatic MNs (α, β, and γ) were discriminated according to the muscle fibres they innervate. Nowadays, further hallmarks can be integrated, as for example molecular, morphological, and electrophysiological properties.

1.3.4.1. Alpha motor neurons

The motor units relying on αMNs can be further classified into (I) slow-twitch, fatigue-resistant (SFR), (II) fast-twitch, fatigue-resistant (FFR), (III) fast intermediate (FI), and (IV) fast-twitch, fatigable (FF) motor units. The MNs included in the different motor units are grouped in slow, intermediate and fast αMNs. The corresponding αMN types can either be discriminated according to their muscle fibres, which they are innervating or by specific hallmarks of morphology and function (Friese *et al.*, 2009; Shneider *et al.*, 2009; Kanning, Kaplan and Henderson, 2010). For example, cell bodies and axon diameters of slow αMNs are smaller compared to the fast αMNs (Burke *et al.*, 1977; Cullheim *et al.*, 1987; Friese *et al.*, 2009; Shneider *et al.*, 2009). This means, they have also slower axon conduction velocities. Further the axons of fast αMNs are more branched and exhibit more presynaptic neuromuscular terminals compared to the other αMN subtypes (Cullheim *et al.*, 1987). Intermediate MNs also have intermediate properties, thus innervation is one of the differences between the fast αMNs and the intermediate αMNs are the muscle fibres they innervate. Based on histochemical and physiological profile of muscles fibres, FF αMN units are restricted to the IIB muscle fibres, the FFR αMNs are innervating IIA muscle fibres, the FI αMN units are innervating IIX muscle fibres and the slow αMN units are restricted to type I muscles fibres. However, the IIB muscle fibres are additionally innervated by a subgroup of βMNs (Manuel, 2011). Fast, intermediate and slow αMN can be assigned to their respective motor unit, although a discrimination between the intermediate IIX fibre units is difficult (Zengel *et al.*, 1985). Further the subgroups of αMN can be classified after their morphology. The membrane input resistance is one parameter, in which the αMNs differ (Kanning, Kaplan and Henderson, 2010). As the fast αMNs possess larger axons and are bigger in soma size, their input resistance is lower compared to slow αMNs. Also, the firing behaviour and the axon conduction velocity is different (Burke *et al.*, 1977; Friese *et al.*, 2009). FF αMN units have a phasic firing pattern and a fast axonal conduction velocity, whereas the slow αMN units have a tonic firing pattern and the slowest axonal conduction velocity. Furthermore, differences in the motor unit size, the neuromuscular junction morphology and synaptic vesicle density can be observed (Friese *et al.*, 2009). Whereas the fast αMNs show a greater complexity in their dendritic arbores, connections, and neuromuscular junctions. Their number of synaptic vesicle density in their terminals is lower compared to the smaller and less complex slow αMNs. Those morphological and electrophysiological differences are important for the function of the different types. Fast αMNs

are activated during short-lasting bouts of forceful contractions, whereas the slow αMNs are mainly needed in long-term tasks (Burke *et al.*, 1995).

In general, αMNs can be discriminated according to their passive electrophysiological properties or morphological properties, for example, their cell size. However, MNs also have specific active electrophysiological properties caused by expression of specific molecular factors like for example, ion channels. Taken together, the smaller, slow αMNs have a higher input resistance and require less synaptic activation to generate an action potential. This means, the slow αMNs are the first ones, to be recruited during a muscle contraction and later the intermediate MNs and as last the fast αMNs (Mendell, 2005). This phenomenon is called "*the size principle"* (Mendell, 2005).

1.3.4.2. Beta motor neurons

The most obscure class of somatic MNs are the beta (β) MNs. Little is known about their anatomically and functional properties. They are smaller in size and less abundant compared to the other MNs subtypes (Manuel, 2011). They are innervating both, the intrafusal as well as the extrafusal muscle fibres simultaneously. This is an exception from the general homogeneity of the motor units (Bessou, Emonet-Dénand and Laporte, 1965). This heterogeneity leads to the control of the muscle contraction as well as to the control of the responsiveness of the sensory feedback from muscle spindles (Bessou, Emonet-Dénand and Laporte, 1965; Adelman *et al.*, 2000; Manuel, 2011). βMNs can be classified into two groups according the fibres they are innervating. The first class is consisting of the static βMNs, innervating the nuclear chain fibres (2B) which are responsible for increasing the firing rate of the Ia and II sensory fibres. On the opposite side, the dynamic βMNs are innervating the nuclear bag fibres and mediate the increase in the stretch-sensitivity of the Ia sensory fibres, which leads to stiffening of the nuclear bag fibre and results in their activation (Manuel, 2011).

1.3.4.3. Gamma motor neurons

Roughly 30 % of the MNs of a motor pool are γMNs (Kanning, Kaplan and Henderson, 2010; Wilkinson, 2021). Morphologically, they have smaller soma compared to αMNs and possess simpler and less branched dendritic trees (Wilkinson, 2021). They are innervating exclusively intrafusal muscle fibres within the muscle spindle. They are mimicking the muscle stretch by increasing progressively the firing rate and therefore the tension (Burke *et al.*, 1977; Celichowski and Krutki, 2019; Catela, 2020). Similar to the βMNs, γMNs can also be grouped into two classes according to the intrafusal muscle fibres they are innervating. The class of static γMNs is innervating the nuclear chain fibres and the static nuclear bag fibres (Manuel, 2011). Whereas the dynamic γMNs are innervating the dynamic nuclear bag fibres (Banks, 2015). γMN are not receiving an Ia monosynaptic input, they are only receiving indirect sensory

information and they are participating only indirectly in the spinal reflex (Shneider *et al.*, 2009; Kanning, Kaplan and Henderson, 2010). An overview of the different MN types and their associated muscle fibres are displayed in the following schematic (figure 1-4).

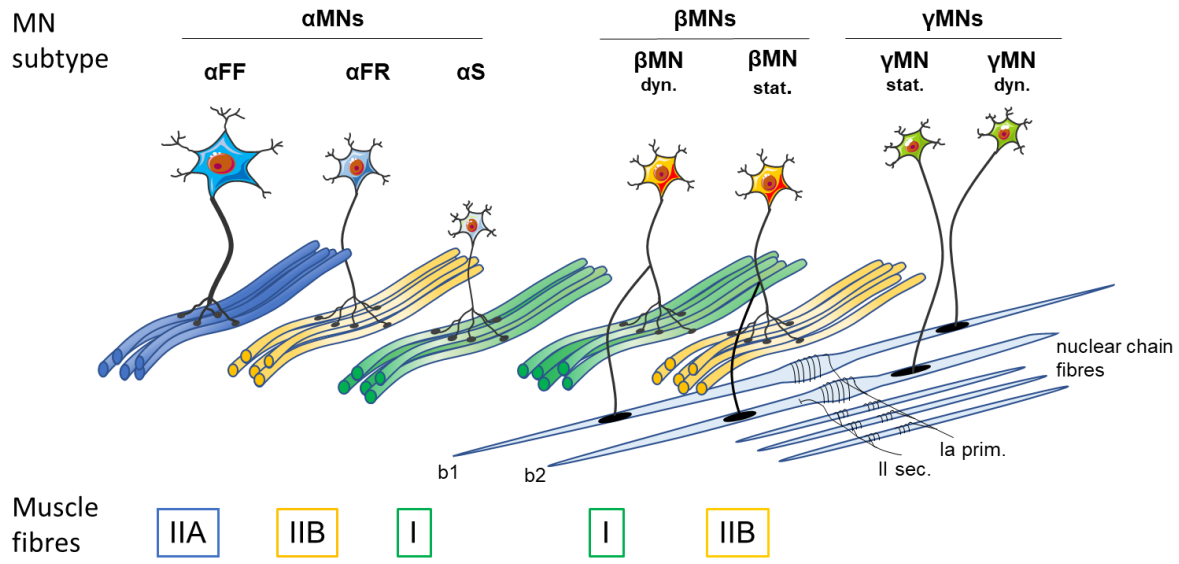

Figure 1-4: *Structural organisation of MNs innervating the corresponding muscle fibres. Somatic MNs can be classified in the three groups of α-, β-, and γMNs. Within the group of motor units with αMN, muscle fibres can be classified in the fast-twitch fatigable (αFF), the fast-twitch fatigue-resistant (αFR), and the slow-twitch fatigue-resistant (αS). They are innervating type IIA, IIB, I, and IIX (not indicated here) muscle fibre respectively. βMNs can be grouped into dynamic (βMN dyn.) and static (βMN stat.) types according the fibres, they are innervating. γMNs can be equally grouped into dynamic (γMN dyn.) and static (γMN stat.) MNs dependent on the innervating nuclear chain fibre. Dynamic properties are described for the βMN dyn. and for the γMN dyn. innervating dynamic nuclear bag fibres. Whereas the static βMNs and γMNs are innervating nuclear chain fibres. Image modified after (Manuel, 2011).*

1.3.5. Molecular marker to identify motor neuron subtypes

Initially, MNs were mainly characterised according to their morphology, electrophysiological properties, and their corresponding muscle fibres (Burke *et al.*, 1995; Manuel, 2011). Nowadays, there are several molecular factors specifically expressed in different subtypes of MNs (Manuel *et al.*, 2019). Postnatal α-and γMNs can be distinguished by the expression of the Neuron-specific nuclear protein (NeuN) (Friese *et al.*, 2009). A high expression level of NeuN throughout the entire cell soma was described for αMNs, whereas γMN have a lack of NeuN expression (Mullen, Buck and Smith, 1992; Friese *et al.*, 2009). Further, *Mnx1* also known as *Hb9* expression can be used to distinguish fast and slow αMNs, as well as γMNs (Arber *et al.*, 1999; Dasen and Jessell, 2009; Shneider *et al.*, 2009; Manuel and Zytnicki, 2019). Furthermore, γMNs can be distinguished from αMNs by the expression of Osteopontin and the Estrogen-related receptor 3 (ERR3) and its paralogue Estrogen-related receptor 2 (ERR2) (Friese *et al.*, 2009; Khan, 2018; Khan *et al.*, 2022). Additionally, γMNs can be discriminated from αMNs by the expression of the Glial-derived neurotrophic factor (GDNF) family receptor

alpha-1 and the serotonin receptor 5-HT_{1D} (Shneider *et al.*, 2009; Enjin *et al.*, 2010; Edwards *et al.*, 2013). There are also some markers to discriminate the subgroups of αMNs, e.g., the Calcitonin gene-related peptide (CGRP), the Matrix metallopeptidase 9 (Mmp9) and Delta-like homologue 1 (Dlk1). They are expressed in some of the αMN subtypes, but not in all of them (Forsgren *et al.*, 1993; Piehl *et al.*, 1993; Kaplan *et al.*, 2014). Mmp9, for example is restricted to the fast and intermediate αMNs, whereas the slow αMNs do not express Mmp9 (Kaplan *et al.*, 2014). Dlk1 is a marker exclusively for the fast αMNs (Müller *et al.*, 2014). Also, Chondrolectin (Chodl) is reported to be expressed in this type of αMN around P11 (Enjin *et al.*, 2010; Morisaki *et al.*, 2016). For the slow αMNs, the synaptic vesicle protein (SV2A) is reported to be expressed exclusively in slow αMNs at the late post-natal days (Chakkalakal *et al.*, 2010). Another marker is the SK3 isoform of the calcium-activated K^+ channel, which was described to be involved in the hyperpolarization of slow αMNs (Edwards *et al.*, 2013).

Most of the identified markers have been linked to MN types based on their expression in MNs with the corresponding cell soma size. However, cell size correlation studies may not be sufficient to determine the specificity of a marker (Manuel and Zytnicki, 2019). There are several markers, which are expressed in more than one type of MNs. Mmp9 as an example is expressed in fast and in intermediate αMNs (Kaplan *et al.*, 2014). Therefore, electrophysiological analysis has to be included to determine the specificity for a certain MN subtype.

There are only few known markers, which in parallel are known determinants of MN function or development. Dlk1 is the most prominent determinant known so far (Müller *et al.*, 2014). It has been shown, that Dlk1 is necessary to induce fast αMN electrophysiological properties in mice and chicken embryos (Müller *et al.*, 2014). By the overexpression of *Dlk1* an increase in rheobase as well as firing frequency was observed, which is consistent with a fast αMN phenotype. On the opposite side, the genetic ablation of *Dlk1* was leading to missing fast αMN properties (Müller *et al.*, 2014). A gene, which is closely associated with Dlk1 is Potassium Voltage-Gated Channel Modifier Subfamily G Member 4 (*Kcng4)*, which is encoding a β-subunit of a K^+ channel (Murakoshi and Trimmer, 1999). *Kcng4* is expressed similarly to Dlk1 in early post-natal embryos and is associated with the tuning of neuronal firing parameters (Wilson, Rempel and Brownstone, 2004). Although, there is evidence that some properties are regulated through *Kcng4*, some biophysical properties might be regulated through further actors. Additionally, Dlk1-dependent fast MN properties might relies on the inhibition of the Notch1 signalling (Müller *et al.*, 2014). Dlk1 properties and functions are topic of the following section (see 1.4.4.). Other known factors necessary to induce MN diversification are ERR2 and ERR3. Both are reported to be expressed in γMNs and important for posture control in mice. The simultaneous knockout of ERR2 and ERR3 leads to lack of γMN properties, like a

low rheobase and a low firing frequency (Khan *et al.*, 2022), whereas their overexpression supports the properties of γMNs. A possible mechanism of how ERR2 might lead to induce the γMN electrophysiological properties is by activation *of the voltage-gated K^+ channel subfamily A type 10* (*Kcna10*). The increased expression of *Kcna10* in chick MNs promotes γMN-like properties, specifically a high input resistance and low firing rate (Khan, 2018; Spiller *et al.*, 2019; Khan *et al.*, 2022).

1.4. The delta-like homologue (Dlk1) protein

1.4.1. Discovery of Dlk1

The delta-like homologue 1 (Dlk1) protein was first identified in the context of amniotic fluid and hereafter described as fetal antigen 1 (FA1) (Fay *et al.*, 1988; Bachmann *et al.*, 1996). In the following years, Dlk1 was discovered several times in different tissues or cell lines independently, explaining the number of differing synonyms. For example, Dlk1 was found in the preadipocytes (*3T3* cells) and named preadipocyte factor 1 (Smas and Sul, 1993). After it was found in lung carcinoma, neuroendocrine tumours and murine *3T3* cells, because of its similarity in the amino acid sequence to the Delta family in *Drosophila melanogaster*, it was given the name Delta-like with the abbreviation Dlk (Laborda *et al.*, 1993). With the discovery of the actual orthologue of Delta in mammals, the previously discovered Dlk1-like was renamed as Dlk1-like homologue 1, however maintaining the acronym Dlk1 (Bettenhausen *et al.*, 1995). In 2014, Dlk1 was found to be associated with postnatal MN development and the specific promotion of fast αMN properties (Müller *et al.*, 2014).

1.4.2. The genomic localisation of the *Dlk1* gene

The murine *Dlk1* gene is located on chromosome 12, while in the human genome it is located on chromosome 14 (Gubina *et al.*, 2000; Wylie *et al.*, 2000). The gene is part of the *Dlk1/Gtl2* locus. *Dlk1* was the first paternally imprinted gene identified in mammals (Gubina *et al.*, 2000). Expression of *Dlk1* starts during embryogenesis in the mesoderm and extends throughout all three germ layer in mammals (Traustadóttir *et al.*, 2019). During embryogenesis, *Dlk1* is expressed in different tissues where it is tissue- and cell type-specifically either becomes downregulated right before birth or remains to continuously expressed. Also, it is expressed in neuronal stem cells in the subventricular zone (Ferrón *et al.*, 2011). Further Dlk1 is expressed in dopaminergic neurons in the ventral midbrain and in the substantia nigra and in hypothalamic vasopressin and oxytocin neurons (Jensen *et al.*, 2001; Christophersen *et al.*, 2007; Bauer *et al.*, 2008; Villanueva, Jacquier and de Roux, 2012; Traustadóttir *et al.*, 2019).

1.4.3. The Dlk1 protein structure

The *Dlk1* gene encodes a glycoprotein, with a predicted size of 41.3 kDa (385 amino acids). This protein is a type 1 transmembrane protein has and has a large N-terminal extracellular domain with epidermal growth factor (EGF)-like repeats, a transmembrane region and a short C-terminal cytosolic region (Smas and Sul, 1993). The two N-terminal EGF-like repeats were referred as Delta or OSM-11 (DOS)-motif (Komatsu *et al.*, 2008).

Dlk1 is modified by alternative splicing, which results in several transcriptional isoforms (Jensen *et al.*, 1994; Wang and Sul, 2006; Miller and Cole, 2014). In human, two isoforms are reported (Deiuliis *et al.*, 2006), whereas in mouse six different isoform are known (figure 1-5) (Smas and Sul, 1993; Mei *et al.*, 2002; Traustadóttir *et al.*, 2019).

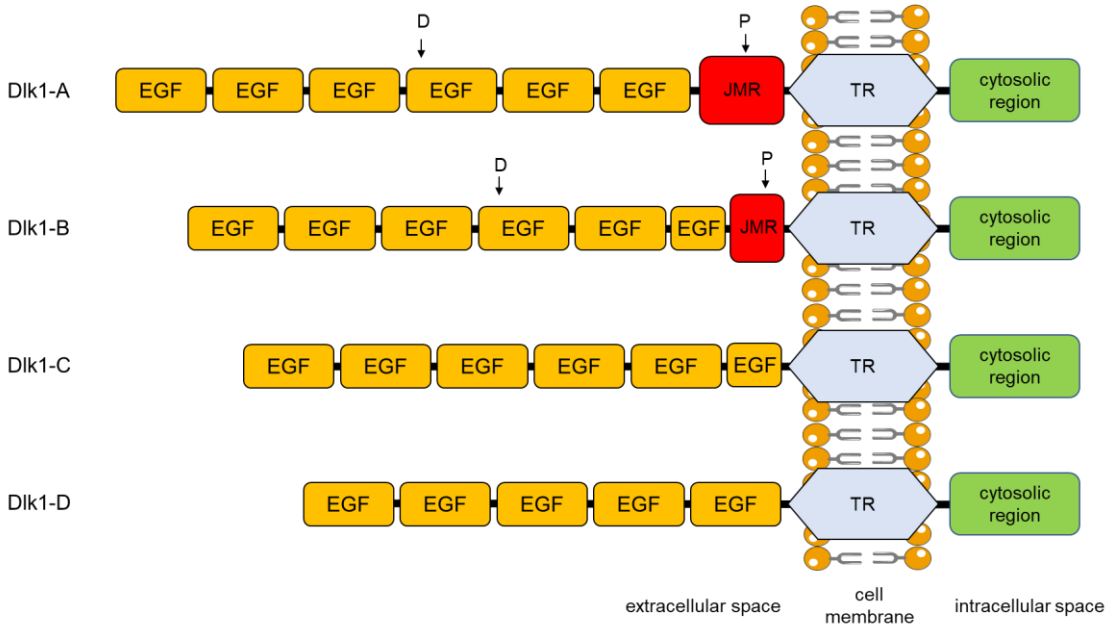

Figure 1-5: *Murine Dlk1 protein structure. Variants of known transcriptional isoforms of Dlk1 share the large extracellular domain with EGF repeats, the transmembrane region and the shorter intracellular cytosolic region. Two isoforms have an extracellular region including six EGF repeats and the JMR (Dlk1 A and Dlk1 B). TACE (Adam17)-mediated cleavage sites are indicated by arrows. The other isoforms are lacking the JMR and have 6 (Dlk1-C), or 5 EGF repeats (Dlk1-D). Dlk1-C and Dlk1-D have two more isoforms (C2 and D2, not displayed here). EGF, epidermal growth factor; D, distal (D) and proximal (P) TACE cleavage site. TACE, tumour necrosis factor alpha converting enzyme, TR, transmembrane region; JMR, juxtamembrane region. Image modified after (Smas, Green and Sul, 1994; Mei et al., 2002).*

A main difference between the six isoforms is the presence of the juxtamembrane cleavage region for the Tumour necrosis factor alpha converting enzyme (TACE)/Adam17 cleavage site (figure 1-5, red box, indicated with JMR) (Wang *et al.*, 2006). Two of the murine isoforms are containing a TACE/Adam17-mediated cleavage site (figure 1-5; Dlk1-A and Dlk1-B). Accordingly, they can be proteolytically cleaved by TACE/Adam17, generating a large

extracellular segment, which is released into the extracellular space (Jensen *et al.*, 1994; Wang and Sul, 2006; Nueda *et al.*, 2008), whereas the other four mouse isoforms are lacking this site and are referred to as membrane-tethered isoforms (figure 1-5; Dlk1-C, -C2, -D, and -D2). Dlk1 is involved in several different processes, depending on the isoform, the cleavage products and the different interaction partners.

1.4.4. Dlk1 protein function

The best understood function is its role as an inhibitor of adipocyte differentiation (Smas and Sul, 1993; Garcés *et al.*, 1999; Mei *et al.*, 2002; Sul, 2009; Hudak *et al.*, 2014). Besides adipogenesis, Dlk1 is known to be involved in osteogenesis, where it inhibits bone formation and stimulates bone resorption (Abdallah *et al.*, 2011). Further, Dlk1 is also involved in muscle development, where it promotes the generation of skeletal muscle fibres by the myogenic program (Charlier *et al.*, 2001; Abdallah *et al.*, 2004; Andersen *et al.*, 2009), whereas it is also inhibiting the regeneration of old muscle fibres (Andersen *et al.*, 2009, 2013). During chondrogenesis, Dlk1 acts as an inhibitor of the PI3K/Akt pathway, which leads to inhibitory effects on cartilage formation (Chen *et al.*, 2011). Additionally, Dlk1 regulates haematopoiesis by promoting the growth of granulocytes, megakaryocytes, and B-cells (Sakajiri *et al.*, 2005; Mirshekar-Syahkal *et al.*, 2013). Furthermore, Dlk1 was found to be involved in neurogenesis. Herein, Dlk1 is expressed in the subgranular zone mainly of astrocytes and is involved in hippocampal neurogenesis contributing to cognition (Ferrón *et al.*, 2011; Whalley, 2011; Montalbán-Loro *et al.*, 2021; Grassi and Pietras, 2022). Further evidence revealed, that Dlk1 is also involved in maintaining the adult stem cell niches in the brain (Ferrón *et al.*, 2011; Surmacz *et al.*, 2012) foetal, and adult bone, some osteoblast cells and in human mesenchymal stem cell (Abdallah *et al.*, 2004). Although there are multiple hints that *Dlk1* is expressed throughout the whole central nervous system, its putative role in the differentiation of MNs had not been addressed until 2014. The evidence for an impact of Dlk1 in the MN diversity was given in 2014, when it was shown that Dlk1 promotes the electrophysiological properties of fast αMNs (Müller *et al.*, 2014). Nevertheless, the exact molecular mechanism through which Dlk1 operates in MN diversification remains unclear so far.

1.4.5. Dlk1 and its molecular interaction partner

Its striking similarity to the Delta like protein (Dll) indicates the possible involvement of Dlk1 in the Notch signalling pathway (Laborda *et al.*, 1993). This pathway is one of best described, yet complex signalling cascades for cell fate decisions and is involved in multiple developmental processes conserved from flies to human (Artavanis-Tsakonas, Rand and Lake, 1999). There are two Notch1 signalling pathways, the canonical and the non-canonical pathway. For the canonical pathway, interaction between the Notch1 membrane protein and the delta/serrate/LAG2 (DSL) domain of a ligand on an adjacent cell is required. For the non-

canonical pathway, the ligands are lacking this DSL motif (Wang, 2011; Guruharsha, Kankel and Artavanis-Tsakonas, 2012). Dlk1 is interacting with Notch1 during tissue development by the non-canonical pathway (Traustadóttir *et al.*, 2016). It seems, that Dlk1 can act cell-autonomous. Herein, Dlk1 interaction could be inhibiting Notch1 signalling and downstream expression of the Notch1 target gene *Hairy and enhancer of split* (*Hes1*). In contrast, the knockdown of *Dlk1* increases the expression of *Hes1* (Baladrón *et al.*, 2001). Further the overexpression of *Hes1* in 3T3 cells was leading to a decreased of *Dlk1* expression, indicating a feedback loop between the two genes (Ross, 2004). The interaction between Notch and Dlk1 was also indicated in a study investigating muscle development. The lack of *Dlk1* was shown to lead to impaired muscles generation (Andersen *et al.*, 2009), caused by a lack of myoblast differentiation due to excess Notch1 signalling activity (Waddell, 2010). There is also evidence, that Dlk1 can act in a Notch-independent manner (Traustadóttir *et al.*, 2016, 2019). As described above, some Dlk1 isoforms contains an extracellular ADAM17/TACE protease cleavage site. After cleavage, the large extracellular soluble protein is released into the extracellular space (Jensen *et al.*, 1994; Wang and Sul, 2006) and can interact with other Dlk1 molecules by binding with its fourth and fifth EGF repeat (Baladrón *et al.*, 2001; Traustadóttir *et al.*, 2016). Further, Dlk1 can bind with the IGF binding protein (IGFBP1) (Nueda *et al.*, 2007), the Cysteine-rich Fgf receptor (CFR) (Miyaoka *et al.*, 2010), Fibronectin (Wang *et al.*, 2010), and also with the Dlk1 homologue Dlk2 (Sánchez-Solana *et al.*, 2011; Navarrete *et al.*, 2017) in mammals (figure 1-6).

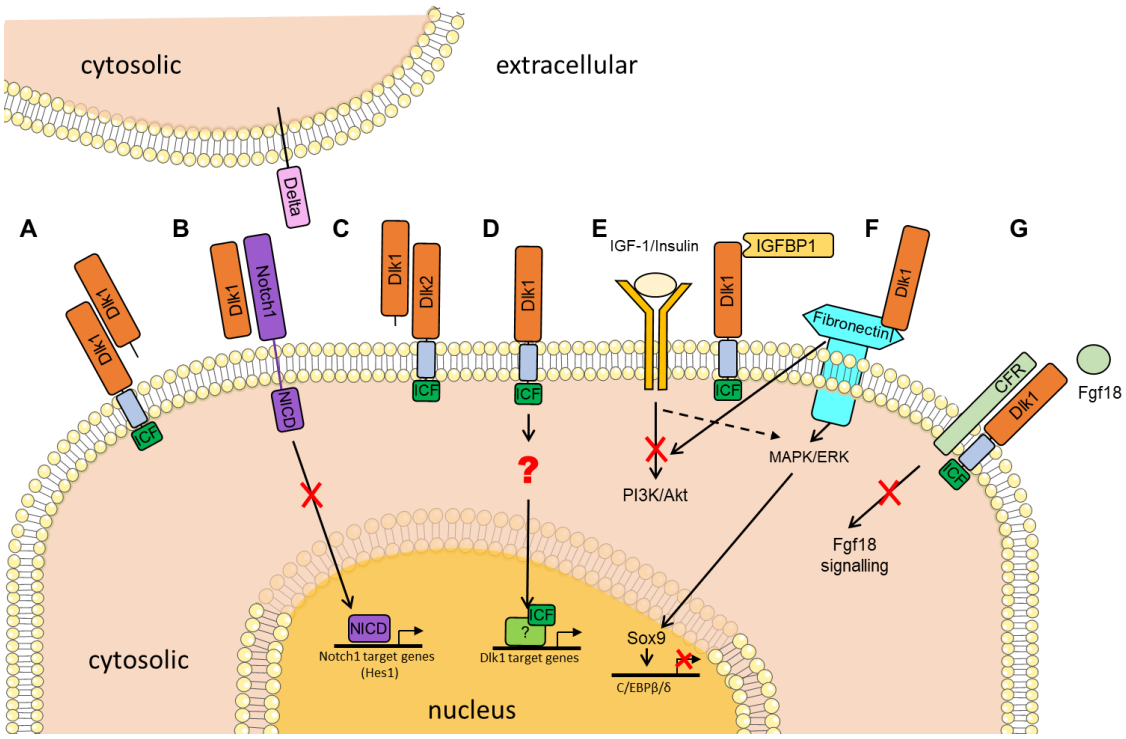

Figure 1-6: *Proposed Dlk1 interaction partners and its complex involvement in signalling pathways.* ***A:*** *Dlk1 is assumed to interact with other Dlk1 proteins by binding to EGF repeats in the extracellular domain.* ***B:*** *Dlk1 is interacting with Notch1 signalling by inhibiting NICD cleavage.* ***C:*** *The homologues Dlk1 and Dlk2 are acting as heterodimer.* ***D:*** *Dlk1 cleavage is assumed to be involved in cancer growth by the ICF cleavage* ***E:*** *Dlk1 is interacting with the IGF-1/insulin receptor to modulate the MAPK/ERK activation level and therefore alternate the Sox9 level for adipogenesis. Further, Dlk1 is binding with the IGFBP1, leading to the increase of free IGF-1. Additionally, Dlk1 is modulating the chondrogenic cell differentiation through inhibition of insulin-dependent Akt-kinase, by the PI3K/Akt pathway.* ***F:*** *Dlk1 inhibits adipocyte differentiation by interaction of the soluble Dlk1 form with Fibronectin. This leads to the activation of the MAPK/ERK signalling and following to an elevated Sox9 level, which blocks the adipogenic transcription factors.* ***G:*** *Dlk1 has also be involved in the skeletal development by the Fgf signalling pathway. CFR, cysteine-rich Fgf receptor; Dlk1/2, Delta-like homologue 1/2; EGF, epidermal growth factor; ICF, HES, hairy and enhancer of split-1; intracellular fragment; IGF, insulin-like growth factors; IGFBP1, IGF binding protein 1; Fgf, fibroblast growth factor; NICD, Notch1 intracellular domain. Image modified after (Traustadóttir et al., 2019).*

1.5. Hypoxia

Hypoxia is defined as the reduction or interruption of the oxygen supply of cells or tissues (Grotta *et al.*, 2021). There are four general causes of hypoxia, which are defining the different types of hypoxias (Pittman, 2011; Grotta *et al.*, 2021). The first type is the hypoxemic type, in which the oxygen pressure is too low to saturate the haemoglobin in the blood (Sarkar, Niranjan and Banyal, 2017). The second type, the anaemic type, occurs when the amount of haemoglobin is too small (Pittman, 2011). The third, the stagnant type, happens because the blood flow is reduced (Morita *et al.*, 2003) and the fourth type is the histotoxic type, which is occurring when the cells or tissues are poisoned (Pittman, 2011; Gaspar and Velloso, 2018).

On one hand, poisoning can occur with carbon monoxide, whereby the haemoglobin is bound and replaces the oxygen in the blood. On the other hand, a poisoning with cyanide can also occur, whereby proteins in the respiratory chain are bound, which disrupts the oxygen transport. The effect of hypoxia is variable. Some tissues can tolerate it better, whereas others sustain severe cell damage or they even require the hypoxic stimulation to develop properly (Dunwoodie, 2009; Patterson and Zhang, 2010; Hiraga, 2018).

1.5.1. Cellular response to hypoxia

The lack of oxygen induces hypoxia-dependent molecular responses at the cellular level. These molecular responses are mainly induced to counteract the lack of oxygen and energy. For example, by increasing glycolysis to generate ATP in an oxygen-independent manner. Further, depending on the affected tissue, erythropoiesis is upregulated in the bone marrow or angiogenesis is increased to improve oxygen supply (Fong and Takeda, 2008; Majmundar, Wong and Simon, 2010). The cellular key players are the hypoxia-induced factor (Hif) transcription factors. One Hif variant, the Hifα, is accumulated under hypoxia and induces the first response to hypoxic stress in the cells (Wang *et al.*, 1995; Kaelin Jr, 2008; Majmundar, Wong and Simon, 2010; Keith, Johnson and Simon, 2011). There are three isoforms of Hifα, namely Hif1α, Hif2α, and Hif3α. Hif1α is ubiquitously expressed, whereas Hif2α and Hif3α expression is restricted to cells of the vascular endothelium, liver parenchyma, and cells of the myeloid linage (Bertout, Patel and Simon, 2008).

In case of sufficient oxygen and nutrition supply of cells and tissues (normoxic conditions), Hif1α and Hif2α undergo an oxygen-dependent hydroxylation of two proline residues by Hif-specific prolyl hydroxylase domain enzymes (PHDs) (figure 1-7) (Keith, Johnson and Simon, 2011). Hydroxylated Hif1α is recognised by the von Hippel-Lindau (VHL) protein, which is part of an E3 ubiquitin ligase complex (Maxwell *et al.*, 1999; Yu *et al.*, 2001; Kaelin Jr, 2008; Sadri and Zhang, 2013). This in turn leads to the rapid degradation of Hif1α and Hif2α by the polyubiquitination proteasomal degradation pathway (Yu *et al.*, 2001; Sadri and Zhang, 2013). Although Hif1α and Hif2α are often co-expressed in multiple cell types and share a hypoxia-induced molecular pathway, Hif1α is most often in focus to analyse hypoxia-induced cellular pathways (Wiesener *et al.*, 2003; Keith, Johnson and Simon, 2011).

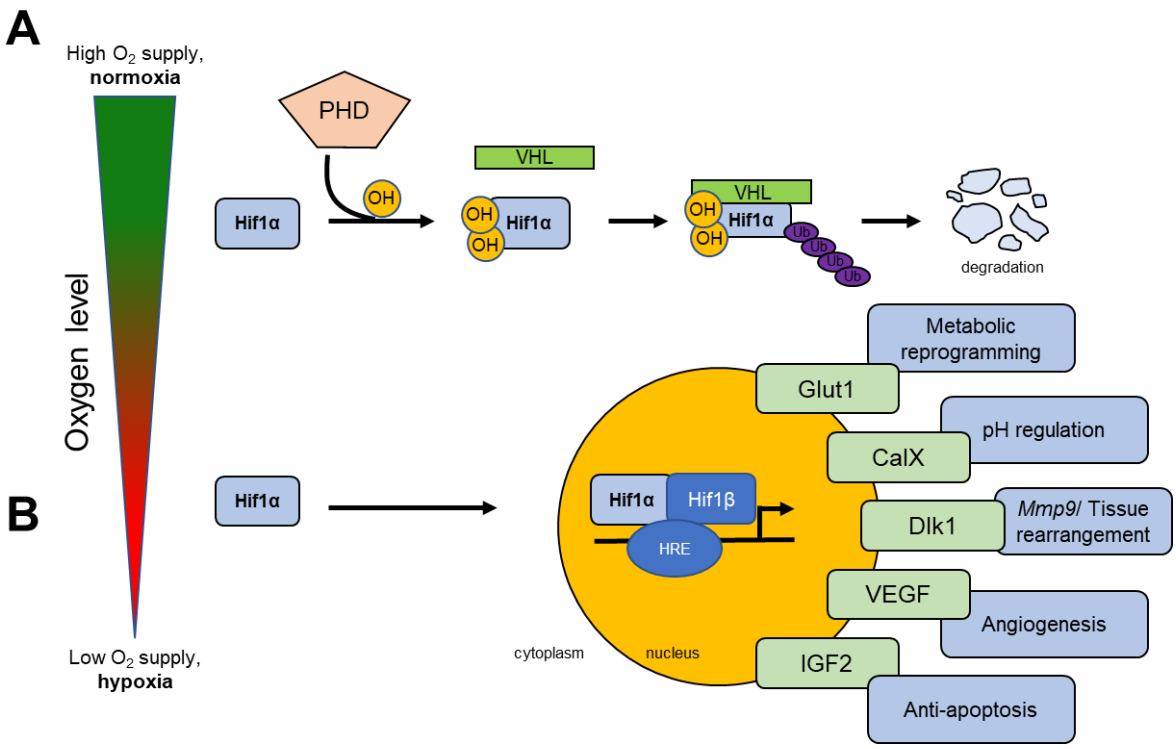

Figure 1-7: *Cellular response to oxygen presence and deprivation.* ***A:*** *During normoxic conditions, Hif1α is hydroxylated by the PHDs. Hydroxylated Hif1α is recognised by the VHL complex, ubiquitinated and degraded by the proteasome.* ***B:*** *Under hypoxic condition, Hif1α is not hydroxylated and therefore, not binding to the VHL complex. The stabilised Hif1α is translocated to the nucleus, where it dimerises with the Hif1β subunit. Together, they are binding to the HREs and induce the expression of hypoxia-related genes, involved in the metastasis reprogramming, angiogenesis, erythropoiesis, cell survival and stem cell self-renewal or pH regulation. CaIX, carbonic anhydrase IX; EPO, erythropoietin; Glut1, glucose transporter; HIF, hypoxia-inducible factor; HRE hypoxia-response element; PhD, prolyl hydroxylase domain proteins; VEGF, vascular endothelial growth factor; VHL, von Hippel-Lindau. Image modified after (Sadri and Zhang, 2013).*

In case of oxygen deprivation, Hif1α is not recognised and hydroxylated by the PHDs. Therefore, Hif1α is not bound by VHL and will not be ubiquitinated and degraded by the proteasome (Sadri and Zhang, 2013). In contrast, it translocates to the nucleus, where it accumulates. The oxygen-sensitive subunit Hif1α is forming a heterodimeric complex with the stable subunit of Hif1β. This complex is binding the hypoxia response elements (HREs). Those HREs are located in the promotor/enhancer region of hundreds of hypoxia-related genes, facilitating the adaption to hypoxia (Iyer *et al.*, 1998; Simon and Keith, 2008). Most of these genes are involved in improving the oxygen supply in the hypoxic region through an increase in red blood cell maturation, angiogenesis, and vascularisation (Krock, Skuli and Simon, 2011; Haase, 2013). Next to involvement in hypoxia regulation, there are also hypoxia-dependent genes related to embryogenesis or stem cell self-renewal (Zhang *et al.*, 2007; Dunwoodie, 2009; Grassi and Pietras, 2022). It is also reported, that hypoxia is one selective inducer to activate different pathways and mechanism during development, cell survival and proliferation

(Fong and Takeda, 2008; Majmundar, Wong and Simon, 2010; Grotta *et al.*, 2021). Also, hypoxia is discussed to have an influence on stem cell maintenance (Sadri and Zhang, 2013; Grassi, Pantazopoulou and Pietras, 2020).

1.5.2. Stroke

Stroke is a potentially lethal cerebrovascular disorder, characterised by the interruption or reduction of the blood flow in the brain or spinal cord. This interruption or reduction of the blood flow results in oxygen and nutrient deprivation, which in turn results in rapid cell death in the affected region (Grotta *et al.*, 2021). Each year, more than 14 million people are affected worldwide. Thus, stroke is one of the most severe health issues, which results often in death or chronic disability, including paralysis, aphasia, dementia as well as loss of advanced brain functions like learning and memory (Linn and Brückmann, 2009; Hasan *et al.*, 2018; Powers, 2020; Virani *et al.*, 2020; Tsao *et al.*, 2022). There are two common forms of stroke, the acute ischemic stroke (87 % of the cases) (Liu, Luo and Wang, 2022) and the haemorrhagic stroke (13 % of the cases) (Chen, Zeng and Hu, 2014). The haemorrhagic stroke is described as the rupture of a vesicle and the uncontrollable blood flow into the surrounding brain regions. The undersupply with oxygen and nutrients of the affected brain region leads to neuronal cell death (Chen, Zeng and Hu, 2014). The ischemic stroke is defined as the rapid disruption of cerebral arterial blood flow and lack of oxygen due to closure of a blood vesicle resulting in the blockage of the blood flow (Liu, Luo and Wang, 2022). The effects observed during a stroke and in the aftermath dependent on a wide range of factors like age, gender, hormonal status, and tissue inflammation. These factors have interactive effects on ischemic stroke risk, outcome, and pathology (Roy-O'Reilly and McCullough, 2018; Ekker *et al.*, 2019; Grotta *et al.*, 2021). Older stroke patients have a longer recovery time, compared to younger patients (Roy-O'Reilly and McCullough, 2018) and the incidence of stroke increases exponentially with age in patients over the age of 35 years (Ekker *et al.*, 2019). Further, a gender difference in the stroke recovery period is observed. In general, women recover faster compared to men after an ischemic stroke (Grotta *et al.*, 2021). Noteworthy, the ischemic recovery difference between the genders has to be considered in correlation to the age. Young men have a higher risk for stroke, in middle-age this reverses and in elderly populations the incidence is higher in women (Roy-O'Reilly and McCullough, 2018). Taken together, stroke incidents can happen throughout the entire population, regardless of age, gender, ethnicity or origin, and causes serious brain damage and cell death (Grotta *et al.*, 2021).

1.6. Influence of oxygen levels on embryogenesis

The level of oxygen plays a crucial role in mammalian embryogenesis. During this process, the embryo undergoes hypoxia (Dunwoodie, 2009; Fathollahipour, Patil and Leipzig, 2019). Hypoxia is discriminated into two types of hypoxic conditions, on one hand, the mild and

physiological hypoxia and, on the other hand, the severe hypoxia. The physiological hypoxia is defined as an oxygen concentration of 2 to 5 % in a microenvironment. The cellular microenvironment, like a stem cell niche describes the cell surrounding, containing physical and chemical signals influencing the cellular behaviour (Sun, Chen and Fu, 2012). In contrast to the physiological hypoxia, severe hypoxia has a drop of the oxygen level below 2 % (Fathollahipour, Patil and Leipzig, 2019). Developmental processes like stem cell fate decision, placenta formation, cardiogenesis, and neurogenesis are requiring hypoxic conditions (Dunwoodie, 2009; Fathollahipour, Patil and Leipzig, 2019; Grassi *et al.*, 2020).

The earliest point in embryogenesis, in which the embryo experiences physiological hypoxia, is during the development of the blastocyst (Harvey *et al.*, 2004; Fathollahipour, Patil and Leipzig, 2019; Nguyen *et al.*, 2020). The blastocyst resembles a spheric structure, consisting of the trophoblast and the ICM. Through the formation of a hollow structure, the blastocyst creates a microenvironment of a physiological hypoxia (2 % oxygen) (Nguyen *et al.*, 2020). The physiological hypoxia O_2 promotes further proliferation of blastocyst cells. In contrast, blastocyst cells, which do not experience the hypoxic condition of ≤ 2 % oxygen, show reduced proliferation rates (Harvey *et al.*, 2004; Ezashi, Das and Roberts, 2005; Nguyen *et al.*, 2020). With differentiation of the embryo into a blastocyst, the formation of the placenta starts. Although, the placenta will later be responsible for the oxygen supply of the embryo, the development of the trophoblast and later of the extra-embryonic ectoderm and the ectoplacental cone requires a hypoxic environment (≤ 2 % O_2). There are more examples for the requirement of hypoxic condition during the embryogenesis, for example. cardiogenesis or bone formation (Amarilio *et al.*, 2007; Dunwoodie, 2009; Ortega *et al.*, 2017).

Next to the cardiogenesis and the bone morphogenesis, the neurogenesis is also a developmental process, where hypoxic conditions have a decisive influence on the cell fate (Amarilio *et al.*, 2007; Dunwoodie, 2009; Ortega *et al.*, 2017). Hypoxia is necessary to maintain neuronal stem cells as well as for the differentiation of various neuronal subtypes (Ferrón *et al.*, 2011; Montalbán-Loro *et al.*, 2021). For example, the differentiation of cortical cell types is highly dependent on hypoxic conditions (Dunwoodie, 2009; Santilli *et al.*, 2010). In the human organism, physiological hypoxia promotes neural stem cell differentiation into neurons and oligodendrocytes, whereas hypoxia under 0.5 % O_2 is required to differentiate into astrocytes (Ortega *et al.*, 2017). The generation of GABAergic neurons requires an O_2 concentration between 2.5 and 5 % O_2, which would also be the oxygen concentration of the physiological hypoxia (Santilli *et al.*, 2010). Hypoxic conditions also facilitate the generation of dopaminergic neuron of marrow-derived mesenchymal stem cells (Zhang *et al.*, 2007).

2. Aims and Objectives

As demonstrated by the literature review above, Delta-like homologue 1 (Dlk1) is involved in multiple processes, such as cancer, adipogenesis, and neurulation. During those processes, Dlk1 is cleaved by the Adam17 secretase and an extracellular fragment is separated. By an additional cleavage, an intracellular fragment (ICF) is cleaved. First preliminary studies about Dlk1 cleavage and the importance of the ICF in MN diversity were previously conducted by our working group. However, the Dlk1 cleavage and the translocation of the ICF to the nucleus remains difficult to detect, likely due to a missing stimulus. Based on previous report (Grassi, Pantazopoulou and Pietras, 2020), it was hypothesized that the missing stimulus could be developmental hypoxia.

2.1. Aim of the study

The aim of this thesis was to study hypoxic-dependent Dlk1 regulation in regard to MN diversification during embryogenesis.

2.2. Objectives

To achieve the aim of this thesis, the following objectives were fulfilled:

The first objective is to clarify, if during embryogenesis hypoxic-dependent Dlk1 regulation could influence MN diversification. This objective will be achieved by analysing immunofluorescence staining of Dlk1 and Hif1α in transversal sections of E12.5 old embryos.

The second goal is to reveal, if hypoxia could influence Dlk1 regulation in ESC-derived MNs and murine brain slices. Therefore, protein concentrations will be measured after hypoxic condition and compared with normoxia.

The third objective is to reveal dynamics and mechanisms of hypoxia-dependent ICF translocation. Therefore, immunofluorescence signal intensities of the ICF-HA will be measured and quantified in the nucleus of ESC-derived MNs.

The fourth goal is to investigate the influence of Adam17 inhibition in the hypoxia-dependent Dlk1 cleavage. To achieve this objective, Adam17 activity is blocked and protein alterations are measured and quantified.

3. Material

3.1. General laboratory material

3.1.1. Consumables

Table 1*: General chemicals*

Name	Catalogue. No	Supplier	City, Country
Amersham™ Protran™ 0.2 µm NC nitrocellulose blotting membrane	10600001	GE Healthcare	Chicago, USA
CellBIND surface culture dish	3295	Corning	Corning, USA
Cell counting 8 channel chambers	80816	Ibidi	Gräfelfing, GER
Cell culture dish 6 cm	430166	Corning	Corning, USA
Cell strainer 40 *µ*m nylon	431750	Corning	Corning, USA
µ-Dish, 35 mm, high wall	81156	Ibidi	Gräfelfing, GER
Parafilm	H666.1	Carl Roth	Karlsruhe, GER
StarSeal Advanced Polyolefin film	E2796-9795	Starlab	Hamburg, GER
Superfrost plus microscope slides	10149870	Thermo Fisher	Darmstadt, GER
Tubes 15 ml	62.554.502	SARSTEDT	Nümbrecht, GER
Tubes 50 ml	62.547.254	SARSTEDT	Nümbrecht, GER
Vacuum filter 0.22 *µ*m pore, 500 ml	431097	Corning	Corning, USA
24 well culture plate	92024	TPP	Trasadingen, CH
96 well PCR Plate, semi skirted	I1402-9700	Starlab	Hamburg, GER

3.1.2. Chemicals

Table 2: *General chemicals*

Compound	Catalogue. No	Supplier	City, Country
1 kilo base pair (kbp) plus ladder	SM1331	Thermo Fisher	Darmstadt, GER
4',6-Diamidin-2-phenylindol (DAPI)	6335.1	Carl Roth GmbH	Karlsruhe, GER
6x DNA loading buffer	R0611	Thermo Fisher	Darmstadt, GER
Agarose, universal	9012-36-6	VWR International	Darmstadt, GER
Albumin Fraction V (BSA)	0163.4	Carl Roth GmbH	Karlsruhe, GER
Ampicillin	69-52-3	Merck KGaA	Darmstadt, GER
Bolt™ 4-12 % Bis-Tris Plus	NW04120BOX	Thermo Fisher	Darmstadt, GER
Bolt™ Antioxidant	BT0005	Thermo Fisher	Darmstadt, GER
Bolt™ MES SDS Running Buffer 20X	B0002	Thermo Fisher	Darmstadt, GER
Bolt™ MOPS SDS Running Buffer 20X	B0001	Thermo Fisher	Darmstadt, GER
Carbenicillin	6344.2	Carl Roth GmbH	Karlsruhe, GER
Chloroform	T901.1	Carl Roth GmbH	Karlsruhe, GER
CRYOSPEED® MED liquid nitrogen		The Linde Group	Pullach, GER
D-Glucose	HN06.3	Carl Roth GmbH	Karlsruhe, GER

Dithiothreitol (DTT)	D1532	Thermo Fisher	Darmstadt, GER
DMSO	D2650	Sigma Aldrich	Taufkirchen, GER
Ethanol (EtOH)	0911.4	Carl Roth GmbH	Karlsruhe, GER
Glycine	HN07	Carl Roth GmbH	Karlsruhe, GER
Fluoromount-G	0100-01	Southern Biotech	Birmingham, USA
Isopropanol	6752.4	Carl Roth GmbH	Karlsruhe, GER
LB Agar	00301241	Invitrogen GmbH	Waltham, USA
LB Broth medium	L3022	Merck KGaA	Darmstadt, GER
Mowiol	0713	Carl Roth GmbH	Karlsruhe, GER
Precision Plus Protein™ All Blue Prestained Protein Standards	1610373	Bio-Rad	Hercules, USA
Skim milk	T145.3	Carl Roth GmbH	Karlsruhe, GER
Sodium deoxycholate protease inhibitor	11873580001	Roche	Mannheim, GER
Sucrose	4621.1	Carl Roth GmbH	Karlsruhe, GER
Super Signal West Femto Maximum Sensivity Substrate	34096	Thermo Fisher	Darmstadt, GER
Tissue-Tek® O.C.T.™ Compound	4583	Sakura	München, GER
TRIS	4855.2	Carl Roth GmbH	Karlsruhe, GER
TritonX100	T8787	Carl Roth GmbH	Karlsruhe, GER
TRIzol reagent	15596026	Thermo Fisher	Darmstadt, GER
Trypan blue stain (0.4%)	15250-061	Thermo Fisher	Darmstadt, GER
Trypsin-EDTA	25300054	Thermo Fisher	Darmstadt, GER
Tween®20	9127.1	Carl Roth GmbH	Karlsruhe, GER

3.1.3. Solutions

3.1.3.1. Solutions for western blot analysis

Table 3: *Solutions for Western blot*

Solution	Constituents' ingredients
5 x Laemmli loading buffer	250 mM (w/v) Tris-HCl, pH 6.8 10 % (v/v) SDS 1.25 % (w/v) Bromophenol blue 10 mM (v/v) EDTA 0.03 % (v/v) β-mecaptoethanol 50 % (w/v) Glycerol
RIPA lysis buffer	50 mM (w/v) Tris-HCl, pH 8.0 0.15 M (w/v) NaCl 0.1 % (v/v) SDS 1 % (v/v) NP-40 0.5 % (w/v) Sodium deoxycholate protease inhibitor (1 pill per 20 ml buffer)
Running buffer	40 x (v/v) MES buffer (B0002, Thermo Fisher) Fill up to in 800 ml ddH_2O
Stripping buffer	0.5 M (w/v) Glycine

	10 % (v/v) SDS 0.03 % (v/v) β-mecaptoethanol pH 2.8
Tris-buffered saline (TBS)	25 mM (w/v) Tris-HCl, pH 7.5 140 mM (w/v) NaCl
TBS-Tween	25 mM (w/v) Tris-HCl, pH 7.5 140 mM (w/v) NaCl 0.05 % (v/v) Tween-20
Western blot transfer buffer	25 mM (v/v) Tris-HCl 192 mM (w/v) Glycine 20 % (v/v) Methanol

3.1.3.2. Solutions for genotyping

Table 4: *Solutions for cloning*

Solution	Content
Duplex buffer 10X	300 mM HEPES 1 M Potassium acetate In ddH_2O; pH 7.5
TAE Buffer 50X	242 g Tris(hydroxymethyl)-aminomethan (Tris) base 0.05 M Ethylenediaminetetraacetic acid (EDTA) 57.1 ml Glacial acetic acid
CCMB80 medium	10 mM Potassium acetate; pH 7.0 80 mM Calcium chloride dihydrate 20 mM Manganese dichloride tetrahydrate 10 mM Magnesium chloride hexahydrate 10 % (v/v) Glycerol adjust pH to 6.4 with 0.1 N HCl
TENS buffer	100 mM Tris; pH 8.0 5 mM EDTA 200 mM Sodium chloride (NaCl) 0.2 % (v/v) SDS

3.1.3.3. Solutions for immunofluorescence analysis

Table 5: *Solutions for Immunofluorescence analysis*

Solution	Content
Blocking solution	Phosphate-buffered saline (PBS) 1 % (w/v) BSA 0.5 % (v/v) TritonX100
Mowiol embedding solution	2.4 g Mowiol 4-88 6.0 g Glycerol 6 ml ddH_2O 12 ml 0.2 M Tris-HCl; pH 8.5

3.2. Cell culture material

3.2.1. Cell lines

The murine embryonic stem cell (ESC) lines used in the following experiments of this thesis were genetically modified by Dr. rer. nat. Matthias Marks. They are based on the G4 mESCs line, which have a F1-hybrid background of 129s6/SvEvTac x C57BL/6NCr. They were maintained as described in section 4.2.2.

1. **Dlk1-HA**

   The Dlk1-HA murine ESC line was generated by the single-stranded oligodeoxynucleotides (ssODNs) modification. The ssODN was used as a donor template in combination of the engineered nucleases for efficient target insertion of small DNA targets.

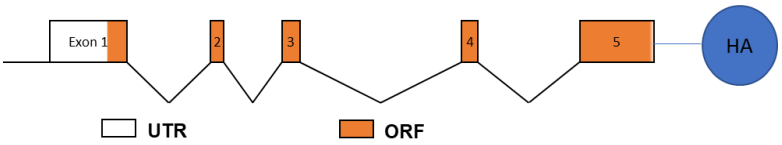

Figure 3-1: *Schematic presentation of the modified Dlk1 murine ESC line. Wt Dlk1 locus, indicating the five exons with the ORF and the UTR regions. HA tag was added by ssODNs at the C-terminus (blue circle). HA, hemagglutinin; ORF, open reading frame; ssODN, single-stranded oligodeoxynucleotides; UTR, untranslated region. Cell line was created by Dr. Marks*

2. **Dlk1$^{\Delta ICF}$**

   The Dlk1$^{\Delta ICF}$ murine ESC line was generated by a CRISPR/Cas9 KO method. The locus of Dlk1 with the CRISPR target site is indicated in the following figure (figure 3-2). The stop codons result in a premature termination of the translation thus leading to a truncated form of Dlk1 missing the ICF. These two separated clones were further expanded to independent cell lines and analysed in the cell culture experiments.

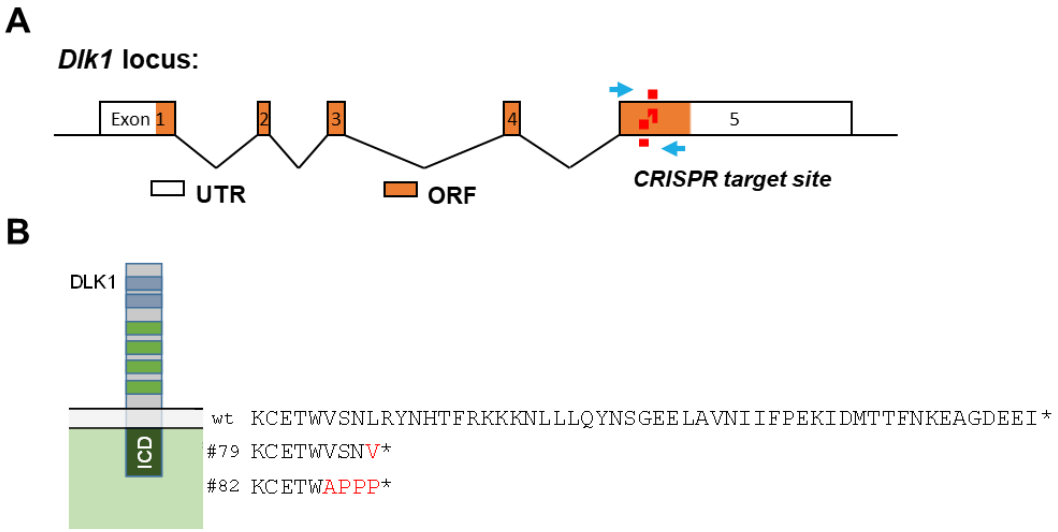

Figure 3-2: *Modified Dlk1ΔICF murine ESC line.* ***A:*** *wt Dlk1 locus, indicating the five exons with the open reading frame (ORF) and the (UTR) regions. CRISPR target sites are indicated in red dashed line, with two nicks to induce a double-stand break-like event (blue arrow).* ***B:*** *The nicks result in a frameshift leading to premature stop codons on the ICF of Dlk1 for two different clones. These clones were expanded in order to create distinct cell lines for further analysis. Cell lines were created by Dr. Marks.*

3.2.2. Cell culture chemicals

Table 6: *Cell culture chemicals*

Compound	Catalogue. No	Supplier	City, Country
B-27 Supplement 50X	17504044	Thermo Fisher	Darmstadt, GER
DBZ	HB3419	HelloBio	Dunshaughlin, IR
Gibco™ MEM solution of non-essential amino acids (100X)	12084947	Thermo Fisher	Darmstadt, GER
5-Fluoro-2‘-deoxyuridine (FDU)	50-91-9	Merck KGaA	Darmstadt, GER
Knockout DMEM	10829018	Thermo Fisher	Darmstadt, GER
DMEM with high glucose-F12	11320033	Thermo Fisher	Darmstadt, GER
FCS ES cell grade	P0607050	PAN-Biotech	Aidenbach, GER
FCS	S0615	PAN Biotech	Aidenbach, GER
Gelatine	9000-70-8	Merck KGaA	Darmstadt, GER
Glycine	HN07.3	Carl Roth GmbH	Karlsruhe, GER
CHIR 99021 (CH)	1386	Axon Medchem	Houston, USA
Laminin	L2020 Sigma	Merck KGaA	Darmstadt, GER
Lipofectamine2000	11668027	Thermo Fisher	Darmstadt, GER
Matrigel® Matrix	356231	Corning	New York, USA
MEK inhibitor PD0325901 (PD)	72182	STEMCELL Technologies	Saint Égrève, FR
TMI-1	PZ0336	Merck KGaA	Darmstadt, GER
Mitomycin C	M0503	ChemCruz	Dallas, USA
ESGRO mouse leukemia	ESG1107	Merck KGaA	Darmstadt, GER

inhibitory factor (LIF)			
Opti-MEM	31985062	Thermo Fisher	Darmstadt, GER
Penicillin Streptomycin	DE17-602E	Lonza	Basel, CH
Phosphate-buffered Saline (PBS)	P04-36500	Pan-Biotech	Aidenbach, GER
Poly-D-ornithine hydrobromide	82682-33-5	Merck KGaA	Darmstadt, GER
Trypan blue stain (0.4%)	15250-061	Thermo Fisher	Darmstadt, GER
TrypLe	12605010	Thermo Fisher	Darmstadt, GER
Trypsin-EDTA	25300062	Thermo Fisher	Darmstadt, GER
Forskolin	HB1348	HelloBio	Dunshaughlin, IR
InSolution smoothened agonist (SAG)	566661	Merck KGaA	Darmstadt, GER
N-2 Supplement 100X	17502-048	Thermo Fisher	Darmstadt, GER

Table 7: *siRNA*

Compound	Catalogue. No	Supplier	City, Country
siRNA Adam17	AM16708	Thermo Fisher	Darmstadt, GER
siRNA control RNA	AM16708	Thermo Fisher	Darmstadt, GER

3.2.3. Cell culture solutions

3.2.3.1. Solutions for stem cell culture

Table 8*: Solutions for cell culture medium*

Solution	Content
ESC medium	Knockout Dulbecco's modified Eagle's medium (DMEM) with 4500 mg/ml glucose and with sodium pyruvate; supplemented with: 15 % (v/v) fetal calf serum (FCS) 1 x (v/v) non-essential amino acids (NEAA) 1 x (v/v) nucleosides 1 x (v/v) penicillin and streptomycin 2 mM L-Glutamine 1 µM β-mercaptoethanol 10 U^{-7} (v/v) murine leukaemia inhibitory factor (LIF)
murine embryonic fibroblast (MEF) medium	DMEM with 4.5 mg/ml glucose and without sodium pyruvate; supplemented with: 10 % (v/v) FCS 2 mM L-Glutamine 1 x (v/v) penicillin and streptomycin
N2B27 medium	Neurobasal medium and Advanced DMEM-F12 Medium at a 1:1 ratio; supplemented with: 1 x (v/v) N2

	1 x (v/v) B27 1 x (v/v) penicillin and streptomycin 1 % (v/v) L-Glutamine 0.04 mg/ml bovine serum albumin (BSA) 0.1 µM β-mecaptoethanol
motor neuron (MN) medium	Neurobasal medium; supplemented with: 2 % (v/v) FCS 1 % (v/v) B27 0.25 % (v/v) L-Glutamine 0.001 % (v/v) β-Mercaptoethanol
2 x ESC freezing medium	Knockout DMEM with 4500 mg/ml glucose and with sodium pyruvate; supplemented with: 20 % (v/v) FCS 20 % (v/v) Dimethylsulfoxid (DMSO)
2 x MEF freezing medium	Regular DMEM with 4.5 mg/ml glucose and without sodium pyruvate; supplemented with: 20 % (v/v) FCS 20 % (v/v) DMSO
MEF resuspension medium	Regular DMEM with 4.5 mg/ml glucose and without sodium pyruvate; supplemented with: 20 % (v/v) FCS 2 mM Glutamine 1 x (v/v) penicillin and streptomycin

3.2.3.2. Solutions for brain slice culture

Table 9: *Solutions for slice culture*

Solution	Content
Artificial cerebrospinal fluid (aCSF) medium	118 mM Sodium chloride 25 mM Sodium hydrogencarbonate 30 mM D-glucose 1 mM Magnesium dichloride 3 mM Potassium chloride 1 mM Sodium dihydrogen phosphate 1.5 mM Calcium chloride 1 x Penicillin and Streptomycin adjusted pH 7.4
Long-term aCSF medium	aCSF; supplemented with: 2 mM Glutamine 1 x (v/v) B27 1 x (v/v) Penicillin and Streptomycin adjusted pH 7.4

3.3. Antibodies

3.3.1. Primary antibodies

Table 10: *Primary antibodies*

Antibody	Catalogue No.	Manufacturer	Host	App.	Dilution
Anti-Dlk1	ab21682	Abcam	rabbit	WB ICC	1:2000 1:500
	H-118	SantaCruz	rabbit	IHC	1:100
Anti-Hif1α	NB100-479	Novus Biologicals	Rabbit	WB ICC IHC	1:1000 1:500 1:1000
Anti-Glut1	NB110-39115	NovusBio	Rabbit	WB	1:1000
Anti-CaIX	NB100-417	NovusBio	Rabbit	WB	1:1000
Anti-HA	ab9110	Abcam	rat	WB ICC	1:1000 1:100
Anti-Mmp9	M9570	Sigma	goat	ICC	1:500
Anti-Adam17	PA527395	Thermo Fisher	rabbit	ICC	1:500
Anti-Iba1	011-27991	Wako	rabbit	WB ICC	1:5000 1:1000
Anti-GFAP	AB5804	Millipore	mouse	WB ICC	1:1000 1:300
Anti-ChAT	ab181023	Abcam	goat	IHC	1:100
Anti-GAPDH	sc-32233	Santa Cruz	goat	WB	1:1000
Anti-VAChT	139 105	Synaptic Systems	guinea pig	IHC	1:1000
Anti-Actin	ab1801	Abcam	Mouse	WB	1:1000
Anti-Actin	ACTN05	Thermo Fisher	Mouse	WB	1:1000
Anti-Tuj1	801202	BioLegend	mouse	WB ICC	1:1000 1:200

3.3.2. Secondary antibodies

Table 11: *Secondary antibodies*

Antibody	Catalogue No.	Manufacturer	Host	App.	Dilution
Anti-rabbit IgG, horseradish peroxi-dase-linked whole AB	17203151	Santa Cruz	donkey	WB	1:10,000
Anti-mouse IgG, horseradish-peroxi-dase-linked whole AB	17193521	Cytiva	sheep	WB	1:10,000
cross-adsorbed Anti-goat IgG (H+L)	31400	Thermo Fisher	goat	WB	1:5,000

Alexa Fluor® 488 anti-mouse IgG	A32766	Thermo Fisher	donkey	ICC	1:200
Alexa Fluor® 555 anti-mouse IgG	A32773	Thermo Fisher	donkey	ICC	1:200
Alexa Fluor® 647 anti-mouse IgG	A32795	Thermo Fisher	donkey	ICC	1:200
Alexa Fluor® 488 anti-rabbit IgG	A32790	Thermo Fisher	donkey	ICC	1:200
Alexa Fluor® 555 anti-rabbit IgG	A32794	Thermo Fisher	donkey	ICC	1:200
Alexa Fluor® 488 anti-goat IgG	A32814	Thermo Fisher	donkey	ICC	1:200
Alexa Fluor® 555 anti-goat IgG	A32816	Thermo Fisher	donkey	ICC	1:200
Alexa Fluor® 647 anti-goat IgG	A32744	Thermo Fisher	donkey	ICC	1:200
Alexa Fluor® 488 anti-guinea pig IgG	A11073	Thermo Fisher	goat	ICC	1:200
Alexa Fluor® 555 anti-rabbit IgG	A32732	Thermo Fisher	goat	ICC	1:200

3.4. Kits

Table 12: *Kits*

Kits	Catalogue No.	Manufacturer	City, Country
CloneJET PCR Cloning kit	K1231	Thermo Fisher	Darmstadt, GER
iQTM SYBR R Green Supermix	1708882	Bio-Rad	Hercules, USA
LIVE/DEAD assay	L3224	Thermo Fisher	Darmstadt, GER
LDH assay kit	G1782	Promega	Madison, USA
QIAGEN Plasmid Maxi kit	12163	Qiagen	Hilden, GER
Qiagen MinElute Gel Extraction kit	28604	Qiagen	Hilden, GER
GeneJET Plasmid Miniprep kit	K0503	Thermo Fisher	Darmstadt, GER
Qiagen RNeasy Mini kit	12125	Qiagen	Hilden, GER
Phusion™ High Fidelity DNA Polymerase	F-530XL	Thermo Fisher	Darmstadt, GER
Pierce BCA Protein Assay kit	5000111	Thermo Fisher	Darmstadt, GER
TUNEL assay kit	11684795910	Merck	Darmstadt, GER

3.5. Equipment

Table 13: *Equipment*

Equipment	Model	Manufacturer	City, Country
Alliance	UVItec15.11	Biometra GmbH	Göttingen, GER
Analyse	2.1	BioDoc	Hannover, GER
Cell counter	Cedex XS	Innovatis	Fairfax, USA
Microscope Olympus	BX51	Olympus Europa SE	Hamburg, GER
Microscope Olympus	IX81	Olympus Europa SE	Hamburg, GER
Confocal Microscope	LSM 710	Carl Zeiss	Oberkochen, GER
qRT PCR thermocycler	MyiQTurbo®2	BioRad	Hercules, USA
Cell culture incubator	HERAcell	ThermoFisher	Darmstadt, GER
PCR Cycler	T Professional Basic	Biometra GmbH	Göttingen, GER
Table-top spectrophotometer	Ultrospec 3100 pro	GE Healthcare	Amersham, UK
Trans-Blot	Turbo®	BioRad	Hercules, USA
UV-light source		X-Cite	Frankfurt a.M., GER
UV Transilluminator		Biometra GmbH	Göttingen, GER
UV Documentation	UVsolo	Biometra GmbH	Göttingen, GER
Hypoxia chamber	C174, customised	BioSpherix	NY, USA
Microtome	VT1200 S	Leica	Wetzlar, GER
Water bath	WNB 14	Memmert	Schwabach, GER

3.6. Software

Table 14: *Software*

Software	Appl.	Manufacturer	City, Country
Cedex XS	Cell count	Innovatis	Fairfax, USA
CLC Main Workbench 8.0.1	Theoretical gene modulation	Qiagen	Hilden, GER
iControl 1.8 SP1	Microplate measurements	Magellan™/ Tecan	Männedorf, CH
CRISPOR	Primer design	(Haeussler et al., 2016)	
Primer-BLAST	Primer design	NCBI	Bethesda, USA
Xcellence Olympus Software	Image processing	Olympus	Tokios, JPN
Zeiss Zen (blue edition)	Image processing	Carl Zeiss	Oberkochen, GER
Microsoft Office (Home and Student 2016)	Text documentation, Data analysis, image composition	Microsoft	Redmond, USA
CellA	Cell imaging	Olympus	Tokios, JPN

Prism (Version 8)	Statistical analysis, plotting of diagrams	GraphPad	San Diego, USA
Alliance™-1D	UV imaging	UVITEC	Cambridge, UK
FIJI/ImageJ	Image processing/ analysis	Schindlin *et al.* 2012	

4. Methods

4.1. Molecular cloning

4.1.1. Competent cells

Competent cells for cloning and deoxyribonucleic acid (DNA) propagation were generated after a modified protocol of Bloom *et. al* (Hanahan, Jessee and Bloom, 1991). Therefore, one single colony was selected, transferred in 2 ml of super optimal broth medium (SOB) and shaked overnight at 18 °C. After around 14 hours of shaking, the optical density (OD) at a wavelength of 600nm value was checked. A fresh culture was inoculated with 250 ml super optimal broth and 1 ml of the overnight culture. This new culture was grown at 25 °C and 24,000 x g in the incubator. The OD was checked regularly (every 30 to 60 minutes (min)) until the OD = 0.3. If the value is reached, the bacteria culture was transferred in on ice, prechilled reactions tubes and centrifuged at 3000 x g, 4 °C and 10 min in a flat bottom centrifuge. The resulting pellet was resuspended gently in a total volume of 80 ml CCMB80 medium, separated in two 50 ml reaction tubes, each with 40 ml CCMB80 medium. After an incubation time of 20 min on ice, the mix was centrifuged at 3000 x g and 4 °C for 10 min. The two pellets were combined by resuspending them in a total volume of 10 ml ice-cold CCMB80 medium. Subsequently, the cells were incubated for 20 min on ice. The bacteria mix was aliquoted directly after the incubation time in 50 µl aliquots and frozen immediately in liquid nitrogen. Competent cells were stored at -80 °C. The CCMB buffer used in the protocol contains glycerol for preservation of the cells.

The competence of the cells was measured as followed. Cells were transformed with the standard pUC19 plasmid. The transformation was performed as described in 4.1.2. 100 µl of reaction were plated on a lysogenic broth (LB) plate, including antibiotics against Carbenicillin (100 ng/ml) and incubated overnight at 37 °C. The next day, the number of grown colonies were counted. Competent cells should yield a ratio of 250-1000 colonies. The further transformation efficiency (TE) is calculated as following.

$$TE = 6 * \text{counted cells} * 10^5 / \text{ug DNA}$$

The expected TE should be reaching a value between $1.5x10^8$ and $6x10^8$ cfu/µg DNA.

4.1.2. Transformation

For the transformation of plasmid DNA into bacteria, Mach1 bacteria were thawed from -80 °C on ice for at least 30 min. Then the plasmid DNA was added to the Mach1 bacteria and incubated again for 30 min on ice. Afterwards, a heat-shock at 42 °C for 45 sec was performed with a recovery period on ice for 3-5 min. After the recovering, the bacteria were supplemented with 1 ml of LB medium and incubated for one hour at 37 °C in the shaker (500 revolutions per

minutes (rpm)). In the meantime, the LB plates with the appropriate antibiotic was incubated a room temperature (RT). For the cloning the px335-G2P plasmid, the integrated ampicillin resistance enables the carbenicillin selection (100 µg/ml). Bacteria were centrifuged for 1 min, RT and 300 x g and plated on the LB plates and incubated overnight at 37 °C upside-down.

4.2. Cell Culture

4.2.1. Maintenance of murine embryonic fibroblast

MEFs were cultured in MEF medium on gelatinised plates. MEFs can be cultivated for a week at 7.5 % CO 2 and 37 °C. MEFs were inactivated by Mitomycin C treatment (2 mg/ml) after expanding the cell number. In brief, 2 mg/ml Mitomycin C were prepared in MEF medium and added to the cells after washing the plates twice with Phosphate-buffered saline (PBS). Mitomycin C treatment is a widely used antibiotic and alkylating agent. It is interacting with double-stranded DNA and results in DNA cross-linking thereby inhibiting DNA synthesis and proliferation. After an incubation time of three hours, the Mitomycin C treatment was stopped by washing the plate again twice with PBS at RT. Then, MEFs were detached by adding Trypsin-EDTA to the cells and incubated for 10 min at 37 °C. The detached cells were collected in fresh MEF medium and centrifuged for 5 min at 180 x g at RT. The pellet was resuspended in a 1:1 mix of MEF medium and 2 x MEF freezing medium. Cells were frozen and stored at -150 °C.

4.2.2. Maintenance of embryonic stem cells

Embryonic stem cells (ESCs) were maintained at 37 °C and 7.5 % CO^2 on gelatinised plates in ESC medium, supplemented with Leukaemia inhibitory factor (LIF). Either ESCs were seeded on a layer of MEF in ESC medium or cells were plated directly on the gelatinised surface in ESC medium, supplemented with two differentiation inhibitors: PD0325901 (PD) (1 µM) and CH90221 (CH) (3 µM). Medium was changed daily and factors were added freshly every day. The cells reached a confluence of about 80 %, cells were trypsinised and splitted in a ratio of 1:4 on a new plate or frozen with 2 x freezing medium in a ratio 1:1. In brief, cells were washed twice with RT PBS and trypsinised with the appropriate amount of Trypsin-EDTA for 10 min at 37 °C. Trypsin-EDTA was inactivated with MEF medium and cell suspension was centrifuged for 180 x g, 5 min at RT. The cell pallet was resuspended in fresh ESC medium, when seeded directly on the MEF layer or with supplementation of PD (1 µM) and CH (3 µM).

4.2.3. Motor neuron differentiation

For the differentiation of ESCs in MNs, ESCs were seeded on a confluent layer of MEFs and maintained according to the standard (see 4.2.2) for at least two passages. Prior to differentiation, plates coated with 0.1 % gelatine were prepared. For the first day of

differentiation, here stated as day 0 (D0), ESCs were trypsinised with 500 µl Trypsin-EDTA for 10 min at 37 °C and 7.5 % CO_2. Detached cells were collected in MEF medium and centrifuged at 180 x g for 5 min at RT. The cell pellet was resuspended with ESC medium and plated on the original 6 cm plate to let the MEFs set down. This process needs an incubation time of 30 min at 37 °C and 7.5 % CO_2. Then, the medium was carefully aspirated while leaving the cell layer intact. Cell medium was replated on a new and freshly coated 6 cm plate and the MEFs freezing process was repeated for 20 min. Afterwards, ESCs were collected and passed through cell strainer with 40 µm pores. The volume was measured and the number of ESCs was determined by using Trypan blue and the Cedex cell counter. For one 6 cm plate, $1.05x10^5$ cells were plated in N2B27 medium, supplemented with 10 ng bFgf to prone the differentiation of ESCs. For the next days the medium was changed every 24 hours. For the next day (D1), medium was changed to N2B27 medium with 10 ng bFgf. At day two of differentiation (D2), medium was changed to N2B27 medium, supplemented with 10 ng bFgf and 5 mM of CH.

For day three of differentiation (D3), medium was changed to N2B27 medium, supplemented with 100 nM synthetic retinoic acid ($ec23^x$) and 500 nM sonic hedgehog agonist (SAG). Next to medium change, cell culture plates were prepared by coating the appropriate number of plates with Poly-D-Ornithin overnight at 37 °C. For day four of differentiation (D4), medium was exchanged to N2B27 medium, supplemented with 100 nM $ec23^x$ and 500 nM SAG twice a day. Furthermore, the coated plates were dried and coated with a mixture of Matrigel and laminin in Neuropan medium and incubated again overnight at 37 °C.

At the beginning of day five of differentiation (D5), coated plates were washed three times with ddH_2O and covered with ddH_2O until further need. Motor neuron progenitor cells (pMNs) were washed with PBS twice and trypsinied with TrypLE for 10 min at 37 °C. Detached cells were covered up with N2B27 medium and centrifuged for 180 x g, 5 min at RT. The cell pallet was resuspended in sterile filtered N2B27 medium, supplemented with 100 nM $ec23^x$, 500 nM SAG and 10 ng/µl DBZ. Single cells were passed through a cell strainer and the number of cells were counted by using Trypan blue and the Cedex cell counter. For a 6 cm plate, $21x10^5$ cells were plated on the prepared plates. For a well of a 12-well-plate, $3.8x10^5$ cells were used. The appropriate number of cells were seeded in sterile-filtered N2B27 medium, supplemented with 100 nM $ec23^x$, 500 nM SAG and 10 ng/µl DBZ.

At day six of differentiation (D6), differentiation medium was changed to MN medium. Therefore, the following components were added to the MN medium (table 15). For long-term cultivation of MNs, medium was changed weekly with the following components (table 16).

Table 15: *Components for motor neuron development*

Compound	Concentration
ec23^x	10 nM
SAG	500 nM
BDNF	10 ng/µl
CNTF	10 ng/µl
Forskolin	10 µM
IBMX	100 µM
FDU	4 µM
Uridine	4 µM

For long-term culture of differentiated MNs, medium was exchanged partially once per week with the following components.

Table 16: *Motor neuron components for long-term culture*

Compound	Concentration
BDNF	10 ng/µl
CNTF	10 ng/µl
Forskolin	10 µM
IBMX	100 µM
FDU	4 µM
Uridine	4 µM

4.2.4. Hypoxic stimulation in motor neurons

4.2.4.1. Hypoxia induction in a motor neuron network

To induce ischemic stimulation in MNs, MNM was replaced partially with Neurobasal medium to induce a full oxygen glucose deprivation (OGD). Then, cells were placed directly afterwards in the customised hypoxia chamber (C174, C21, Biospherix, Parish, NY, USA; provided by AG Habib, UK Aachen). Initially experiments revealed an optimal time period of OGD (<0.2 % O_2) of 45 min. Oxygen levels were monitored continuously (PreSens, Regensburg, Germany). Temperature (set at 37 °C), pressure (1 bar) and pH were controlled and monitored in the chamber and in the cell medium during the hypoxic stimulation. MNs under normoxia were maintained at 37 °C, 7.5 % CO_2, and 1 bar. During the post-hypoxic reperfusion time, medium was changed to MN medium partially with long-term factors (table 16).

4.2.4.2. TMI-1 treatment in motor neurons

To inhibit Adam17, MNs were treated with TMI-1 (PZ0336, Merck). Medium of differentiated MNs (see 4.3.2.) were exchanged to MN medium with long-term factors (table 16) and additional TMI-1. The optimal concentration was determined in an external experiment. Hereafter, MNs were treated for one hour prior to OGD condition with 0.5 µM TMI-1 and

respectively the volume of DMSO for control samples at 37 °C, 7.5 % CO_2, and 1 bar. During the entire hypoxic stimulation (<0.2 % O_2), and the respective normoxic condition (37 °C, 7.5 % CO_2, 1 bar), TMI-1 and DMSO were incubated. During the post-hypoxic reperfusion time, medium was changed to MN medium with long-term factors in several steps (table 16).

4.2.4.3. Chemical transfection of motor neurons

For a Lipofectamin2000 transfection, differentiated MNs (see 4.3.2.) were lipofectamine-transfected with siRNA two days before hypoxic stimulation. Prior to transfection, the transfection mix was prepared. In brief, part I was prepared by mixing 125 µl Opti-MEM with 1 µg siRNA. Part II was prepared by mixing 125 µl Opti-MEM with 25 µl Lipofectamine2000. Both parts were combined without mixing and incubated for 20 min at RT. Subsequently, the transfection mix was added dropwise to the cell medium, while swirling slightly. For the reaction, cells were incubated at 37 °C, 7.5 % CO_2 for 6 hours. Afterwards, medium was replaced with MN medium with additional long-term factors (table 16) and incubated for 48 hours prior to hypoxia/OGD stimulation (see 4.2.4.1.). During the post-hypoxic reperfusion time, medium was changed to MN medium with long-term factors in several steps (table 16).

4.2.5. Sample generation from *in vitro* differentiated motor neurons

4.2.5.1. RNA extraction

To analyse the expression of different genes, the ribonucleic acid (RNA) was collected from ESCs at different time points. Therefore, $3.5x10^5$ ESCs were seeded on gelatinized 6 cm cell culture dishes and maintained at least for two days in ESC medium, supplemented with PD (1 µM) and CH (3 µM). For time points during differentiation, ESCs were differentiated as described in 4.3.2. For all time points, medium was changed to PBS in several steps to wash the cells. After sucking off the medium, 500 µl TRIzol were applied to lyse the cells from two different 6 cm dishes. The TRIzol samples were stored at -20 °C until further processing. To extract RNA from the cell samples, TRIzol was used to lyse the cells and the RNA extraction kit (RNeasy Mini Kit, Qiagen) was used to purify the RNA after the manufacture instruction. The final RNA concentration was measured due to the TECAN plate reader and the corresponding iControl 1.8 SP1 software.

4.2.5.2. cDNA synthesis

For the transcription of the RNA to complementary DNA (cDNA), the iScriptTM selected cDNA synthesis kit (Qiagen) was used according to the manufactures protocol with the following modifications. In brief, 500 ng of RNA were used for further proceeding. After performing the instructed steps of transcription, a final step was included. To prevent the denaturation of the

cDNA by enzymes, 1 µl of DNase I was added to the cDNA and incubated for 30 min at 37 °C. Afterwards, the cDNA sample was stored at -20 °C.

4.2.5.3. Cell protein lysates

For protein lysates from ESCs, $3.5x10^5$ cells were seeded on gelatinized 6 cm cell culture dishes and maintained for two days in ESC medium, supplemented with PD (1 µM) and CH (3 µM). Then, cells were collected for protein analysis. If MNs were analysed, cells were differentiated as described in 4.3.2. and analysed after 21 days of differentiation. For both lysate conditions, medium was changed to PBS in several steps. Then, the PBS medium mix was suck off and 100 µl of Radioimmunoprecipitation assay buffer (RIPA) lysis buffer was added. The cells were removed with a cell scraper and transferred into a new reaction tube. Afterwards, samples were incubated for 30 min on ice and followed by centrifuged for 30 min at 13,000 x g at 4 °C. The supernatant was determined as RIPA-soluble fraction and used for Western blot analysis (see 4.4.1).

4.3. Animal experiments

4.3.1. Mouse maintenance

The mouse lines used in this thesis are based on the C57BL/6 mouse line and were, with the permission by the state office for environments and consumer protection (LANUV), used for the research in this thesis. The C57BL/6 mice were kept at the Institute for Animal Research according to the rules of the Federation of European Laboratory Animal Science (FELASA). In summary, maximal 4 littermates were hold per cage (type II, “Euronorm”). The storage room for the cage were temperature to 20– 24 °C, the humidity of 45-65 % and had a light dark cycle of 12 hours. Food and water were provided *ad libitum*. Breeding pairs were separated in a further cage under the same conditions.

4.3.2. Embryo extraction

The females in mating were checked daily for the presence of a vaginal plug. This is considered of a successful fertilisation and indicates E0.5 of development. In addition, a daily weight check was performed as a further indicator of pregnancy. Starting from the date of the vaginal plug, the pregnant female animals are sacrificed at E12.5 by cervical dislocation before the embryos were removed. The embryos were removed by caesarean section from the female. The preparation is carried out in a PBS solution on ice. Embryos up to E12.5 are transferred directly into a 4 % PFA-containing PBS solution after preparation and thus sacrificed.

4.3.3. Brain extraction

To prepare the brain slices of early post-natal mice (P5 to P8), mice were sacrificed with scissors and the brain was dissected carefully. Afterwards, the brains were directly transferred into ice-cold artificial cerebrospinal fluid (aCSF) and proceed for slice culture. C57BL/6 mice, at the appropriate age (2-8 month and 8-18 month), were sacrified with isoflurane and perfused with ice-cold aCSF. The brain was carefully dissected and transferred in ice-cold aCSF for further processing.

4.3.4. Brain slice culture

For coronal slices, 350 µm thin slices were cut with the vibrating-blade microtome (Leica, VT1200 S) and kept in ice-cold, carbonated aCSF while processing. For cultivation, slices were transferred onto 30 mm Millicell-CM tissue culture inserts with 0.4 mm pores (Millipore) in six-well culture dishes with long-term aCSF. The slices were cultivated in a HERAcell (Thermo Fisher) cell culture incubator at 37 °C and 5 % CO_2 level.

4.3.5. Hypoxia induction in slice culture

To induce hypoxic stimulation, the brain slices were placed in the customised hypoxia chamber (Biospherix; provided by AG Habib, UK Aachen). Initially experiments of the working group of Dr. med. Dr. rer. nat. Habib revealed an optimal time period of OGD (<0.2 % O_2) of 30 min (data unpublished). Oxygen levels were monitored continuously in the aCSF and in the chamber (PreSens). Temperature (set at 37 °C), pressure (1 bar) and pH were controlled and monitored in the chamber and in the cell medium during the hypoxic stimulation. Brain slices under normoxia were maintained at 37 °C, 5 % CO_2, and 1 bar. During the post-hypoxic reperfusion time, brain slices were maintained at 37 °C, 5 % CO_2 and 1 bar.

4.3.6. Sample generation mouse

4.3.6.1. Mouse protein lysates

For protein lysates purified from mouse brain slices, the slices were washed in PBS and then transferred into a fresh Eppendorf reaction tube with 300 µl RIPA. Afterwards, samples were incubated for 30 min on ice followed by centrifugation for 30 min at 13,000 x g at 4 °C. The supernatant was defined as RIPA-soluble fraction and used for Western blot analysis (see 4.4.1.).

4.4. Analysis

4.4.1. Bradford protein measurement

To use an equal protein amount for each different conditions in the Western blot (WB) analysis, the protein concentration was determined. Therefore, the Bradford protein assay (DC protein

assay, Bio-Rad) was used according to the manufacture introduction. In brief, the standard curve was prepared by using specific amount of BSA, diluted with RIPA lysis buffer (0.2 µg/µl; 0.5 µg/µl; 0.8 µg/µl; 1.0 µg/µl; and 1.5 µg/µl). For the analysis, the premix of Solution A (alkaline copper tartrate solution) and solution S (surfactant solution) were prepared and mixed with 5 µl of the lysates. Further, solution B (dilute Folin reagent) was added and incubated for 15 min in the dark at RT. The absorbance was measured by the TECAN plate reader and the corresponding iControl 1.8 SP1 software. The protein concentration was calculated due to the standard curve.

4.4.2. Western blot

To determine the differences in protein level, the Western blot (WB) analysis was performed. Therefore, lysates from ESC or mouse samples were measured to analyse the protein concentration (see 4.4.1.). To compare different conditions, 30 µg of each cell lysate were used and 5x Laemmli Buffer was added for a final concentration of 1x. The mixture was incubated for 5 min at 95 °C. In the meantime, the precast gel (Bolt™ 4-12 % Bis-Tris Plus) was prepared. The gel was clamped in the chamber and the chamber was filled with the running buffer (20 X Bolt™ MES SDS Running Buffer, Thermo Fisher). 500 µl of Bolt™ antioxidant were added in the Fooling running buffer. The heated lysates were loaded on the SDS page and fooling the proteins were separated by electrophoresis (80 V for 2 hours). The semi-dry transfer to a nitrocellulose membrane was performed in the Trans-Blot Turbo® (Biorad) for 15 min and 225 V. This was followed by blocking the membrane for 1 hour with 5 % skim milk or 5 % BSA solution. The primary antibody was prepared at the concentration shown in table 10 in the corresponding blocking solution. The membrane was incubated overnight at 4 °C on a rotator with the primary antibody. The next day, the membrane was washed three times with TBS-T for 10 min each. Further the membrane was incubated with the corresponding secondary antibody in the blocking solution at RT for one hour. All dilutions for the primary and secondary antibodies are listed in table 10 and table 11. After incubation with the secondary antibody, three washing steps with TBS-T were following. The proteins of interest were detected by applying the Pierce® Electrochemiluminescence (ECL) Western Blotting Substrate detection kit (Thermo Fisher) according to the manufacturer's instructions and imaging the reaction by the Alliance LD4 documentation system (Biometra).

4.4.3. Immunofluorescence analysis *in vitro*

ESCs were seeded on sterile coverslips in 12-well plates coated as described in 4.3.2. At the time point of interest, ESCs were washed with PBS in several steps and fixed afterwards with 4 % Paraformaldehyde (PFA) for 5 min. Therefore, the half of the volume was removed and the same volume of 4 % PFA was added. After 5 min, the whole volume was removed and another step of incubation with 4 % PFA for 10 min at RT was performed. Afterwards, the fixed

cells were washed three times with PBS and covered with blocking solution for one hour at RT. Subsequently, the primary antibody solution was prepared by diluting the antibody in blocking solution and incubating the cells overnight at 4 °C. The next day, the fixed ESCs were washed three times with RT PBS and incubated for another hour with the corresponding secondary antibody and DAPI dye to stain the nucleus. After this incubation time, the fixed ESCs were washed again three times with PBS at RT and once with ddH_2O. Afterwards, the coverslips were mounted in Mowiol on microscope slides. After another 16 h for drying, cells could be analysed by microscopy.

4.4.4. Immunofluorescence analysis *in vivo* samples

4.4.4.1. Embryo preparation

E12.5 embryos were harvested (see 4.3.2.) and fixed with 4 % PFA for 2.5 hours at 4 °C. Afterwards, fixed embryos were washed overnight in PBS at 4 °C. The next day, embryos were dehydrated for cryoprotection with 30 % sucrose (in PBS) by incubation for at least eight hours at 4 °C. Afterwards, embryos were cut half under the forelimb buds and embedded in moulds (15x 15 mm) using Tissue TEC O.C.T compound (Sakura) and frozen on dry-ice. Embedded embryos were long-term stored at -20 °C. Embedded embryos were further cut to 12 µm slices with the Leica cryostat at -18 °C to -22 °C. Slices were collected on SuperFrost Plus microscope slides by first drying the slices for 10 min at RT and the slides were subsequently stored at -20 °C.

4.4.4.2. Immunofluorescence staining of embryos

Brain slices of the embryos were prepared (see 4.3.3.) and thawed at RT for at least 10 min. The embryonic cryosections were washed three times with PBS and covered with blocking solution (0.5 % TritonX100 and 1 % BSA in PBS) for one hour at RT. Afterwards, the primary antibody solution was prepared by diluting the antibody in blocking solution and incubating the cryosection overnight at 4 °C in a damp and dark chamber. The next day, cryosections were washed three times with PBS at RT and incubated another hour with the corresponding secondary antibody and DAPI dye to stain the nucleus. After this incubation time, the fixed embryonic cryosections slices were washed again three times with PBS at RT and once with dH_2O. Afterwards, the embryo slices were mounted using Mowiol to the high precision microscope cover glasses (170±5 µm, 24×60 mm, no.1.5H). With dried Mowiol, slices could be imaged by microscopy.

4.4.4.3. Brain slice preparation

Brain slices were prepared (see 2.4.5.) and either cultivated or implemented in hypoxic stimulation experiment (see 3.3.5.). In both cases, at the time point of interest, brain slices

were collected and washed with PBS and fixed afterwards with 4 % PFA for three hours at 4 °C. Afterwards, the fixed brain slices were washed three times with PBS, dehydrated for cryoprotection by incubation in 30 % sucrose overnight at 4 °C. The next day, brain slices were embedded in moulds (15x 15 mm) using Tissue TEC O.C.T compound (Sakura) and frozen on dry-ice. Embedded brain slices were long-term stored at -20 °C.
Slices were further cut to 12 µm thin slices with the Leica cryostat at -18 °C to -22 °C. Slices were collected on SuperFrost Plus microscope slides. Subsequently the slides were dried for 10 min at RT and stored at -20 °C.

4.4.4.4. Immunofluorescence staining of brain slices

Immunofluorescence staining and in combination with TUNEL staining were performed by the laboratory technician Louisa-Carole Neumann. In brief, cryoslices were defrosted at room temperature and washed with PBS: Afterwards, cryoslices were incubated for 30 min in the streamer oven. After cooling down the slices, they were placed in PBS again for 5 min. Followed by 30 min incubation in 3 % normal goat serum (NGS) at RT. The primary antibody was diluted in 3 % NGS. The microscope slides with the primary antibody were embedded in a damp and dark chamber and incubated overnight at 4 °C. The next day, cryoslices were washed again for 5 min in PBS and incubated afterwards with the secondary antibody, corresponding to the host of the primary antibody. After additionally washing with TBS for 10 min of the cryoslices, they were incubated with the TUNEL master mix (Merck) for three hours. The TUNEL staining was performed according to the manufactures protocol and additionally covered with parafilm. Afterwards, the cryosections were again washed with TBS and briefly stained with DAPI. Finally, cryosections were embedded in Fluoromount-G and covered with microscope cover slips (170±5 µm, 24×60 mm, no.1.5H) and dried at room temperature until further microscopic imaging.

4.4.5. Quantitative real-time PCR

To perform the semi-quantitative real-time PCR (semi-qRT PCR) analysis, 500 µg RNA were transcribed into cDNA as described in 4.2.5.1 and to stop the reaction 80 µl of ddH_2O were added. Further, the iQTM SYBR R Green Supermix kit (Bio-Rad) was used according the manufacturer's protocol. In brief, 1 µl of cDNA was mixed with 8 µl of SYBR Green, 1 µl of the primer mix and 10 µl ddH_2O. The following exon-spanning primers were designed with the Primer-BLAST tool from the National Center for Biotechnology Information (NCBI) and ordered at the Sigma Aldrich. For every gene, a technical triplicate was performed and analysed in the same qRT-PCR performance. For statistical analysis, three different technical replicates within three independent biological replicates were calculated.

Table 17: *Quantitative real-time PCR primers*

Primer	Sequence fwd (5'-3')	Sequence rev (5'-3')
Rps29	GAAGTTCGGCCAGGGTTCC	GAAGCCTATGTCCTTCGCGT
Hprt	GGCCAGACTTTGTTGGATTT	CAGATTCAACTTGCGCTCAT
Oct4	TGTTCCCGTCACTGCTCTGG	TTGCCTTGGCTCACAGCATC
Olig2	GAACCCCGAAAGGTGTGGAT	TTCCGAATGTGAATTAGATTTGAGG
Chat	GTGAGGAGGTGCTGGACTTAC	CCCCAAACCGCTTCACAATG
Dlk1	TCTTGCTCCTGCTGGCTTTC	ACATGGCACCTGCAGACATT
Pmm2	AGGGAAAGGCCTCACGTTCT	AATACCGCTTATCCCATCCTTCA
Mmp9	GTCCAGACCAAGGGTACAGC	ATACAGCGGGTACATGAGCG
Pax6	CATGGCAAACAACCTGCCTATG	GCACGAGTATGAGGAGGTCTGAC
NeuN	TCCAACCCGGCCTCTCG	TTTCAACGGGTTCAGCGTTC
Mnx1	GTTGGAGCTGGAACACCAGT	GGAACCAAATCTTCACCTGAGT
Tubb3	GCGCATCAGCGTATACTACAA	TTCCAAGTCCACCAGAATGG
Adam17 #1	TTATCCCACGACGTGTTCCG	GACGAGCTGAACCTAACCCC
Adam17 #2	GACGCTGCAGCTTGAATGAG	ACGGTTTTGAGAAGGACCCC

4.4.6. Live-Dead assay

To determine the viability of the MN network in different experimental setups, the LIVE/DEAD assay (L3224, Thermo Fisher) was performed. With the bi-colour assay, it is possible to determine the viability of a cell population, based on the plasma membrane integrity and esterase activity. Therefore, the polyanionic dye calcein AM (AM), which is staining living cells in green (excitation/emission ~495 nm/~515 nm) is combined with ethidium homodimer-1 (EthD-1). EthD-1 is staining dead cells in red (excitation/emission ~495 nm/~635 nm). MNs were washed with PBS in several steps, until PBS has replaced the medium. Then, the PBS was removed and the mixture of AM and EthD-1 was covering the cells and incubating for 30 min. In the following, the MNs were washed again with PBS and were imaged with a live imaging microscope (Olympus IX81, Olympus) using a 20x air-immersion objective.

4.4.7. LDH assay

The viability was measured, using the CytoTox 96 Non-Radioactive Cytotoxicity Assay (Promega) according to the manufacturer's instructions. In brief, 50 µl of the cell medium was collected in a 96-well plate of the desired time point and incubated in a 1:1 mixture of the LDH master mix. The lactate dehydrogenase (LDH) was released and the levels were measured in a 30 min time frame due to the fluorescence conversion from violet (tetrazolium) into red (formazan) via the TECAN reader with a script written by Aaron Fehr. Hereafter, the amount of converted LDH is proportionally to the number of dead cells.

5. Results

5.1. Analysing localised hypoxia in relation to Dlk1 expression during embryogenesis

Motor neurons (MNs) are generated with beginning of the embryonic day E10.5 in the mouse (Smas and Sul, 1993; Müller, 2012). At this embryonic day, *in situ* experiments revealed *Dlk1* mRNA expression exclusively in MN progenitor cells (pMNs) (Müller, 2012; Khan *et al.*, 2022). With ongoing development (E12.5), *Dlk1* mRNA is also detectable in the ventral horn of the spinal cord, which is corresponding to the region of post-mitotic MNs (Müller, 2012). Therefore, the developmental stage of E12.5 was chosen to address the putative impact of oxygen levels on the MN diversification during development.

In a first step, E12.5 days old wild-type embryos were extracted, fixed and embedded in Tissue-Tek OCT medium. A transversal cut was performed to expose the regions of interest where Dlk1 is supposed to be expressed. After generating cryosections, co-immunodetection of Dlk1 and the vesicular acetylcholine transporter (VAChT) was performed (figure 5-1). VAChT is expressed by cholinergic neuron including αMNs.

The transversal sections of the E12.5 days old embryo were generated at the level of the heart (figure 5-1, A and B). From dorsal to ventral, many structures are recognisable as the neural tube, notochord, forelimb bud and the heart, which is surrounded by the thoracic wall and includes the pericardial cavity. The immunofluorescence reveals a high fluorescence signal in the heart region. Further, small regions in the forelimb bud, neural tube and internal organs have a high fluorescence signal for Dlk1. In contrast to this, VAChT was mainly immunodetected in the mantle layer of the ventral neural tube, consistent with its expression by postmitotic MNs. At E12.5 Dlk1 was mainly detected in pMN adjacent to the VAChT-positive mantle layer containing postmitotic MNs (figure 5-1 C, C’ and C”).

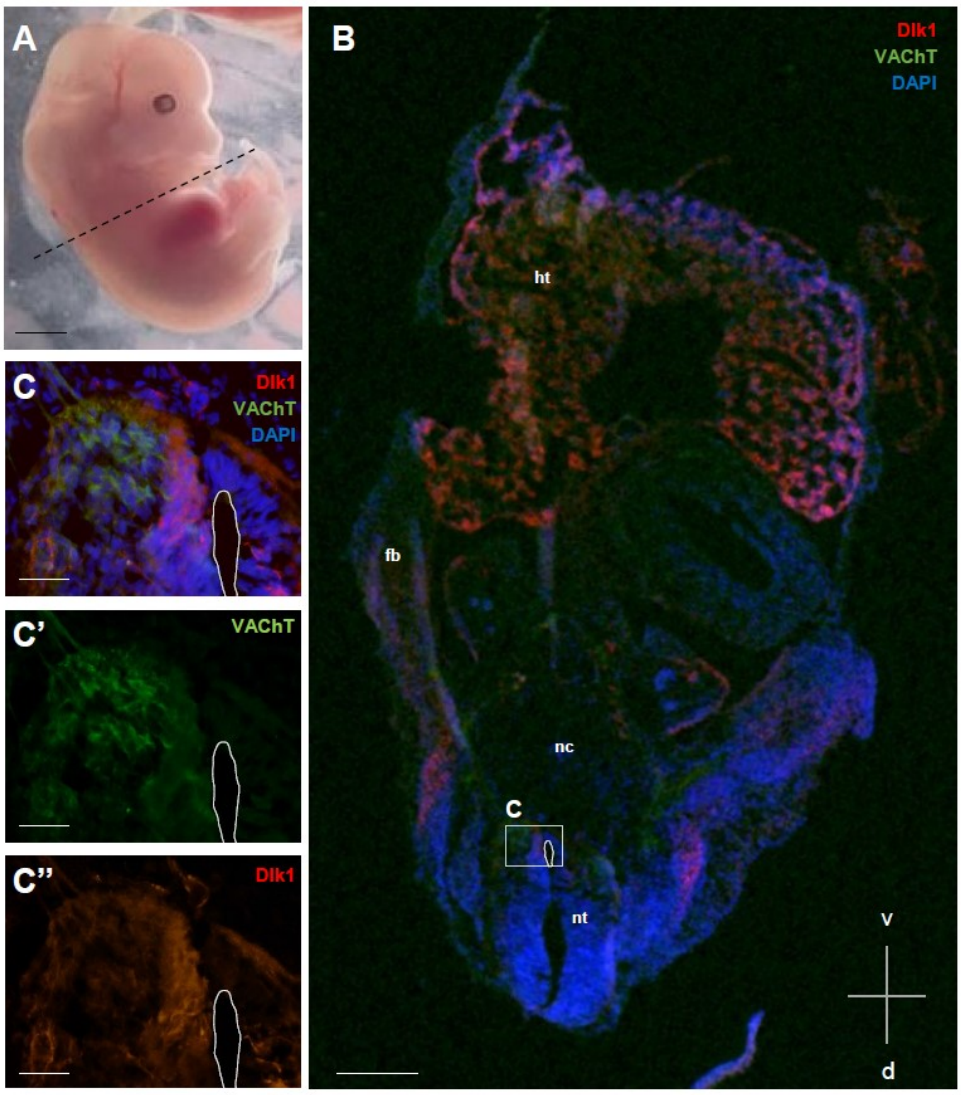

Figure 5-1: *Dlk1 staining in transversal section of E12.5 embryos.* ***A:*** *Collected E12.5 embryo, Theiler stage 21 with indicated transversal section plane (black dashed line)* ***B:*** *Overview of sectioned region with co-immunostaining of Dlk1, VAChT, and DAPI.* ***C:*** *Higher magnification of boxed region in B (C) with co-immunostaining of Hif1α, VAChT, and DAPI. Lumen of neural tube is indicated (white dashed line).* ***C' and C'':*** *Single immunofluorescence image of VAChT and Dlk1 respectively, with indicated lumen of the neural tube (white dashed line). Scale bar represents 1 mm (A), 100 µm (B) and 20 µm (C). fb, forelimb bud; d, dorsal; ht, heart; nc, notochord; nt, neural tube; v, ventral.*

To address the question whether lower levels of oxygen occur during embryogenesis and if those are influencing the diversification of MN subtypes, the regions of low oxygen were further analysed. Therefore, one of the most prominent cellular markers for hypoxic stress, the hypoxia-induced factor 1α (Hif1α) was used (Jewell *et al.*, 2001; Semenza, 2007). Hif1α is stabilised in low intracellular oxygen conditions, whereas it is rapidly degraded under physiological oxygen levels by the ubitiquin/proteasome pathway (figure 1-7) (Semenza, 2007). To address the question of a Hif1α stabilisation in E12.5 embryos overlaps with the regions of Dlk1 activity and motor neurogenesis, co-immunodetection of Hif1α and VAChT were performed (figure 5-2).

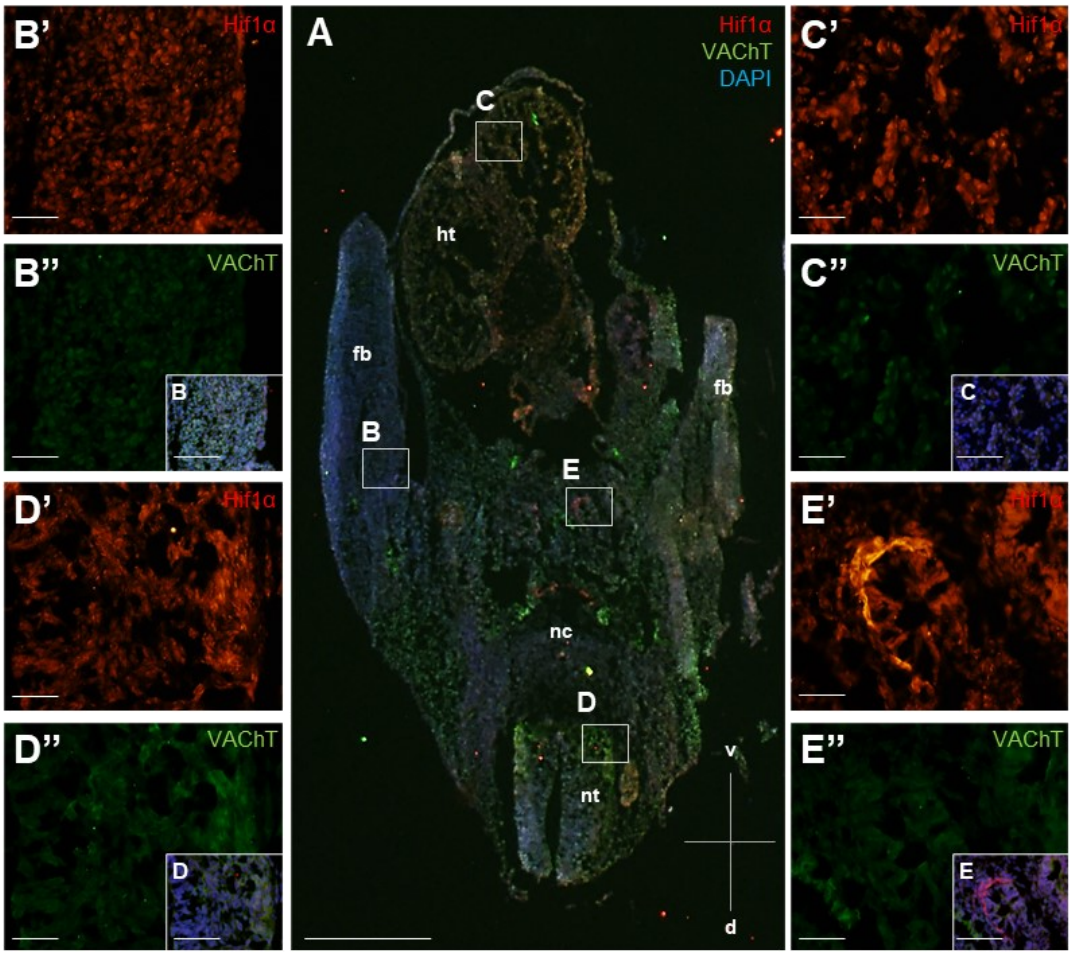

Figure 5-2: *Hif1α stabilisation in E12.5 embryos.* ***A:*** *Overview of sectioned region of E12.5, Theiler stage 20 with co-immunostaining of Hif1α, VAChT, and DAPI.* ***B:*** *Higher magnification of boxed region in A (B, C, D, and E) with co-immunostaining of Hif1α, VAChT, and DAPI.* ***B', C', D',*** *and* ***E':*** *Hif1α immunofluorescence signal of VAChT in the selected regions (B-E).* ***B'', C'', D'',*** *and* ***E'':*** *VAChT immunofluorescence signal in the selected regions (B-E). Scale bar represents 1 mm (A), 100 µm (B) and 20 µm (C). fb, forelimb bud; d, dorsal; ht, heart; nc, notochord; nt, neural tube; v, ventral.*

An overview of the whole transversal section with different stainings (nucleus (blue), VAChT in (green), and Hif1α (red)) is displayed (figure 5-2). The co-immunostaining of VAChT and Hif1α showed a higher signal of Hif1α in the heart region (figure 5-2, C) and in multiple smaller areas throughout the whole transversal section, especially small regions of the internal organs lighting up for the Hif1α signal, as well as the remaining somites (figure 5-2, A), consistent with previous reports (Tam and Loebel, 2007). To analyse Hif1α expression in more detail, higher magnifications were done (forelimb bud (B), heart (C), neural tube (D), and internal organs (E)), to see the localisation of Hif1α (figure 5-2, B', C', D', and E'). As In parallel, VAChT co-immunostainings were used to identify regions of MNs (figure 5-2, B'', C'', D'', and E''). In the four selected sections, the forelimb bud (B), the heart (C), the neural tube (D), and the internal organs (E) a high Hif1α signal were detectable. No restricted overlap in VAChT and Hif1α expression was observed in these experiments (figure 5-2, B'', C'', D'', and E'') and the overall Hif1α signal was very high and not readily distinguishable VAChT-positive or negative cells in

the embryo, possibly reflecting pleiotrophic roles of hypoxia signalling during embryogenesis. Thus, in regard to the investigation of a possible regulation of Dlk1 by hypoxia, the analysis of Hif1α expression in the mouse embryo was inconclusive. Therefore, embryonic stem cell (ESC)-derived MNs were tested for their suitability to permit a detailed study of the role of hypoxia in the regulation of Dlk1 activity and MN functional diversification.

5.2. Dlk1 expression in embryonic stem cell-derived motor neurons

5.2.1. Neuronal differentiation

ESCs have two main characteristic features, namely pluripotency and self-renewal (Bain *et al.*, 1995). Pluripotency means ESCs can differentiate into every cell type of the three germlines. Self-renewal means their constant proliferation without losing their stem cell properties (Bain *et al.*, 1995). For the *in vitro* differentiation of the ESCs into MNs, a precisely determinate cascade of steps has to be followed to recapitulate the *in vivo* conditions of the equivalent in the embryo (figure 5-3) (Wichterle *et al.*, 2002; Mazzoni *et al.*, 2013; Gouti *et al.*, 2014).

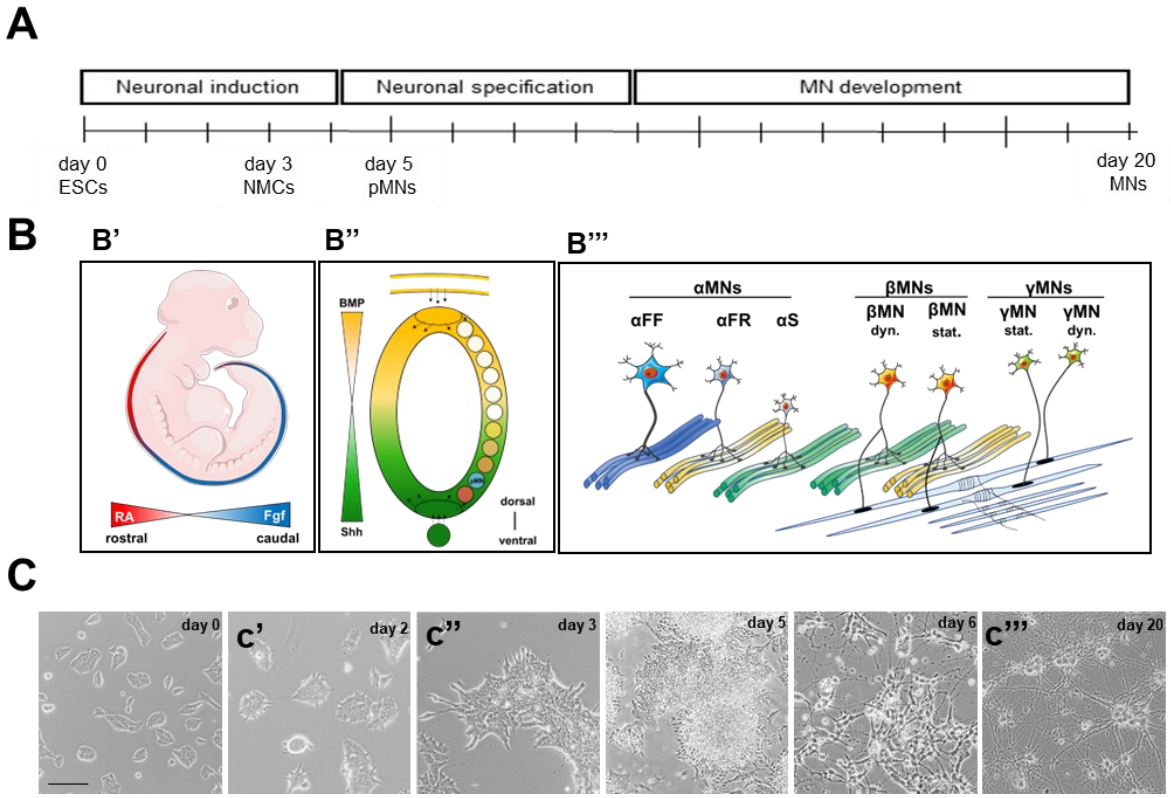

Figure 5-3: *Differentiation of ESC-derived MN.* ***A:*** *Schematic representation of the differentiation steps and neuronal stages to be recapitulated in vitro differentiation.* ***B:*** *Schematic representations of axis formation (rostral caudal (RC) axis; B'), ventral dorsal (VD axis; B'') during neurogenesis and motor neuron subtypes innervating corresponding muscles fibres (B'''),* ***C:*** *Morphological changes during in vitro differentiation from murine embryonic stem cells to a MN network.* ***C', C'',*** *and* ***C''':*** *Corresponding images to B', B'', and B''' in the in vitro differentiation. Scale bar represents 100 µm. αFF, alpha fast-twitch, fatigable motor unit; αFR, alpha fast-twitch resistante, motor unit; αS, alpha slow motor unit; BMP, bone morphogene protein family; dyn, dynamic; ESCs, embryonic stem cells; MNs, motor neurons; NMCs, neuromesodermal lineage; pMNs, motor neuron progenitor domains; Shh, sonic hedgehog; stat, static. Figure modified after (Manuel, 2011; Stifani, 2014a).*

For the differentiation of ESCs to MNs, the *in vivo* steps of motor neurogenesis are recapitulated in three successive phases, namely neural induction, neural specification and MN differentiation (figure 5-3). The naïve ESC culture was forming round to oval dome-shaped colonies, showing characteristic sharply delineated and brightly illuminated edges in phase contrast microscopy (day 0) (figure 5-3, C). Starting with the differentiation protocol, ESCs were separated and treated first with basic fibroblast growth factor (bFgf) to induce a primed state of pluripotency. The separation was leading to the regrow of the single cells to small, jagged colonies. By further treatment with glycogen synthase kinase (GSK) 3 inhibitor, the WNT signalling pathway is induced, which leads to generation of cells of the neuromesodermal lineage (NMCs) (day 3, figure 5-3, C). Following this, the neural RC and DV axis is induced by the treatment with a specific concentration of CHIR99021 (CH), ec23 and Smoothened agonist (SAG). CH is an inhibitor of glycogen synthase kinase 3 (GSK-3) and acts as Wnt activator, whereas SAG as smoothened agonist, modulates the coupling of Smo with the downstream

effectors and therefore activates the Shh pathway. The last component is ec23, which is a synthetic retinoic acid (RA) and represent the counterpart of Wnt. Morphologically, colonies are spread over the plate and grow to amorphic massive colonies during day 3 to 5 (figure 5-3, C). At the stage of pMNs (day 5), single cell separation induced terminal differentiation and promotes neurite outgrowth on a large number of cells. With further cultivation (day 6 onwards), those networks of neurites got more prominent and the neuritic structures more stable. Remaining mitotically active cells were removed by the addition of FDU and Uridine in the MN medium. Uridine causes the inhibition of cell growth and differentiation (Sokoloski *et al.*, 1991). 5-fluoro-2′-deoxyuridine (FDU) is inhibiting the mitosis through disruption of the microtubules. This results in an almost pure neuronal culture (figure 5-3, C). This cell population was further analysed with various neural markers to analyse the pureness of the differentiated network (figure 5-4).

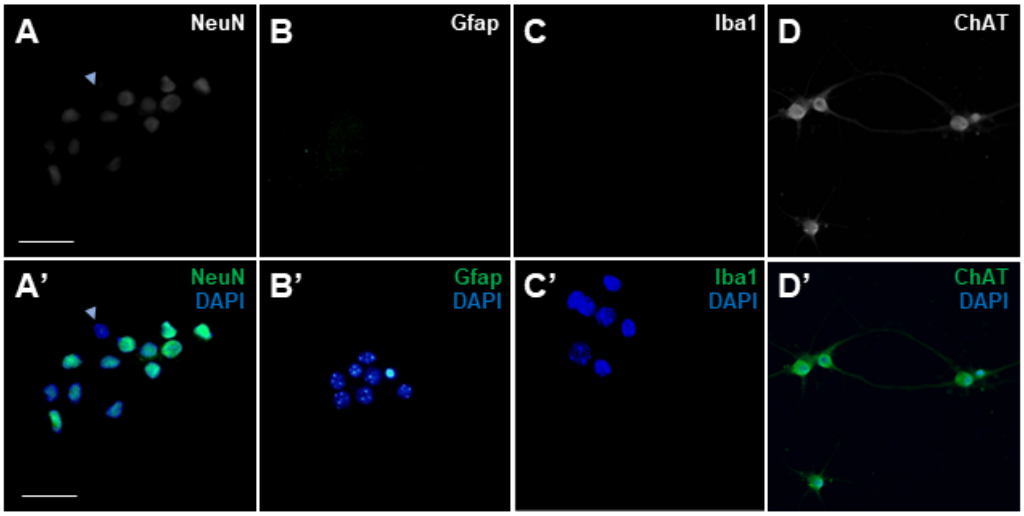

Figure 5-4: *ESC-derived MN population analysed with specific molecular markers.* ***A:*** *Representative images of NeuN immunofluorescence staining. Grey scale of NeuN (A) and merge picture (**A',** NeuN, green; DAPI, blue). Arrow indicates a non-neuronal cell by DAPI^{+} but NeuN^{-} staining.* ***B:*** *Representative images of Gfap immunofluorescence staining. Grey scale of Gfap (B) and merge picture (**B',** Gfap, green, DAPI, blue). C: Representative images of Iba1 immunofluorescence staining. Grey scale image of Iba1 (C) and merge picture (**C',** Iba1, green, DAPI, blue).* ***D:*** *Representative images of ChAT immunofluorescence staining. Grey scale of ChAT (D) and merge picture (**D',** ChAT green, DAPI, blue). The scale bar represents 25 µm. ChAT, Choline Acetyltransferase; Gfap, glial fibrillary acidic protein; Iba1, ionised calcium-binding adapter molecule 1; NeuN, neuronal nuclei.*

Thereby, NeuN, was used as a marker for neurons (figure 5-4, A). Most cells were positive for NeuN, nevertheless, some cells could be detected which were also negative for NeuN (figure 5-4, A; blue arrowhead). Further, glial fibrillary acidic protein (Gfap) was immunodetected to visualise glial cells and ionised calcium-binding adapter molecule 1 (Iba1) to mark astrocytes in the day 20 population (figure 5-4, B and C, respectively). The differentiated cell population was negative for Gfap and Iba1, which means there were no glial cells or astrocytes present. Further, immunodetection for Choline Acetyltransferase (ChAT)

was used to determine the number of MNs (figure 5-4, D). This revealed that the majority of the cells were also positive for ChAT. Nevertheless, individual ChAT$^-$ cells could be observed. This indicates that the differentiated MN population was not entirely pure. Those cells types should be further analysed by co-immunostaining with more or all markers simultaneously to identify the NeuN$^-$ cell types.

During differentiation, various genes are involved in determining a specific cell type. Those can be used as molecular markers to analyse the success of the differentiation (figure 5-5). Samples were collected from the whole cell population at seven different time points (feeder-free ESCs (day 0), NMCs (day 3), pMN (day 5 and day 7), mature MNs (day 10 and day 20) and used for total RNA extraction followed by cDNA synthesis and analysis by semi-quantitative real time PCR (semi-qRT PCR). The expression levels of all transcription factor genes investigated were displayed relative to the ESCs stage and normalised to the housekeeping gene *Pmm2*.

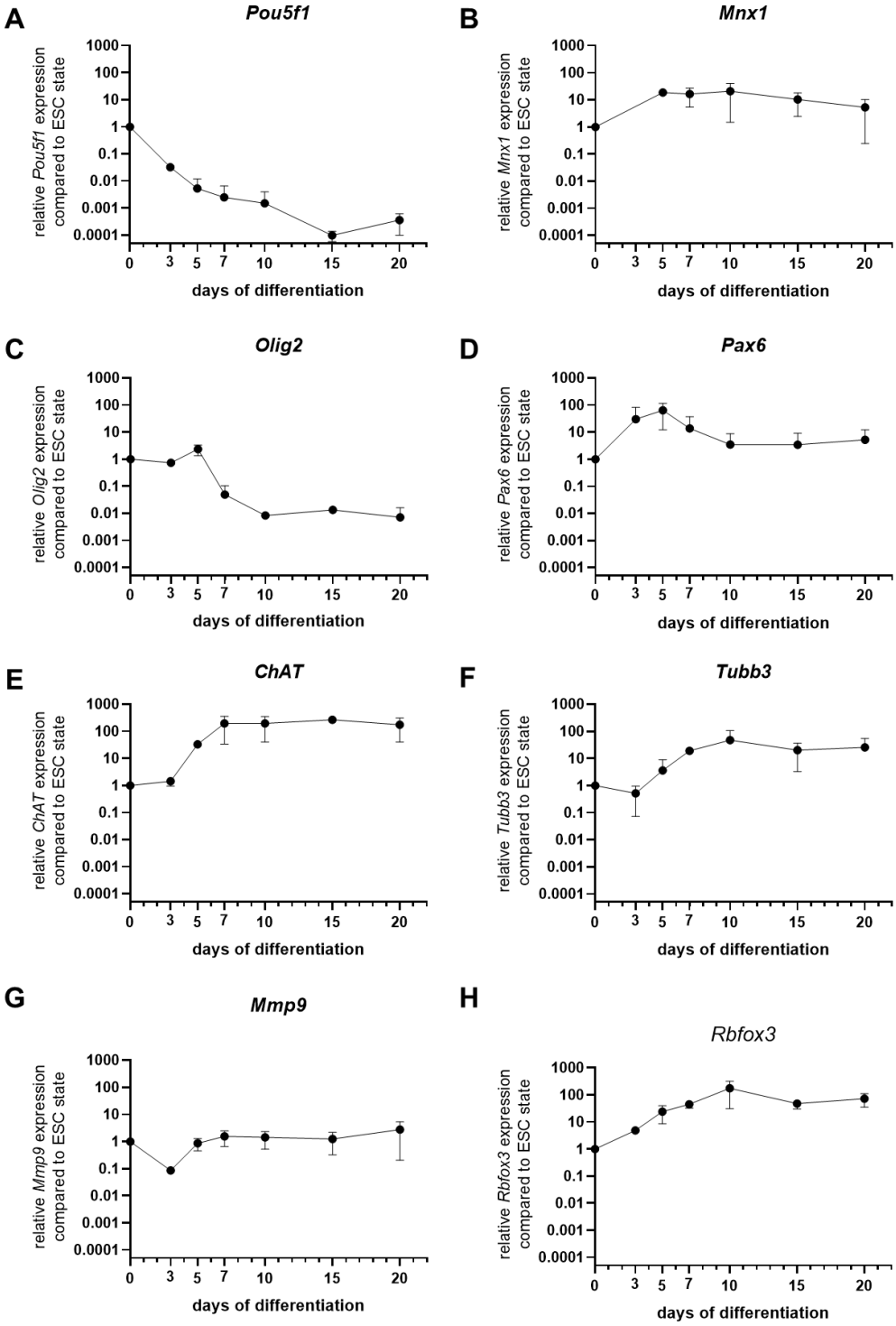

Figure 5-5: *Analysis of the differentiation of ESC-derived MNs based on molecular markers.* ***A:*** *Relative expression of the ESC marker Pou5f1.* ***B*** *to* ***H:*** *Relative expression level of the pMN marker Olig2 (B) and Pax6 (C); the pan neural marker Tubb3 (F), and Rbfox3 (H); the MN marker Mnx1 (D), and ChAT (E) as well as a specific marker for αMN, Mmp9 (G). Expression levels are shown relative to day 0 and normalised to the housekeeping gene Pmm2. ChAT, Choline Acetyltransferase; Mmp9, Matrix Metalloprotease 9; Mnx1, Motor Neuron And Pancreas Homeobox 1; Olig2, Oligodendrocyte Transcription Factor 2; Pax6, Paired box protein 6; Pou5f1, POU Class 5 Homeobox 1; Rbfox3, RNA Binding Fox-1 Homolog 3; Tubb3, Tubulin Beta 3 Class III.*

During the priming of ESCs, they convert from a naïve state to the primed pluripotency state of epiblast stem cells (EpiSCs). In line with this, *Pou5f1* was highly expressed in ESCs, but expression levels were continuously reducing until day 15 of differentiation. Day 20 had a slight increase in the expression of *Pou5f1* compared to the lowest level at day 15 of differentiation. The genes *Olig2* and *Pax6* (figure 5-5, C and D respectively) are known to be involved in MN specification and their expression peaked about day 5 of differentiation. Afterwards, the expression of *Olig2* was reduced compared to the ESCs state, whereas the expression level of *Pax6* became again comparable with its expression levels in ESCs. The genes *Mnx1* (also known as *Hb9*) (figure 5-5, B), *ChAT* (figure 5-5, E), *Tubb3* (figure 5-5, F), *Mmp9* (figure 5-5, G), and *NeuN* (figure 5-5, H) were expressed at higher levels in mature neurons, compared to the ESC state. *Mnx1* was only slightly increased in the expression level compared to the ESC state. The expression reached a slight elevated plateau between day 5 to day 10, with a slight reduction at day 7 and decreased afterwards. In contrast to this, *ChAT* had a steep increase in the level transcripts from day 3 to day 5 and continued to increase till day 7, while afterwards its levels remained nearly stabile. *Tubb3* had a similar course of expression levels as *ChAT*. Nevertheless, the increase of *Tubb3* transcripts appeared later in differentiation and its transcripts levels were comparatively reduced at day 3. The peak of *Tubb3* expression was at day 10 and levels remained stable during the further timepoints. The gene *Mmp9* was expressed at lower levels at day 3 compared to the ESC stage, but afterwards reached similar levels compared to those of the ESCs. Only towards the end of the observation time of the differentiation, it seemed that *Mmp9* levels slightly increased above the ESC stage. For *NeuN* the expression was increasing continuously till day 10, though afterwards dropped back to the expression levels, observed at day 7.

5.2.2. Dlk1 expression in embryonal stem cell-derived MNs

Next to the genes, which are involved in the differentiation of ESCs to MNs, genes unique for one subtype of MNs can also be useful to analyse the composition of the neuronal population. Dlk1 is only expressed in fast αMNs and be considered as molecular marker (Müller *et al.*, 2014). The transcript level of Dlk1 during the differentiation is displayed in the following graph (figure 5-6, A). The level was compared between the ESC state and six different timepoint during the differentiation, including NMCs, pMNs and mature neurons.

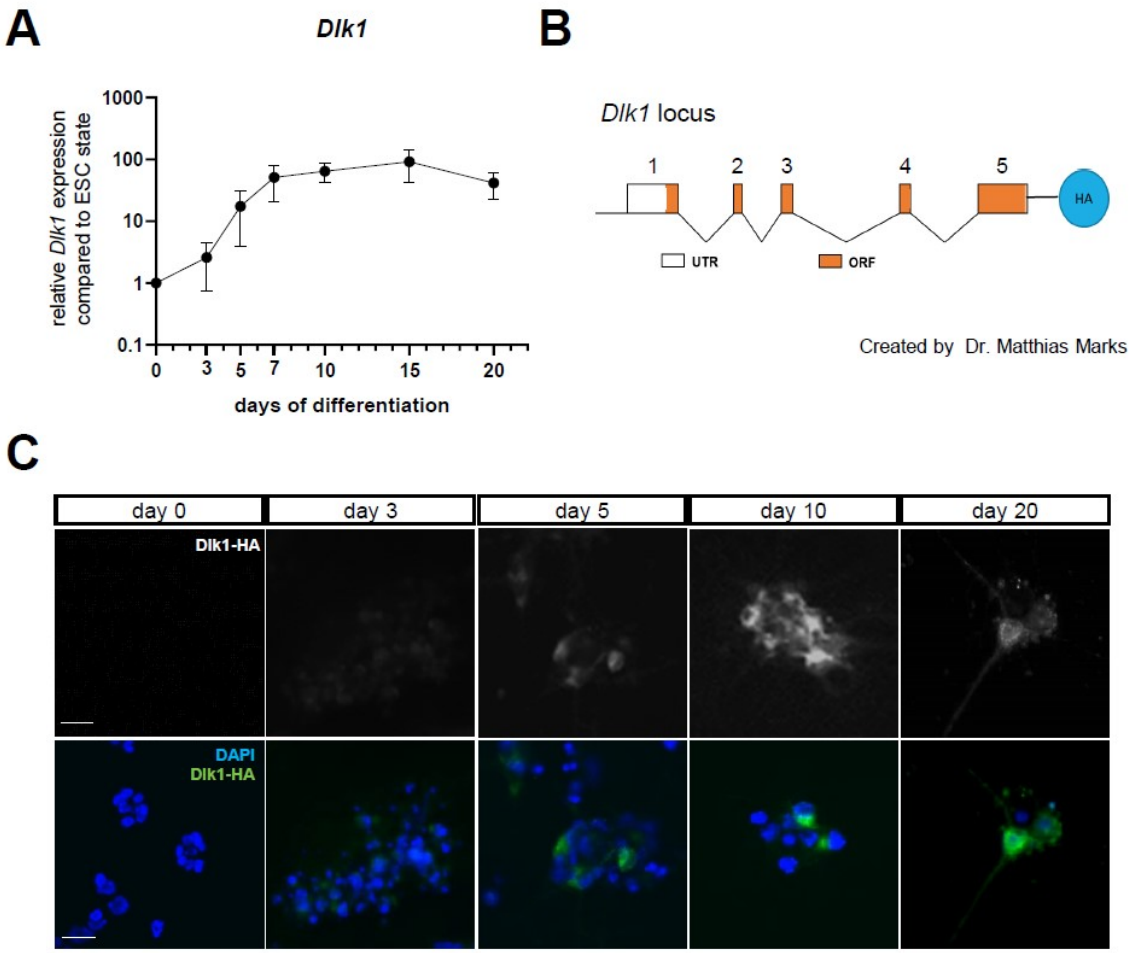

Figure 5-6: *Expression of Dlk1 on mRNA and protein level.* ***A:*** *Dlk1 expression levels during the differentiation of ESCs into MNs. mRNA level was plotted in relation to the ESC state (day 0) and normalised to the housekeeper Pmm2.* ***B:*** *Schematic representation of the genetically modified Dlk1 genomic locus, with numbered ORFs (numbers above)* ***C:*** *Representative immunostaining of Dlk1-HA at different timepoints during the differentiation process. Scale bar represents 20 µm. ORF, open reding frame; UTR, untranslated region; HA, hemagglutinin; Pmm2, Phosphomannomutase 2.*

The differentiated ESC line used in this experiment has the advantage of carrying a modified *Dlk1* gene encoding epitope-tagged Dlk1 (figure 5-6, B). By a genetic modification using CRISPR/Cas9 technology, the endogenous Dlk1 protein was tagged at its C-terminus with a single HA-epitope (see 3.2.1). Thus, it was possible to detect Dlk1 during the course of the differentiation using an HA-epitope specific antibody. Using this detection method, Dlk1 was not observed at the ESC stage (figure 5-6; C; day 0). It became slightly detectable in the colonies from day 3 onwards. At day 5, Dlk1 could be visualised in single cells and from day 10 till day 20, the signal intensity further increased compared to day 5. At day 10, Dlk1 was detectable in a subset up cells with different intensity (figure 5-6, C; day 10). Noteworthy, the observation that Dlk1 was detected only in a subset of cells was confirmed at day 20.

To follow up this subset-specific expression in the cell population at day 20, in a next step co-immunostainings were performed with a marker for fast and intermediate αMNs, namely Dlk1 and Mmp9 (Kaplan *et al.*, 2014; Spiller *et al.*, 2019) to identify the ratio of cell type specific subgroup at this time point of differentiation (figure 5-7).

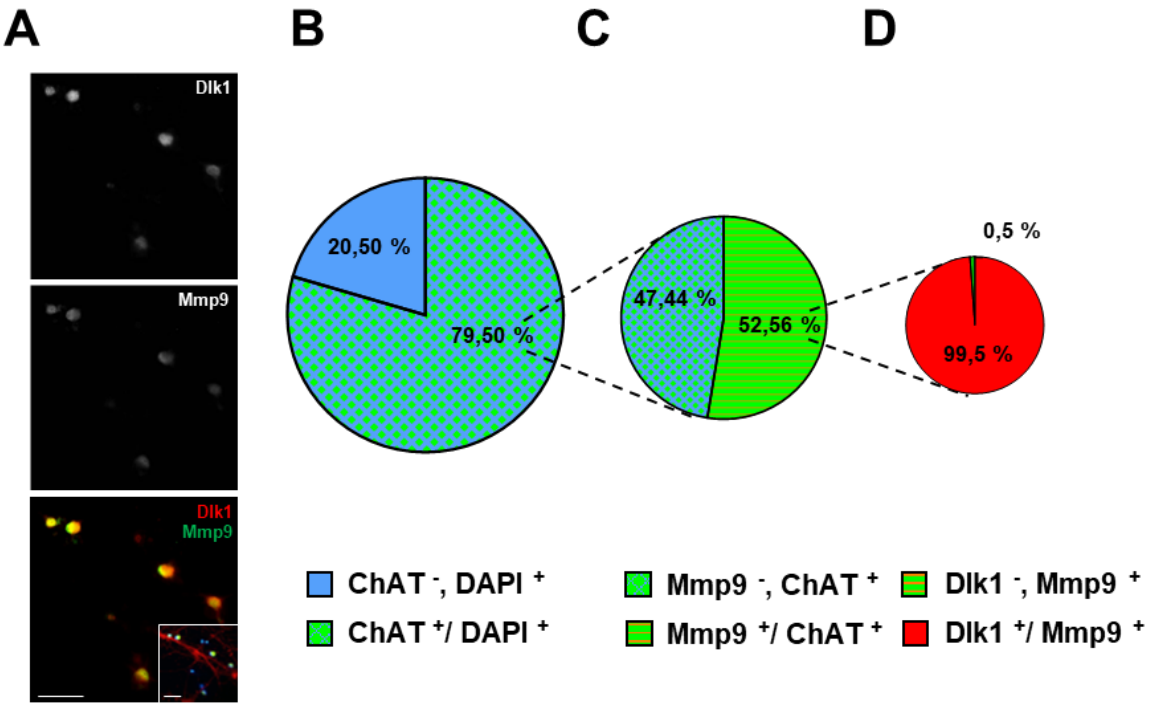

Figure 5-7: *Subtype analysis in ESC-derived MNs.* ***A:*** *Representative images of co-immunostaining of Mmp9 and Dlk1 as separate images (grey scale) and merged with DAPI (lower row). Quantification of a total number of 300 DAPI$^+$ cells per condition of the full-length Dlk1 in relation to the total number of cells.* ***B:*** *Quantification of ChAT$^+$ cells (blue-green checked) per total number of cells (DAPI$^+$; blue).* ***C:*** *Mmp9$^+$ cells (green-orange striped) per ChAT$^+$ cells (blue-green checked).* ***D:*** *Mmp9$^+$ cells (red) per Mmp9$^+$ cells (green-orange striped). The scale bar represents 20 µm. ChAT, Choline Acetyltransferase, ESCs, embryonic stem cells; Mmp9, Matrix Metalloprotease; MNs, motor neurons.*

The quantification of the ChAT$^+$ cell revealed a ratio of 80 % MNs in the entire cell population (DAPI$^+$) (figure 5-7, B). This confirmed a mostly pure MN population at day 20 of differentiation. Further, the ratio of different MN subtypes was analysed by staining with Mmp9 and Dlk1 antibodies. Mmp9 as a marker for the larger intermediate and fast αMN (Kanning, Kaplan and Henderson, 2010) revealed a subgroup of neurons positive for Mmp9 in the culture. This subgroup comprised around 52 % of all ChAT$^+$ MNs (figure 5-7, C) and is hereafter referred to the fast and intermediate MN subgroup. Dlk1 is also an unique marker for fast αMNs (Müller *et al.*, 2014). In line with that, Dlk1 was found to be detectable in a subgroup of DAPI$^+$ cells. The quantification revealed, that nearly 99 % of all Mmp9 positive cells were found to be Dlk1 positive (figure 5-7, A and D). Sporadically, there are also some MNs either positive only for Dlk1 or for only Mmp9 (1 %).

5.3. Establishing hypoxia experimental setup

5.3.1. Motor neurons survival under hypoxia conditions

Although some factors are known, the molecular mechanisms for the determination of the fast αMN identity remain still largely elusive (Kaplan *et al.*, 2014; Müller *et al.*, 2014; Khan *et al.*, 2022). In 2020, the laboratory of Pietras found a relation between Dlk1 and hypoxia in high grade glioma cells (Grassi, Pantazopoulou and Pietras, 2020). They found that the lack of oxygen can induce Dlk1 cleavage and the translocation of Dlk1 intracellular fragment (ICF) to the nucleus in cancer (Grassi, Pantazopoulou and Pietras, 2020). The hypothesis that this may represent a mechanism through which Dlk1 activity is regulated in MN diversification was investigated in the following part of this thesis. Hypoxia is per definition the lack of oxygen in a cell or tissue. Due to oxygen-deprivation Hif1α is stabilised in the cell (Wang and Semenza, 1993; Semenza, 2007), which leads to further molecular responses of the cell (Simon and Keith, 2008; Grassi *et al.*, 2020; Grassi, Pantazopoulou and Pietras, 2020). To induce cellular responses after hypoxia, the duration of the hypoxic stimulation has to be determined. The viability of the MN-derived in *in vitro* differentiation from mouse ESCs is unknown so far. Based on time periods in other *in vitro* experiments with different cell types (personal communication with Dr. rer. nat. Dr. med. P. Habib, unpublished data), the hypoxic stimulation was restricted either to 30, 45, or 60 min and always compared to the physiological control (normoxia) (figure 5-8).

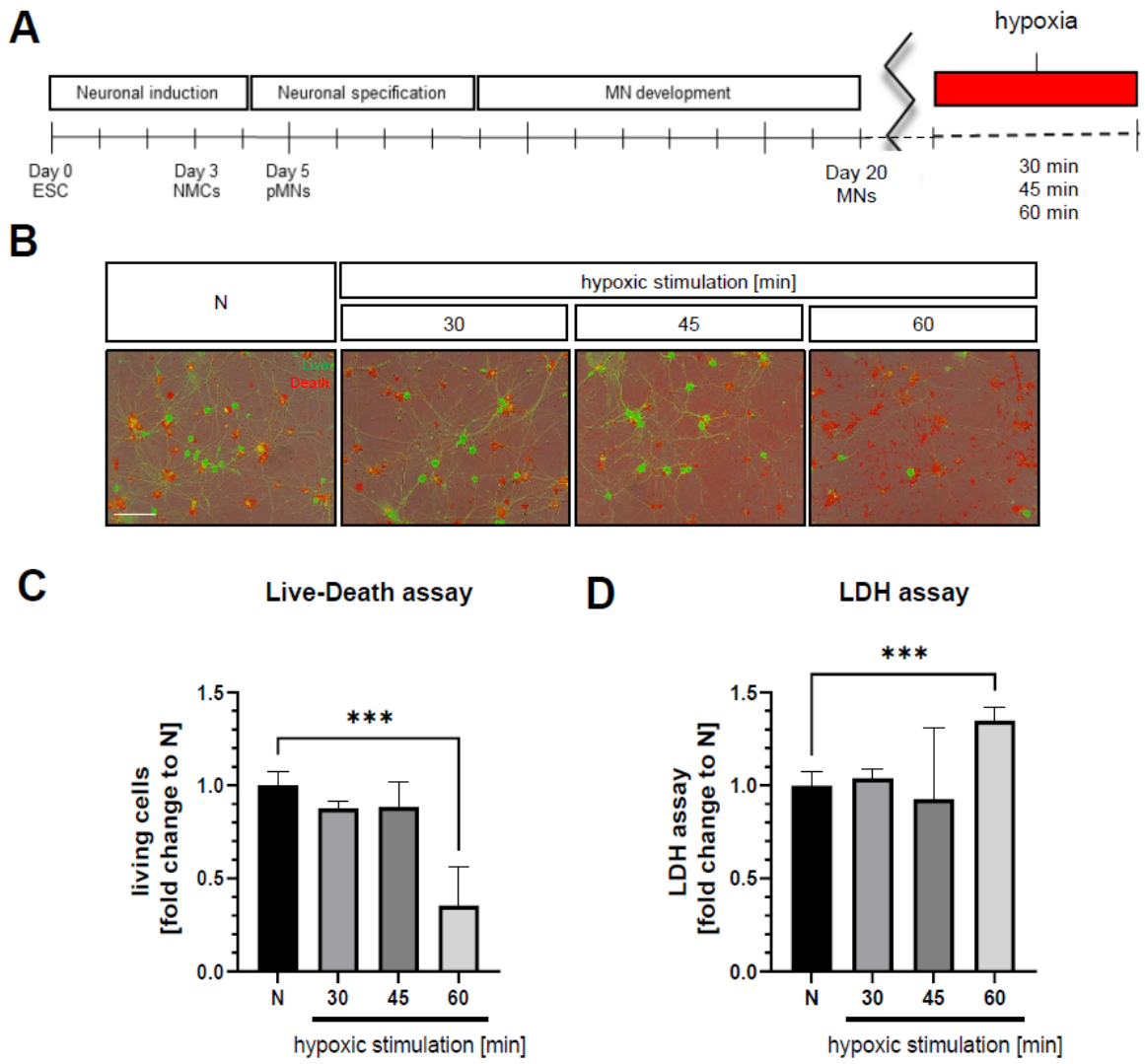

Figure 5-8: *Survival of ESC-derived MNs under hypoxic conditions.* ***A:*** *Schematic timeline for the experimental setup. After differentiation of ESCs into MNs in vitro for 18-22 days, mature MNs were subjected to hypoxic condition for 30, 45, or 60 min and compared to normoxia (N).* ***B:*** *Live-Death assay stains living cells in green (Calcein AM) and dead cells in red (Ethidium-Homodimer-1). Scale bar represents 100 µm.* ***C:*** *Quantification of living cells by Live-Death staining (B). Values are shown relative to the number of living cells under normoxia.* ***D:*** *Quantification of an LDH assay to determine the lactate-dehydrogenase release. The values are proportional to the amount of dying cells. LDH activities are shown relative to LDH activity under normoxia. Significance in comparison with normoxia were tested with t-tests (*** P<0.001). ESC, embryonic stem cells; LDH, lactate dehydrogenase; NMCs, neuro mesodermal cells; pMNs motor progenitor cells; MNs, motor neurons; N, normoxia.*

In order to verify cell viability and the kinetic of the molecular response 18-22 days old ESC-derived MNs were subjected to three different hypoxia protocols (30, 45, and 60 min). To analyse the impact of hypoxia on the ESC-derived MNs were first subjected to a Live-Death staining (figure 5-8, B). Calcein AM (green) stains all living cells and ethidium-homodimer-1 (red) stains all dead cells (Slack *et al.*, 1998). The number of living cells were counted for the normoxia sample and after a period of either 30, 45 or 60 mins of hypoxia and plotted relative to the normoxic condition (figure 5-8, C). Compared to normoxia, the number of living cells was

not significantly different after 30 and 45 min of hypoxia. After 60 min of hypoxia, significantly less viable cells could be detected compared to the normoxic sample. Those results were verified with a lactate dehydrogenase (LDH) assay (figure 5-8, D). The LDH release due to plasma membrane damage was measured and quantified in comparison to the normoxia. In relation to the normoxic control, the amount of released LDH was similar when cells were subjected to either 30 min or 45 min of hypoxia, whereas after 60 min of hypoxia the release of LDH was significantly higher.

5.3.2. Hypoxia-induced Hif1α stabilisation and Dlk1 regulation

After assaying the cell viability, the stabilisation of Hif1α protein is the most prominent parameter to analyse the hypoxia response in cells and tissues (Wang *et al.*, 1995; Kaelin Jr, 2008; Fähling, 2009). The presence of oxygen leads to the hydroxylation of Hif1α, which results in the binding of the von Hippel-Lindau (VHL) E3 ligase complex, which in turn results in the direct ubiquitination and degradation by the proteasome (Kaelin Jr, 2008; Sadri and Zhang, 2013). In the case of a lack of oxygen, Hif1α is not hydroxylated and thus not binding to the VHL E3 ligase complex, preventing its degradation (Sadri and Zhang, 2013). This allows Hif1α accumulation and translocation into the nucleus, where it can act as a transcription factor (Jewell *et al.*, 2001; Simon and Keith, 2008; Dunwoodie, 2009; Haase, 2013; Grassi *et al.*, 2020; Wakhloo *et al.*, 2021). Known target genes of this signalling cascade are the transmembrane protein carbonic anhydrase IX (CaIX), which is involved in the pH regulation of cells (Sadri and Zhang, 2013; Wakhloo *et al.*, 2021), and the glucose transporter 1 (Glut1) (Harvey *et al.*, 2004). Those genes are hypoxia-related genes, which are supporting the efficiency of the Hif1α stabilisation and therefore the successful activation of hypoxia-dependent regulation processes (figure 5-9).

Hypoxic conditions were generated by placing the cells in a hypoxic chamber, in which the oxygen concentration can be reduced to 0.1 %, by replacing the oxygen with nitrogen (N_2). Further parameters, like temperature (37 °C), pressure (990 hPa) and humidity (83.5 %) were under permanent control. The chamber was provided and the experimental setup were performed in close cooperation with the group of Dr. rer. Dr. med. P. Habib, UK Aachen.

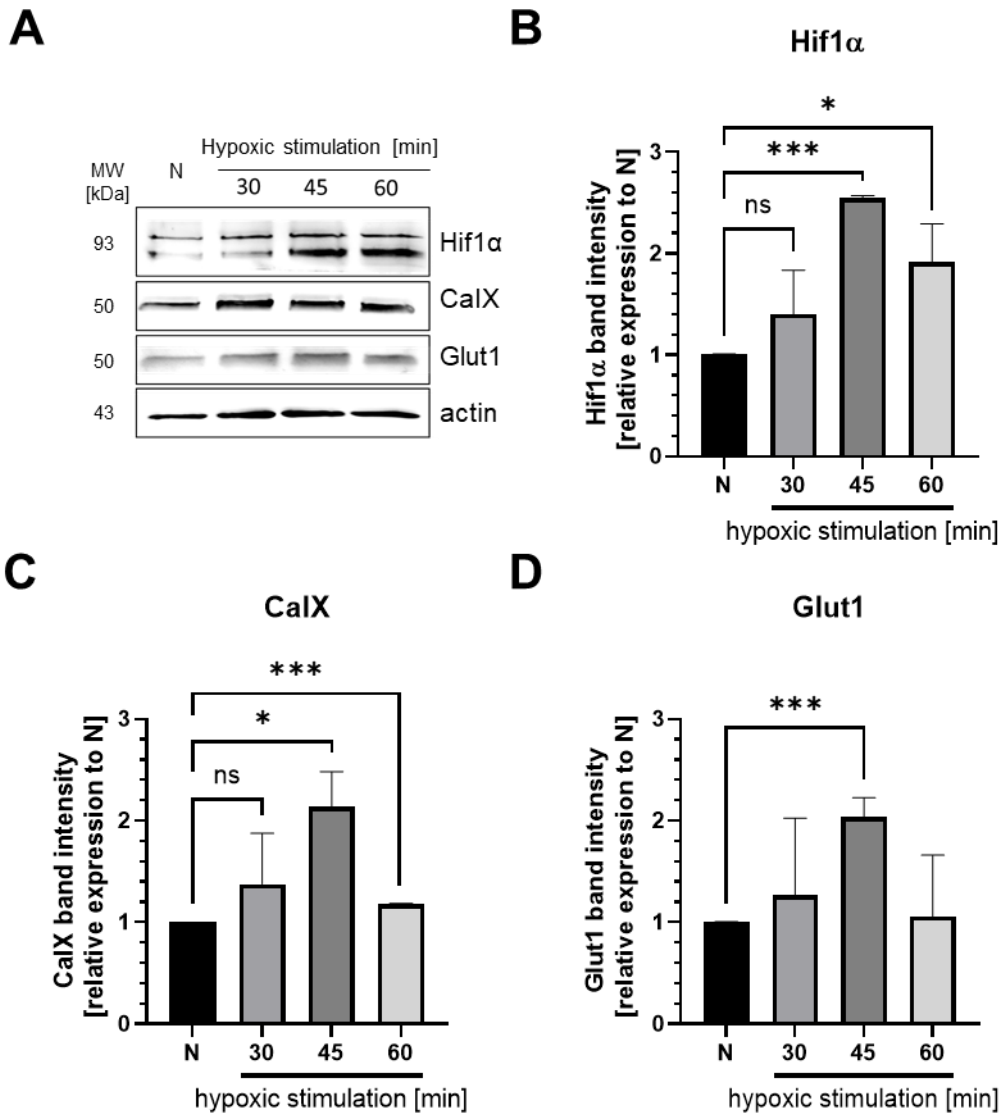

Figure 5-9: *Hypoxia-induced Hif1α stabilisation in the ESC-derived MN network.* ***A:*** *Western blot analysis of cell lysates from cells after 30, 45, or 60 min of hypoxia.* ***B:*** *Quantification of the densiometric analysis of Hif1α stabilisation in cells under different periods of hypoxic stimulation and compared to normoxia.* ***C*** *and* ***D:*** *Quantification of the densiometric analysis of Hif1α downstream factors CaIX (C) and Glut1 (D) after 30, 45, or 60 min of hypoxia compared to normoxia. Actin was used as loading control. Significance was tested with t-tests (* P<0.05; *** P<0.001). CaIX, carbonic anhydrase IX; Glut1, glucose transporter 1; MW, molecular weight; N, normoxia.*

Western blot analysis revealed that the hypoxic conditions applied to the ESC-derived MNs resulted in an increased abundance of Hif1α after 30, 45, and 60 min, likely due to the stabilisation of the protein (figure 5-9, B). While quantitatively there was a slight increase of Hif1α detectable after 30 min of hypoxia, significantly elevated protein levels were detected after 45 min and 60 min of hypoxia. For the Hif1α downstream target CaIX, there was an increase after 30 min of hypoxia and statistically increased after 45 min and 60 min of hypoxia. However, after 60 min, the CaIX protein concentration was drastically reduced compared to the 45 min of oxygen deprivation (figure 5-9, C). The CaIX protein level after 60 min of hypoxia,

was nearly back to normal level. Glut1 levels were slightly, but not significantly increased after 30 min compared to normoxia (figure 5-9, D). Nevertheless, after 45 min of hypoxia, there was a higher increase compared to 30 min and significantly increased compared to normoxia. After 60 min, the protein level of Glut1 was reduced again, comparable to normoxic conditions and similar to the CaIX protein level after 60 min.

With the evidence of successful hypoxia, by confirming the Hif1α stabilisation and the activation of the direct hypoxia-dependent transcription factors CaIX and Glut1, the further steps were to analyse the hypoxia-dependent Dlk1 response. The three different time periods of hypoxia were also used for analysing the specific response of Dlk1 (figure 5-10).

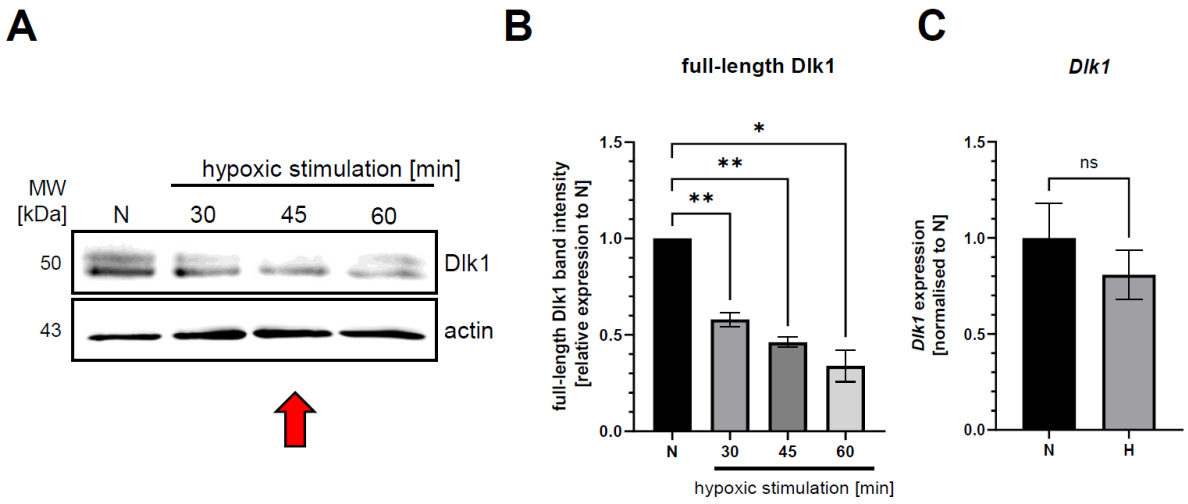

Figure 5-10: *Hypoxia-induced reduction of Dlk1 protein levels in the ESC-derived MN network.* ***A:*** *Western blot analysis of Dlk1 from cells after 30, 45, or 60 min of hypoxia compared to normoxia. For detection a Dlk1-specific antibody was used. Actin was applied as loading control.* ***B:*** *Quantification of the densiometric analysis of (A) relative to normoxia, n = 3.* ***C:*** *Dlk1 mRNA expression levels after hypoxic stimulation, compared to normoxia, n = 3. Quantifications were tested with t-tests (* P<0.05; ** P<0.005). N, normoxia; MW, molecular weight.*

Western blot analysis revealed that the Dlk1 protein levels were significantly reduced after hypoxia, independent the time of oxygen deprivation (figure 5-10, A and B). After 30 min of hypoxia a significant reduction was observed, while 45 min of hypoxia resulted in a significant reduction of full-length Dlk1 protein levels. The lowest significant reduction was observed after 60 min under hypoxia. Noteworthy, all Dlk1 blots detected a double band in the western blot, independent of hypoxic stimulation (figure 5-10, A). The band detected above the expected molecular weight of 50 kDa changed intensity similar to the expected band at 50 kDa for the 30 min and 45 min hypoxic stimulation compared to normoxia. Nevertheless, after 60 mins of hypoxia the Dlk1 was only slightly visible. For this analysis and all following analysis, both bands were used.

As the hypoxia-dependent reduction could be the result of altered *Dlk1* gene expression, the transcript level of *Dlk1* was analysed using semi-qRT PCR. The quantification of the transcript level showed no significant difference between the hypoxia-stimulated cells and the cells under normoxic condition (figure 5-10, C).

Based on the outcome of the cell viability assay, the Hif1α stabilisation and the abundance of the Hif1α downstream targets CaIX and Glut1, a hypoxic period of 45 min with 0.1 % O_2 concentration was used for all further experiments performed on the ESC-derived MNs (figure 5-10, A, arrow). Since the hypoxic stimulation should only be activate the hypoxic-induced pathways and not stimulate the apoptotic pathway, further experiments were performed with 45 min of hypoxic stimulation.

5.4. Dlk1 regulation *in situ*

ESC-derived MNs stimulated by hypoxia showed a reduction in the full-length Dlk1 protein levels, which was not resulting from reduced *Dlk1* expression levels. The alteration of Dlk1 in MNs after a hypoxic stimulation raised the question whether the observation was based on the *in vitro* culture of MNs or the differentiation of ESCs into MNs itself and therefore an *in vitro* artifact. To clarify if this, an additional approach of *ex vivo* was used. Because the *in situ* long-term cultivation of spinal cord slices containing unfortunately not possible, because MNs in these preparations typically survive only for a couple of hours (Dr. Müller, personal communication). To circumvent this problem, murine brain slices were used, which have long been established for using long-term slice cultures. *Dlk1* is expressed in the brain, especially in astrocytes in neural stem cell niches, as well as in the dopaminergic neurons in the hypophysis and the subgranular zone of the dentate gyrus (Ferrón *et al.*, 2011; Montalbán-Loro *et al.*, 2021; Grassi and Pietras, 2022).

5.4.1. Establishing brain slice culture

The murine brain has over seven million neurons with 1 $x10^{12}$ synaptic connections. The neurons are forming a complex network with diverse cell types (Erö *et al.*, 2018). They are a central component of the microstructure of CNS circuits (Schwarz *et al.*, 2010). In order to maintain this microcircuit and the influence of the various neuronal structures, acute living slices cultures were generated. The three-dimensional (3D) structure of brain slices enables the inclusion of multiple cell types, which might interact with the neurons and could influence the outcome of the experiment (Eguchi *et al.*, 2020).

After preparation of the brain, it was sectioned into 300 µm thick slices which were cultivated on Millicell-CM tissue culture inserts with 0.4 mm pores in six-well culture dishes. The slices are surrounded by artificial cerebrospinal fluid (aCSF) medium to provide the essential factors

for survival. The brain slices had a compact structure and were surrounded by aSCF medium to mimic the liquor in the brain. The preparation and slicing of the brain resulted in few damaged neurons, cell-cell connections and brain structures. To exclude preparation artifacts and investigate the optimal time point to perform hypoxic stimulations the viability of the brain slices was determined. Therefore, the viability of the cultivated brain slices was analysed after one, three, seven, fourteen and twenty-one days after plating. Therefore, the number of NeuN$^+$ cells and the Terminal deoxynucleotidyl transferase dUTP nick end labelling (TUNEL)/NeuN$^+$ double positive cells were counted (figure 5-11).

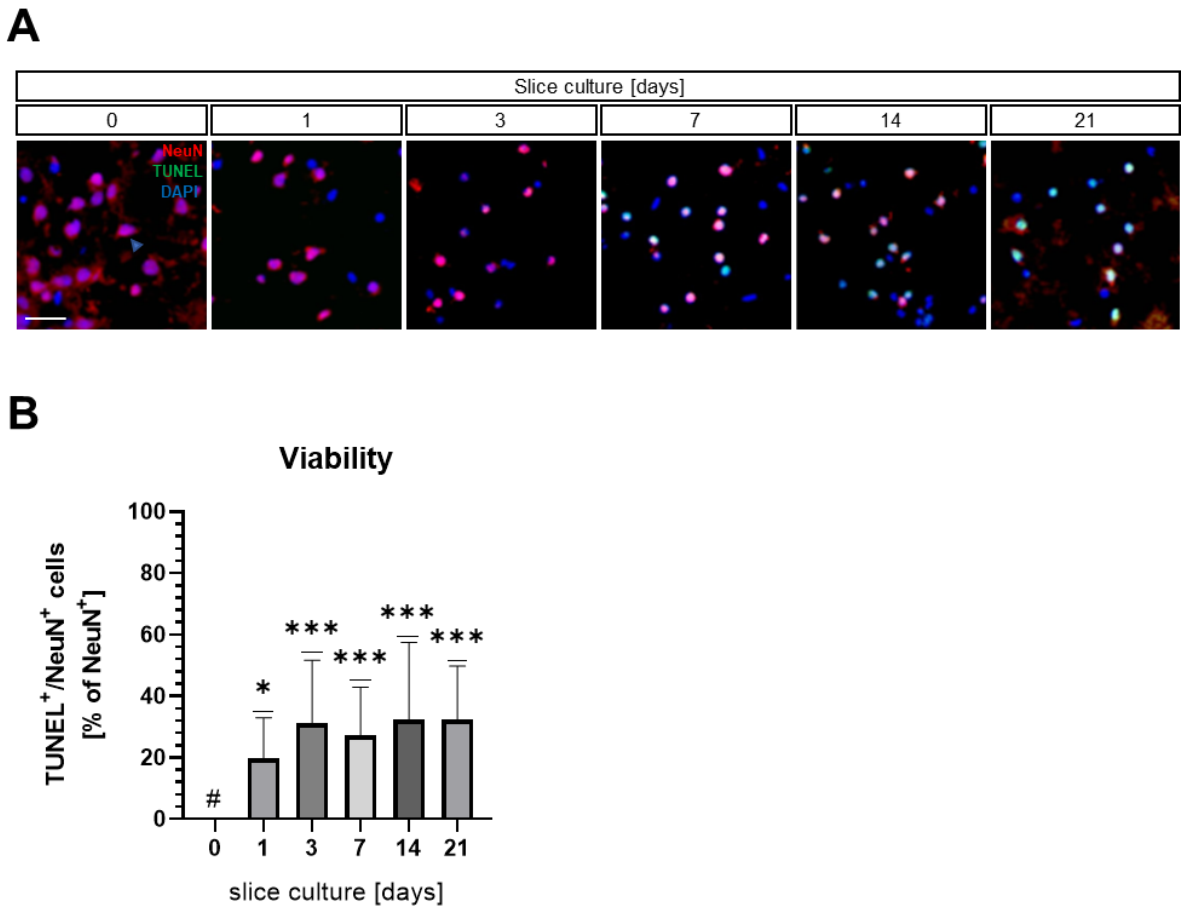

Figure 5-11: *Viability of neurons in brain slices over the cultivation period of three weeks.* ***A:*** *Representative images of immunofluorescence staining's for neurons (NeuN, red), combined with a TUNEL (green) and DAPI (blue) staining for the days (0; 1; 3; 7; 14 and 21) after preparation. The scale bar represents 25 µm.* ***B:*** *Quantification of 2000 cells per condition. Significances were tested with a one-way ANOVA, n = 2. (* P<0.05; *** P<0.001). Significance referees to the normoxia (#). NeuN, neuronal nuclear protein; TUNEL, Terminal deoxynucleotidyl transferase dUTP nick end labeling.*

At the day of the dissection (day 0), the sections showed barley any dying cells, whereas slices cultivated for one day revealed a percentage of 20 % and after three days there was an increase in the number of NeuN$^+$ and TUNEL$^+$ cells (30 %). With this time point, the mean number of NeuN$^+$ and Tunel$^+$ cells were fluctuating around 30 % for all further time points (7,

14, and 21 days). Based on this quantification, the ideal cultivation period of the brain slices was determined to be one day (24 hours) before the hypoxia experiment starts.

For humans, hypoxic deprivation results often in stroke. However, people react differently to stroke depending on how old they are, what gender they are and what ethnicity they are (Roy-O'Reilly and McCullough, 2018; Ekker *et al.*, 2019; Grotta *et al.*, 2021; Tsao *et al.*, 2022). Older humans are far more sensitive to hypoxia than younger ones (Ekker *et al.*, 2019; Grotta *et al.*, 2021). Beside this age aspect, there is also a gender differences reported in humans (Roy-O'Reilly and McCullough, 2018). In general, women are less likely to suffer from an ischaemic stroke compared to men. Therefore, the difference in the recovering from an ischaemic stroke between the gender must be considered together with age. Young men have a higher risk of stroke compared to women, this reverses in middle age, and in older populations women are more likely to suffer from a stroke (Ekker *et al.*, 2019). Those gender and age aspects can also be transferable to mice (Liu *et al.*, 2009; Manwani *et al.*, 2013), which could show that young adult female mice have smaller infarct volumina, better neurological functions and faster recovery time, compared to the same aged male mice. With ongoing age, the difference between the gender, were equivalently severe (Manwani *et al.*, 2013).

Investigating on brain slices as useful approach to study Dlk1 processing after hypoxic stimulation, brain slices of different gender and age were analysed. The brain slices were generated from mice either in an age range of 2-5 month or 8-18 month. Initial experiments revealed useful slices with a high expression of Dlk1 (supplement figure 6). Slices from the selected region were used for all further experiments. Those brain slices were further cultivated for one day, followed by hypoxic stimulation identically from previous experiments (figure 5-12).

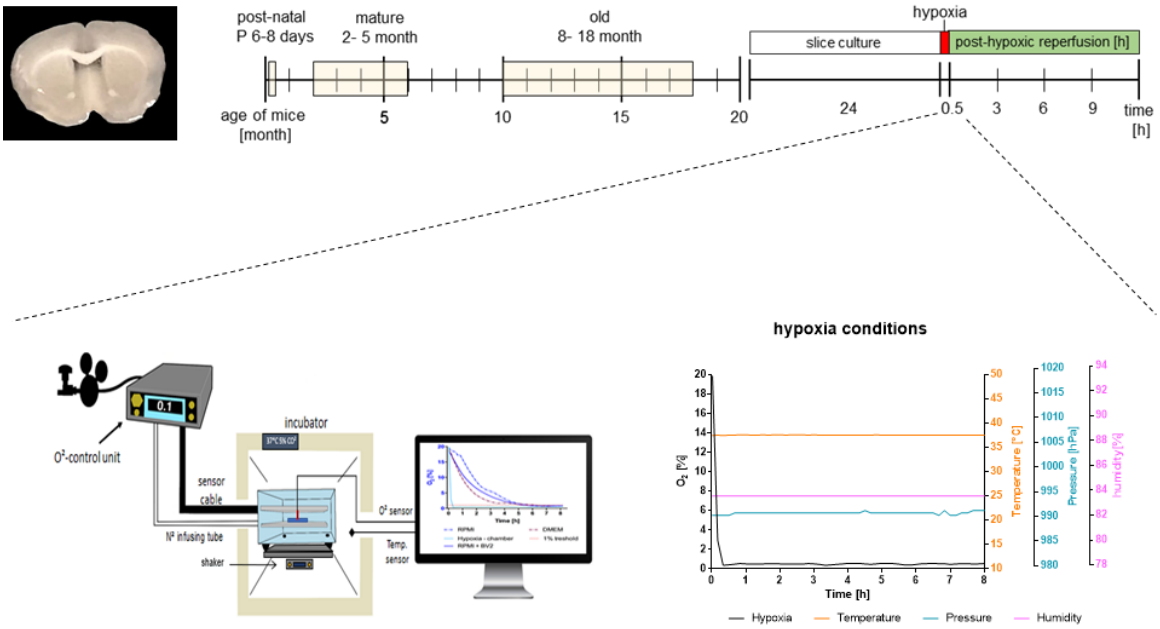

Figure 5-12: *Experimental setup to analyse hypoxia mediated Dlk1 processing in murine brain slices. Brain slices were divided in three different age groups (post-natal P 6-8 days; mature 2-5 month; old 8-18 month) depending on the reaction to hypoxia. After 24 h of culturing, the hypoxia experiment was performed under controlled conditions of stable temperature (37 °C), pressure (990 hPa), and humidity (83.5 %). Further, slices was observed beyond the oxygen deprivation in the post-hypoxic reperfusion time. Image was provided by E. Arik and modified after the individual experimental setup.*

Hypoxia induction in brain slices is similar to the induction of hypoxia in cultured ESC-derived MNs. This acute period of oxygen deprivation is followed by the post-hypoxic reperfusion time. The period of hypoxia activates cellular recovery mechanisms to restore the oxygen supply of the brain and repair mechanisms, such as angiogenesis, neurogenesis and synaptogenesis (Eltzschig and Eckle, 2011). However, it is common that serious damage occur during reperfusion period as a result of the post-hypoxic reperfusion injury (Wu *et al.*, 2018). Therefore the 24 hours after hypoxia were investigated in the experiment to analyse the full-length Dlk1 processing (figure 5-12, upper panel). The optimal time period of hypoxic stimulation for the brain slices was determined to be 30 min (unpublished data and personal communication Dr. rer. nat. Dr. med. P. Habib, UK Aachen) and induced a time-dependent Hif1α stabilisation (figure 5-13). The Hif1α stabilisation, as well as the induction of the downstream targets CaIX and Glut1 were verified in brain slices from 2-5 months old and 8-18 months old mice. Furthermore, the gender difference was separately evaluated. First results revealed similar levels of Hif1a after hypoxic stimulation in male and female mice. As no significant differences between males and females mice emerged (supplement figure 3, supplement figure 4), only the male mice blots were presented in the following figures, whereas the quantifications of both sexes was displayed.

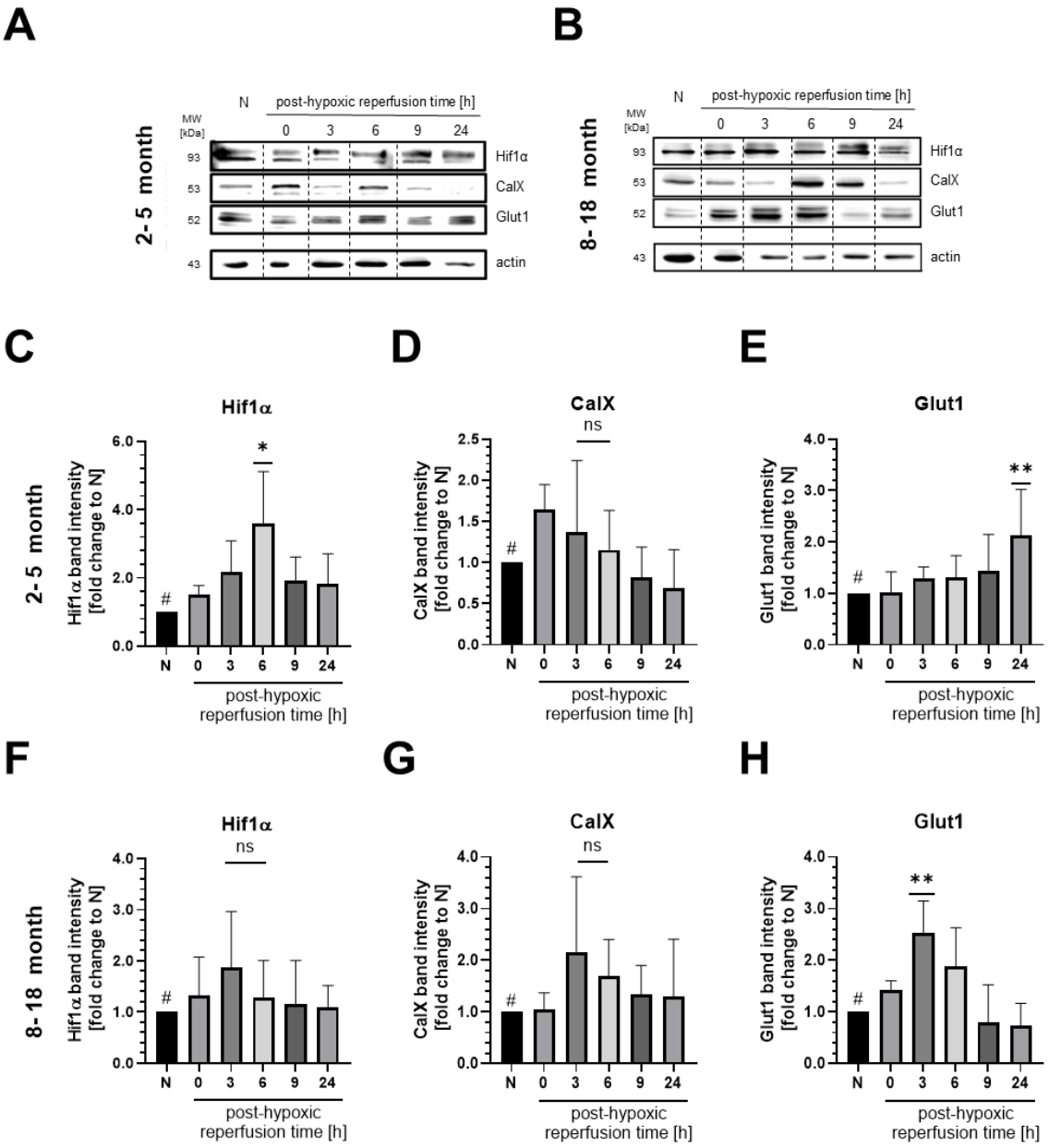

Figure 5-13: *Hypoxia-induced Hif1α stabilisation and downstream targets CaIX and Glut1 in murine brain slices.* ***A:*** *Combined western blot image from male brain slices of 2-5 month old mice at normoxia, after 30 min of hypoxia, and post-hypoxia reperfusion time.* ***B:*** *Combined western blot images from male brain slices of 8-18 month old mice at normoxia after 30 min of hypoxia, and post-hypoxia reperfusion time.* ***C:*** *Quantification of the densiometric analysis of Hif1α stabilisation after hypoxia and reperfusion time compared to normoxia, pooled from male and female response.* ***D*** *and* ***E:*** *Quantification of the densiometric analysis of the downstream factors CaIX (C) and Glut1 (D), pooled from male and female response.* ***F:*** *Quantification of the densiometric analysis of Hif1α stabilisation after hypoxia and reperfusion time compared to normoxia, pooled from male and female response.* ***G*** *and* ***H:*** *Quantification of the densiometric analysis of the downstream factors of Hif1α stabilisation CaIX (G) and Glut1 (H). Actin was used as loading control. Quantifications were tested with a one-way ANOVA, n = 4. (* P<0.05, ** P<0.005). Significance referees to the normoxia (#).*

In 2-5 months old mice Hif1α levels were slightly increased directly after three hours of oxygen deprivation compared to the normoxic condition (figure 5-13, A and C-E). With ongoing

reperfusion time, Hif1α was significantly increasing after 6, 9 and 24 hours of post-hypoxic reperfusion time compared to normoxia (figure 5-13, C). The regulation of CaIX was only slightly increased directly after the 30 min of hypoxic stimulation, whereas after 3 and 6 hours post-hypoxic reperfusion time, CaIX level was comparable to that in normoxia conditions. With further post-hypoxic reperfusion time, CaIX was dropping even below the level of that seen in normoxia (figure 5-13, D). Glut1 was not increasing post-hypoxia and also not in the three and six hours post-hypoxic reperfusion time. However, after 9 and 24 hours post-hypoxic reperfusion time, Glut1 expression levels were significantly increasing, compared to those observed under normoxic conditions (figure 5-13, E).

Compared to the 2-5 months old mice, the hypoxic stimulation of brain slices from 8-18 months old mice, resulted in a lower, not significant Hif1α stabilisation (figure 5-13, F). Directly after hypoxia, Hif1α is slightly increased compared to normoxia, which was more pronounced in younger mice. In younger mice (2-5 months), Hif1α stabilisation was slightly reduced at three hours post-hypoxic reperfusions time compared to 0 hours post-hypoxic reperfusion time. At the same time points, the Hif1α level was still increasing in older mice (8-18 months). With ongoing post-hypoxic reperfusion time, Hif1α levels were again reduced, compared to those in young mice. In comparison to the young mice, the protein levels of hypoxia-induced factor CaIX was increased directly after the acute phase of hypoxia, until reaching a peak at six hours post-hypoxic reperfusion time for the older mice. With ongoing post-hypoxic reperfusion time, CaIX levels were reduced again (figure 5-13, G). The Glut1 protein levels were elevated in the older mice after the acute phase of hypoxia, compared to those observed in normoxia (figure 5-13, H). At three hours post-hypoxic reperfusion time, Glut1 levels had reached its maximum. In young mice, the Glut1 protein level was increasing during the complete post-hypoxic reperfusion time, with a peak after 24 hours post-hypoxic reperfusion time. All in all, younger mice showed less Hif1α stabilisation and also the induction of the hypoxia-induced factors was less compared to those observed in older mice.

There are multiple cell death pathways implicated in the pathogenesis of ischemic stroke, including intrinsic and extrinsic apoptosis (Tuo, Zhang and Lei, 2022). To quantify the cell death rate in the brain slices, slices of young and old mice were stimulated with a hypoxic condition, and fixed at the desired time points during the post-hypoxic reperfusion time. Further, the slices were stained with antibodies recognising NeuN and TUNEL to highlight the $NeuN^+$ cells and the mortality of the cells was quantified (figure 5-14). First results revealed similar levels of the viability of $NeuN^+$ neurons after hypoxic stimulation in male and female mice. As no significant differences between male and female mice emerged, only the male mice blots were presented in the following figures, whereas the quantifications of both sexes were displayed (supplement figure 5).

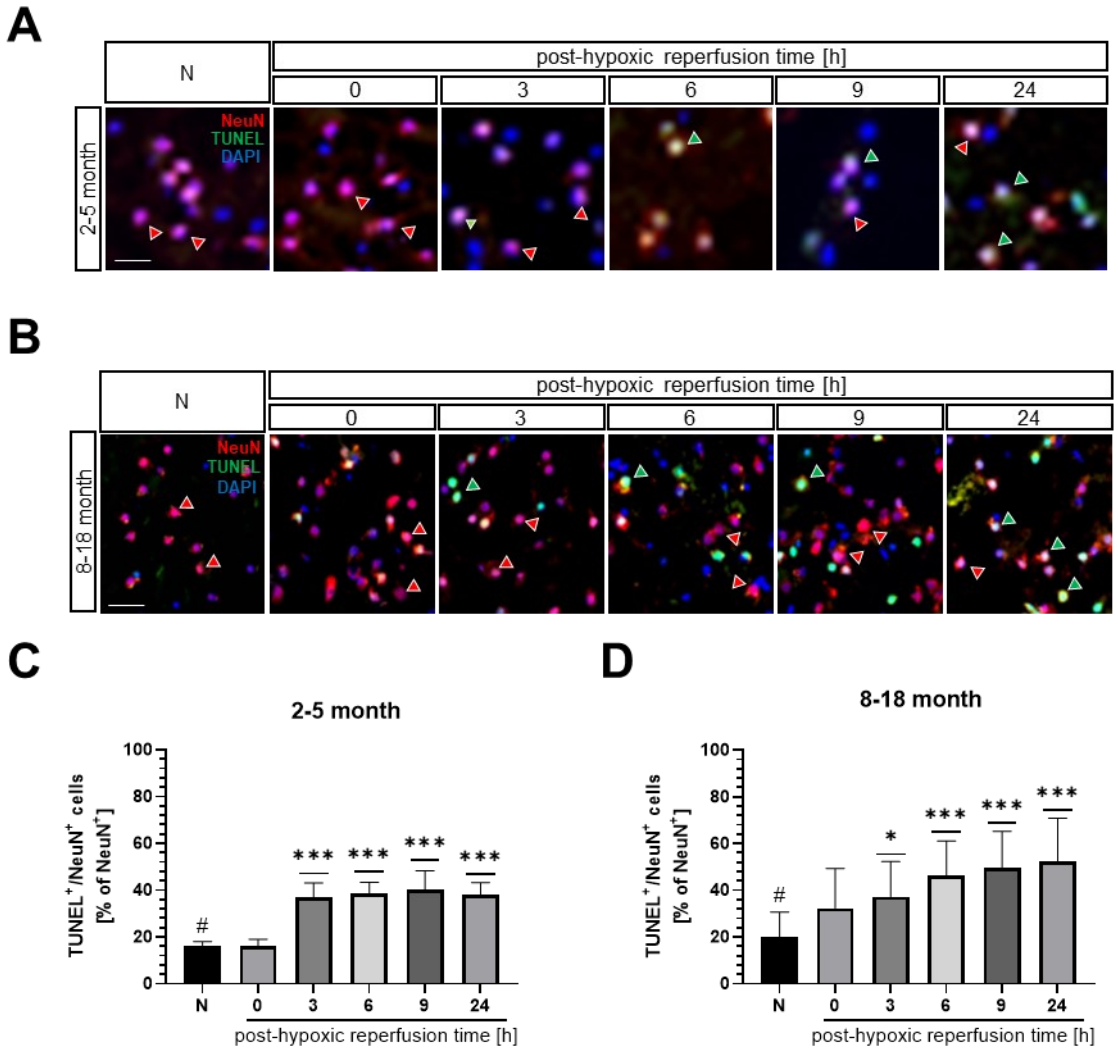

Figure 5-14: *Viability of neurons in brain slices after hypoxia.* ***A*** *and* ***B****: Representative images of immunofluorescence staining's for neurons (NeuN⁺, red arrowhead), combined with a TUNEL (green, arrowhead) and DAPI (blue) staining for the normoxia, hypoxia and the time points of the post-hypoxic reperfusion time (3, 6, 9, and 24h) for mature mice (A, 2-5 month) and old mice (B; 8-18 month). Scale bars represent 25 µm.* ***C*** *and* ***D:*** *Quantification of a total of 2000 cells per condition per age. Quantifications were tested with a one-way ANOVA, n = 2 (C) and n = 4 (D). (* P<0.05, ** P<0.005; *** P<0.001). Significance referees to the normoxia (#). N, normoxia, NeuN, neuronal nuclear protein; TUNEL, Terminal deoxynucleotidyl transferase dUTP nick end labeling.*

The mortality of neurons was analysed by the count of NeuN$^+$ and TUNEL$^+$ cells (figure 5-14, A and B; green arrowhead) and calculating the proportion to NeuN$^+$ cells (figure 5-14, A and B; red arrowhead) in brain slices of young mature (figure 5-14, A and C) and old mice (figure ***5-14***, B and D). For the brain slices of young mature mice, the mortality was not elevated after the acute period of hypoxia. After three hours of post-hypoxic reperfusion time, the proportion of the NeuN$^+$ and TUNEL$^+$ were significantly increased, compared to the total number of NeuN$^+$ cells. The percentage of dead cells in normoxia condition was around 16 %, compared to the total number of neurons (DAPI$^+$). For the brain slices of 8-18 month old mice (figure 5-14, D),

the percentage of 20 % dead cells in the normoxia condition was comparable to those from the normoxia of the younger mice (figure 5-14, C). Within three hours of post-hypoxic reperfusion time, there was a significant elevation in the number of dead cells relative to the NeuN$^+$ cells. Over the entire post-hypoxic reperfusion time, the numbers of dead cells were increasing. No significant differences were observed between male and female (supplement figure 5). After verifying that murine brain slices could be used as an additional approach to address the question about Dlk1 regulation after hypoxic stimulation, those brain slices were further used to quantify Dlk1 protein level *in situ*.

5.4.2. Dlk1 regulation by hypoxia in early post-natal and adult brain slices

Dlk1 regulation after hypoxic stimulation brain slices of mice with different ages were analysed in brain slices derived from early post-natal days 6 to 8 (P 6-8), young mature (2-5 months) and old (8-18 months) mice (figure 5-15).

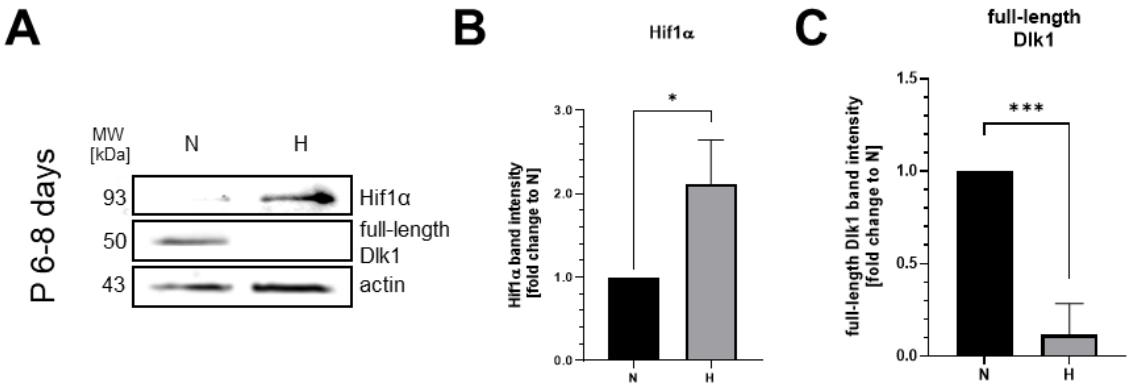

Figure 5-15: *Hypoxia-induced Dlk1 processing in post-natal murine brain slices.* ***A:*** *Representative western blot image from brain slices of early post-natal mice (P 6-8 days) cultured in normoxic conditions or after 30 min of hypoxia.* ***B:*** *Quantification of densiometric analysis of Hif1α stabilisation after hypoxia compared to normoxia, n = 3.* ***C:*** *Quantification of densiometric analysis of Dlk1 processing after hypoxia compared to normoxia, n = 3. Actin was used as loading control. Quantifications were tested with T-test analysis (* P<0.05, *** P<0.001). H, hypoxia; MW, morlecular weight; N, normoxia.*

Brain slices of young early post-natal mice were obtained and cultured as previously for brain slices of mature mice (figure 5-12). In summary, they were exposed to hypoxic stimulation of 30 min 0.1 % oxygen and analysed in regard to the success of the hypoxic induction. The Hif1α stabilisation showed a significant increase after 30 min of hypoxic stimulation, compared to normoxia (figure 5-15, B). Based on the Hif1α stabilisation, Dlk1 protein was investigated and compared between normoxic control and after hypoxic conditions. Interestingly, Dlk1 protein levels were significantly reduced to 15 % compared to normoxia (figure 5-15, C).

Following the P 6-8 old mice, the older mice were also investigated about the alteration on the Dlk1 protein levels after hypoxic condition compared to control conditions, in brain slices, expressing comparable levels of Dlk1 (supplement figure 1 and supplement figure 2).

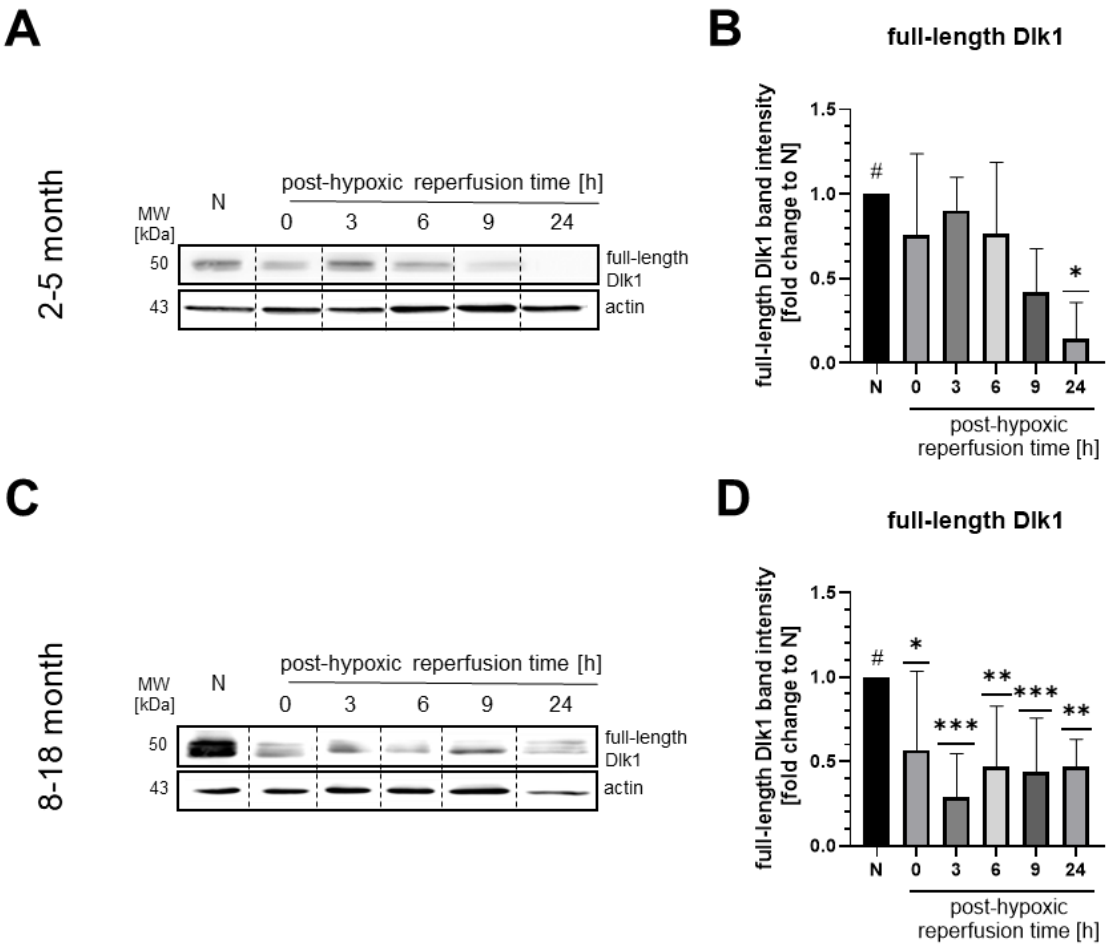

Figure 5-16: *Hypoxia-induced Dlk1 processing in mature murine brain slices.* ***A:*** *Composed western blot image from male brain slices of 2-5 month old mice after 30 min of hypoxia and post-hypoxia reperfusion time (3; 6; 9; and 24 h).* ***B:*** *Quantification of densiometric analysis of Dlk1 protein level after hypoxia and reperfusion time compared to normoxia in mature mice of 2-5 month old mice, n = 4.* ***C:*** *Composed western blot image from male brain slices of 8-18 month old mice at normoxia, after 30 min of hypoxia, and post-hypoxia reperfusion time.* ***D:*** *Quantification of densiometric analysis of Dlk1 protein level after hypoxia and reperfusion time compared to normoxia in mature mice of 8-18 month, n = 8. Actin was used as loading control. Quantifications were tested with a one-way ANOVA (* P<0.05, ** P<0.005; *** P<0.001). Significance referees to the normoxia (#). MW, molecular weight; N, normoxia.*

Interestingly, full-length Dlk1 was significantly reduced after hypoxic stimulation compared to normoxia in brain slices of the young and older mature mice (figure 5-16). In the brain slices of young mature mice, full-length Dlk1 was reduced by about 50 % compared to normoxia (figure 5-16, B). Dlk1 levels were slightly higher after three hours of post-hypoxic reperfusion time. The older (8-18 months) mice showed a similar reduction of Dlk1 levels after the acute phase of hypoxia about 50 %, compared to normoxia. Following the post-hypoxic reperfusion time, Dlk1 was about as low in the protein levels, compared to the acute phase after hypoxia.

Nevertheless, slight fluctuations in the Dlk1 protein levels could be detected in the post-hypoxic reperfusion time. The three and six hours post-hypoxic reperfusion showed more decrease in the Dlk1 protein levels compared to the acute phase of hypoxia (0 hour). At nine and twenty-four hours post-hypoxic reperfusion time, Dlk1 levels were slightly elevated again at round 45 % compared to the normoxia condition. For both ages of mice, no gender-specific differences in the Dlk1 protein levels were detected (supplement figure 6).

Taken together, Dlk1 is regulated in ESC-derived MNs as well as in brain slices, which leads to the question about the underlying mechanism, which was investigated in the following parts of this thesis.

5.5. Hypoxia-induced Dlk1 cleavage

5.5.1. Hypoxia-induced Hif1α stabilisation in ESC-derived MNs

To analyse the causes of the hypoxia-reduction of full-length Dlk1 in more detail, the ESC-line Dlk1-HA was used to differentiate MNs. Those ESC-derived MNs were subjected to hypoxic stimulation and the C-terminally epitope tagged Dlk1 protein analysed after hypoxia. The observed reduction of full-length Dlk1 protein levels (figure 5-10, A; figure 5-15, figure 5-16, D) could have four different reasons: (I) a down-regulation of transcription, (II) proteolytic degradation of the entire protein or (III) a cleavage process that abrogates detection by the Dlk1-specific antibody used. To investigate the possibility of hypoxia-induced changes in gene expression, *Dlk1* expression was analysed be semi-qRT PCR (figure 5-10, C). Thereby, no significant reduction of the expression levels after hypoxia were detected. To address the two other possibilities, ESCs were used to analyse the reduction of Dlk1 in regard to possible cleavage of the Dlk1 protein.

It is known, that the post-hypoxic reperfusion time is more crucial to analyse hypoxia-induced pathways. It includes the time period after the oxygen deprivation, when the molecular pathways to recover the physiological parameters proceed (Eltzschig and Eckle, 2011; Wu *et al.*, 2018). Therefore, next to the acute phase of hypoxia (0 h) a post-hypoxic reperfusion time of three hours was included in the analysis. As before, the Hif1α stabilisation as well as the upregulation of its downstream targets CaIX and Glut1 served again as control for successful hypoxic stimulation.

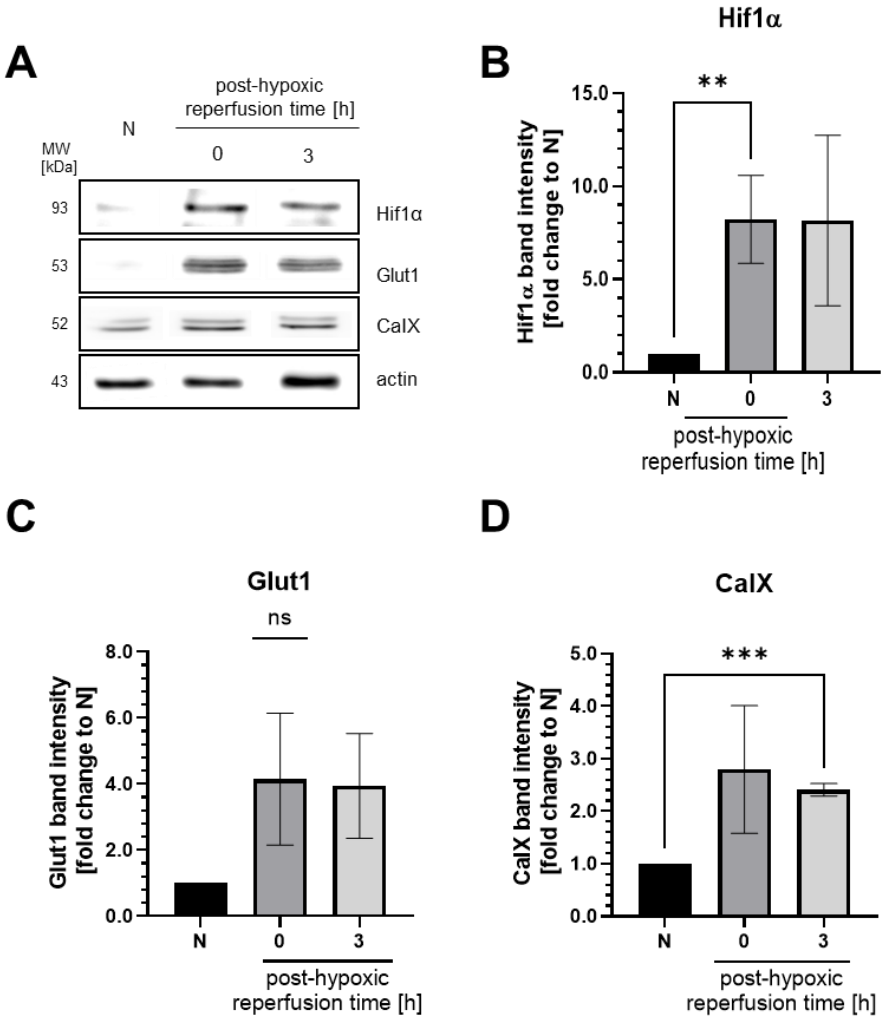

Figure 5-17: *Hypoxia results in a stabilisation of Hif1α and the targets CaIX and Glut1 in ESC-derived MN network.* ***A:*** *Representative western blot for samples from 45 min of hypoxia and three hours of post-hypoxia reperfusion time, compared to samples from normoxia.* ***B:*** *Quantification of the densiometric analysis of Hif1α stabilisation after hypoxia and reperfusion time compared to normoxia, n = 3.* ***C*** *and* ***D:*** *Quantification of the densiometric analysis of the downstream factors of Hif1α stabilisation Glut1 (C) and CaIX (D), n = 3. Actin was used as loading control. Quantifications were tested with a T-test analysis (** P<0.005; *** P<0.001). CaIX, carbonic anhydrase IX; Glut1, glucose transporter; MW, molecular weigth; N, normoxia.*

As previously established (figure 5-9) and reconfirmed here by immunoblot, 45 min of hypoxia directly resulted in Hif1α stabilisation and increase of its targets CaIX and Glut1 (figure 5-17, A). These enrichments in Hif1α (figure 5-17, B), CaIX (figure 5-17, C) and Glut1 (figure 5-17, D) protein levels were maintained at three hours of post-hypoxic reperfusion time. From these findings it can be assumed that the hypoxia was successful and triggered an intracellular response. After establishing the Hif1α stabilisation in the ESC-derived MNs, the focus was on the Dlk1 protein regulation after hypoxia. First, the question about the full-length Dlk1 regulation in the context of the cellular localisation was addressed.

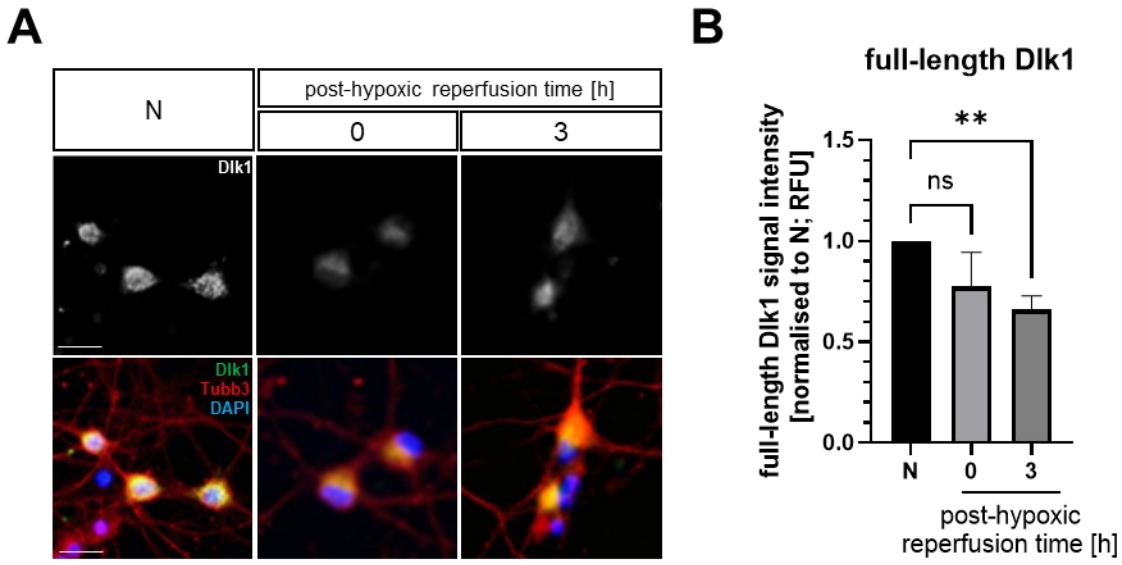

Figure 5-18: *Immunofluorescence of the Dlk1 detected by the Dlk1-specific antibody.* ***A:*** *Representative grey scale images of the Dlk1 signal intensity at normoxia, after 45 min of hypoxia, and after additional three hours of post-hypoxic reperfusion time (upper row) and merged images of staining's of Dlk1 (green), Tubb3 (red) and DAPI (blue) (lower row). Scale bars represent 15 µm.* ***B:*** *Quantification of a total number of 300 cells per condition, n = 3. Quantifications were tested with a one-way ANOVA (** P<0.005). N, normoxia; RFU, relative fluorescence unit; Tubb3, Tubulin Beta 3 Class III.*

When comparing the immunofluorescence intensity after 45 min of hypoxic, three hours post-hypoxic reperfusion time and normoxia conditions, Dlk1 signal intensity varied between these conditions (figure 5-18, A). The highest signal intensity was measured in the normoxia condition, while the oxygen deprivation decreased the signal of the full-length Dlk1 directly after hypoxia and significantly after three hours reperfusion time about 25 % (figure 5-18, B). The images revealed details of the subcellular Dlk1 localisation. In normoxia, a punctate Dlk1 signal is observed in the whole soma, particularly enriched in the perinuclear region. This region was also preferable binding region for other commercially available human Dlk1 antibodies, cited on the webpage of *"The Human Protein Atlas"*. This overlap in the Dlk1 localisation might indicate the specificity and functionality of the antibody used. This punctate signal was also observed after 45 min of hypoxia and three additional hours of post-hypoxic reperfusion time.

To further address the question whether Dlk1 reduction is because Dlk1 is cleaved in a way that the Dlk1 antibody could not bind anymore, the Dlk1-HA ESC line was taken advantage of. The used ESC line was genetically modified by Dr. M. Marks by adding an HA epitope tag at the C-terminus of the ICF (figure 3-1; unpublished data). Dlk1 is a type 1 transmembrane protein. It consists of an N-terminal extracellular region (ECD), followed by the transmembrane (TM) region and the short C-terminal intracellular region (ICF) (figure 1-5, A, figure 5-19, A). After Dlk1 stimulation, it can be cleaved by different proteases at its ECD and ICF and leaves

behind the membrane-bound region (figure 5-19, B) (Smas and Sul, 1993; C. H. Jensen *et al.*, 1994; Wang and Sul, 2006). The cleavage of the ECD is, among others, possibly catalysed by the disintegrin- and metalloprotease 17 (Adam17) (Jensen et al., 1994; Wang and Sul, 2006; Traustadóttir et al., 2019). This first cleavage leads then to the second cleavage of the ICF (Grassi, Pantazopoulou and Pietras, 2020).

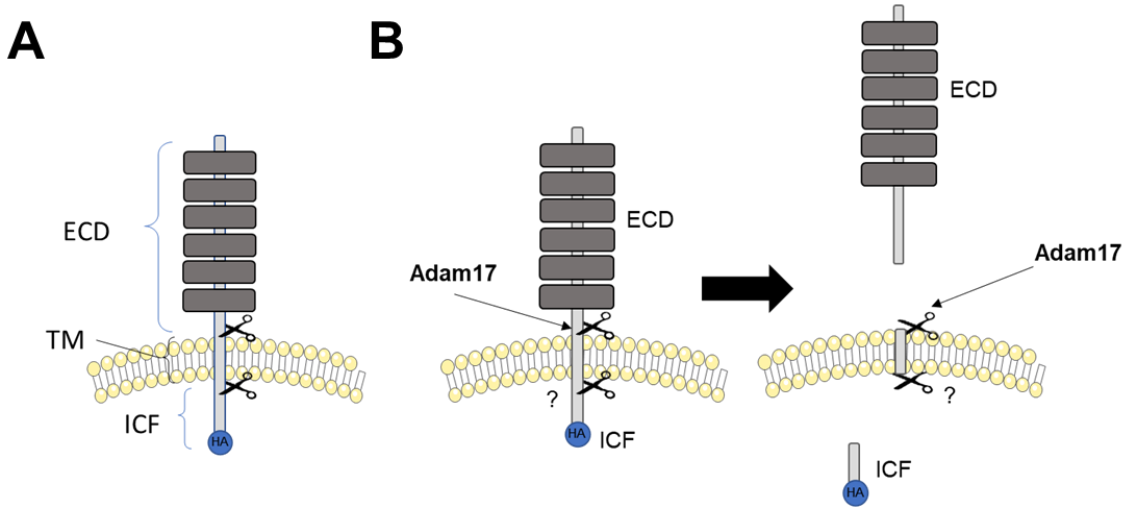

Figure 5-19: *Dlk1 protein and the predicted Dlk1 processing after hypoxic stimulation.* ***A:*** *Dlk1 protein with ECD, the TM and the ICF.* ***B:*** *Dlk1 is predicted to be cleaved by Adam17 at the ECD, followed by a cleavage at the ICF from a so far unknown protease. ECD, extracellular fragment; ICF, intracellular fragment; HA, hemagglutinin; TM, transmembrane region.*

The protease responsible for the second cleavage is not known yet. Both cleaved segments can either interact with themselves or with further interaction partners (Wang *et al.*, 2006; Nueda *et al.*, 2008; Traustadóttir *et al.*, 2017). It is assumed that the ICF itself might translocate to the nucleus, where it can have transcription co-factor-like activities (Subhashini, 2016; Grassi, Pantazopoulou and Pietras, 2020). As the processing of Dlk1, especially of the ICF, is the main focus of the following experiments, the different Dlk1 fragments should be discriminated. Therefore, the following antibodies were used (figure 5-20).

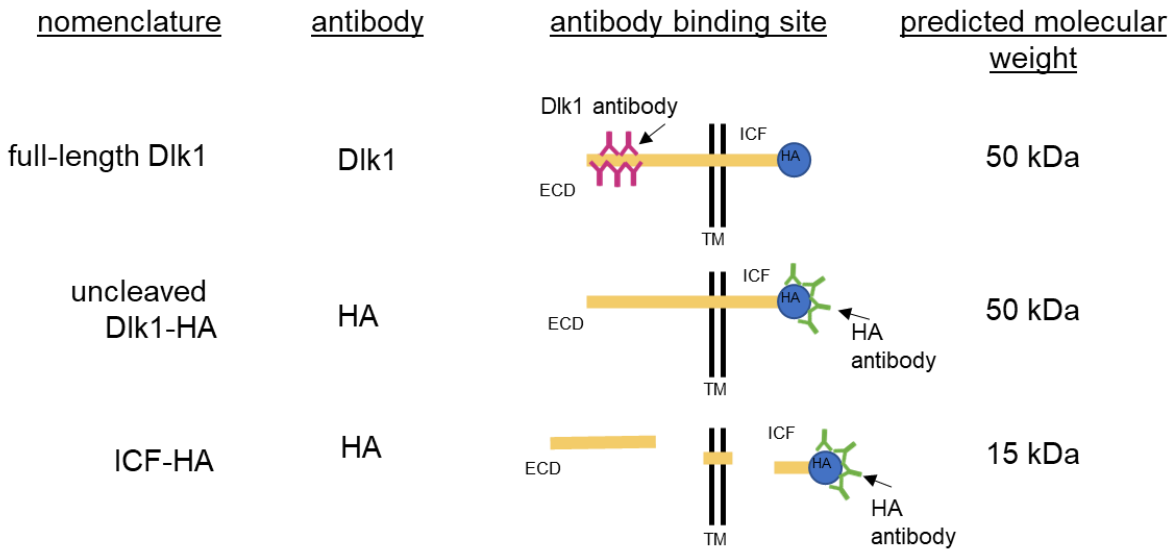

Figure 5-20: *Overview of nomenclature, antibody binding sites and expected molecular weight detectable in western blot analysis. Full-length Dlk1 is detected by a commercially available antibody, which binds at the ECD of Dlk1, whereas the uncleaved Dlk1-HA the full-length Dlk1 describes, which is detected by the HA antibody. The ICF-HA is one cleavage product of Dlk1 detected with the HA antibody. ECD, extracellular fragment; ICF, intracellular fragment; HA, hemagglutinin.*

Therefore, in the used experimental setup, possible Dlk1 cleavage products were discriminated as the full-length Dlk1, detectable with a commercially available antibody, as well as the uncleaved Dlk1-HA and the ICF-HA detected by an HA-epitope specific antibody. This allowed a detection of Dlk1 in immunoblot analysis twice at a molecular weight of around 50 kDa and using the HA-specific antibody once at 15 kDa (figure 5-20). Those two antibodies could also be used in the immunofluorescence analysis, as they are overlapping in a co-immunostaining (supplement figure 7). Nevertheless, with the HA co-immunostaining it is not possible to discriminate between the full-length and ICF of Dlk1. Only the Dlk1 immunofluorescence staining could reveal exclusively the full-length Dlk1. Therefore, it provides more details about the subcellular localisation rather than Dlk1 protein processing.

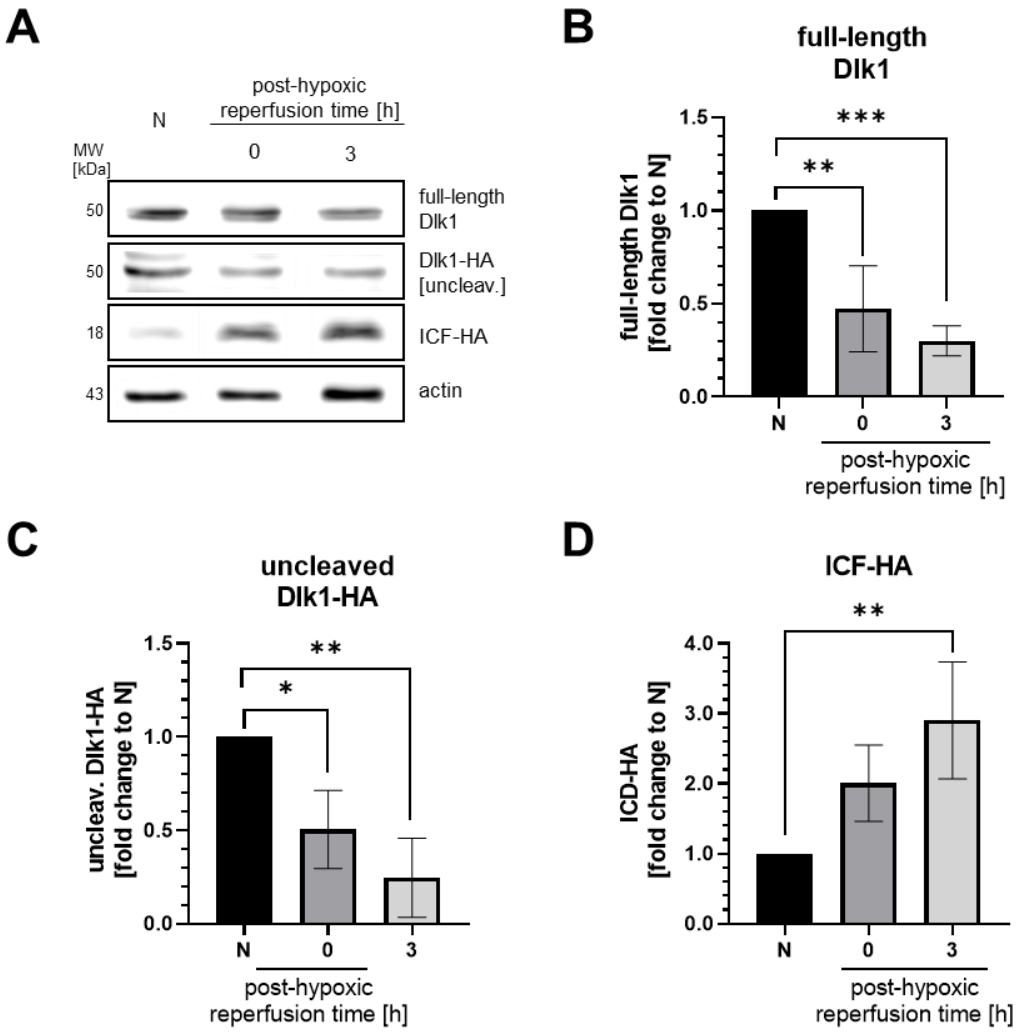

Figure 5-21: *Dlk1 cleavage after hypoxic stimulation.* ***A:*** *Representative western blots of normoxia, 45 min of hypoxia, and three hours of post-hypoxia reperfusion time.* ***B:*** *Quantification of the densiometric analysis of the full-length Dlk1 signal intensity after hypoxia and reperfusion time compared to normoxia, n = 3* ***C:*** *Quantification of the densiometric analysis of uncleaved Dlk1-HA signal intensity after hypoxia and reperfusion time compared to normoxia, n = 3* ***D:*** *Quantification of the densiometric analysis of the ICF-HA signal after hypoxia and reperfusion time compared to normoxia, n = 3. Actin was used as loading control. Quantifications were tested with t-tests (* P<0.05; ** P<0.005; *** P<0.001). uncleav., uncleaved Dlk1-HA; HA, hemagglutinin; MW, molecular weight; N, normoxia.*

The full-length Dlk1 was clearly detectable in normoxia, but significantly reduced after post-hypoxia and the post-hypoxic reperfusion time compared to normoxic conditions (figure 5-21, B). Similar results were detected for the full-length Dlk1 protein variant using the HA-epitope-specific antibody (figure 5-21, C; Dlk1-HA). Given that the HA-specific antibody also allows the detection of the ICF of Dlk1, a second band at a size of approximately 15 kDa was detectable in the immunoblot analysis (figure 5-21, D; ICF-HA). While the ICF was hardly detectable in the normoxia, hypoxia resulted in an enrichment of the ICF that became significant after the three hours of post-hypoxic reperfusion time (figure 5-21, D).

5.5.2. ICF-HA localisation after hypoxic stimulation

The increasing ICF-HA signal after hypoxia and post-hypoxic reperfusion time indicates cleavage of Dlk1 as a response to hypoxia (figure 5-21, D). Although it is known that Dlk1 is promoting the fast αMN properties, it is not clear how Dlk1 is promoting these properties (Müller *et al.*, 2014). Because of the different splice variants and the different cleavage sites, different varies are formed depending on the tissue or developmental stage investigated (Wang *et al.*, 2006). Most of the interactions of Dlk1 in any described pathways are reported to be the soluble ECD of Dlk1 (Wang and Sul, 2006; Nueda *et al.*, 2008; Traustadóttir *et al.*, 2016). However, it has been shown that the ECD is not responsible for promoting fast αMN properties (Müller *et al.*, 2014). In contrast to the well-known ECD, little is known about the function of the ICF. However, based on the similarity to the Notch1 signalling (Laborda *et al.*, 1993), it was assumed that the ICF might play a role in the pathway to promote fast αMN properties.

Nevertheless, the localisation and the downstream activity of the ICF after cleavage in fast αMNs remains largely unknown. To further investigate the localisation of the ICF-HA, an immunofluorescence analysis was performed using the HA-epitope-specific antibody on ESC-derived MNs cultured either under normoxia or subjected to hypoxia with or without three hours of post-hypoxic reperfusion time (figure 5-22). Z-stack confocal images of the cells were taken by starting the imaging at the lowest and highest position of the ICF-HA signal. This gave a region of 101.61 µm x 101.61 µm x 15.00 µm (X x Y x Z) with 16 individual images. Thereafter, the distance between the single images was 0.94 µm. However, to get an overview through the whole cell, every third individual image was observed (optical section: 3^{th}, 6^{th}, 9^{th}, and 12^{th}) (supplement figure 8). This leads to a distance between the images of 2.81 µm. Based on the susception that the ICF is transported into the nucleus, the nucleus region was examined more closely. Suspecting a nucleus of 10 µm, it should be observed in at least three of the images. Since the ninth layer intersects the nucleus approximately in the middle in all samples, this was studied in more detail (figure 5-22).

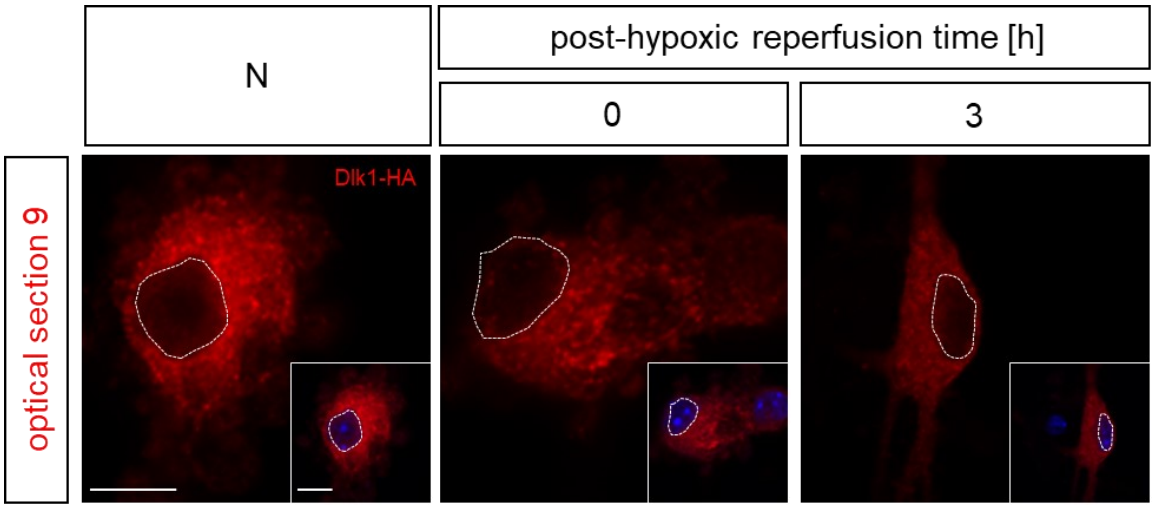

Figure 5-22: *Immunofluorescence of the Dlk1-HA localisation. Confocal images of the Dlk1-HA signal of the selected 9th optical section of cells under normoxia, after 45 min of hypoxia, and after additional three hours of post-hypoxic reperfusion time. Merged staining's of HA and DAPI are implicated. The nucleus was marked by the dashed line to visualise the possible translocation of ICF. The scale bar represents 10 µm. ICF, intracellular fragment; HA, hemagglutinin, N, normoxia.*

Immunostaining of Dlk1-HA on the ninth optical section of the Z-stacks, showed uniformly distributed puncta of the Dlk1 signal in all three conditions (normoxia, post-hypoxic reperfusion time of 0 hour and 3 hours) (figure 5-22). Contrary to the ubiquitously and even signal of td-tomato, Dlk1 is detectable in puncta in different intensities throughout the soma of the cell. This kind of signal is concordant with that obtained using the Dlk1 antibody. However, the nucleus seems to be left out partially. The region of the dashed line, seems to be also Dlk1 positive. However, the signal does not reveal an obvious translocation of the ICF-HA for any condition. Though it has to be noted that the used antibody detects the full-length protein as well as the intracellular part. To gain a better subcellular resolution of the nuclear region, Z-stacks were combined in way that only the nucleus region was considered. To address the differences of the HA antibody exclusively in the nucleus, a maximum intensity projection (MIP) of the Z-stacks of all conditions was produced (Zeiss, Zen 3.0 software). Hereby, the $DAPI^+$ region was determined. This reduced the number of optical sections from 17 to 6-8 images. All nucleus positive optical sections were projected together in the MIP. Afterwards, the area of the nucleus was examined by determining the nucleus in the $DAPI^+$ image. Following this, the same area was used to quantify the pixel intensity of the HA signal (figure 5-23). The signal intensity of the HA-antibody in this area was then plotted relative to normoxia (figure 5-23, B).

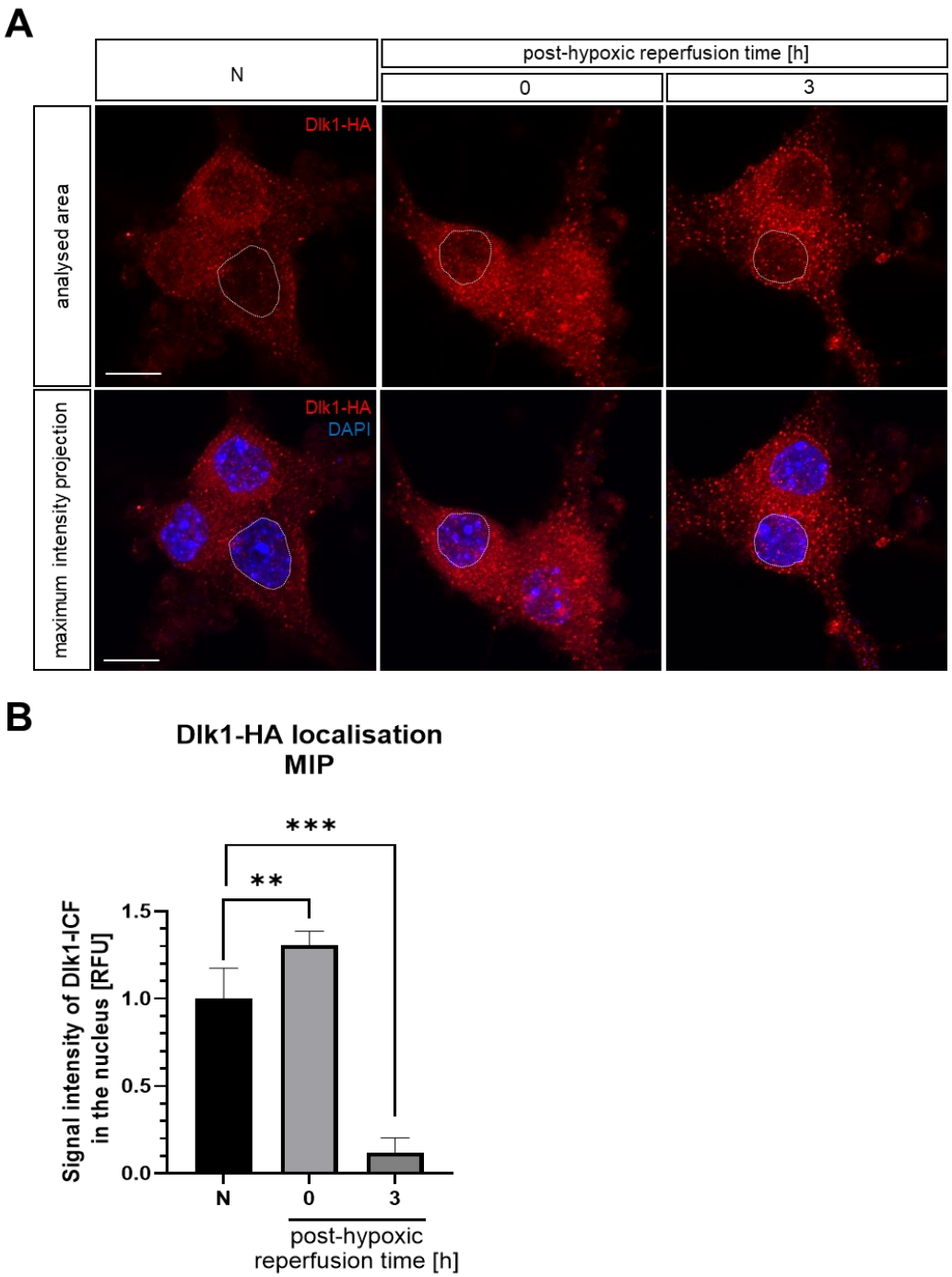

Figure 5-23: *Immunofluorescence analysis of the subcellular Dlk1-HA localisation.* ***A:*** *Confocal images of the nucleus positive optical sections (judged by DAPI staining) of z-stack images of cells in normoxia, post-hypoxia and three hours of post-hypoxic reperfusion time were combined by MIP. The areal of the nucleus was determined based on the DAPI counterstaining (dotted line). The scale bar represents 10 µm.* ***B:*** *Quantification of the HA signal intensity in the nuclear region (dotted line in A). Quantifications were performed on four (N), six (0h), and three (3h) cells with t-tests (** P<0.005; *** P<0.001). HA, hemagglutinin; ICF, intracelular fragment; MIP, maximum intensity projection; RFU, relative fluorescence unit.*

The quantification of the detected HA signal intensity exclusively in the nucleus (figure 5-23, A) revealed a significant increase directly after hypoxia (figure 5-23, B). Interestingly, after the

three hours post-hypoxic reperfusion time, the signal was significantly reduced. This reduction was around 90 % of the normoxia level (figure 5-23, B). The increased ICF-HA after hypoxia detected in western blot (figure 5-21, D) without an obvious alteration of *Dlk1* expression levels (figure 5-10, C) showed that hypoxia can alters the post-translational processing of Dlk1. Further, the observed increase in nuclear signal of the Dlk1-HA immunofluorescence (figure ***5-23***, B) might be indicative of a translocation of the ICF into the nucleus directly after hypoxia. This could explain the gene alterations for the fast αMN properties.

5.5.3. Dlk1 cleavage might act as transcription factor to mediate Matrix metalloprotease gene expression

In the previous experiments, it was shown, that the ICF-HA is cleaved and subsequentially translocated into the nucleus. There, the ICF-HA might act as transcription factor to alternate specific genes expression to promote fast αMN properties. One of the suspected target genes is the matrix metalloprotease IX (Mmp9). *Mmp9* gene regulation is associated with Dlk1-independent processes, like matrix formation, cell metabolism and tissue invasion (Ingraham *et al.*, 2011) and in Dlk1-dependent processes in cancer cell regulations (Li *et al.*, 2014; Grassi, Pantazopoulou and Pietras, 2020). The question arose, whether the *Mmp9* gene expression and/or the Mmp9 protein processing could also be dependent on Dlk1 cleavage in ESC-derived MNs or if this effect was specific to cancer cells. To address the influence of a hypoxia-induced Dlk1 cleavage on the *Mmp9* gene regulation or Mmp9 protein processing, semi-qRT PCR and immunofluorescence staining's were performed.

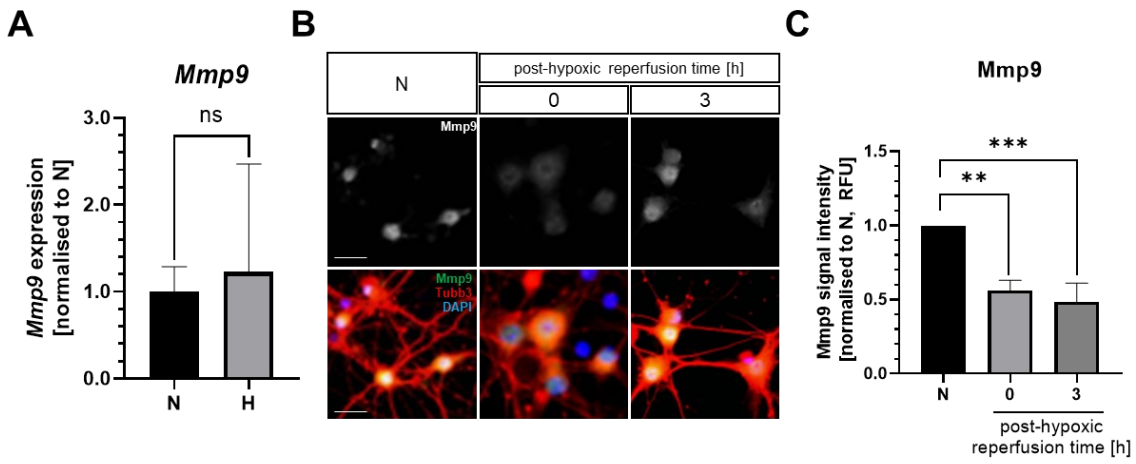

Figure 5-24: *Hypoxia-induced Mmp9 regulation.* ***A:*** *Hypoxia-induced Mmp9 gene expression was analysed after hypoxia in relation to normoxia and plotted normalised to the housekeeper Pmm2. Quantifications were tested with independent t-test, n = 3.* ***B:*** *Representative grey scale images of immunofluorescence Mmp9 staining after post-hypoxic and three hours of post-hypoxic reperfusion time compared to normoxia (upper row) and merged images with staining of Mmp9, Tubb3 and DAPI (lower row). The scale bar represents 20 µm.* ***C:*** *Quantification of Mmp9 signal intensity in the different conditions. A total number of 100 cells were analysed per condition. Quantifications were tested with the one-way ANOVA analysis, n = 3 (** P<0.005; *** P<0.001). H, hypoxia; Mmp9, matrix metalloprotease; N, normoxia; Pmm2, Phosphomannomutase 2; RFU, relative fluorescence unit; Tubb3, Tubulin Beta 3 Class III.*

Comparing *Mmp9* gene expression in normoxia and post-hypoxia, *Mmp9* expression is slightly, but not significantly increased after hypoxia compared to normoxia (figure 5-24, A). Subsequently, hypoxia-induced alteration in the Mmp9 protein regulation were further analysed by comparing the immunofluorescence signal intensities in normoxia, post-hypoxia and the three hours post-hypoxic reperfusion time. The signal intensity is most intense in the normoxia condition, whereas the signal is significantly reduced after the hypoxia (figure 5-24, B and C). After the post-hypoxic reperfusion time, the signal intensity is even more reduced compared to post-hypoxia.

5.6. Dlk1 cleavage mediated by Adam17

Dlk1 is reported to be cleaved by the protease Adam17 (Smas, Green and Sul, 1994). Adam17 is a membrane bound metalloprotease. It is involved in multiple processes of the body function and development (Zunke and Rose-John, 2017). So far, Adam17 has more than 80 substrates, from cytokines, growth factors, receptors and many cell adhesion molecules (Scheller *et al.*, 2011). It is believed that 10 % of all cell surface proteins are proteolytically cleaved by Adam17 to release a soluble protein (Kawahara *et al.*, 2014; Zunke and Rose-John, 2017). One of those cell membrane substrates is Dlk1 (Wang and Sul, 2006). Depending on the Dlk1 variant, there can be multiple cleavage sites in the Dlk1 protein. There are up to two cleavage sites at the ECD, as well as one in the juxtamembrane region and another one more distally in one of the EGF repeats (figure 1-5) (Wang and Sul, 2006; Wang *et al.*, 2006; Grassi and Pietras, 2022).

Furthermore, another cleavage site is reported to be intracellularly (Subhashini, 2016). The cleavage of the ECD of Dlk1 has been extensively reported (C. H. Jensen *et al.*, 1994; Smas, Green and Sul, 1994; Wang and Sul, 2006; Ferrón *et al.*, 2011; Traustadóttir *et al.*, 2019). However, little is known about the dynamics of the ICF cleavage. In a recent experiment, the juxtamembrane region was deleted, which includes one of the cleavage sites of Adam17. This deletion was leading to a membrane-bound Dlk1 (Grassi, Pantazopoulou and Pietras, 2020). The comparison of membrane-bound Dlk1 and cleavable Dlk1 revealed the importance of the cleavage for tissue invasiveness and migration in glioma cells (Grassi, Pantazopoulou and Pietras, 2020). Thereafter, the cleavage of Dlk1 by Adam17 was investigated in the following experiments.

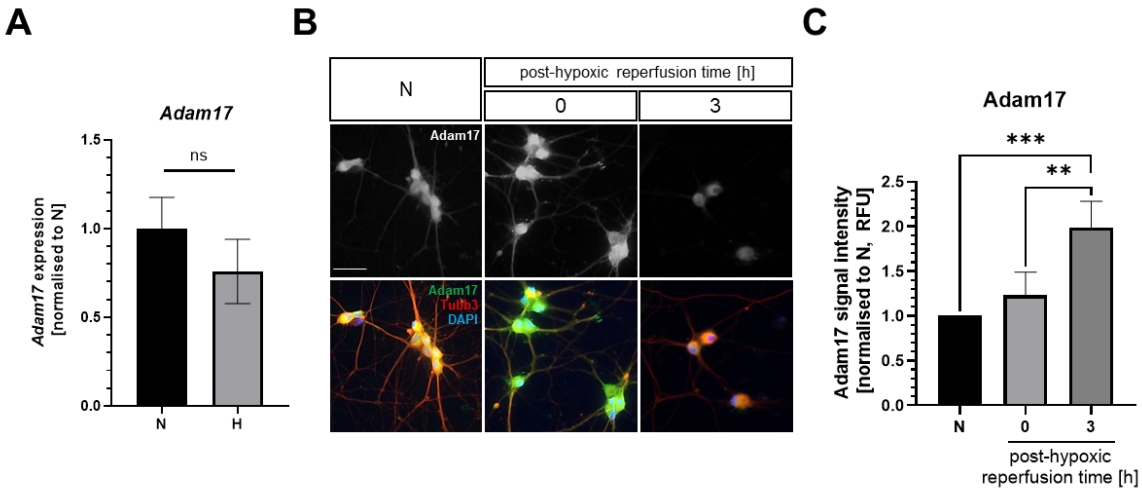

Figure 5-25: *Hypoxia-induced regulation of Adam17.* ***A:*** *Hypoxia-induced Adam17 gene expression was analysed after hypoxia in relation to normoxia and plotted normalised to the housekeeper Pmm2. Quantifications were tested with independent t-test, n = 4.* ***B:*** *Immunofluorescence staining's of Adam17 (gray scale in top row, green in bottom row) and Tubb3 (red in bottom row) under normoxia, after 45 min of hypoxia, and after hypoxia with additional three hours of post-hypoxic reperfusion time. Counterstaining with DAPI. Scale bar represents 20 µm.* ***C:*** *Quantification of Adam17 signal intensity in the different conditions. A total number of 100 cells per condition were analysed with the ordinary one-way ANOVA, n = 4 (** P< 0.005; *** P<0.001). H, hypoxia; N, normoxia; Pmm2, Phosphomannomutase 2; RFU, relative fluorescence unit; Tubb3, Tubulin Beta 3 Class III.*

Adam17 is one of the proteases cleaving Dlk1 at the ECD and the TM region (Smas, Green and Sul, 1994; Wang and Sul, 2006). The activity of the Adam17 secretase is known to be influenced by hypoxia (Wang, Feng and Li, 2013; Lian *et al.*, 2019). In ESC-derived MNs, hypoxia induced no significant differences in the expression of *Adam17* after 45 min of hypoxia compared to normoxia (figure 5-25, A). Given that the gene expression was not found to be affected, the Adam17 protein was analysed by immunofluorescence staining (figure 5-25, B) and the signal intensities quantified (figure 5-25, C). The detected signal intensities for Adam17 were only slightly elevated after hypoxia, but significantly increased after three hour of post-hypoxic reperfusion time compared to normoxia.

5.6.1. Dlk1 cleavage inhibition by siRNA

The previous results suggest a stabilisation of Adam17 by hypoxia. However, it is reported, that Adam17 is cleaving Dlk1. To analyse this possibility, *Adam17* was knocked down by a short interference RNA (siRNA) directly in ESC-derived MNs. ESCs were differentiated over 18-22 days and then transfected with *control* (*ctr*) siRNA and *Adam17* siRNA 48 hours prior hypoxic stimulation (see 4.2.4.3.).

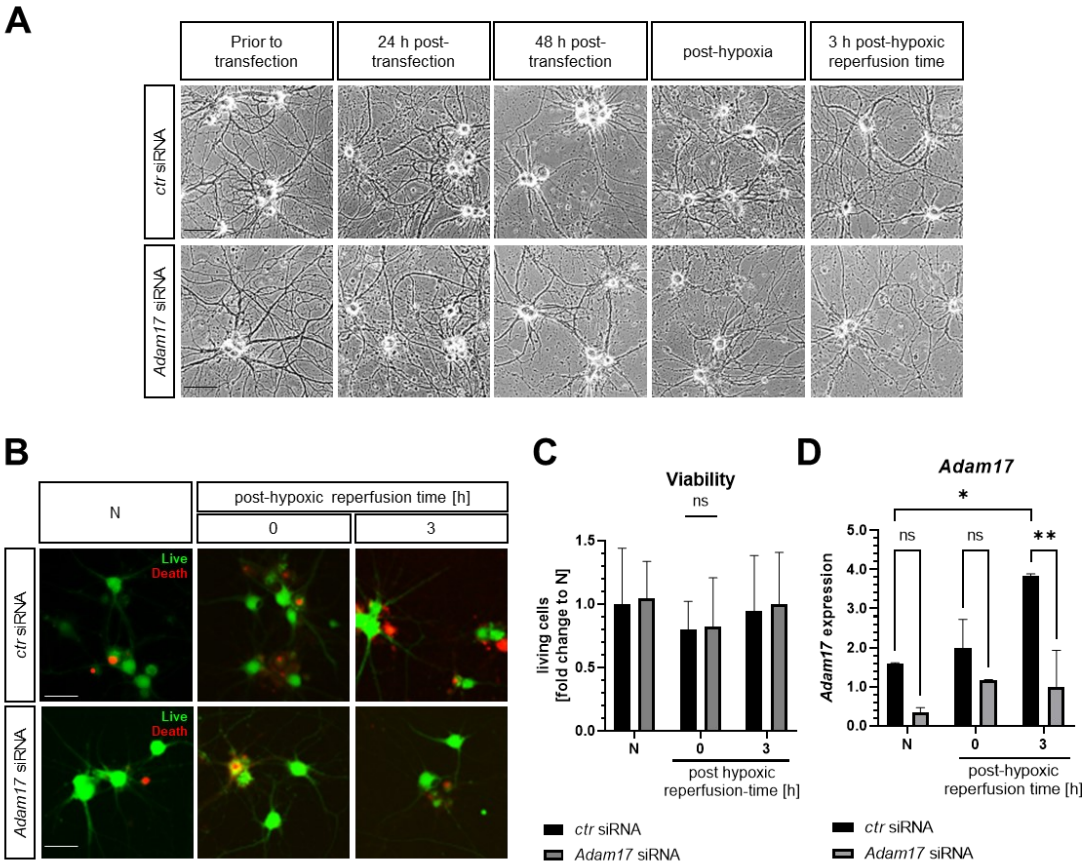

Figure 5-26: *Knockdown of Adam17 by siRNA does not impact on cell morphology and viability.* ***A:*** *Phase contrast images of MN networks before transfection and hypoxia, and after transfection either with an Adam17 siRNA or a ctr siRNA 24- and 48 hours post-transfection, after hypoxia, and after three hours of post-hypoxic reperfusion time. Scale bar represent 20 µm.* ***B:*** *Live-Death assay stains living cells with Calcein AM (green) and dead cells with Ethidium-Homodimer-1 (red). Staining's were compared between normoxia (N), directly after hypoxia, and after three hours post-hypoxic reperfusion time. Scale bar represent 25 µm.* ***C:*** *Quantification of living cells in the Live-Death staining (B). Living cells were shown relative to the number of living cells under normoxia in cells transfected with the ctr siRNA. Quantifications were tested with the one-way ANOVA analysis. n = 2.* ***D:*** *Hypoxia-induced Adam17 gene expression was analysed after hypoxia and post-hypoxic reperfusion time in relation to normoxia in MNs transfected either with control or Adam17 siRNA. Those samples were plotted normalised to the housekeeper Pmm2 (* P<0.05, **P<0.005). Quantifications were tested with the one-way ANOVA analysis. n = 2. ctr, control; H, hypoxia; N, normoxia, Pmm2, Phosphomannomutase 2, siRNA, short interference RNA.*

The morphology of the MNs was observed before and after siRNA transfection, as well as directly after hypoxia and after post-hypoxic reperfusion time (figure 5-26, A). The morphology

of the MNs showed no differences regarding density, adhesion to the dishes or morphology of the neurites, neither for transfected *Adam17* siRNA nor of *control (ctr)* siRNA. The regular observation of the MNs under normoxia, after hypoxia and after three hours post-hypoxic reperfusion time were amended with a Live-Death staining (see 4.2.4.3.) (figure 5-26, B). No obvious differences between *ctr* and *Adam17* siRNA transfected cells or between the conditions could be detected, which was supported by the quantification of the Calcein AM (green) fluorescence signal marking the living cells (figure 5-26, C). Compared to normoxia, the number of living cells was not significantly different at normoxia, post-hypoxia or post-hypoxic reperfusion time irrespective of the transfected siRNA. Semi-qRT PCR revealed that *Adam17* transcripts were significantly reduced after knockdown with *Adam17* siRNA, compared to transfections with *ctr* siRNA 48 hours after the transfection (figure 5-26, D). The *ctr* siRNA led to an increase of *Adam17* mRNA levels after hypoxia, which became significant after three hours of post-hypoxic reperfusion time compared to normoxia. Using the RNAi pathway with *Adam17*-specific siRNAs, a knockdown to 80 % in normoxia was measured (figure 5-26, D). Furthermore, the knockdown directly after hypoxia was less efficient compared to normoxia condition. The difference between the *Adam17* mRNA levels in MNs transfected with *ctr* siRNA, compared to MNs transfected with Adam17 was about 40 %. After three hours post-hypoxic reperfusion time, a knockdown efficiency of 80 % could be detected by calculating the relative transcript level after *ctr* siRNA transfections of each time point and calculated the relative mRNA level after transfected with *Adam17* siRNA (figure 5-26, A). The knockdown of *Adam17* resulted in increased signal intensities compared to the control. Interestingly, after three hours of post-hypoxic reperfusion time, when the knockdown efficiency for *Adam17* was highest, similar band intensities for the full-length Dlk1 as well as ICF-HA were observed between the *Adam17* knockdown and *ctr* siRNA transfected cells.

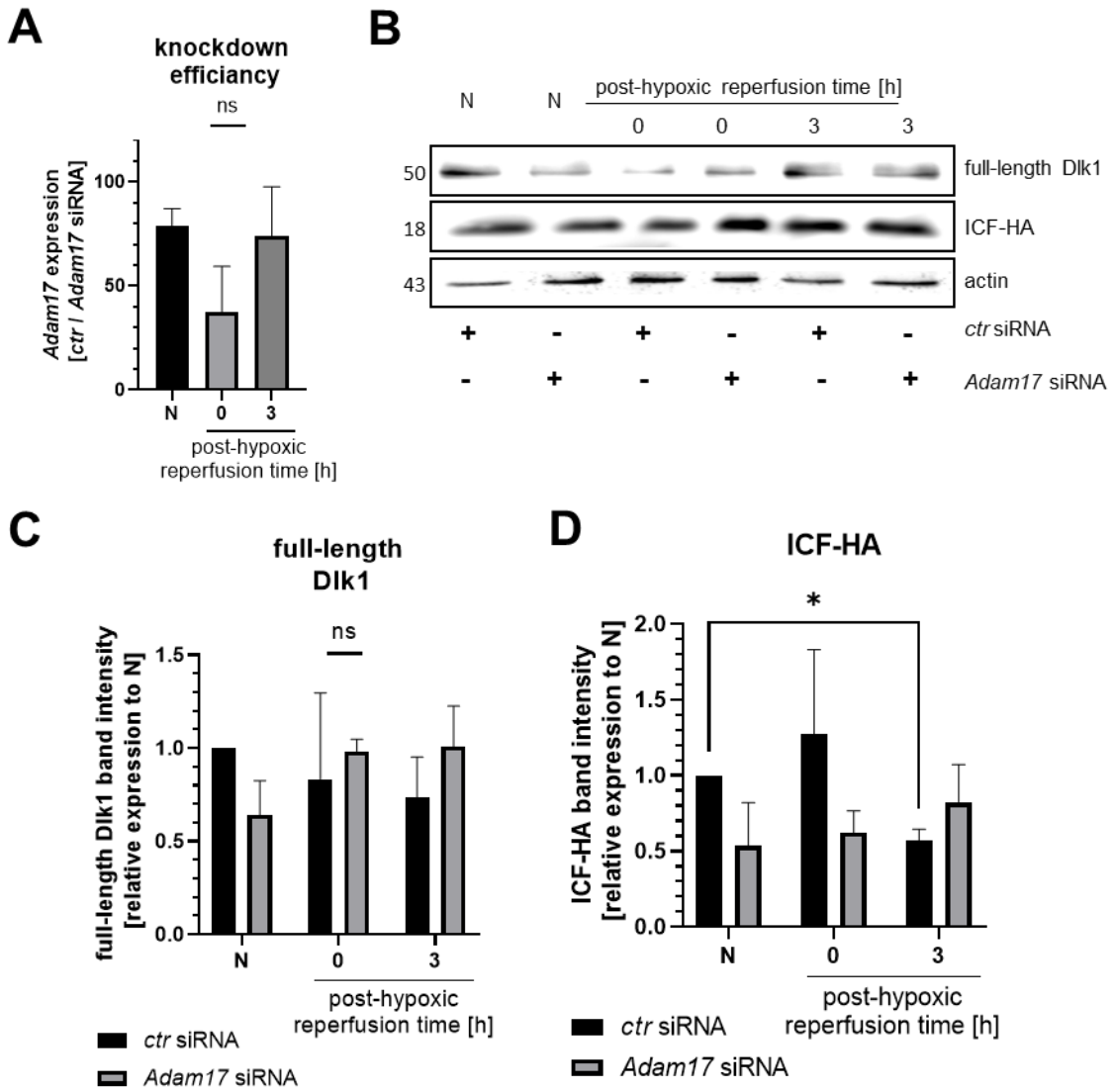

Figure 5-27: *Knockdown of Adam17 in MN networks under hypoxia.* ***A:*** *Calculated Adam17 knockdown efficiency. From semi-qRT PCR results (figure 5-26, D), the reduction of mRNA level for every time point was plotted.* ***B:*** *Representative western blot of MN networks, either with Adam17 knockdown or with ctr siRNA transfection, under normoxia, directly after hypoxia, and after three hours post-hypoxic reperfusion time. Transfection with ctr or Adam17 siRNA respectively is indicated below.* ***C:*** *Quantification of the full-length Dlk1 band intensity in normoxia, post hypoxia, and three hours post-hypoxic reperfusion time, in transfected MNs with Adam17 siRNA and control siRNA. n = 3* ***D:*** *Quantification of the ICF-HA band intensity in normoxia, post-hypoxia, and three hours post-hypoxic reperfusion time, in transfected MNs with Adam17 siRNA and control siRNA. n = 3. Actin was used as loading control. Quantifications were tested with the two-way ANOVA analysis (* P<0.05). ctr, control; ICF, intracellular fragment; N, normoxia; siRNA, short interference RNA.*

The knockdown resulted in a reduction of *Adam17* mRNA levels after hypoxic stimulation (figure 5-27, A). Therefore, the hypoxia-induced Dlk1 cleavage was further analysed by performing western blot analysis (figure 5-27, B). Under normoxia, the western blot of whole cell population lysates of MNs transfected with *Adam17* siRNA showed less signal for the full-length Dlk1, compared to MNs transfected with *ctr* siRNA (figure 5-27, C). This trend reversed

after oxygen deprivation. With the transfection of the *Adam17* siRNA, there was more full-length Dlk1 compared to the control MNs transfected with *ctr* siRNA. With the additional three hours of post-hypoxic reperfusion time, the full-length Dlk1 was even more reduced in the control MNs, compared to the MNs transfected with *Adam17* siRNA. Those MNs showed a comparable level of the full-length Dlk1 as after the acute phase of hypoxia, which is higher compared to normoxia. The hypoxia-induced effects were comparable to those from previous experiments (figure 5-21). Additionally, the ICF-HA was investigated. The transfection of *Adam17* siRNA was leading to a decrease in the protein levels in normoxia conditions (figure ***5-27***, D). With hypoxic stimulation, the control MNs transfected with *ctr* siRNA showed a higher ICF-HA level compared to normoxia. Whereas, the MNs, transfected with *Adam17* siRNA show less ICF-HA level, compared to the control MNs. After three hours of post-hypoxic reperfusion time, the level of ICF-HA was similar in the control and *Adam17* knockdown MNs. The amount of ICF-HA in control MNs was higher than after post-hypoxic stimulations. Taken together, the MNs transfected with *ctr* siRNA are showing similar effects for the full-length Dlk1 and the ICF-HA compared to previous results.

5.6.2. Inhibition of Dlk1 cleavage by Adam17 inhibitor TMI-1

5.6.2.1. Establishing Adam17 inhibitor TMI-1

Previously, it was shown that hypoxia induction leads to an increase in the signal intensity of Adam17, while the knockdown of Adam17 appeared to reduce Dlk1 cleavage. To further investigate the activity of Adam17 in Dlk1 processing, an Adam17 inhibitor was chosen to block Adam17-dependent cleavage. The Thiomorpholine hydroxamate inhibitor (TMI-1) is a potent Adam17 inhibitor, which inhibits successfully LPS-induced TNF-α secretion in human primary monocytes and human blood (Zhang *et al.*, 2004). Additionally, it has been reported that TMI-1 is inhibiting Dlk1 cleavage in high-grade glioma cells (Grassi, Pantazopoulou and Pietras, 2020). The optimal concentration of TMI-1 was first tested by analysing its impact on cell morphology and the effects on full-length Dlk1 in immunoblots and further in comparison to the uncleaved Dlk1-HA and ICF-HA in western blot analysis.

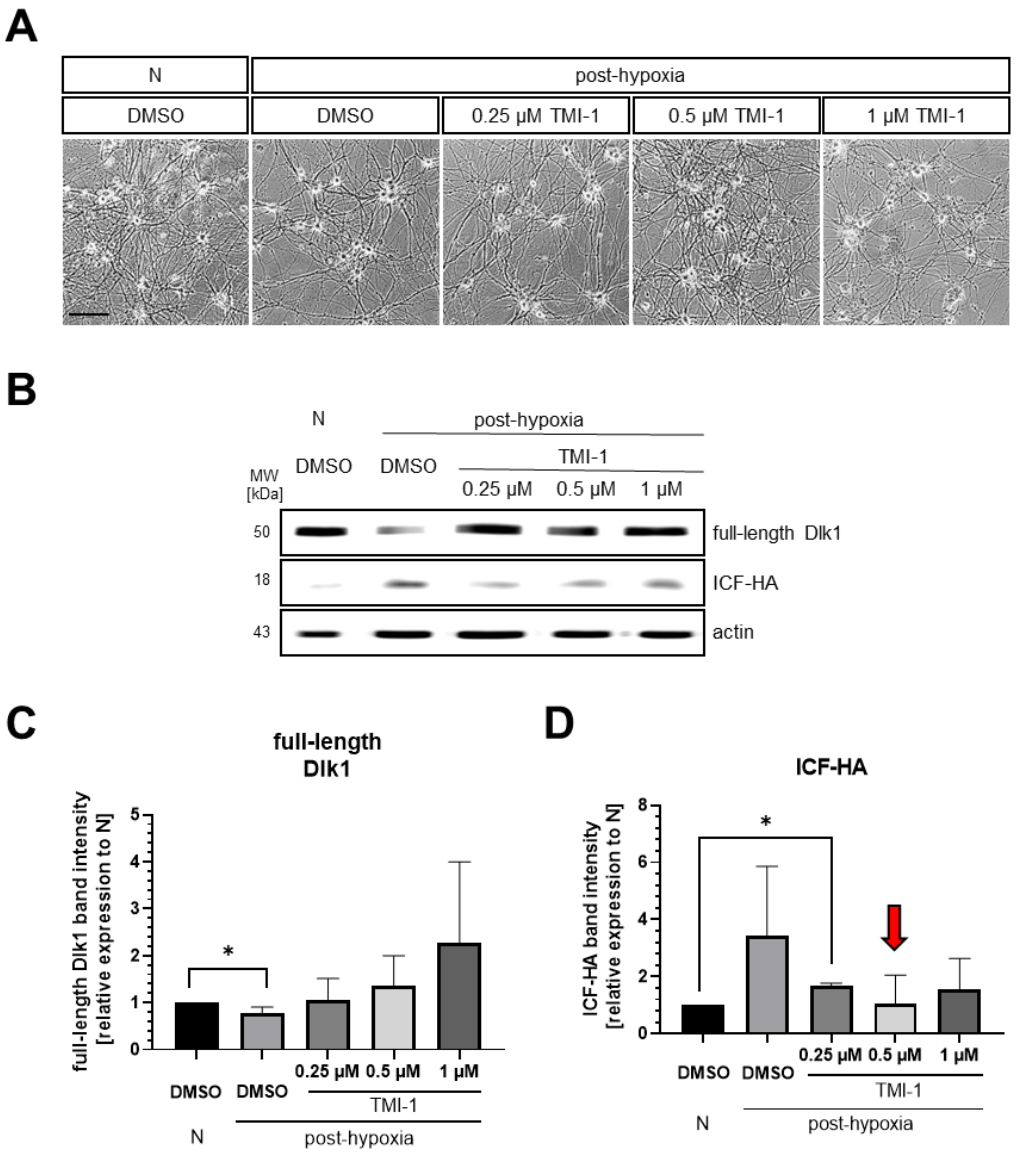

Figure 5-28: *Chemical inhibition of Adam17 by TMI-1.* ***A:*** *Morphological changes of MN network treated with different concentrations of TMI-1 or DMSO as control under normoxia (N) and after 45 min of hypoxia. Scale bar represents 100 µm.* ***B:*** *Representative western blot of whole population protein lysates of MN network in normoxia and post hypoxia, treated with different concentrations of TMI-1 or DMSO as control. β-actin was used as loading control.* ***C:*** *Quantification of the densiometric analysis of full-length Dlk1 signal from B relative to normoxia. n = 2.* ***D:*** *Quantification of the densiometric analysis of ICF-HA signal intensity from B relative to normoxia. n = 2. Arrow indicate the optimal TMI-1 concentration. Significances were tested with T-tests analysis (* P<0.05). ICF, intracellular fragment; HA, hemagglutinin, MW, molecular weight; N, normoxia.*

Treatment of MNs for one hour with the Adam17 inhibitor TMI-1 did not show any obvious changes in the morphology or in the neurite stability for any of the used concentrations in comparison to the untreated DMSO control irrespective of the oxygen conditions (figure 5-28, A). Western blot analysis verified that the full-length Dlk1 was significantly reduced after hypoxic stimulation, compared to normoxia for the DMSO control groups (figure 5-28, C). In contrast, in MNs treated with 0.25, 0.5, and 1 µM of TMI-1 the band intensity for the full-length

Dlk1 increased with higher inhibitor concentrations. As Adam17 activity might result in cleavage of the full-length Dlk1 in the ECD and the ICF-HA, the oxygen deprivation led to an increase of the ICF-HA signal intensity of the DMSO treated control group (figure 5-28, D). While the cells treated with 0.25 µM TMI-1 showed still a significant increase for ICF-HA signal intensity compared to normoxia, this increase was blocked by 0.5 µM and 1 µM TMI-1 treatment. Based on those results and on published data from the group of Pietras (Grassi, Pantazopoulou and Pietras, 2020), all further TMI-1 experiments were performed with a concentration of 0.5 µM TMI-1 for one hour before hypoxia.

After having determined the optimal concentration of the Adam17 inhibition, the experimental setup was established with the TMI-1 concentration of 0.5 µM TMI-1. Therefore, the Hif1α stabilisation was investigated and confirmed by the hypoxia-dependent gene regulation of CaIX and Glut1 for TMI-1 and DMSO control group.

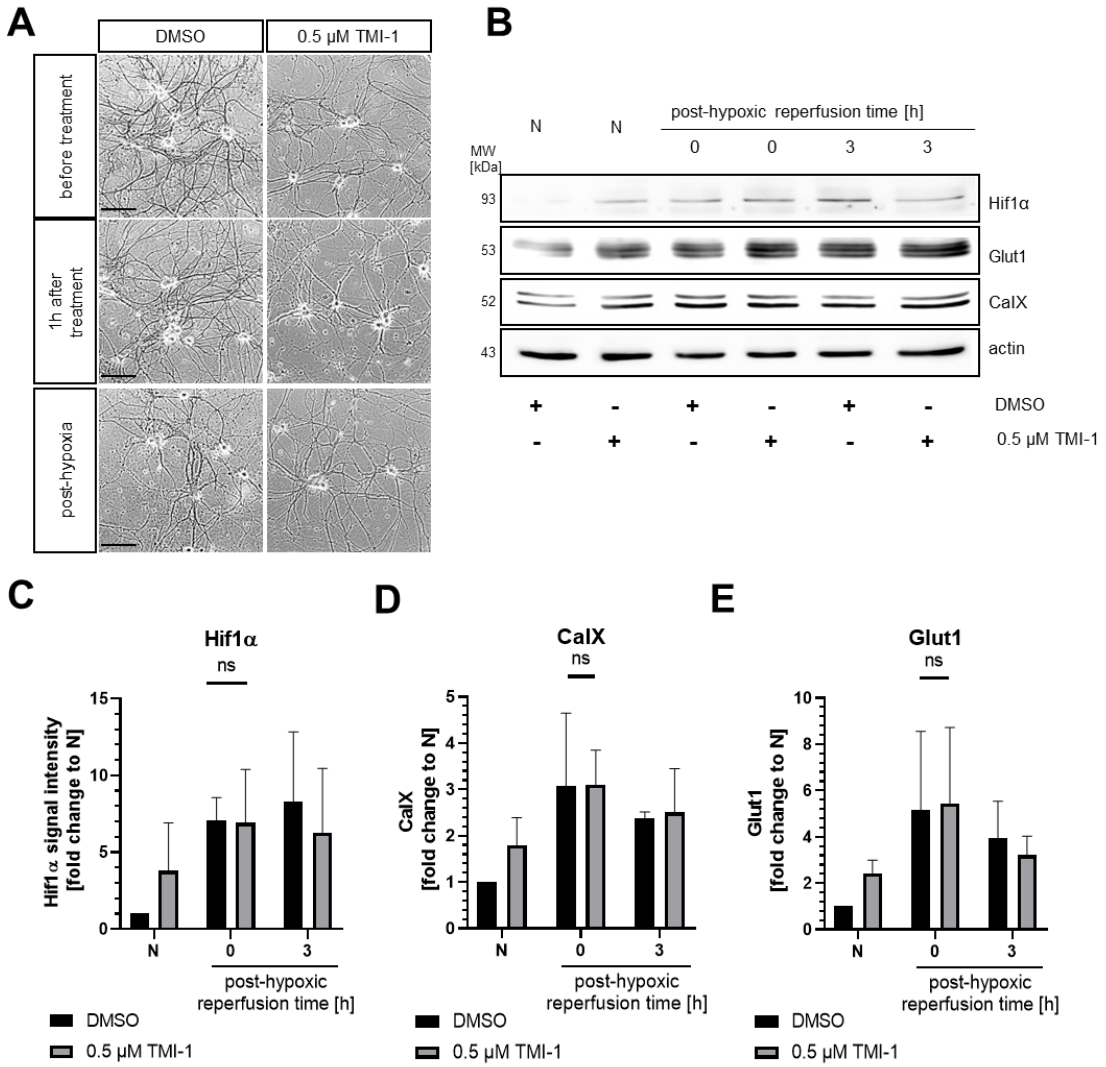

Figure 5-29: *Hif1α response to Adam17 inhibition in ESC-derived motor neuron network.* ***A:*** *Morphological changes of the MN network treated with 0.5 µM TMI-1 and DMSO as control for the time point before treatment, after one hours of treatment and post-hypoxia. Scale bar represents 100 µm.* ***B:*** *Representative western blot for MN network in normoxia, post hypoxia, and three hours post-hypoxic reperfusion time, treated with 0.5 µM TMI-1 compared to DMSO control.* ***C:*** *Quantification of Hif1α stabilisation in normoxia, post hypoxia, and three hours post-hypoxic reperfusion time, treated with 0.5 µM TMI-1 compared to DMSO control. n = 2.* ***D*** *and* ***E:*** *Quantification of CaIX (D) and Glut1 (E) signal intensity in normoxia, post hypoxia, and three hours post-hypoxic reperfusion time, treated with 0.5 µM TMI-1 compared to DMSO control. n = 2. Actin was used as loading control. Significances were tested with two-way ANOVA analysis. HA, hemagglutinin; MW, molecular weight; N, normoxia.*

The ESC-derived MNs did not show any obvious changes in regard to the morphology or network stability when treated with TMI-1 in normoxia, after one hour of treatment or after 45 min hypoxic stimulation (figure 5-29). Next, the Hif1α stabilisation was compared between normoxia, post-hypoxia and three hours of post-hypoxic reperfusion time in treated and untreated MNs. The inhibition of Adam17 has no direct impact on the Hif1α stabilisation (figure ***5-29***, C). In normoxia, Hif1α is increased by treatment with TMI-1, compared to the control. With oxygen deprivation, Hif1α is stabilised more in treated and untreated control MNs

compared to normoxia. Between the two groups, no obvious difference in the signal intensity at post-hypoxia is observed. With the additional three hours of post-hypoxic reperfusion time, Hif1α stabilisation is higher compared to post-hypoxia in untreated control, but treated MNs have less Hif1α stabilised compare to untreated control. For the downstream factors of Hif1α, CaIX and Glut1, TMI-1 treatment seamed to reveal no significance differences (figure 5-29, D and E). In normoxia, MNs showed for both downstream factors a higher signal intensity after Adam17 inhibition, compared to the control group. With the oxygen deprivation, CaIX and Glut1 were even expressed at higher levels, compared to the treated group in normoxia. There was no difference in the expression levels between the treated and the control group in post-hypoxia and also not after the three additional hours of post-hypoxic reperfusion time. For both factors, the signal was slightly decreased after the three hours of post-hypoxic reperfusion time, compared to the post-hypoxic condition.

5.6.2.2. Hypoxia-induced Dlk1 cleavage inhibited by Adam17 inhibitor

After establishing the experimental setup for the Adam17 inhibition using TMI-1 its effects on Dlk1 regulations were analysed. It was concluded that the Dlk1 antibody, which is binding Dlk1 at the N-terminus, can only detect the full-length Dlk1 and the ECD of Dlk1 (figure 5-20). As Dlk1 is cleaved by Adam17 and the cleaved ECD is released into the intracellular space, it is washed away with the supernatant in the experimental approach used. Therefore, only the uncleaved full-length Dlk1 is detectable. Therefore, only the direct impact on the full-length Dlk1 was considered by inhibiting Adam17 one hour prior to hypoxic stimulation. Control MNs were treated with the similar volume of DMSO as the volume in which 0.5 µM TMI-1 was dissolved.

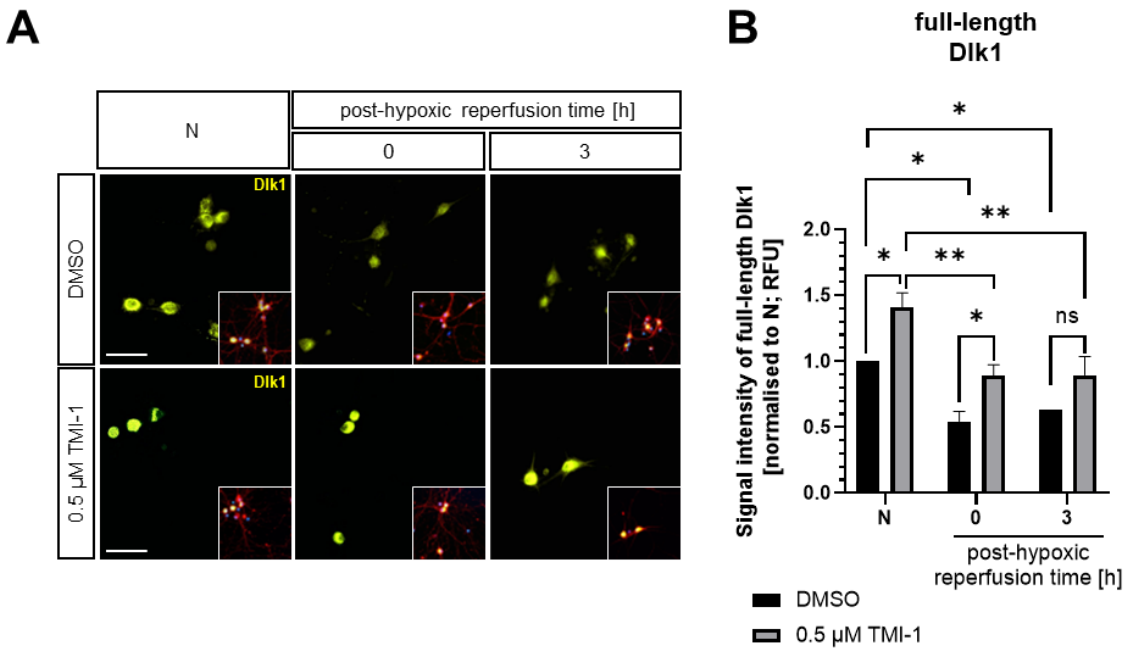

Figure 5-30: *Immunofluorescence of the full-length Dlk1 after inhibition of Adam17.* ***A:*** *Representative images of the full-length Dlk1 signal intensity at normoxia, after 45 min of hypoxia, and additional three hours of post-hypoxic reperfusion time (upper row) and with treatment of 0.5 µM TMI-1 for one-hour prior hypoxia (lower row).* ***B:*** *Quantification of the signal intensity of the full-length Dlk1 in total number of 100 cells per condition normalised to MNs, treated with DMSO under normoxic conditions. Quantifications were tested with a one-way ANOVA, n = 3 (* P<0.05, ** P<0.005). The scale bar represents 20 µm. Additional statistical analysis are displayed in the supplement figure 9. N, normoxia; RFU, relative fluorescence units.*

The full-length Dlk1 signal intensity was higher after treating the cells with TMI-1, compared to the control cells in normoxia (figure 5-30, supplement figure 9). After the cells have been deprived of oxygen, untreated cells showed a significantly decreased signal intensity compared to normoxia. Whereas the cells treated with TMI-1 show less decrease in the signal intensity compared to the control DMSO treated MNs. After the three hours of post-hypoxic reperfusion time, DMSO and TMI-1-treated MNs showed similar signal intensities for the full-length Dlk1. Nevertheless, the signal intensities in both conditions were higher compared to the signals after the acute period of hypoxia, but less intense compared to normoxia in the DMSO treated MNs (figure 5-30, B). Further, these results were also verified in western blot

and the analysis extended to the ICF-HA cleavage after Adam17 inhibition (figure 5-31).

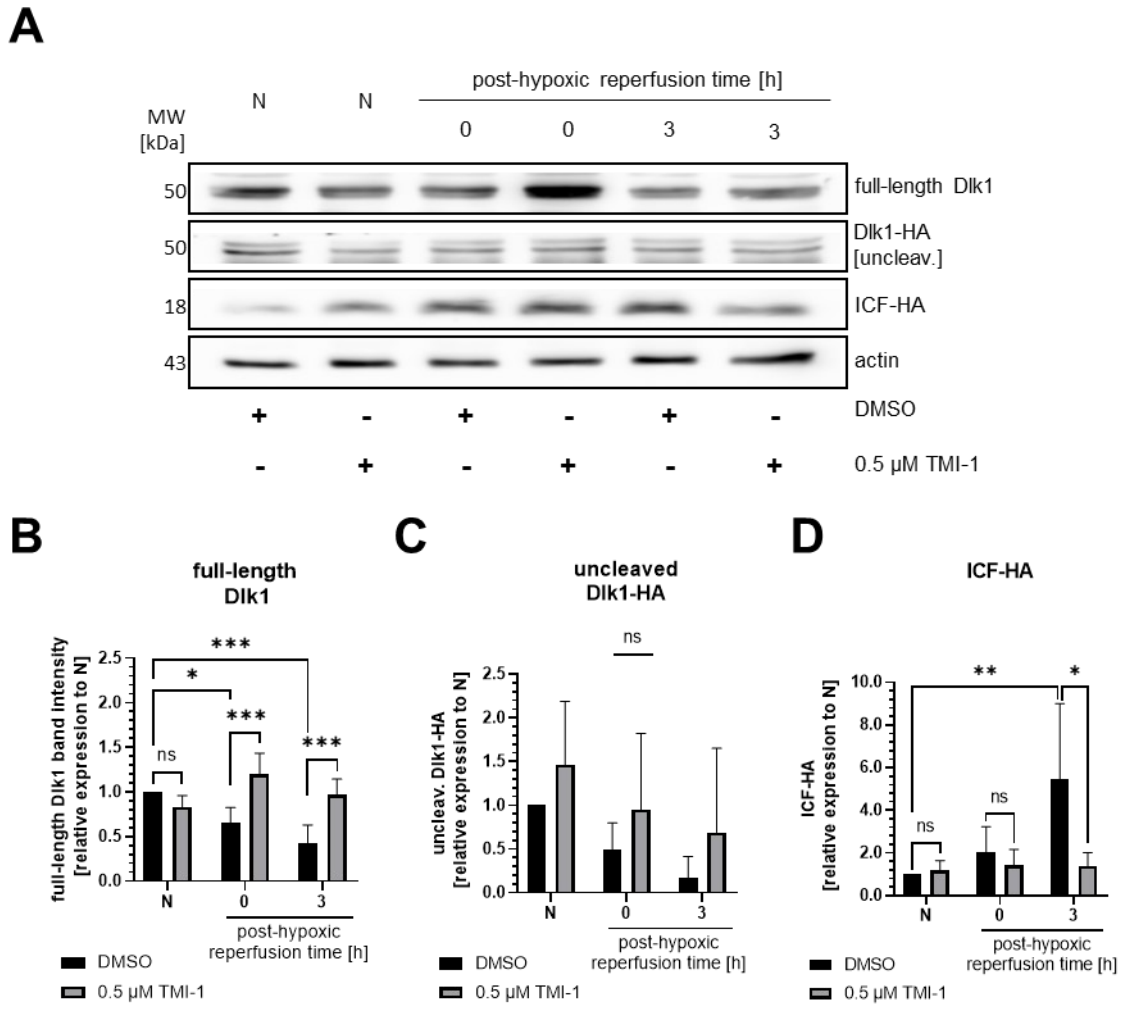

Figure 5-31: *Dlk1 cleavage after hypoxic stimulation.* ***A:*** *Representative western blot for samples either treated with TMI-1 or with DMSO under normoxia (N), 45 min of hypoxia, or three hours of post-hypoxia reperfusion time.* ***B:*** *Quantification of full-length Dlk1 signal intensity after hypoxia and reperfusion time compared to normoxia treated with DMSO, n = 3* ***C:*** *Quantification of uncleaved Dlk1-HA signal intensity after hypoxia and reperfusion time compared to normoxia treated with DMSO, n = 3* ***D:*** *Quantification of ICF-HA signal intensity after hypoxia and reperfusion time compared to normoxia treated with DMSO, n = 3. Actin was used as loading control. Quantifications were tested with a two-way ANOVA (* P<0.05, ** P<0.005; *** P<0.001). Further significances are displayed in the supplement figure 10. MW, molecuar weight; ICF, intracellular fragment.*

The full-length Dlk1 was significantly reduced in the untreated cells post-hypoxia, compared to normoxia. Whereas, cells treated with 0.5 µM TMI-1 showed unaffected band intensities after hypoxia and after three hours of post-hypoxic reperfusion time, compared to normoxia (figure ***5-31***, B). The uncleaved Dlk1-HA showed an increase in cells after the hypoxic stimulation, compared to normoxia. The TMI-1-treated MNs, as well as the untreated MNs both showed increased uncleaved Dlk1-HA band intensities compared to normoxia. After the three hours of post-hypoxic reperfusion time, both conditions showed a decrease in the uncleaved Dlk1-HA band intensities, compared to the normoxia (figure 5-31, C). The ICF-HA revealed a slight

increase in the band intensities between the normoxia and post-hypoxia and further also a significant increase after the three hours of post-hypoxia reperfusion time (figure 5-31, D). Nevertheless, cells which were treated with 0.5 µM TMI-1 revealed no increase in the band intensity compared to the DMSO control group for the normoxia and post-hypoxia. Whereas after three hours of post-hypoxic reperfusion time there is a significant reduction in ICF-HA treated with 0.5 µM TMI-1, compared to the DMSO-treated MNs (figure 5-31, D). Taken together, the results suggest that Dlk1 is cleaved by Adam17 and that the ICF-HA is enriched in the hypoxic-stimulated MNs.

5.6.2.3. Mmp9 segregation is independent on hypoxia-induced Dlk1 cleavage

Previous results showed that hypoxia is influencing *Mmp9* gene expression (figure 5-24). Further it was reported that the ICF-HA could act as transcriptional co-factor to induce *Mmp9* expression. To address the question whether Dlk1 cleavage could alternate Mmp9 protein expression or its processing, Dlk1 cleavage was inhibited by TMI-1 and Mmp9 protein expression was analysed.

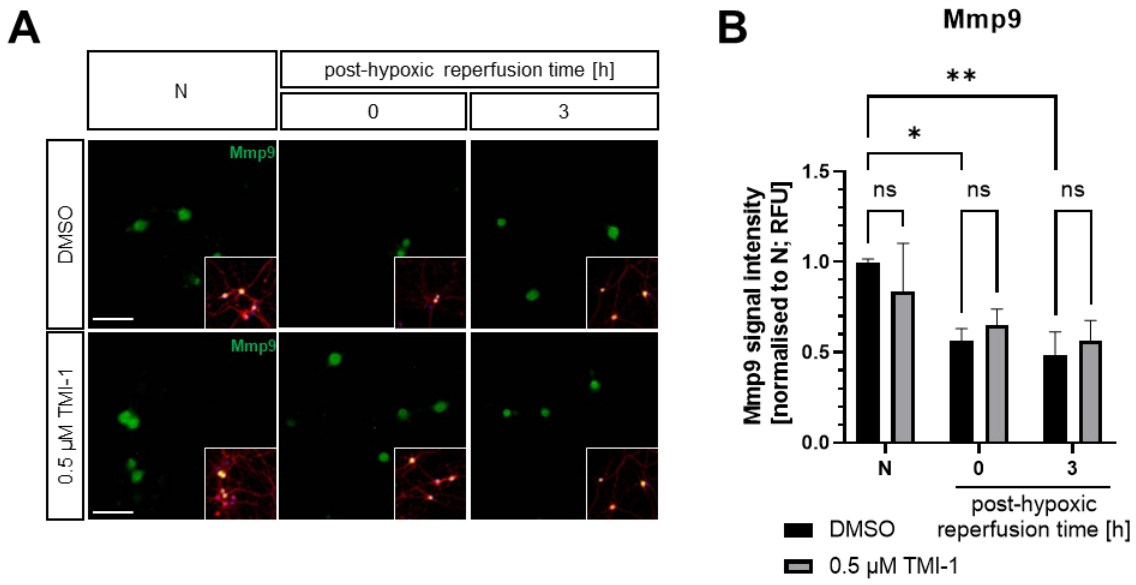

Figure 5-32: *Hypoxia-induced Mmp9 regulation in ESC-derived motor neuron network with Adam17 inhibition.* ***A:*** *Representative immunofluorescence images of Mmp9 signal intensity after 45 min of hypoxia and additional three hours of post-hypoxic reperfusion time compared to normoxia (upper row) and with treatment of 0.5 µM TMI-1 for one-hour prior hypoxia (lower row). Inserted pictures are merged images of Mmp9 (green); Tubb3 (red); and DAPI staining. Scale bar represents 20 µm.* ***B:*** *Quantification of the signal intensity of the full-length Dlk1 in total number of 300 cells per condition displayed normalised to nomoxia treated with DMSO, n = 3. Quantifications were tested with a two-way ANOVA (* P<0.05, ** P<0.005). Additional quantifications are displayed in the supplement figure 11. Mmp9, matrix metalloprotease 9; RFU, relative fluorescence unit; Tubb3, Tubulin Beta 3 Class III.*

Immunofluorescence signal intensity comparison revealed a significant reduction in the Mmp9 signal intensity after hypoxia for DMSO control cells, but not for treated cells: for the three

hours for post-hypoxic reperfusion time, both conditions were significantly reduced compared to normoxia (figure 5-32, supplement figure 11). For both time points of post-hypoxia and post-hypoxic reperfusion time, cells treated with the Adam17 inhibitor showed higher signals compared to the DMSO control group.

5.7. *Dlk1$^{\Delta ICF}$* ESC-derived MNs show similar proportion of Mmp9^{+} MNs

The working hypothesis was that Dlk1 is cleaved intracellularly followed by the translocation of the Dlk1-ICF into the nucleus and thereby an activation of presumably fast αMN-specific Dlk1 target genes. To analyse if the cleaved ICF had an effect on the fast αMN gene expression, Dlk1-HA ESCs and the Dlk1$^{\Delta ICF}$ ESC lines (created by Dr. M. Marks) were differentiated into MNs and at day 18-22 immunostained for ChAT and Mmp9. ChAT staining was used to mark MNs and Mmp9 to label the fast and larger intermediate αMN subpopulation (Kaplan et al., 2014). Hereafter, the number of Mmp9^{+}/ ChAT^{+} cells were compared between the Dlk1-HA and the Dlk1$^{\Delta ICF}$ cell lines. The two Dlk1$^{\Delta ICF}$ mESC line were generated by CRISPR/Cas9-mediated gene targeting (see 3.2.1 and figure 3-2). The CRISPR target site in the *Dlk1* locus was cleaved, and indirect repair resulted in a frame-shift in which stop codons assured premature termination of the translation. Thereby, different variant of the truncated form of Dlk1 missing the ICF were generated. These different variants were used as internal control.

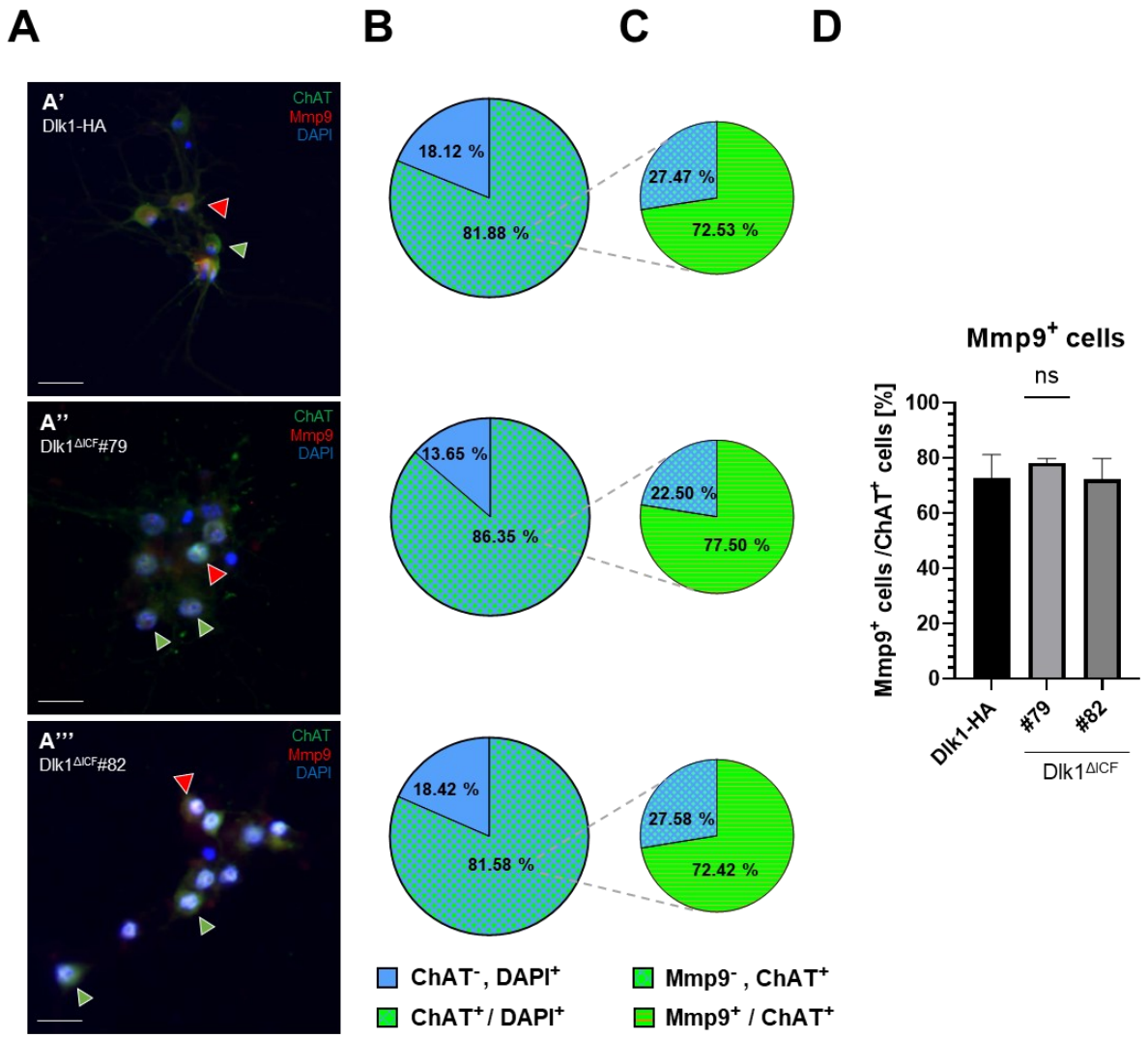

Figure 5-33: *Mmp9⁺ cell proportion in Dlk1 modified ESC-derived MN population.* ***A:*** *Representative images of ChAT (green); Mmp9 (red) and DAPI (blue) staining in Dlk1-HA and Dlk1$^{\Delta ICF}$ cell lines (#79; #82). The scale bar represents 20 µm.* ***B:*** *Quantification of ChAT^{+} cells (blue-green checked) per total number of cells (DAPI^{+}; blue).* ***C:*** *Mmp9^{+} cells (green-orange striped) per ChAT^{+} cells (blue-green checked).* ***D:*** *Bar graph of Mmp9^{+} and ChAT^{+} cells per total number of ChAT^{+} cells with statistical analysis. total number of 500 cells per condition. Quantifications were tested with a t-test analysis, n = 3. ChAT, Choline Acetyltransferase; ICF, intracellular fragment; HA, hemagglutinin; Mmp9, matrix metalloprotease.*

The ratio of ChAT^{+} cell per total cell number for the wild-type *Dlk1-HA* cell line was found to be around 80 %, while the Dlk1$^{\Delta ICF}$ cell lines showed similar results in the ratios of Chat^{+}/ DAPI^{+} cells (figure 5-33, A and B). The Dlk1$^{\Delta ICF}$#72 cell line had 86.35 % of Chat^{+}/ DAPI^{+} cells. Also, the Dlk1$^{\Delta ICF}$#82 cell line had 81.58 % of ChAT^{+}/ DAPI^{+} cells. In summary, no differences were observed in the ratio of ChAT $^{+}$ cells and DAPI^{+} (total) cells, indicating that the differentiation of MNs *per se* seemed to have been independent of Dlk1-ICF. Immunostainings for Mmp9 were used to test whether the generation of the Dlk1-dependent fast-like αMN subtype was affected (figure 5-33,A and C). ChAT $^{+}$ and Mmp9^{-} cells were indicative of slow-like αMNs,

βMNs, or γMNs (Kaplan *et al.*, 2014) (figure 5-33, C; blue-green arrows), while ChAT^{+} and Mmp9^{+} double-positive cells represented fast and intermediate-like αMNs (figure 5-33, C; green-orange stripes). The Dlk1-HA cell line had around 72,53 % of Mmp9^{+}/ ChAT^{+} cells, whereas the *Dlk1*$^{\Delta ICF}$ cell lines showed 77,50 % (Dlk1$^{\Delta ICF}$#72) and 72,42 % (*Dlk1*$^{\Delta ICF}$*#82*) of Mmp9^{+}/ ChAT^{+} cells, respectively. These ratios showed no significant difference in the numbers of fast or intermediate-like αMNs (figure 5-33, D). These similar ratios of Mmp9^{+}/ ChAT^{+} cells might have indicated that the ICF of Dlk1 has no direct influence at least on *Mmp9* gene expression. Thereafter, Mmp9 might not be the best candidate to evaluate the Dlk1-ICF-dependent subpopulation of MNs.

5.8. Contributions

The cell lines used to address the question of the possible mechanism of Dlk1 cleavage, were generated by Dr. M. Marks (figure 3-1 and figure 3-2).

Additionally, the cell culture experiments were performed with the help of my colleagues Dr. M. Marks, A. Michely, L. Braun, and A. Hansknecht. They helped me out with medium changes and differentiation of ESCs into MNs. Especially, A. Michely was assisting during the time-consuming hypoxia experiments with collecting the samples and also with medium changes and differentiations of ESCs into MNs.

Further, L. Neumann was contributing to this thesis by slicing the embedded mouse brains and further performing all immunofluorescence and TUNEL staining of brain slices.

6. Discussion

Delta-like homologue 1 (Dlk1) was previously identified as a determinant of motor neuron (MN) development and diversification. Previous studies in mice and chicken embryos revealed a critical role of Dlk1 in the promotion of fast αMN gene expression and function (Müller et al., 2014). Nevertheless, the exact molecular mechanism(s) underlying the promoting fast αMN identity remained elusive. Experiments to identify Dlk1 interaction partners and stimulations of the Dlk1 pathway were not sufficient to elucidate the complete pathway through which it operates.

The role of Dlk1 regarding developmental and functional aspects has been studied in multiple tissues. For examples, the group of Pietras showed Dlk1 expression in high grade gliomas, where Dlk1 was proteolytically cleaved by tumour necrosis factor-α-converting enzyme (TACE), also known as A disintegrin and metalloprotease 17 (Adam17) (TACE/Adam17) after hypoxic stimulation (Grassi et al., 2020). This leads to the separation of Dlk1 into an extracellular domain (ECD) and intracellular fragment (ICF). The ICF translocated into the nucleus, where it altered genes involved in vascularisation and tissue remodelling is linked to tumour growth (Grassi et al., 2020). Based on the finding that Dlk1 cleavage can be induced by a hypoxic stimulus, the question arose whether Dlk1 processing during embryogenesis and MN development was also mediated by hypoxia. In mouse, MN development during embryogenesis starts from embryonic day 10.5 (E10.5) and continues beyond birth (Wolpert *et al.*, 2007). During embryogenesis, hypoxic conditions have been shown to be involved in various processes such as osteogenesis and myogenesis (Simon and Keith, 2008; Dunwoodie, 2009). To study whether MN diversification was stimulated by hypoxic conditions as well, wild-type embryos were analysed in this thesis in regard to altered oxygen levels during embryogenesis (see 5.1.).

6.1. Hypoxia influences embryogenesis

It has been reported that *Dlk1* is expressed in inner organs, such as the pancreas, salivary gland, adrenal gland, lung, heart and liver at E12.5 in the mouse embryo (Garcia-Gallastegi *et al.*, 2019; Traustadóttir *et al.*, 2019). To initially address the question whether proteolytic Dlk1 cleavage was initiated by hypoxic conditions during differentiation of MNs, E12.5 mouse embryos were analysed by immunohistochemistry and analysed in regard to the distribution of Dlk1 and hypoxia-induced factor 1α (Hif1α). Immunofluorescence signals could be detected in the spinal cord, forelimb, and some inner organs e.g., the hearth. The slight Dlk1 signal in the forelimb could be linked to the involvement of Dlk1 in bone and skeletal muscles development (Chen *et al.*, 2011; Andersen *et al.*, 2013). Further, Dlk1 is localised in different inner organs. Especially, the heart showed a high expression of Dlk1, which is in line with the involvement

of Dlk1 in cardiofibroblasts differentiation (Rodriguez *et al.*, 2019). Further Dlk1 expression in inner organs could reflect the Dlk1 involvement in branching morphogenesis of the lung and in the salivary glands (Yevtodiyenko and Schmidt, 2006; Traustadóttir *et al.*, 2019).

To address the question whether MN development could involve hypoxic conditions, the cellular hypoxia response was analysed by studying the expression of Hif1α. Hif1α is one of the most intensively studied factors influenced by hypoxic conditions (Wang *et al.*, 1995; Semenza, 2007). Under normoxic conditions, Hif1α is degraded through the ubiquitin/proteasome pathway, whereas it is stabilised under hypoxic conditions (figure 1-7) (Sadri and Zhang, 2013). Beside the hypoxic stabilisation of Hif1α, different hypoxic-independent processes of Hif1α are known. For example, it has been reported that Hif1α is involved in cardiogenesis, bone formation, and neurogenesis (Dunwoodie, 2009; Himmels *et al.*, 2017). A deletion of Hif1α leads to mouse embryos with lower body weight, heart mass, malformed for- and hindlimbs and reduced sympathetic innervation of the heart, compared to wild-type embryos (Romana *et al.*, 2019). Additionally, it is reported, that Hif1α is associated with the branching of blood vessels in the spinal cord by acting through Vegf (Himmels *et al.*, 2017), which supports the idea that hypoxic conditions could be presence in the spinal cord.

Although most cells are expressing Hif1α, only in hypoxia-stimulated cells Hif1α is stabilised and translocate to the nucleus, which enables discriminating between cells under hypoxic and normoxic conditions by using antibodies recognising Hif1α. Contrary to the expectation, in the experiments conducted in this thesis no discrete regions of Hif1α stabilisation could be detected. Instead, Hif1α was detected at even levels throughout the embryo. The failure to detect differences in Hif1α levels between tissues in the soma and nucleus could be explained by high levels of Hif1α in normoxic condition, which could be caused by pseudo-hypoxic conditions. Pseudo-hypoxia can be induced by activated growth factor signalling, independently of oxygen deprivation (Mohlin *et al.*, 2017). Such hypoxia-independent elevation of Hif1α levels could have made discrimination between pseudo-hypoxically stimulated cells and cells under hypoxic condition not possible by the experimental approach used. Additionally, due to high levels of Hif1a expression the protein may escape degradation in the cytosol and translocate into the nucleus, where it would be protected from degradation. Therefore, the question of a possible hypoxic influence on MN development had to be addressed by other experimental approaches.

6.2. Embryonic stem cell derived motor neurons as a model for hypoxia studies

A well-known model system for MN studies are ESC-derived MNs, which were investigated in this thesis in regard to effects of hypoxic stimulations. In contrast to primary MNs, which cannot be cultivated for long-term experiments, ESCs are able to be cultured for long periods. Further ESCs can be genetically modified and subsequentially differentiated to the desired cells, including MNs. Thus, ESC-derived MNs were assessed as a potential model system to analyse the effects of hypoxia on MN development and differentiation. To address the question whether hypoxia could influence fast αMN development, ESCs were differentiated into MNs over a period of 20 days, according to a modified version of a previously established protocol (Wichterle *et al.*, 2002; Bibel *et al.*, 2004; Gouti *et al.*, 2014; Sagner *et al.*, 2018). This ESC-derived MN culture was analysed by immunofluorescence with different neuronal markers to identify its cellular composition. The cells of the population were almost entirely positive for the general neuronal marker NeuN, indicating the efficient differentiation into a neuronal linage. Further, the cell population did not contain any $GFAP^+$ and $Iba1^+$ cells, which point out the absence of astrocytes and glial cells. However, the NeuN immunofluorescence reveal also some $DAPI^+$ but $NeuN^-$ cells. These cells could either be other non-neural cell type or $NeuN^-$ neurons. The latter could be neurons of a variety of identities, including olfactory mitral cells, retinal photoreceptors, cerebellar Purkinje cells, sympathetic chain ganglion cells, inferior olivary neurons, some cerebellar interneurons or Cajal-Retzius cells of the neocortex, as these cells have been described as NeuN negative (Mullen, Buck and Smith, 1992; Wolf *et al.*, 1996; Sarnat, Nochlin and Born, 1998; Weyer and Schilling, 2003) or they could possibly have been gamma motor neurons, which are $NeuN^-$. Indeed, as the differentiation protocol enforces posterior CNS characteristics, posterior cells, such as sprinkle MNs were more likely. Beside the neuronal types, other cell types are less likely but might be possible, as ESCs can develop into all cells of the three germ layers (Bibel *et al.*, 2004). Finally, $NeuN^-$ cells could also be surviving murine embryonic fibroblasts, which have been used during the cultivating period of ESCs to maintain them in the pluripotent state. Although based on the differentiation protocol, feeder cells should be removed with the beginning of the differentiation process, it is possible that feeder cells could have survived the process of differentiation. Based on the ChAT immunofluorescence, the majority (90 %) of the differentiated neurons appeared to be MNs. Nevertheless, some of the cells were negative for ChAT, indicating the presence of other neuronal cell types. Hereafter, only $Chat^+$ and $NeuN^+$ cells were considered for further experiments.

The successful differentiation of the ESCs into MNs was further verified by analysing the expression of transcription factors that mark different stages of differentiation, including (I) ESC marker, (II) MN progenitor (pMN) markers, (III) pan-neural markers, and (IV) mature MN

markers. For instance the ESC marker gene *Pou5f1, encoding the* pluripotency transcription factor Oct4 (Schöler *et al.*, 1990; Shi and Jin, 2010; Kuzmin *et al.*, 2019), was expressed at high levels at the beginning of differentiation and decreased with further differentiation (Schöler *et al.*, 1990; Niwa, 2001). Parallel to the decrease of *Pou5f1* transcription, the mRNA levels of the MN progenitor transcription factor gene *Paired Box 6* (*Pax6)* and *Oligodendrocyte Transcription Factor 2* (*Olig2)* began to rise. Upon exiting the cell cycle, the expression of the pMN marker genes and determinants *Pax 6* and *Olig2* are downregulated as the cells exit the cell cycle and transition from pMNs to MNs (Sagner *et al.*, 2018). The semi-quantitative real time PCR (semi-qRT PCR) revealed a similar expression dynamic between those two markers. For the *in vitro* differentiation, the observed expression of all of these factors thus indicated the successful differentiation process from ESC to pMN and finally to MNs. However, slightly in contrast to the literature (Sagner *et al.*, 2018), which reported expression of *Pax6* and *Olig2* preceding that both genes were already upregulated at day 5 of differentiation. In detail, the previous work stated that *Pax6* transcription should peak at day 3 and drastically decline afterwards (Sagner *et al.*, 2018). In this work, the expression of *Pax6* increased drastically between day 0 and day 3, yet reaching its peak at day 5. However, as an expression levels for each individual day were not determined in the present work, it cannot be ruled out that *Pax6* expression already peaked at day 4 of differentiation. This effect could also explain the shifted peak in the expression of *Olig2*, which was at day 5 of differentiation. However, prior studies reported *Olig2* expression reaching its maximum at day 6 of differentiation (Sagner *et al.*, 2018), but the relative expression levels at day 6 of differentiation was not analysed in detail in this study. Notably, an independent analysis in the research group using the same modified protocol revealed the same relative timing of expression for both marker genes (Liauchuk, 2021).

With the inhibition of the cell-cell interactions through trypsinisation on one hand, on the other hand the inhibition of Notch signalling by the γ-secretase inhibitor dibenzazepine (DBZ), the transient activation of *Olig2* was achieved and a large number of MNs were obtained in the differentiation. *In vivo*, Olig2 is regulating further transcriptions factors, such as Islet-1 (Isl1), and Islet-2 (Isl2), which in turn induce transcription factor *Mnx1* in post-mitotic MNs. Mnx1 suppresses the expression of interneuron-specific genes in MNs and to induce the maturation of MNs *in vivo* (Arber *et al.*, 1999; Thaler *et al.*, 2002; Catela, 2020). In the *in vitro* differentiation, *Mnx1* showed an increase in the expression from day 5 onwards, indicating successful generation of post-mitotic MNs. Additionally, the cells were found to express the pan-neuronal markers *Tubulin Beta 3 Class III* (*Tubb3)* and *RNA Binding Fox-1 Homolog 3* (*Rbfox3)*, which together with the cholinergic neuron marker *ChAT*, indicated successful differentiation into ‘mature’ MNs. Finally, *Dlk1* expression was found to increase during the pMN generation until day 7, consist with its expression in pMNs (Müller 2012).

Together with the results obtained by immunofluorescence analysis, these results clearly demonstrated the successful differentiation of ESCs into MNs. The next question was whether the MN differentiation protocol would promote the generation of the full range of MN subtypes, including α, β, and γ MNs, as well as the αMN subtypes (fast, intermediate and slow). As this thesis is focussing on the fast αMN subpopulation and the influence of hypoxia on the αMN diversity, the ESC-derived MN population was analysed specifically in regards to αMN diversity. *Mmp9* is known to be expressed in fast and intermediate αMNs, whereas MN expression of *Dlk1* is restricted exclusively to the fast αMN subtype (Kaplan *et al.*, 2014; Müller *et al.*, 2014). A closer investigation of the ESC-derived MN population revealed that ~50 % of the total Chat^{+} cells were Mmp9^{+} (figure 5-7, C). Further, 99 % of the Mmp9^{+} MNs were Dlk1^{+}, while only ~1 % of the Chat^{+} MNs were Dlk1^{+} and Mmp9^{-}. Although previous research found that *Dlk1* expression is downregulated in the later post-natal stages *in vivo* (after P15), in the *in vitro* differentiation *Dlk1* did not seems to be significantly downregulated in the ESC-derived MNs within the 20 days of differentiation, which was also observed with the Dlk1-HA cell line. Together with the results obtained in the gene expression studies this could indicate that the MNs within the 20 days of differentiation were not yet fully matured. Moreover, independent experiments using the same modified protocol could no decrease in *Dlk1* expression could be observed within 40 days of differentiation (Liauchuk, 2021). It is possible that the ESC-derived MNs were held in a not fully matured state by the culture conditions, the absence of presynaptic inputs and/or the absence of muscle fibres with which MNs form neuromuscular junctions (NMJs) *in vivo* and which may be required for the final maturation of MNs.

The temporal regulation of expression of *Mmp9* and *Dlk1* in the ESC-derived MNs also differed somewhat from that in the *in vivo* situation. *In vivo*, *Mmp9* expression is upregulated with MN maturation, while *Dlk1* is downregulated in mature MNs (Cherukuri, 2012; Müller, 2012). In the present *in vitro* analysis, *Mmp9* mRNA levels revealed stable expression with only slight fluctuations during the process of differentiation. It is possible that the early expression of *Mmp9* during *in vitro* differentiation reflected its previously reported expression in the inner cell mass (ICM) of the blastocyst stage embryo (Kim and Yoon, 2019). However, there are different explanations. One study reported that *Mmp9* is expressed in the trophoblast during the blastocyst implantation (Martìnez-Hernandez *et al.*, 2010). Nevertheless, a further study reported that *Mmp9* is expressed in cultured ESCs and its expression might be influenced by the increased proliferation rate effected by the hypoxia-induced canonical Wnt/β catenin signalling pathway (Ingraham *et al.*, 2011). This could indicate that *Mmp9* is also expressed in the *in vitro* differentiation and subsequently resulting in unchanging mRNA levels of *Mmp9* during the process of MN differentiation from ESCs.

While the persistent expression of Dlk1 suggested that the ESC-derived MNs did not fully mature, the finding that the cell populations consisted of up to 50 % of $Mmp9^{+}$ and $Dlk1^{+}$ cells suggested that MN functional diversification nevertheless proceeded to a large extent during the *in vitro* differentiation process. Therefore, it was decided that the ESC-derived MNs could be used to address the impact of a hypoxic conditions on Dlk1 activity and MN diversification.

6.3. Hypoxia mediated Dlk1 regulation

Knowing, that hypoxia could influence neuronal differentiation (Simon and Keith, 2008; Fathollahipour, Patil and Leipzig, 2019; Li *et al.*, 2021), the experimental conditions to assess the effect of hypoxic stimuli had to be established in MN cell culture conditions, as the effects of hypoxia on MNs have been barely investigated. In a recent publication, one hour with 1 % O_2 was used for the hypoxic stimulation of primary human MNs, which informed about the critical O_2 concentration used in the stimulation of ESC-derived MNs (Fiskum, Sandvig and Sandvig, 2021). In this thesis, the optimal time period of 45 min of oxygen deprivation for the ESC-derived MNs was determined as 45 min, which was based on the minimal time of significant Hif1α stabilisation and the initiation of hypoxia-induced downstream factors, before the onset of significant cell death. After 60 min of oxygen deprivation, the MN network exhibited an excessive number of dead cells and correspondingly an increased LDH level compared to normoxia. This indicated that a hypoxic stimulus of 60 min is too long and as the apoptotic pathway was already induced. Since cellular processes are addressed, Hif1α was also considered. Those results were supported by changes in the expression of the downstream factors glucose transporter 1 (Glut1) and the transmembrane protein carbonic anhydrase IX (CaIX) (Harvey *et al.*, 2004; Sadri and Zhang, 2013; Wakhloo *et al.*, 2021). Glut1 is directly associated with hypoxia- induced gene expression and leads to an increase in the necessary energy supply of the cells, whereas CaIX is known to be associate with the pH regulation (Wakhloo *et al.*, 2021). These experiments therefore set the conditions to investigate the impact of oxygen deprivation on Dlk1 processing and MN diversification.

6.4. Dlk1 regulation in murine brain slices

Hypoxic stimulated MNs showed reduced Dlk1 protein levels, which was not an effect of decreased *Dlk1* transcription levels. This observation raised the question whether the observed reduction in full-length Dlk1 levels could also be observed in neurons in their native tissue context, which in turn was addressed through an *in situ* experimental approach. This could not be performed with MNs within the spinal cord, however, because of the extreme sensitivity of spinal MNs towards axonal and dendritic damage, which in these preparations cannot be avoided. As an alternative, there are three main sources of MNs available *ex vivo*;

(I) ESC-derived MNs, (II) primary MNs from embryos, and (III) iPSC-derived MNs (Gouti *et al.*, 2014; Bucchia *et al.*, 2018; Sagner *et al.*, 2018). As an alternative to this *in vitro* protocol a model better resembling the *in vivo* situation was chosen by using acute living brain slice cultures to analyse Dlk1 regulation after hypoxic stimulation. The three-dimensional (3D) structure of brain slices enables the inclusion of multiple cell types within their native tissue context into the analysis (Eguchi *et al.*, 2020). As *Dlk1* is known to be expressed in the brain throughout the whole life-span, this approach therefore allowed studying the impact of hypoxia on neuronal Dlk1 processing *in situ*.

Before addressing the question, if Dlk1 regulation is triggered by hypoxia in brain slice cultures, specific protocols had to be established for this purpose. It is known, that brain slices are a well-established approach to study brain disorders (Yuan *et al.*, 2012; Cui *et al.*, 2013; Feber, 2019). Also, *Hif1α* expression and hypoxia- induced apoptotic protein regulation are already characterised in brain slices (Yuan *et al.*, 2012; Cui *et al.*, 2013). However, hypoxic induction and effects have to be adjusted to the established experimental setup. By analysing the viability of $NeuN^+$ neurons, the optimal post-extraction recovery period for brain slices was determined. Thereafter, the time period to culture those brain slices was set to be about one day. This decision was based on the recovery time of neurons after preparation, the observation with other cell types, as glial and astrocytes and the minimisation of neuronal cell, which are occurring during longer cultivation periods. After cultivating the brain slices for one day, they were stimulated in the hypoxia chamber. Following the stimulation, the viability and the cellular response in terms of Hif1α stabilisation and Glut1 and CaIX upregulation were analysed for a time period of 24 hours (here after named as post-hypoxic reperfusion time). The detected Hif1α stabilisation and also the increase of the protein levels for both hypoxia-regulated genes indicate the successful induction of cellular hypoxic response.

As the induction of cellular hypoxic response in brain slices mimics the condition of a stroke, further aspects should be considered (Grotta *et al.*, 2021). Non-modifiable risk factors in human and mice for stroke are the gender and the age of the affected patients (Roy-O'Reilly and McCullough, 2018; Ekker *et al.*, 2019). Both factors play a decisive role in the course and severity of the stroke (Roy-O'Reilly and McCullough, 2018). Therefore, gender and age differences were comparatively analysed. To summarise, gender differences were not observed, neither regarding the Hif1α stabilisation, nor in the induction of the downstream factors, CaIX and Glut1 (supplement figure 3 and supplement figure 4). This contradicts the literature, stating a more severe outcome of stroke in male compared to female mice (Alkayed *et al.*, 1998). For the age as another decisive factor, there are no significant differences between the ages 2-5 month old (young mice) (supplement figure 3) and 10-18 month old (mature mice) (supplement figure 4). These results are in contradiction to the literature, indicating a difference in the stroke outcome at different age. Especially, young female mice

have a higher estrogen levels, which appears to have a protective effect regarding the outcome of stroke (Alkayed *et al.*, 1998; Manwani *et al.*, 2013; Grotta *et al.*, 2021). With increasing age, the gender-specific differences in the murine stroke model should be diminished (Liu *et al.*, 2009; Manwani and McCullough, 2011; Manwani *et al.*, 2013). A possible explanation for the difference in the results could have been that in the *ex vivo*-condition the cultured brain slices lack the blood flow and exposure to hormones. To clarify these possibilities, further experiments have to be performed with larger sample sizes.

After establishing the suitability of brain slices as a model system to study Dlk1 regulation, various experiments were conducted in order to analyse the dynamics of the Dlk1 protein under oxygen-deprived conditions. Western blot analysis revealed a significant reduction of the detectable Dlk1 protein in hypoxic stimulated brain slices. This was observed in all mice, regardless of age or gender. For young mature (2-5 month) and old (8-18 month) mice, Dlk1 was reduced immediately after induction of hypoxia. This is in line with the observation in ESC-derived MNs and with the publication by Grassi *et al* (Grassi, Pantazopoulou and Pietras, 2020). During the ongoing post-hypoxic reperfusion time, Dlk1 was decreased even more in young mature mice. This might indicate a process leading to the initial reduction of Dlk1 continuing after reperfusion. This might indicate that Dlk1 processing itself is independent from the oxygen-deprivation and hypoxia is only needed as an initial trigger signal. For older mice, Dlk1 reduction was also observed during the post-hypoxic reperfusion time. However, at this stage, Dlk1 protein levels were more fluctuating (figure 5-16). The lowest Dlk1 protein concentration was detected after six hours of post-hypoxic reperfusion time in this experiment. This means that the Dlk1 processing continued at least until six hours after hypoxia. In the time period of six to nine hours, the amount of the Dlk1 protein levels began to increase. The increased Dlk1 level after 9 and 24 hours of post-hypoxic reperfusion time, respectively, were comparative to that observed after six hours, which may indicate a normalisation of Dlk1 protein levels. To summarise, the reduction in the Dlk1 protein was in line with the reduction observed in ESC-derived MNs, indicating that this was not a cell culture-specific effect, but a general feature of Dlk1 regulation.

6.5. Dlk1 regulation triggered by hypoxia in embryonic stem cell-derived motor neurons

The brain slice cultures showed the decrease in the Dlk1 protein amount also after and beyond the acute hypoxic stimulation during the post-hypoxic reperfusion time. This dynamics in the reduced Dlk1 protein levels, compared to normoxia, were also observed in ESC-derived MNs by immunofluorescence. The signal intensity of Dlk1 was progressively reduced after the acute phase of hypoxia and kept decreasing after three hours of post-hypoxic reperfusion. This is in line with the results observed in brain slice culture. In addition, the immunofluorescence gave

insights into the subcellular localisation of Dlk1 protein. In normoxia, Dlk1 was detected ubiquitously in the entire cell, whereas after hypoxia it concentrated at the perinuclear area. This re-localisation was previously observed in murine orexin neurons (Harris et al., 2020). Further, the Dlk1 protein reduction might be explainable by the fact, that the Dlk1 antibody is no longer able to detect its epitope due to some kind of post-translational processing or secretion.

The type 1 single pass transmembrane protein Dlk1 possesses a large ECD, including six epidermal growth factor (EGF) repeats. A second cleavage leads to a short intracellular fragment (ICF). The extracellular juxtamembrane cleavage site is one of the up to two extracellular proteolytic cleavage sites depending on the actual Dlk1 isoform. A second cleavage site is located closer to the N-terminus (see figure 1-5) (Smas, Green and Sul, 1994; Wang and Sul, 2006). Thereafter, Dlk1 can be cleaved by TACE/Adam17 at the ECD cleavage site (Wang and Sul, 2006; Traustadóttir et al., 2019). Because of alternative splicing and the different cleavage sites, different Dlk1 isoforms can be generated, depending on the tissue or developmental stage (Wang et al., 2006). Nevertheless, little is known about the ICF and its function. The analysis of a genetically modified ESC-derived MNs, in which Dlk1 is bearing a C-terminal HA-tag was used. Thus, after cleavage of the Dlk1 protein, the ICF (hereafter termed ICF-HA) could be traced by applying an anti-HA antibody. Hereafter, it was possible to discriminate between the full-length membrane-bound uncleaved Dlk1 and the soluble ICF-HA by applying the respective antibodies.

Indeed, the ESC-derived MNs were shown to possess two forms of Dlk1, according to western blot analysis: the full-length Dlk1 (~50 kDa) and the cleaved ICF-HA (~18 kDa). This observation was partially in line with previous studies (Wang and Sul, 2006; Subhashini, 2016; Grassi, Pantazopoulou and Pietras, 2020). In terms of the ICF, discrepancies of the processing are reported. On one hand, the ICF is described to be 11 kDa in size (Wang and Sul, 2006), but further investigations could detect a stable, cleaved ICF with a size of 9 kDa, which might have been the product of an additional intracellular cleavage (Subhashini, 2016). This third cleavage was further reported as alternative Adam17-dependent cleavage after hypoxia in astrocytes (Grassi and Pietras, 2022). In this thesis, the ICF showed a molecular weight of 18 kDa as judged by comparison with the molecular weight standard. Including the fact that the ICF was HA-tagged and western blot molecular weight standards are not accurate at such low molecular weights, the protein fragment was concluded to represent the actual size of the ICF of Dlk1.

With hypoxic stimulation both, the levels of the full-length Dlk1 and the uncleaved Dlk1-HA were significantly decreasing, whereas that of ICF-HA was significantly increasing. The decrease in the full-length Dlk1 and the parallel increase in ICF-HA indicate a cleavage of the

protein, triggered by hypoxia. Although Gassi *et al.* were not focussing on that detail, the reduction of full-length Dlk1 levels was also observed in high-grade glioma cells (Grassi, Pantazopoulou and Pietras, 2020). Further, their work could show the appearance of the ICF only after hypoxia induction. In this thesis, the ICF-HA was also detectable under normoxic condition. This might be a result of either the MN culture conditions, cell-specific differences in protease levels or (more likely) because MNs have already shown a certain level of Hif1α stabilisation even under normoxic conditions (see figure 5-17, B). That the ECD was not detected in these experiments was expected, as the ECD is released into the medium, which was not separately collected and analysed in these experiments and thus it could not be immunodetected.

6.6. Localisation of the intracellular Dlk1 fragment after hypoxic stimulation

So far, evidence has been provided that the Dlk1 ICF could be cleaved by Adam17 cleavage, after which it may translocate to the nucleus (Subhashini, 2016; Grassi, Pantazopoulou and Pietras, 2020; Grassi and Pietras, 2022). However, little is known about the function and processing of the ICF. It has been hypothesised that the ICF acts as transcription co-factor, as it cannot bind DNA itself. Thereafter, the ICF, acting as a transcription co-factor could be responsible for determining fast αMN-related function (Müller *et al.*, 2014). To address this question, the subcellular localisation of the ICF was traced by using the HA-specific antibody and the Dlk1-HA tag of the cell line. In normoxia conditions, both HA and full-length Dlk1 signals showed similar punctate localisation patterns.

To compare the HA signal distribution in the nucleus before and after hypoxic stimulation, the layer, which included the nucleus was identified. This was the 9th optical section for all analysed MNs. The immunofluorescence analysis of the 9th optical section did not reveal a significant the translocation of the ICF-HA to the nucleus for any condition, which appeared to contradict previous findings (Grassi *et al.*, 2020). Reasons for these discrepancies might have been the narrow area in the fluorescence analysis or hypoxic stimulation being insufficient to induce the cleavage and the subsequential translocation of the ICF. Therefore, an additional quantification of the immunofluorescence signal of the ICF-HA was performed with only individual optical sections of the Z-Stack, including the DAPI^{+} regions being analysed, excluding the surrounding soma regions. Furthermore, the maximum intensity projection (MIP) was used to condense the individual optical sections fluorescence intensity into one single image. Within this image, the nucleus was traced back by using the DAPI signal. This analysis indeed revealed a higher level of ICF-HA in the nucleus after hypoxic induction, indicating the translocation of the ICF into the nucleus in MNs just as in glioma cells (Grassi, Pantazopoulou and Pietras, 2020).

The exact mechanism underlying the translocation of the ICF into the nucleus was not published so far. Preliminary data indicates, that the ICF is translocated to the nucleus in association with the Nuclear factor of activated T-cells (Nfatc4) (Subhashini, 2016). This transcription factor regulates gene expression in response to intracellular Ca^{2+} levels. Upon release of the second messenger Ca^{2+} from the endoplasmic reticulum (ER), the ions can activate the phosphatase Calcineurin (Rao, Luo and Hogan, 1997; Elisa *et al.*, 2009). This activation leads to the phosphorylation of Nfatc4 and subsequently to its translocation to the nucleus (Subhashini, 2016). This pathway might be responsible for the co-translocation of the ICF into the nucleus. Based on this pathway, one reason for the low level of translocation of ICF-HA found in the ESC-derived MNs could be the bottle neck effect, as the amount of Nfatc4 protein could have been insufficient to shuttle the ICF. Another very likely reason could be that the 45 min time of hypoxia was too short to promote a more pronounced translocation of Dlk1-ICF into the nucleus, since the previous experiments in glioma cells involved hypoxia stimulation for 48h periods (Grassi, Pantazopoulou and Pietras, 2020), a time that would by far exceed the possible survival of ESC-derived MNs.

Although the Grassi *et al*. studied Dlk1 cleavage by hypoxic stimulation, they did not include any such analysis after post-hypoxic reperfusion time (Grassi *et al.*, 2020). In this thesis, a drastically decreased nuclear localisation of the HA signal in the nucleus was observed after three hours post-hypoxic reperfusion time. This result seemed to contradict to the results from western blot analysis, which indicates an increase in the ICF after the acute phase of oxygen deprivation, as well as after three hours of post-hypoxic reperfusion time. The cause of this reduction of the intranuclear ICF-HA signal could either be (I) an active transport of the ICF out of the nucleus, or less likely (II) the blockage of the transport into the nucleus and the subsequential degradation. Another idea would be that the nuclear ICF acts as a feedback signal to induce the inhibition of further ICF transport to the nucleus. Thus, it is possible that in MNs the translocation of the Dlk1-ICF into the nucleus happens much faster and that by the time it was analysed the reverse process of nuclear export had already been initiated. However, to address these possibilities further experiments are necessary to investigate the changes in shorter or longer time intervals and in more detail. Additionally, the nuclear localisation dynamics of possible interaction partners, such as Nfatc4 should be investigated, for example by chromatin immunoprecipitation (ChIP) and co-immunodetection.

6.7. Matrix metalloproteinase 9 is affected by Dlk1 cleavage

The observation that Dlk1 ICF-HA is cleaved and likely translocated into the nucleus could indicate a role as a transcriptional co-factor in the activation or repression of MN-related genes. One of the suspected target gene encodes the *Matrix metalloproteinase 9* (*Mmp9*). It is

associated with multiple processes, like stemness, cell metabolism and cancer cell invasion (Grassi, Pantazopoulou and Pietras, 2020). Fast αMNs and large intermediate αMNs can be distinguished from other subtypes by the presence of Mmp9 as a marker protein (Kaplan *et al.*, 2014). Beside the identification of the MN subtypes, it is also reported, that *Mmp9* expression is increased by Dlk1 in cancer cells, but has not been addressed whether this activity was mediated by Dlk1-ICF (Li *et al.*, 2014). The observed slight increase in the *Mmp9* transcript levels in ESC-derived MNs upon hypoxic stimulation indicates an influence of hypoxia also on the transcription of *Mmp9*, which had previously been shown in various reports for cancer cells (Li et al., 2014; Grassi, Pantazopoulou and Pietras, 2020). In contrast to the slight increase at the mRNA level, the Mmp9 protein level was showing a significant decrease after hypoxic stimulation and after three hours of post-hypoxic reperfusion time, compared to normoxia. Based in the fact, that *Mmp9* mRNA levels did not decrease, it is suggested a regulation of Mmp9 through protein degradation or its shedding from the cell-surface. Mmp9 is essential in the restructuring and remodelling of the extracellular matrix (Huang, 2018). Especially, Mmp9 is involved in tumour-dependent remodelling for the vascularisation in cancer-affected tissues (Christoffersson *et al.*, 2015). To address the importance of Dlk1 cleavage for Mmp9 regulation, further experiments in brain slices should be conducted. However, the results indicate a mechanism linking hypoxia directly to Mmp9 release.

6.8. Dlk1 cleavage

6.8.1. Impacts of reducing *Adam17* mRNA levels on Dlk1 processing

The mechanism and the effects of Dlk1 ECD cleavage has been reported by various studies (Jensen *et al.*, 1994; Smas, Green and Sul, 1994; Wang and Sul, 2006; Ferrón *et al.*, 2011; Traustadóttir *et al.*, 2019). However, most of the reports are exclusively analysed the extracellular cleavage of Dlk1. Beside the extracellular cleavage, however, it was also reported that there is an additional cleavage of Dlk1 at the intracellular segment (Subhashini, 2016; Grassi and Pietras, 2022). Furthermore, Grassi *et al.* reported that the wild-type cleavable Dlk1 form is responsible for Mmp9 secretion and an increase in the *Vegf* expression, as a membrane-bound Dlk1 variant lacking the extracellular cleavage site these effects were not observed, suggesting that the second, intracellular cleavage is dependent on the first, extracellular cleavage (Grassi, Pantazopoulou and Pietras, 2020). In this thesis it could be shown that Adam17 activity can indeed be influenced by hypoxia in ESC-derived MNs, in line with previous reports in macrophages and cancer cells (Wang, Feng and Li, 2013; Lian et al., 2019). Interestingly, *Adam17* expression levels were not elevated, but Adam17 protein levels were increased after hypoxic stimulation. The finding of reduced *Adam17* mRNA levels contrasts with previous findings that found Hif1α stabilisation promoting an increase in *Adam17* transcript levels in macrophages (Lian *et al.*, 2019), suggesting that in MNs Adam17, like

Mmp9, is rather regulated at the protein level, either through stabilisation or decreased shedding from the cell surface.

In this thesis, it was addressed through siRNA-mediated knockdown whether Adam17 would be involved in Dlk1 cleavage in MNs as well. After demonstrating the successful knockdown of *Adam17* expression, Dlk1 cleavage was analysed in ESC-derived MNs. After stimulating MNs by oxygen deprivation, MNs transfected with *Adam17* siRNA showed increasing full-length Dlk1 protein levels compared to ctr MNs, which supports the idea that Dlk1 cleavage was mediated by an induction of Adam17 activity by hypoxia. However, after the three hours of post-hypoxic reperfusion time, the full-length Dlk1 protein levels were again similar in MNs transfected either with *ctr* or *Adam17* siRNA. As it was increasing after three hours post-hypoxic reperfusion time to 80 % reduction in mRNA level and should result in inhibition of the cleavage of Dlk1. This should further lead to an increase in the full-length Dlk1 protein level. However, including the results of the protein level of the ICF after knockdown of *Adam17*, it seems that *Adam17* siRNA did have an effect on proteolytic activity. Under normoxic conditions, the ICF protein level was reduced in MNs transfected with *Adam17* siRNA compared to MNs transfected with *ctr* siRNA. After the hypoxic stimulation, the ICF-HA level was increased in MNs transfected with *ctr* siRNA while still reduced in MNs transfected with *Adam17* siRNA. By *Adam17* knockdown, the cleavage of Dlk1 should be inhibited and subsequently, less ICF-HA detectable. However, after three hours of post-hypoxic reperfusion time, the ICF-HA level was reduced in MN transfected either with *Adam17* siRNA as well as transfected with *ctr* siRNA. This indicated, that after three hours of post-hypoxic reperfusion time, the effects of the reduced cleavage of Dlk1 are independent of the *Adam17* mRNA level. Taken together, the effect which leads to the increase in the ICF-HA protein level seemed to be partially independent of the *Adam17* mRNA concentration, and more likely dependent of the Adam17 protein function. Therefore, to address the Adam17 function on Dlk1 cleavage, an additional approach with in inhibitor was performed.

6.8.3. Dlk1 cleavage is inhibited by an Adam17 inhibitor

6.8.3.1. Impacts of blocking Adam17 protein function on Dlk1 processing

The thiomorpholin hydroxamate inhibitor (TMI-1) is a potent Adam17 inhibitor. TMI-1 was initially described as inhibitor of LPS-induced TNF-α secretion in human primary monocytes and human blood (Zhang *et al.*, 2004). Furthermore, TMI-1 was shown to successfully inhibit Dlk1 cleavage in high grade glioma cells (Grassi, Pantazopoulou and Pietras, 2020). Therefore, TMI-1 was used to investigate the impact of Adam17 protein function in hypoxia- induced Dlk1 ICF shedding. MNs withstood the treatment with all TMI-1 concentrations tested without obvious differences. Consistent with the previous report, steadily increasing full-length Dlk1 protein levels with increasing TMI-1 concentration and decreasing ICF-HA levels were observed. Adam17 inhibition also resulted in an increase of full-length Dlk1

levels and a reduction in ICF-HA levels despite hypoxia induction. This increase was higher than the initial normoxia full-length Dlk1 levels in the 1 µM TMI-1 treated cells, which was likely an effect of newly synthesised Dlk1 accumulating due to inhibited proteolytic cleavage by Adam17. Taken together, TMI-1 was inhibiting Adam17 function, blocking the cleavage of the full-length Dlk1 into the ECD and ICF, indicating that indeed it appears to be the regulation of Adam17 at the protein function level that is relevant for Dlk1 processing. Taken together, these results confirmed that the ICF is proteolytically cleaved off the full-length Dlk1 protein by the Adam17 protease.

6.8.3.2. Mmp9 secretion is independent on Dlk1 intracellular fragment cleavage

To analyse the possibility, that the ICF might act as transcriptional co-factor, *Mmp9* expression was investigated. However, hypoxic stimulated MNs did show an elevated Mmp9 transcript level. Data generated in this study suggested that Mmp9 protein could be shredded from the cell surface after hypoxic stimulation. If this regulation is dependent on the Adam17-mediated ICF-HA cleavage, the Mmp9 secretion would be prevented by the treatment with the Adam17 inhibitor TMI-1. However, MNs, treated with TMI-1 show the same reduction in the signal intensity for the tested hypoxic stimulations as the control treated MNs, suggesting that Dlk1 cleavage and release of the ICF-HA were not responsible for the Mmp9 protein levels. Thus, in MNs the hypoxia-mediated reduction of Mmp9 levels appears to be achieved in a manner differing from that previously reported for glioma cells (Grassi, Pantazopoulou and Pietras, 2020).

6.9. Dlk1$^{\Delta ICF}$ shows similar results in proportion of fast motor neurons

It has been hypothesised that Dlk1 processing by Adam17 via proteolytic cleavage is followed by translocation of the ICF into the nucleus and subsequently the activation of fast αMN-specific genes (figure 7-1). To analyse if the cleaved ICF has an effect on the proportion of fast αMN, Dlk1$^{\Delta ICF}$ ESCs were differentiated into MNs to address whether the absence of the Dlk1-ICF would disrupt MN functional diversification and specifically, fast αMNs specification. Two independent Dlk1$^{\Delta ICF}$ ESC lines were used as internal control, which differed in their mutation leading to truncation of Dlk1 shortly after the transmembrane segment. The preliminary analysis of both lines focused on the proportion of Mmp9^{+} (“fast”) MNs of the total population of ChAT^{+} MNs, which was previously in this study found to be usually be ~50 %. Notably, in this experiment a difference in the proportion of Mmp9^{+} cells (~80 %) compared to those obtained in the previous experiments was also found for the control (Dlk1-HA) cell line, suggesting that slight differences in culture conditions can have large impacts on the diversification of MNs during their differentiation from ESCs. The comparison between the Dlk1-HA cell line with the Dlk1$^{\Delta ICF}$ cell lines showed similar ratios for the ChAT^{+} and the Mmp9^{+}

cells. This could either indicate that the ICF was not influencing Dlk1-dependent MN diversification or that the Dlk1$^{\Delta ICF}$ MNs might have differed at another level, such as in their electrophysiological properties. However, it could also be that Mmp9 was not the most adequate marker to discriminate the fast MNs from other MN subtypes, because of its possible regulation at the post-transcriptional level independent of MN subtype identity. The observation that differentiation of ESCs into MNs did not yield stable proportions of Mmp9^{+} MNs across different experiments may point in this direction. In any case, more comprehensive analysis using additional MN subtype-specific markers, such as Err2; Err3, OPN and Timp3 (Morisaki *et al.*, 2016) Liauchuk, 2021; Khan *et al.*, 2022) should be applied to conclusively discriminate and analyse the exact composition of the MN population in regards to the different MN subtypes. In addition to the cellular composition, electrophysiological analysis should be used to address a possible influence of the ICF on MN subtype-specific properties independent of MN subtype identity proper. Taken together, the truncation of the Dlk1 protein largely eliminating the ICF could not change the proportion of Mmp9^{+} MNs and further experiments with different markers and approaches have to be performed to determine its influence on MN cell fate decisions.

7. Conclusion

This thesis focused on the study of the hypoxia-dependent regulation of Delta-like homologue 1 (Dlk1) and its role in motor neuron (MN) functional diversification. Based on previous observations on Dlk1 processing in response to hypoxia in gliomas and that spinal MNs remain avascular during their initial development (Himmels *et al.*, 2017), it was hypothesized that Dlk1 could be stimulated by low-level oxygen conditions (hypoxia) to promote MN functional diversification.

During embryogenesis the “classical” hypoxia pathways mediated by Hif1α can also be activated independent of hypoxia, it is therefore difficult to attribute exclusively to low oxygen conditions. As an alternative approach permitting precisely controlled oxygen deprivation, the impact of hypoxia on Dlk1 processing and MN diversification was studied in murine embryonic stem cell (ESC)-derived MNs. It was first shown that ESCs could be differentiated to a MN expressing markers for fully differentiated MNs, such as NeuN and ChAT. Moreover, ~50 % of the ESC-derived MNs were positive for both Dlk1 and Mmp9, suggesting that MN functional diversification at least to some extent proceeds similar to that *in vivo*. Next it was shown that in ESC-derived MNs exposed to hypoxic conditions Hif1α is stabilised and then translocated to the nucleus. The MNs thus showed the hallmarks of the cellular hypoxia response, including the upregulation of Hif1α target genes *CaIX, Glut1* and *Adam17*. The Adam17 protease, in turn, may lead to an increase in the cleavage of Dlk1, which indeed was observed as a reduction in Dlk1 full-length protein levels and an increase in the levels of the Dlk1 intracellular fragment (ICF). This Dlk1 cleavage could be effectively reduced by blocking Adam17 protein activity, but not by reducing *Adam17* RNA levels, which could suggest that, in contrast to other cell types, hypoxia-dependent Adam17 activity is regulated in a transcription-independent manner in MNs. It was further shown by this study that, after hypoxia-mediated increase in Dlk1 cleavage, Dlk1-ICF translocates transiently into the nucleus, while being shuttled out of the nucleus after restoring normoxic conditions. It was hypothesised that once in the nucleus, the ICF could subsequently act as a transcriptional co-factor (figure 7-1). However, preliminary results suggested that deletion of the ICF by CRISPR-Cas9-mediated gene targeting did not apparently alter the proportion of Mmp9^{+} ESC-derived MNs. It remains possible, however, that Dlk1, operating through its ICF. However, the ICF, may not influence MN functional diversification *per se*, but rather specifically the implementation of fast αMN properties, a possibility that awaits further study.

To summarise, this thesis could show that Adam17 activity regulated by hypoxic stimulation can induce the cleavage of Dlk1 in MNs. The cleaved ICF of Dlk1 translocated to the nucleus, where is could function by altering gene expression activity related to fast αMN properties (figure 7-1).

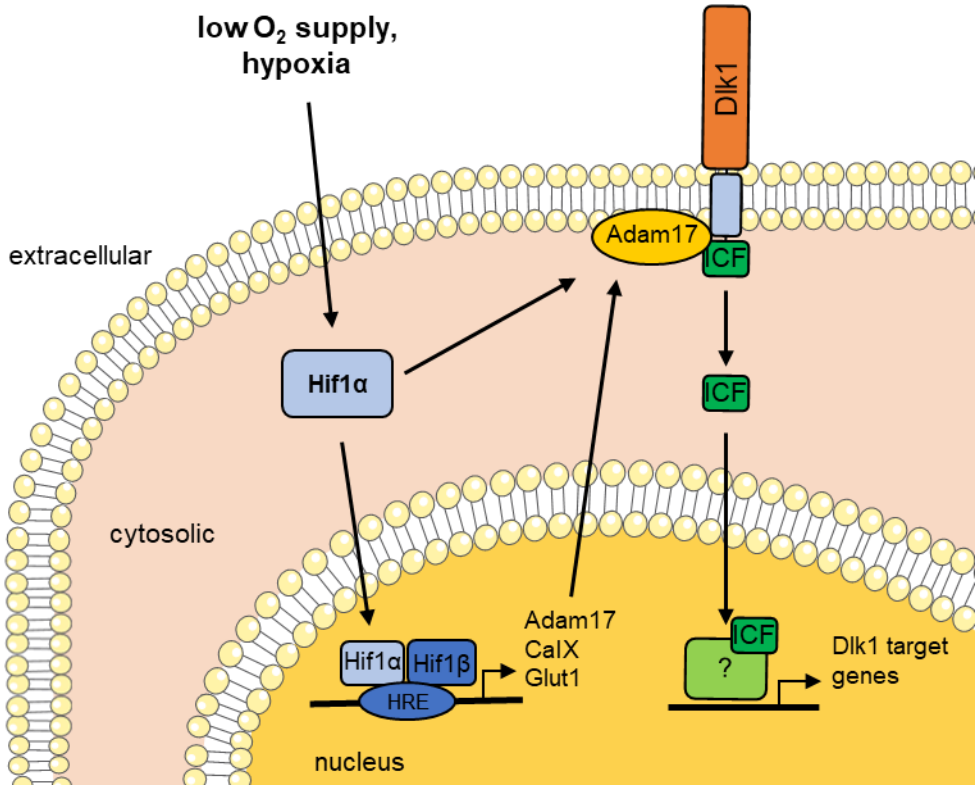

Figure 7-1: *Summary and predicted molecular mechanism of fast alpha MNs property aquisition. Low oxygen levels are inducing the stabilisation of Hif1α, which is translocated to the nucleus and subsequentially binding with Hif1β to form a dimer. The dimer can bind to the HRE of target gene regulatory elements and activate the transcription of Adam17, CaIX and Glut1. At the same time, Hif1α can also activate Adam17 activity, which leads to a cleavage of Dlk1. The cleaved ICF translocate to the nucleus and alters Dlk1 target genes to promote fast αMN properties. CaIX, carbonanhydrase IX; Glut1, glucose transporter 1; Hif1α/β, hypoxia-induced factor subunit 1α/β; HRE, Hif-response element; ICF, intracellular fragment; MNs, motor neurons.*

8. Outlook

Based on the achieved results, further questions and possible approaches arise to clarify the underlying mechanism which induces fast αMN properties. However, during this thesis, some challenges have raised, which should be addressed in additional experiments. One challenge was the specificity of Mmp9 as a molecular marker to identify the fast αMN population amongst the ESC-derived MNs. Contradictory to the literature, *Mmp9* expression was already elevated during the differentiation process. Therefore, research into the *Mmp9* expression dynamics should be extended. Either by including further molecular markers, as for example, Err2, Err3, Timp3, OPN, which could give a closer hint on the MN subtypes or in combination with electrophysiological analysis to identify the different electrophysiological properties of the different MN subtypes *in vitro* culture.

Furthermore, the translocation of the ICF raises further questions. The slight increase after hypoxic stimulation should be further addressed by altering the duration of the hypoxic stimulus or other conditions. The duration of the hypoxic stimulus (like for example, 30 min, 35 min, 40 min) or other conditions like the post-hypoxic reperfusion time or the oxygen level could be fined-tuned. Also, the translocation of the ICF into the nucleus and the further progression should be analysed. Therefore, a chromatin immunoprecipitation (ChIP) could be an adequate method to address this question.

Beside the performed experiments, it would be interesting, if hypoxic stimulation could change the proportion of MN subtypes during the developmental stage of pMNs. Thereafter, pMN might be investigated by varying oxygen conditions and analysed in regard to the different MN types they generate. Additionally, electrophysiological analysis should be performed to clarify the properties of those differentiated MNs. At last, the $Dlk1^{\Delta ICF}$ mouse line could be analysed in regard to their MN composition and MN functionality.

9. Appendix

Supplement figures

Supplement figure 1:

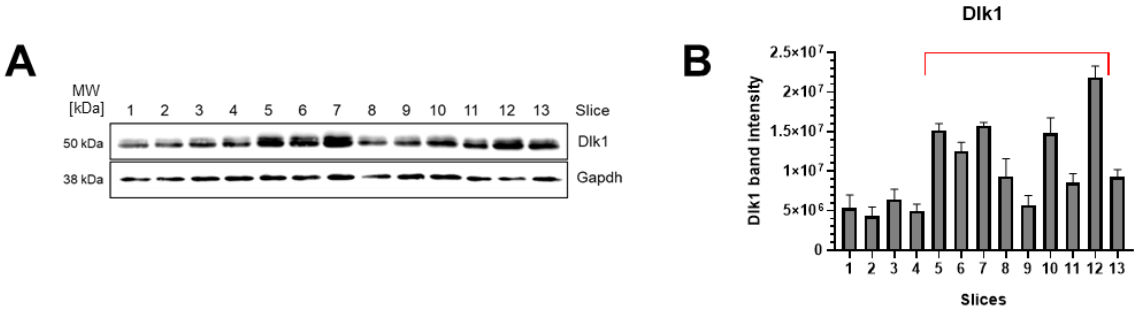

Supplement figure 1: *Dlk1 expression in murine brain slices.* ***A:*** *Representative western blot image from Dlk1 expression in all brain slices generated from one individual brain.* ***B:*** *Quantification of the densitometrical analysis of Dlk1 expression. GAPDH was used as loading control. Used brain slices are indicated with the red bar. MW, molecular weight.*

Supplement figure 2:

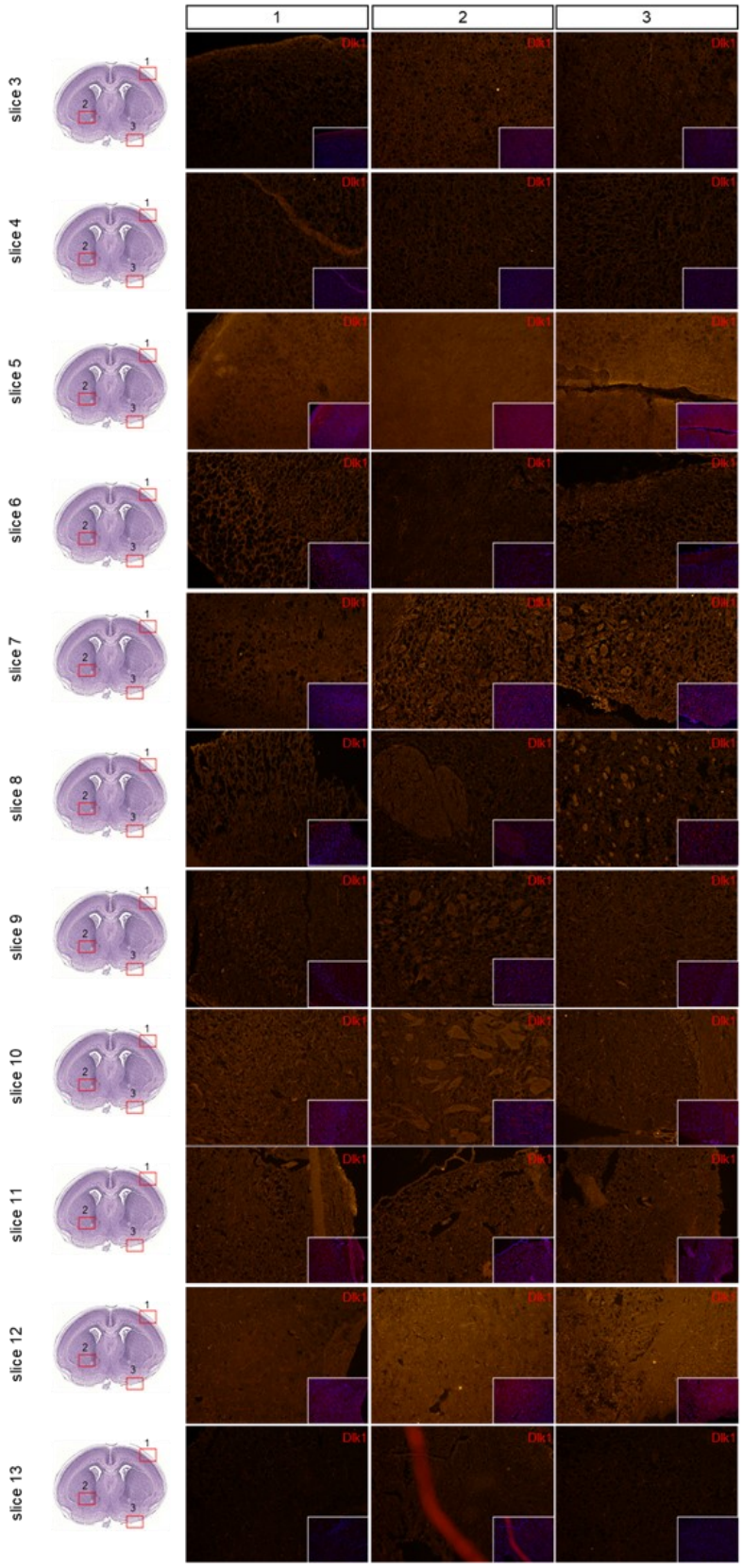

Supplement figure 2: *Immunofluorescence analysis of Dlk1 expression in murine brain slices. Individual brain slices of a wild-type mouse were stained with Dlk1 and fluorescence intensities were compared. Slices 5-8 were used for further experiments.*

Supplement figure 3:

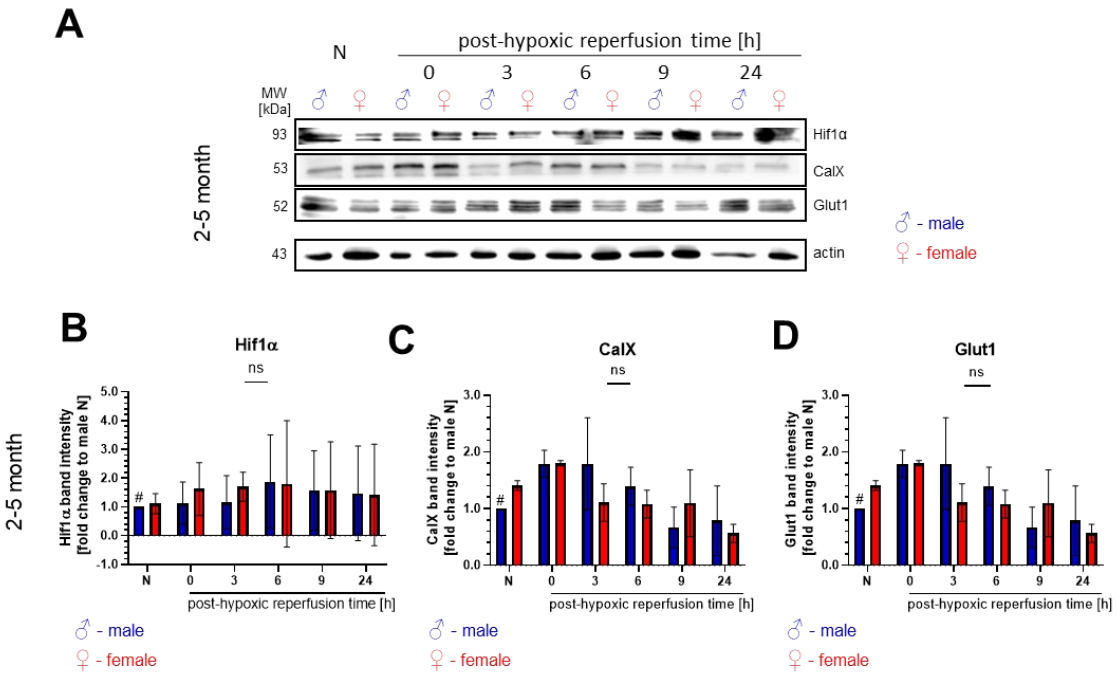

Supplement figure 3: *Hypoxia-induced Hif1α stabilisation and downstream targets CaIX and Glut1 in murine brain slices of 2-5 month old mice* ***A:*** *Representative western blot image from male and female brain slices of 2-5 month old mice after 30 min of hypoxia and post-hypoxia reperfusion time.* ***B:*** *Quantification of the densiometric analysis of Hif1α stabilisation after hypoxia and reperfusion time compared to normoxia for male and female responses.* ***C*** *and* ***D:*** *Quantification of the densiometric analysis of the downstream factors CaIX (C) and Glut1 (D), for male and female responses. Actin was used as loading control. Quantifications were tested with a one-way ANOVA, n = 3. CaIX, carbonic anhydrase IX, Glut1, glucose transporter 1; MW, molecular weight; N, normoxia.*

Supplement figure 4:

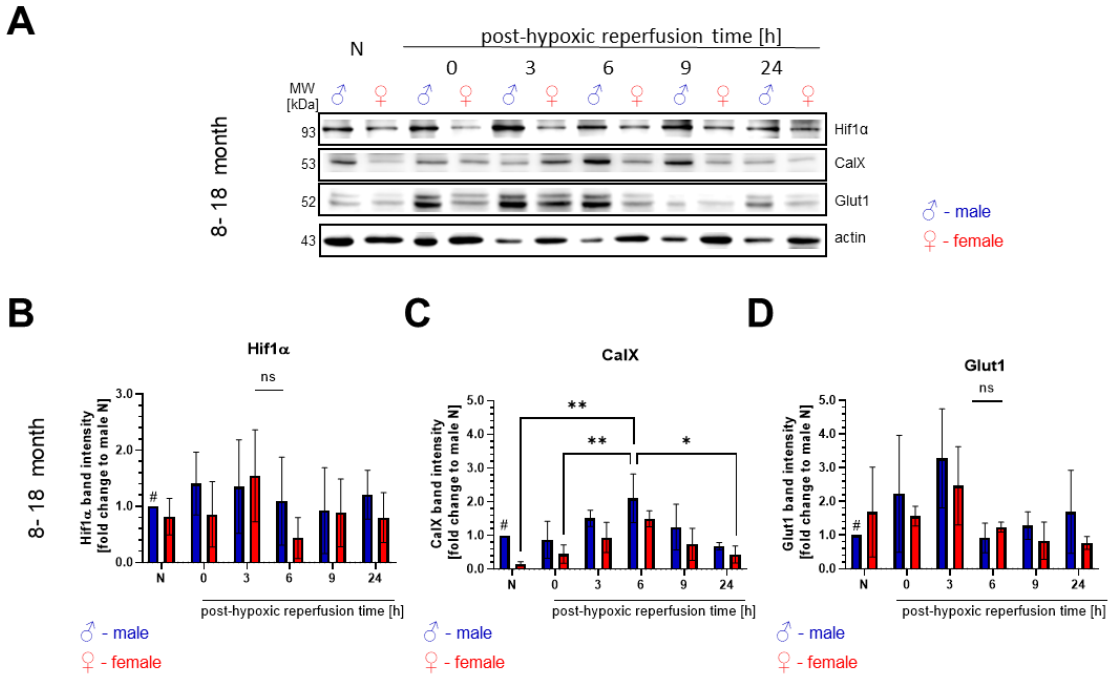

Supplement figure 4: *Hypoxia-induced Hif1α stabilisation and downstream targets CaIX and Glut1 in murine brain slices of 8-18 month old mice.* ***A:*** *Representative western blot image from male and female brain slices of 8-18 month old mice after 30 min of hypoxia and post-hypoxia reperfusion time.* ***B:*** *Quantification of the densiometric analysis of Hif1α stabilisation after hypoxia and reperfusion time compared to normoxia, for male and female responses.* ***C*** *and* ***D:*** *Quantification of the densiometric analysis of the downstream factors CaIX (C) and Glut1 (D), for male and female responses. Actin was used as loading control. Actin was used as loading control. Quantifications were tested with a one-way ANOVA, n = 3 (* P<0.05, ** P<0.005). Significance referees to the normoxia (#). CaIX, carbonic anhydrase IX, Glut1, glucose transporter 1; MW, molecular weight; N, normoxia.*

Supplement figure 5:

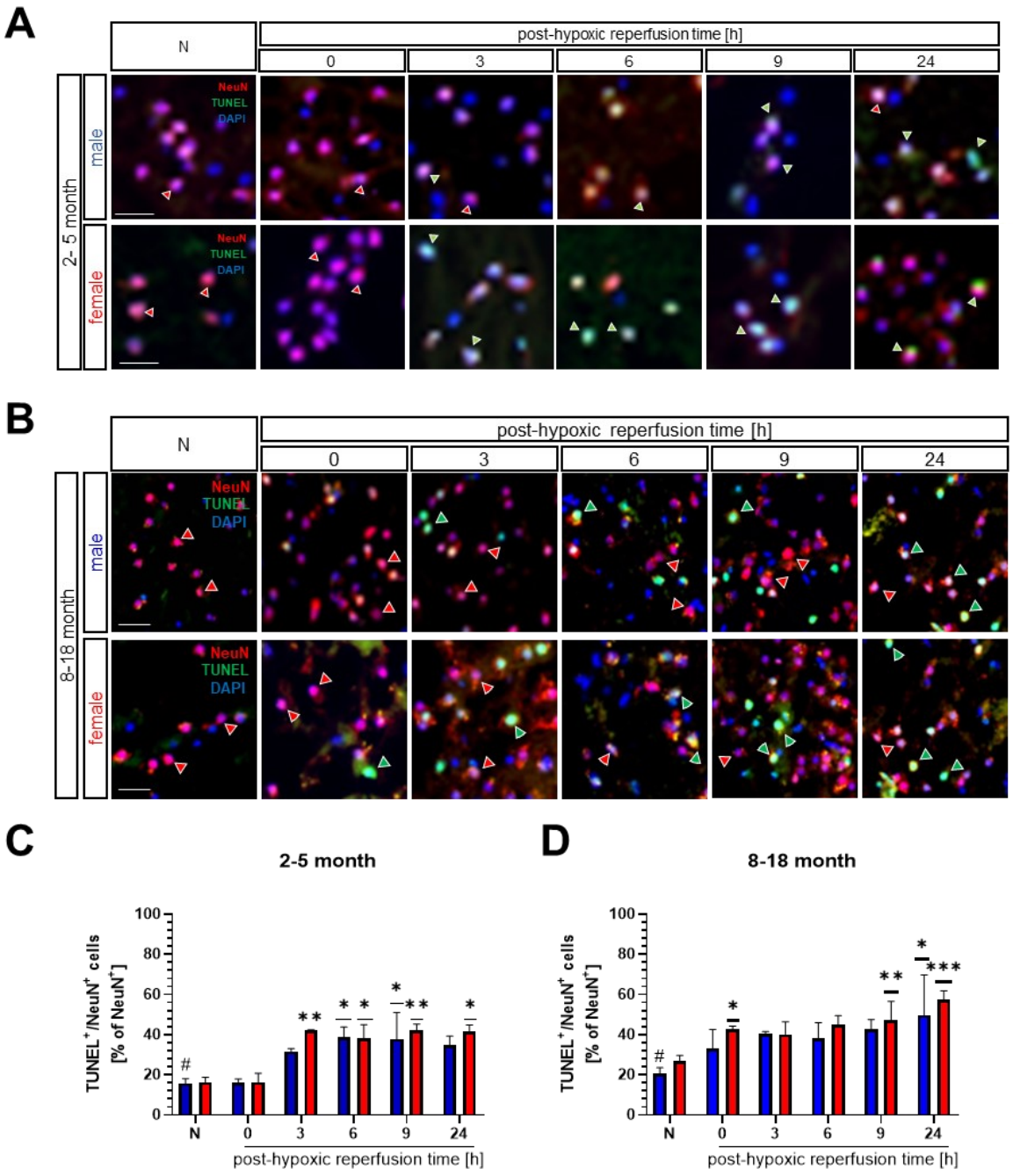

Supplement figure 5: *Viability of neurons in brain slices after hypoxia.* ***A*** *and* ***B:*** *Representative images of immunofluorescence staining's for neurons (NeuN⁺, red arrowhead), combined with a TUNEL⁺ (green, arrowhead) and DAPI⁺ (blue) staining for the normoxia, hypoxia and the time points of the post-hypoxic reperfusion time (3, 6, 9, and 24 h) for mature male and female mice (A, 2-5 month) and old male and female mice (B; 8-18 month). Scale bars represent 25 µm.* ***C*** *and* ***D:*** *Quantification of a total of 2000 cells per condition per age. Quantifications were tested with a one-way ANOVA, n = 2 (C), n = 4 (D) (* P<0.05, ** P<0.005; *** P<0.001). Significance referees to the normoxia (#). N, normoxia; NeuN, neuronal nuclei; TUNEL, TdT-mediated dUTP-biotin nick end labelling.*

Supplement figure 6:

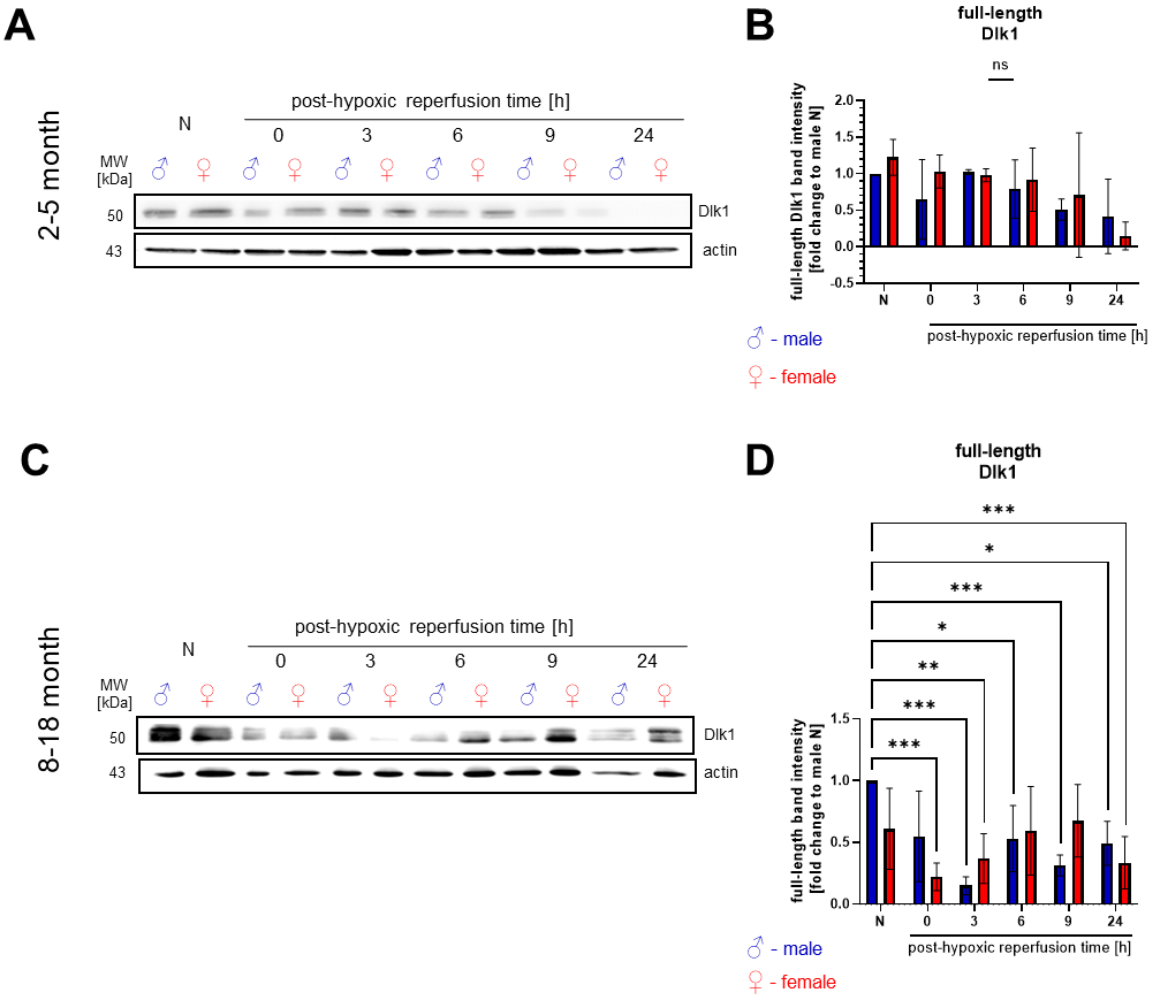

Supplement figure 6: *Hypoxia-induced Dlk1 processing in brain slices of mature mice.* ***A:*** *Representative western blot image from male brain slices of 2-5 month old mice after 30 min of hypoxia and post-hypoxia reperfusion time (3; 6; 9; and 24 h).* ***B:*** *Quantification of densiometric analysis of Dlk1 protein level after hypoxia and reperfusion time compared to normoxia in mature mice of 2-5 month old mice, n = 3.* ***C:*** *Representative western blot image from male brain slices of 8-18 month old mice after 30 min of hypoxia and post-hypoxia reperfusion time.* ***D:*** *Quantification of densiometric analysis of Dlk1 protein level after hypoxia and reperfusion time compared to normoxia in mature mice of 8-18 month. n = 4. Actin was used as loading control. Quantifications were tested with a two-way ANOVA (* P<0.05, ** P<0.005; *** P<0.001). MW, molecular weight; N, normoxia.*

Supplement figure 7:

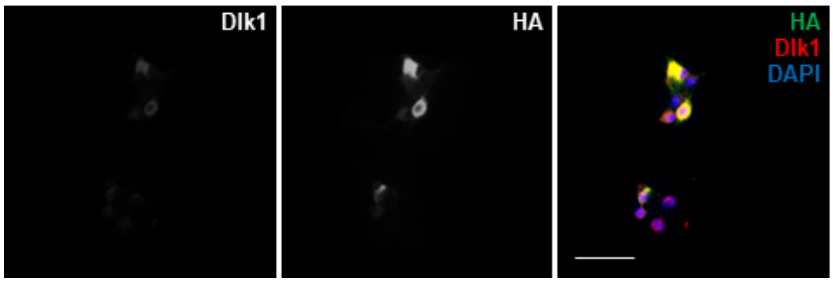

Supplement figure 7: *Immunofluorescence of the Dlk1-HA co-localisation. Representative grey scale images of Dlk1 (left image), HA (middle image) and merged (HA, green; Dlk1, red; and DAPI, blue) (right image). Scale bar represents 100 µm. HA, hemagglutinin.*

Supplement figure 8:

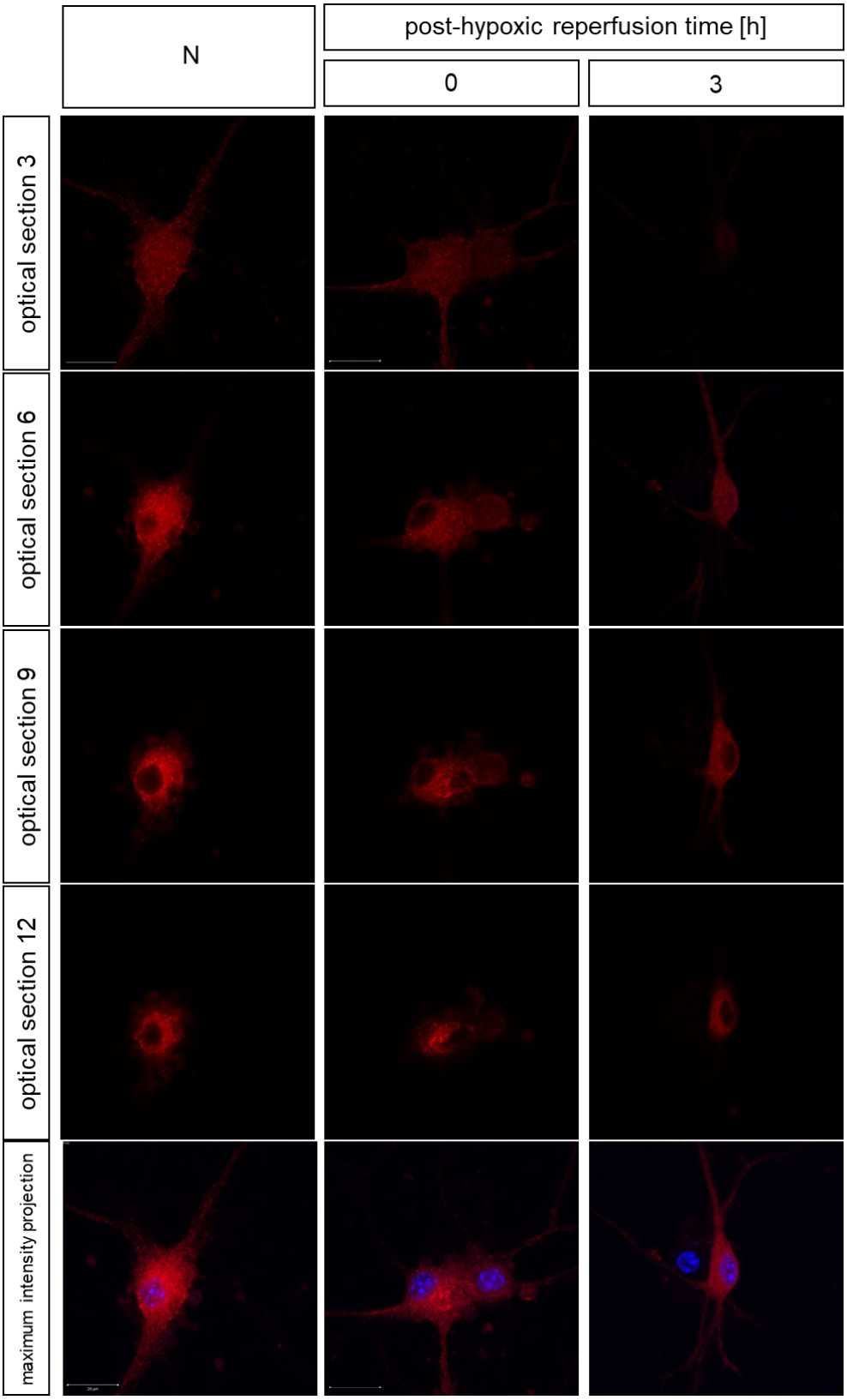

Supplement figure 8: *Immunofluorescence of the Dlk1-HA localisation. Confocal images of the Dlk1-HA signal of the optical section under normoxia, after 45 min of hypoxia, and after additional three hours of post-hypoxic reperfusion time. Merged image of Dlk1-HA staining with DAPI in the maximum intensity projection (lowest row). Scale bar represents 20 µm. HA, hemagglutinin; N, normoxia.*

Supplement figure 9:

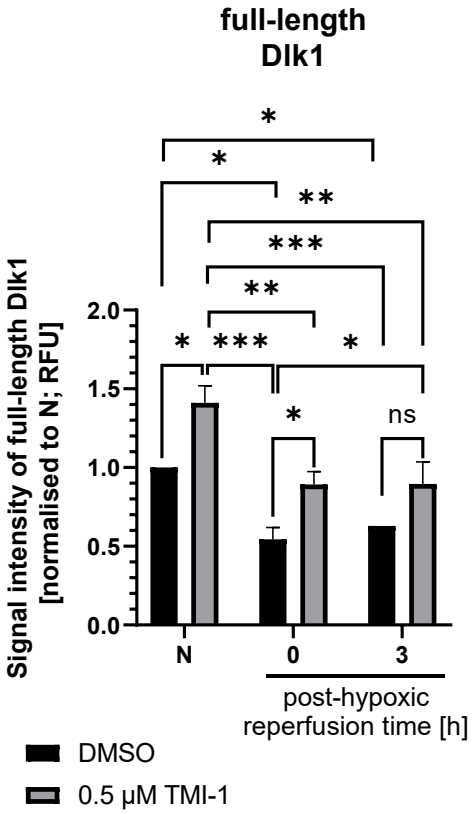

Supplement figure 9: *Additional quantification of immunofluorescence signal of the full-length Dlk1 signal intensities after inhibition of Adam17 in figure 5-30. Quantifications were tested with a two-way ANOVA, n = 3 and all significant differences are displayed (* P<0.05, ** P<0.005; *** P<0.001). N, normoxia, RFU, relative fluorescence units.*

Supplement figure 10:

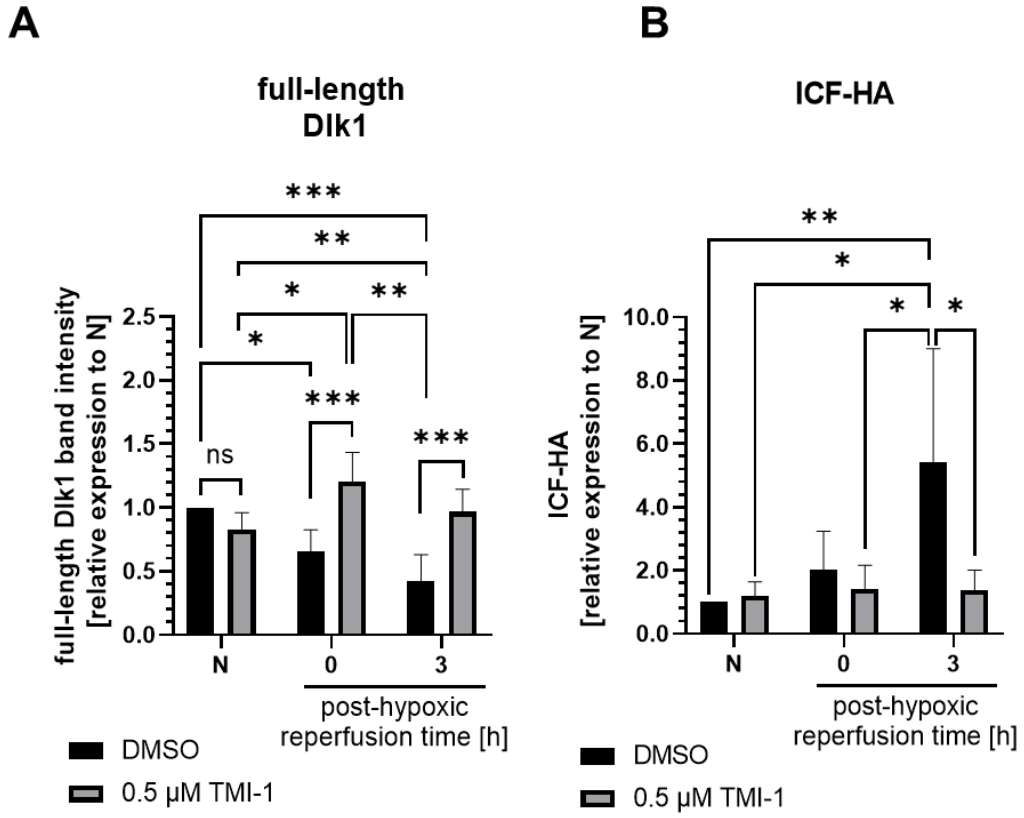

Supplement figure 10: *Additional quantification of western blot analysis of Dlk1 cleavage after inhibition of Adam17.* ***A:*** *Quantifications of full-length Dlk1 band intensities were tested with a two-way ANOVA, n = 3 (* P<0.05, ** P<0.005; *** P<0.001).* ***B:*** *Quantifications of ICF-HA band intensities were tested with a two-way ANOVA, n = 3 (* P<0.05, ** P<0.005; *** P<0.001). ICF, intracellular fragment; N, normoxia.*

Supplement figure 11:

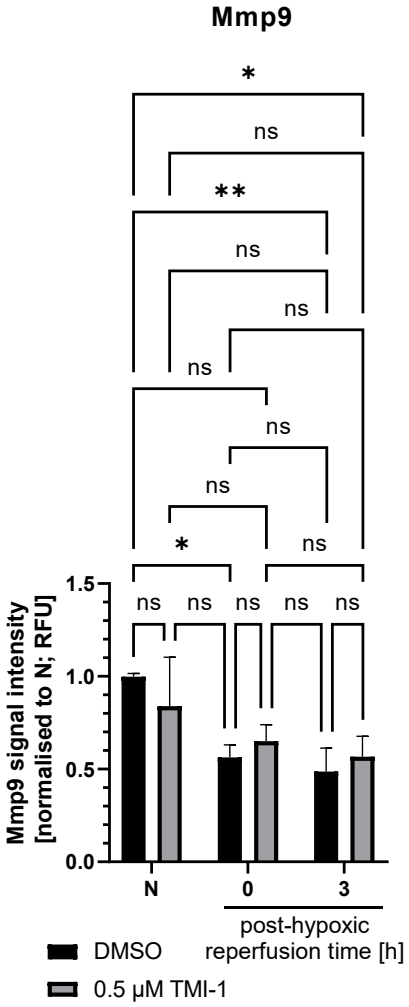

Supplement figure 11: *Additional quantification of immunofluorescence analysis of Mmp9 regulation in ESC-derived motor neuron network with Adam17 inhibition. Quantification of the signal intensity of Mmp9 in figure 5-32 were tested with a two-way ANOVA, n = 3 (* P<0.05, ** P<0.005). N, normoxia; Mmp9, matrix metalloprotease 9; RFU, relative fluorescence units.*

Bibliography

Abdallah, B. M. *et al.* (2004) 'Regulation of human skeletal stem cells differentiation by Dlk1/Pref-1', *Journal of Bone and Mineral Research*. Wiley Online Library, 19(5), pp. 841–852.

Abdallah, B. M. *et al.* (2011) 'DLK1 is a novel regulator of bone mass that mediates estrogen deficiency-induced bone loss in mice.', *Journal of bone and mineral research : the official journal of the American Society for Bone and Mineral Research*. United States, 26(7), pp. 1457–1471. doi: 10.1002/jbmr.346.

Acloque, H. *et al.* (2009) 'Epithelial-mesenchymal transitions: the importance of changing cell state in development and disease', *The Journal of clinical investigation*. Am Soc Clin Investig, 119(6), pp. 1438–1449.

Adelman, D. M. *et al.* (2000) 'Placental cell fates are regulated in vivo by HIF-mediated hypoxia responses', *Genes & development*. Cold Spring Harbor Laboratory Press, 14(24), pp. 3191–3203. doi: 10.1101/gad.853700.

Agalliu, D. *et al.* (2009) 'Motor Neurons with Axial Muscle Projections Specified by Wnt4/5 Signaling', *Neuron*. Cell Press, 61(5), pp. 708–720. doi: 10.1016/J.NEURON.2008.12.026.

Akay, T. *et al.* (2014) 'Degradation of mouse locomotor pattern in the absence of proprioceptive sensory feedback', *Proceedings of the National Academy of Sciences*. National Acad Sciences, 111(47), pp. 16877–16882.

Alkayed, N. J. *et al.* (1998) 'Gender-linked brain injury in experimental stroke.', *Stroke*. United States, 29(1), pp. 159–65; discussion 166. doi: 10.1161/01.str.29.1.159.

Amarilio, R. *et al.* (2007) 'HIF1α regulation of Sox9 in necessary to maintain differentiation of hypoxic prechondrogenic cells during early skeletogenesis', *Development*, 134(21), pp. 3917–3928. doi: 10.1242/dev.008441.

Andersen, D. C. *et al.* (2009) 'Characterization of DLK1+ cells emerging during skeletal muscle remodeling in response to myositis, myopathies, and acute injury.', *Stem cells (Dayton, Ohio)*. United States, 27(4), pp. 898–908. doi: 10.1634/stemcells.2008-0826.

Andersen, D. C. *et al.* (2013) 'Dual role of delta-like 1 homolog (DLK1) in skeletal muscle development and adult muscle regeneration', *Development*, 140(18), pp. 3743–3753. doi: 10.1242/dev.095810.

Arber, S. *et al.* (1999) 'Requirement for the Homeobox Gene Hb9 in the Consolidation of Motor Neuron Identity', *Neuron*. Cell Press, 23(4), pp. 659–674. doi: 10.1016/S0896-6273(01)80026-X.

Artavanis-Tsakonas, S., Rand, M. D. and Lake, R. J. (1999) 'Notch signaling: cell fate control and signal integration in development.', *Science (New York, N.Y.)*. United States, 284(5415), pp. 770–776. doi: 10.1126/science.284.5415.770.

Attardi, A. *et al.* (2018) 'Neuromesodermal progenitors are a conserved source of spinal cord with divergent growth dynamics', *Development*, 145(21), p. dev166728. doi: 10.1242/dev.166728.

Bachmann, E. *et al.* (1996) 'Mouse fetal antigen 1 (mFA1), the circulating gene product of mdlk, pref-1 and SCP-1: isolation, characterization and biology', *Reproduction*. Bristol, UK: Bioscientifica Ltd, 107(2), pp. 279–285. doi: 10.1530/jrf.0.1070279.

Bain, G. *et al.* (1995) 'Embryonic stem cells express neuronal properties in vitro', *Developmental biology*. Elsevier, 168(2), pp. 342–357.

Baladrón, V. *et al.* (2001) 'Specific regions of the extracellular domain of dlk, an EGF-like homeotic protein involved in differentiation, participate in intramolecular interactions.', *Frontiers in bioscience : a journal and virtual library*. United States, 6, pp. A25-32. doi: 10.2741/A582.

Banks, R. W. (2015) 'The innervation of the muscle spindle: a personal history', *Journal of Anatomy*. Wiley Online Library, 227(2), pp. 115–135.

Bardot, E. S. and Hadjantonakis, A. K. (2020) 'Mouse gastrulation: Coordination of tissue patterning, specification and diversification of cell fate', *Mechanisms of Development*. Elsevier, 163(February), p. 103617. doi: 10.1016/j.mod.2020.103617.

Bauer, M. *et al.* (2008) 'Delta-like 1 participates in the specification of ventral midbrain progenitor derived dopaminergic neurons.', *Journal of neurochemistry*. England, 104(4), pp. 1101–1115. doi: 10.1111/j.1471-4159.2007.05037.x.

Bedzhov, I. *et al.* (2014) 'Developmental plasticity, cell fate specification and morphogenesis in the early mouse embryo', *Philosophical Transactions of the Royal Society B: Biological Sciences*. Royal Society, 369(1657), p. 20130538. doi: 10.1098/rstb.2013.0538.

Bel-Vialar, S., Itasaki, N. and Krumlauf, R. (2002) 'Initiating Hox gene expression: in the early chick neural tube differential sensitivity to FGF and RA signaling subdivides the HoxB genes in two distinct groups'. Oxford University Press for The Company of Biologists Limited.

Bertout, J. A., Patel, S. A. and Simon, M. C. (2008) 'The impact of O2 availability on human cancer.', *Nature reviews. Cancer*, 8(12), pp. 967–975. doi: 10.1038/nrc2540.

Bessou, P., Emonet-Dénand, F. and Laporte, Y. (1965) 'Motor fibres innervating extrafusal and intrafusal muscle fibres in the cat', *The Journal of physiology*, 180(3), pp. 649–672. doi: 10.1113/jphysiol.1965.sp007722.

Bettenhausen, B. *et al.* (1995) 'Transient and restricted expression during mouse embryogenesis of Dll1, a murine gene closely related to Drosophila Delta.', *Development (Cambridge, England)*. England, 121(8), pp. 2407–2418. doi: 10.1242/dev.121.8.2407.

Bianchi, L. M. (2018) *Developmental Neurobiology*.

Bibel, M. *et al.* (2004) 'Differentiation of mouse embryonic stem cells into a defined neuronal lineage', *Nature neuroscience*. Nature Publishing Group, 7(9), pp. 1003–1009.

Briscoe, J. *et al.* (2000) 'A Homeodomain Protein Code Specifies Progenitor Cell Identity and Neuronal Fate in the Ventral Neural Tube', *Cell*. Cell Press, 101(4), pp. 435–445. doi: 10.1016/S0092-8674(00)80853-3.

Briscoe, J. and Ericson, J. (2001) 'Specification of neuronal fates in the ventral neural tube', *Current Opinion in Neurobiology*. Elsevier Current Trends, 11(1), pp. 43–49. doi: 10.1016/S0959-4388(00)00172-0.

Briscoe, J. and Thérond, P. P. (2013) 'The mechanisms of Hedgehog signalling and its roles in development and disease', *Nature reviews Molecular cell biology*. Nature Publishing Group, 14(7), pp. 416–429.

Bucchia, M. *et al.* (2018) 'Limitations and Challenges in Modeling Diseases Involving Spinal Motor Neuron Degeneration in Vitro ', *Frontiers in Cellular Neuroscience* . Available at:

https://www.frontiersin.org/article/10.3389/fncel.2018.00061.

Buckingham, M. *et al.* (2003) 'The formation of skeletal muscle: from somite to limb', *Journal of anatomy*. Wiley Online Library, 202(1), pp. 59–68.

Burke, A. C. *et al.* (1995) 'Hox genes and the evolution of vertebrate axial morphology', *Development*, 121(2), pp. 333 LP – 346. Available at: http://dev.biologists.org/content/121/2/333.abstract.

Burke, R. E. *et al.* (1977) 'Anatomy of medial gastrocnemius and soleus motor nuclei in cat spinal cord.', *Journal of neurophysiology*. United States, 40(3), pp. 667–680. doi: 10.1152/jn.1977.40.3.667.

Catela, C. *et al.* (2016) 'Hox proteins coordinate motor neuron differentiation and connectivity programs through Ret/Gfrα genes', *Cell reports*. Elsevier, 14(8), pp. 1901–1915.

Catela, C. (2020) 'Chapter 7 - Patterning and generation of neural diversity in the spinal cord', in Rubenstein, J. et al. (eds). Academic Press, pp. 137–155. doi: https://doi.org/10.1016/B978-0-12-814405-3.00007-2.

Celichowski, J. and Krutki, P. (2019) 'Chapter 4 - Motor Units and Muscle Receptors', in Zoladz, J. A. B. T.-M. and E. P. (ed.). Academic Press, pp. 51–91. doi: https://doi.org/10.1016/B978-0-12-814593-7.00004-9.

Chakkalakal, J. V *et al.* (2010) 'Retrograde influence of muscle fibers on their innervation revealed by a novel marker for slow motoneurons', *Development (Cambridge, England)*. 2010/09/15. Company of Biologists, 137(20), pp. 3489–3499. doi: 10.1242/dev.053348.

Chang, C. and Hemmati-Brivanlou, A. (1998) 'Cell fate determination in embryonic ectoderm', *Journal of neurobiology*. Wiley Online Library, 36(2), pp. 128–151.

Charlier, C. *et al.* (2001) 'The callipyge mutation enhances the expression of coregulated imprinted genes in cis without affecting their imprinting status', *Nature Genetics*, 27(4), pp. 367–369. doi: 10.1038/86856.

Chen, L. *et al.* (2011) 'Delta-like 1/fetal antigen-1 (Dlk1/FA1) is a novel regulator of chondrogenic cell differentiation via inhibition of the Akt kinase-dependent pathway.', *The Journal of biological chemistry*, 286(37), pp. 32140–32149. doi: 10.1074/jbc.M111.230110.

Chen, S., Zeng, L. and Hu, Z. (2014) 'Progressing haemorrhagic stroke: categories, causes, mechanisms and managements', *Journal of Neurology*, 261(11), pp. 2061–2078. doi: 10.1007/s00415-014-7291-1.

Cherukuri, P. (2012) *Molecular correlates of spinal motor neuron functional specification and plasticity*.

Chesnutt, C. *et al.* (2004) 'Coordinate regulation of neural tube patterning and proliferation by TGFbeta and WNT activity.', *Developmental biology*. United States, 274(2), pp. 334–347. doi: 10.1016/j.ydbio.2004.07.019.

Christoffersson, G. *et al.* (2015) 'Matrix metalloproteinase-9 is essential for physiological Beta cell function and islet vascularization in adult mice.', *The American journal of pathology*. United States, 185(4), pp. 1094–1103. doi: 10.1016/j.ajpath.2014.12.009.

Christophersen, N. S. *et al.* (2007) 'Midbrain expression of Delta-like 1 homologue is regulated by GDNF and is associated with dopaminergic differentiation', *Experimental neurology*. Elsevier, 204(2), pp. 791–801.

Close, R. I. (1972) 'Dynamic properties of mammalian skeletal muscles.', *Physiological Reviews*.

American Physiological Society, 52(1), pp. 129–197. doi: 10.1152/physrev.1972.52.1.129.

Cohen, M. *et al.* (2015) 'Ptch1 and Gli regulate Shh signalling dynamics via multiple mechanisms', *Nature Communications*, 6(1), p. 6709. doi: 10.1038/ncomms7709.

Copp, A. J., Greene, N. D. E. and Murdoch, J. N. (2003) 'The genetic basis of mammalian neurulation', *Nature Reviews Genetics*. Nature Publishing Group, 4, p. 784. Available at: https://doi.org/10.1038/nrg1181.

Cuevas, J. B. T.-R. M. in B. S. (2015) 'The Somatic Nervous System☆', in. Elsevier. doi: https://doi.org/10.1016/B978-0-12-801238-3.05364-2.

Cui, H. *et al.* (2013) 'Expression of hypoxia-inducible factor 1 alpha and oligodendrocyte lineage gene-1 in cultured brain slices after oxygen-glucose deprivation☆', *Neural Regeneration Research*, 8(4). Available at: https://journals.lww.com/nrronline/Fulltext/2013/08040/Expression_of_hypoxia_inducible_factor_1_alpha_and.5.aspx.

Cullheim, S. *et al.* (1987) 'Membrane area and dendritic structure in type-identified triceps surae alpha motoneurons.', *The Journal of comparative neurology*. United States, 255(1), pp. 68–81. doi: 10.1002/cne.902550106.

Dasen, J. S. *et al.* (2005) 'A Hox Regulatory Network Establishes Motor Neuron Pool Identity and Target-Muscle Connectivity', *Cell*. Cell Press, 123(3), pp. 477–491. doi: 10.1016/J.CELL.2005.09.009.

Dasen, J. S. *et al.* (2008) 'Hox Repertoires for Motor Neuron Diversity and Connectivity Gated by a Single Accessory Factor, FoxP1', *Cell*. Cell Press, 134(2), pp. 304–316. doi: 10.1016/J.CELL.2008.06.019.

Dasen, J. S. and Jessell, T. M. (2009) 'Chapter Six Hox Networks and the Origins of Motor Neuron Diversity', *Current Topics in Developmental Biology*. Academic Press, 88, pp. 169–200. doi: 10.1016/S0070-2153(09)88006-X.

Dasen, J. S., Liu, J.-P. and Jessell, T. M. (2003) 'Motor neuron columnar fate imposed by sequential phases of Hox-c activity', *Nature*. Macmillan Magazines Ltd., 425, p. 926. Available at: https://doi.org/10.1038/nature02051.

Dasen, J. S. and Rosenfeld, M. G. (2001) 'Signaling and Transcriptional Mechanisms in Pituitary Development', *Annual Review of Neuroscience*. Annual Reviews, 24(1), pp. 327–355. doi: 10.1146/annurev.neuro.24.1.327.

Deiuliis, J. A. *et al.* (2006) 'Alternative splicing of delta-like 1 homolog (DLK1) in the pig and human', *Comparative Biochemistry and Physiology Part B: Biochemistry and Molecular Biology*, 145(1), pp. 50–59. doi: https://doi.org/10.1016/j.cbpb.2006.06.003.

Dessaud, E., McMahon, A. P. and Briscoe, J. (2008) 'Pattern formation in the vertebrate neural tube: a sonic hedgehog morphogen-regulated transcriptional network'. Oxford University Press for The Company of Biologists Limited.

Dunwoodie, S. L. (2009) 'The Role of Hypoxia in Development of the Mammalian Embryo', *Developmental Cell*. Elsevier Inc., 17(6), pp. 755–773. doi: 10.1016/j.devcel.2009.11.008.

Edwards, I. J. *et al.* (2013) 'Na⁺/K⁺ ATPase α1 and α3 Isoforms Are Differentially Expressed in α- and γ-Motoneurons', *The Journal of*

Neuroscience, 33(24), pp. 9913 LP – 9919. doi: 10.1523/JNEUROSCI.5584-12.2013.

Eguchi, K. *et al.* (2020) 'Advantages of Acute Brain Slices Prepared at Physiological Temperature in the Characterization of Synaptic Functions ', *Frontiers in Cellular Neuroscience* . Available at: https://www.frontiersin.org/article/10.3389/fncel.2020.00063.

Ekker, M. S. *et al.* (2019) 'Stroke incidence in young adults according to age, subtype, sex, and time trends.', *Neurology*. United States, 92(21), pp. e2444–e2454. doi: 10.1212/WNL.0000000000007533.

Elisa, C. *et al.* (2009) 'NFAT isoforms control activity-dependent muscle fiber type specification', *Proceedings of the National Academy of Sciences*. Proceedings of the National Academy of Sciences, 106(32), pp. 13335–13340. doi: 10.1073/pnas.0812911106.

Eltzschig, H. K. and Eckle, T. (2011) 'Ischemia and reperfusion--from mechanism to translation', *Nature medicine*, 17(11), pp. 1391–1401. doi: 10.1038/nm.2507.

English, A. W., Wolf, S. L. and Segal, R. L. (1993) 'Compartmentalization of muscles and their motor nuclei: the partitioning hypothesis', *Physical Therapy*. Oxford University Press, 73(12), pp. 857–867.

Enjin, A. *et al.* (2010) 'Identification of novel spinal cholinergic genetic subtypes disclose Chodl and Pitx2 as markers for fast motor neurons and partition cells.', *The Journal of comparative neurology*. United States, 518(12), pp. 2284–2304. doi: 10.1002/cne.22332.

Ericson, J. *et al.* (1996) 'Two Critical Periods of Sonic Hedgehog Signaling Required for the Specification of Motor Neuron Identity', *Cell*. Cell Press, 87(4), pp. 661–673. doi: 10.1016/S0092-8674(00)81386-0.

Ericson, J. *et al.* (1997) 'Pax6 Controls Progenitor Cell Identity and Neuronal Fate in Response to Graded Shh Signaling', *Cell*. Cell Press, 90(1), pp. 169–180. doi: 10.1016/S0092-8674(00)80323-2.

Erö, C. *et al.* (2018) 'A Cell Atlas for the Mouse Brain ', *Frontiers in Neuroinformatics* . Available at: https://www.frontiersin.org/article/10.3389/fninf.2018.00084.

Evans, M. J. and Kaufman, M. H. (1981) 'Establishment in culture of pluripotential cells from mouse embryos', *Nature*, 292(5819), pp. 154–156. doi: 10.1038/292154a0.

Ezashi, T., Das, P. and Roberts, R. M. (2005) 'Low O2 tensions and the prevention of differentiation of hES cells.', *Proceedings of the National Academy of Sciences of the United States of America*, 102(13), pp. 4783–4788. doi: 10.1073/pnas.0501283102.

Fähling, M. (2009) 'Cellular oxygen sensing, signalling and how to survive translational arrest in hypoxia', *Acta Physiologica*. John Wiley & Sons, Ltd, 195(2), pp. 205–230. doi: https://doi.org/10.1111/j.1748-1716.2008.01894.x.

Fathollahipour, S., Patil, P. S. and Leipzig, N. D. (2019) 'Oxygen regulation in development: Lessons from embryogenesis towards tissue engineering', *Cells Tissues Organs*, 205(5–6), pp. 350–371. doi: 10.1159/000493162.

Fay, T. N. *et al.* (1988) 'Two fetal antigens (FA-1 and FA-2) and endometrial proteins (PP12 and PP14) isolated from amniotic fluid; preliminary observations in fetal and maternal tissues', *European Journal of Obstetrics & Gynecology and Reproductive Biology*, 29(1), pp. 73–85. doi: https://doi.org/10.1016/0028-2243(88)90167-0.

Feber, J. le (2019) 'In Vitro Models of Brain Disorders', *In Vitro Neuronal Networks*. Springer, pp. 19–49.

Ferrón, S. R. *et al.* (2011) 'Postnatal loss of Dlk1 imprinting in stem cells and niche astrocytes regulates neurogenesis', *Nature*. Nature Publishing Group, 475(7356), pp. 381–385.

Fiskum, V., Sandvig, A. and Sandvig, I. (2021) 'Silencing of Activity During Hypoxia Improves Functional Outcomes in Motor Neuron Networks in vitro ', *Frontiers in Integrative Neuroscience* . Available at: https://www.frontiersin.org/article/10.3389/fnint.2021.792863.

Fong, G.-H. and Takeda, K. (2008) 'Role and regulation of prolyl hydroxylase domain proteins.', *Cell death and differentiation*. England, 15(4), pp. 635–641. doi: 10.1038/cdd.2008.10.

Forsgren, S. *et al.* (1993) 'Calcitonin gene-related peptide expression at endplates of different fibre types in muscles in rat hind limbs.', *Cell and tissue research*. Germany, 274(3), pp. 439–446. doi: 10.1007/BF00314540.

Francius, C. (2013) 'Generating spinal motor neuron diversity : A long quest for neuronal identity Generating spinal motor neuron diversity : a long quest for neuronal identity', (April 2014). doi: 10.1007/s00018-013-1398-x.

Francius, C. and Clotman, F. (2014) 'Generating spinal motor neuron diversity: a long quest for neuronal identity', *Cellular and Molecular Life Sciences*, 71(5), pp. 813–829. doi: 10.1007/s00018-013-1398-x.

Friese, A. *et al.* (2009) 'Gamma and alpha motor neurons distinguished by expression of transcription factor Err3', *Proceedings of the National Academy of Sciences*. Proceedings of the National Academy of Sciences, 106(32), pp. 13588–13593. doi: 10.1073/pnas.0906809106.

Gao, Y. *et al.* (2011) 'Epigenetic regulation of gene expression in porcine epiblast, hypoblast, trophectoderm and epiblast-derived neural progenitor cells', *Epigenetics*. Taylor & Francis, 6(9), pp. 1149–1161.

Garcés, C. *et al.* (1999) 'Adipocyte differentiation is modulated by secreted delta-like (dlk) variants and requires the expression of membrane-associated dlk.', *Differentiation; research in biological diversity*. England, 64(2), pp. 103–114. doi: 10.1046/j.1432-0436.1999.6420103.x.

Garcia-Gallastegi, P. *et al.* (2019) 'Similarities and differences in tissue distribution of DLK1 and DLK2 during E16.5 mouse embryogenesis', *Histochemistry and Cell Biology*. doi: 10.1007/s00418-019-01778-4.

Gaspar, J. M. and Velloso, L. A. (2018) 'Hypoxia Inducible Factor as a Central Regulator of Metabolism - Implications for the Development of Obesity', *Frontiers in neuroscience*. Frontiers Media S.A., 12, p. 813. doi: 10.3389/fnins.2018.00813.

Genc, B., Gozutok, O. and Ozdinler, P. H. (2019) 'Complexity of Generating Mouse Models to Study the Upper Motor Neurons: Let Us Shift Focus from Mice to Neurons.', *International journal of molecular sciences*, 20(16). doi: 10.3390/ijms20163848.

Goodman, F. R. and Scambler, P. J. (2001) 'Human HOX gene mutations', *Clinical Genetics*. John Wiley & Sons, Ltd (10.1111), 59(1), pp. 1–11. doi: 10.1034/j.1399-0004.2001.590101.x.

Gouti, M. *et al.* (2014) 'In Vitro Generation of Neuromesodermal Progenitors Reveals Distinct Roles for Wnt Signalling in the Specification of Spinal Cord and Paraxial Mesoderm Identity', *PLOS Biology*. Public Library of Science, 12(8), p. e1001937. Available at:

https://doi.org/10.1371/journal.pbio.1001937.

Granit, R. and Henatsch, H. D. (1956) 'Gamma control of dynamic properties of muscle spindles', *Journal of Neurophysiology*, 19(4), pp. 356–366.

Grassi, E. S. *et al.* (2020) 'Niche-derived soluble DLK1 promotes glioma growth', *Neoplasia (United States)*. Elsevier Inc., 22(12), pp. 689–701. doi: 10.1016/j.neo.2020.10.005.

Grassi, E. S., Pantazopoulou, V. and Pietras, A. (2020) 'Hypoxia-induced release, nuclear translocation, and signaling activity of a DLK1 intracellular fragment in glioma', *Oncogene*, 39(20), pp. 4028–4044. doi: 10.1038/s41388-020-1273-9.

Grassi, E. S. and Pietras, A. (2022) 'Emerging Roles of DLK1 in the Stem Cell Niche and Cancer Stemness', *Journal of Histochemistry and Cytochemistry*. SAGE Publications Ltd, pp. 17–28. doi: 10.1369/00221554211048951.

Greene, N. D. E. and Copp, A. J. (2009) 'Development of the vertebrate central nervous system: formation of the neural tube', *Prenatal Diagnosis*. John Wiley & Sons, Ltd, 29(4), pp. 303–311. doi: https://doi.org/10.1002/pd.2206.

Grotta, J. *et al.* (2021) *Stroke, Pathophysiology, Diagnosis, and Management*.

Gubina, E. *et al.* (2000) 'Assignment of dlk (Dlk1) to mouse chromosome band 12E-F1 by in situ hybridization.', *Cytogenetics and cell genetics*, 88(3/4), pp. 322–323.

Guruharsha, K. G., Kankel, M. W. and Artavanis-Tsakonas, S. (2012) 'The Notch signalling system: recent insights into the complexity of a conserved pathway.', *Nature reviews. Genetics*, 13(9), pp. 654–666. doi: 10.1038/nrg3272.

Haase, V. H. (2013) 'Regulation of erythropoiesis by hypoxia-inducible factors.', *Blood reviews*, 27(1), pp. 41–53. doi: 10.1016/j.blre.2012.12.003.

Hanahan, D., Jessee, J. and Bloom, F. R. (1991) '[4] Plasmid transformation of Escherichia coli and other bacteria', *Methods in Enzymology*. Academic Press, 204, pp. 63–113. doi: 10.1016/0076-6879(91)04006-A.

Harrington, M. J., Chalasani, K. and Brewster, R. (2010) 'Cellular mechanisms of posterior neural tube morphogenesis in the zebrafish', *Developmental Dynamics*. John Wiley & Sons, Ltd, 239(3), pp. 747–762. doi: https://doi.org/10.1002/dvdy.22184.

Harris, T. *et al.* (2020) 'DLK1 Expressed in Mouse Orexin Neurons Modulates Anxio-Depressive Behavior but Not Energy Balance', *Brain Sciences* . doi: 10.3390/brainsci10120975.

Harvey, A. J. *et al.* (2004) 'Oxygen-regulated gene expression in bovine blastocysts.', *Biology of reproduction*. United States, 71(4), pp. 1108–1119. doi: 10.1095/biolreprod.104.028639.

Hasan, T. F. *et al.* (2018) 'Diagnosis and management of acute ischemic stroke', in *Mayo Clinic Proceedings*. Elsevier, pp. 523–538.

Hiiragi, T. and Solter, D. (2004) 'First cleavage plane of the mouse egg is not predetermined but defined by the topology of the two apposing pronuclei', *Nature*. Nature Publishing Group, 430(6997), pp. 360–364.

Himmels, P. *et al.* (2017) 'Motor neurons control blood vessel patterning in the developing spinal cord', *Nature Communications*, 8(May 2016). doi: 10.1038/ncomms14583.

Hines, P. J. and Marx, J. (1996) *Developmental neurobiology*, *Science*. doi: 10.1126/science.274.5290.1099.

Hiraga, T. (2018) ‘Hypoxic Microenvironment and Metastatic Bone Disease’, *International Journal of Molecular Sciences* . doi: 10.3390/ijms19113523.

Hogan, B., Costantini, F. and Lacy, E. (1986) ‘Manipulating the mouse embryo: a laboratory manual’. Cold spring harbor laboratory Cold Spring Harbor, NY.

Huang, H. (2018) ‘Matrix Metalloproteinase-9 (MMP-9) as a Cancer Biomarker and MMP-9 Biosensors: Recent Advances’, *Sensors* . doi: 10.3390/s18103249.

Hudak, C. S. *et al.* (2014) ‘Pref-1 marks very early mesenchymal precursors required for adipose tissue development and expansion’, *Cell reports*. 2014/07/31, 8(3), pp. 678–687. doi: 10.1016/j.celrep.2014.06.060.

Hunt, C. C. and Kuffler, S. W. (1951) ‘Further study of efferent small-nerve fibres to mammalian muscle spindles. Multiple spindle innervation and activity during contraction’, *The Journal of physiology*. Wiley-Blackwell, 113(2–3), p. 283.

Hynes, M. *et al.* (2000) ‘The seven-transmembrane receptor smoothened cell-autonomously induces multiple ventral cell types’, *Nature neuroscience*. Nature Publishing Group, 3(1), pp. 41–46.

Ille, F. *et al.* (2007) ‘Wnt/BMP signal integration regulates the balance between proliferation and differentiation of neuroepithelial cells in the dorsal spinal cord’, *Developmental biology*. Elsevier, 304(1), pp. 394–408.

Ingraham, C. A. *et al.* (2011) ‘Matrix Metalloproteinase (MMP)-9 Induced by Wnt Signaling Increases the Proliferation and Migration of Embryonic Neural Stem Cells at Low O_2 Levels *’, *Journal of Biological Chemistry*. Elsevier, 286(20), pp. 17649–17657. doi: 10.1074/jbc.M111.229427.

Ishihara, Y. and Fukuda, T. (2016) ‘Immunohistochemical investigation of the internal structure of the mouse subiculum’, *Neuroscience*, 337, pp. 242–266. doi: https://doi.org/10.1016/j.neuroscience.2016.09.027.

Iyer, N. V *et al.* (1998) ‘Cellular and developmental control of O2 homeostasis by hypoxia-inducible factor 1α’, *Genes & development*. Cold Spring Harbor Lab, 12(2), pp. 149–162.

Jacob, J. and Briscoe, J. (2003) ‘Gli proteins and the control of spinal-cord patterning’, *EMBO reports*. John Wiley & Sons, Ltd Chichester, UK, 4(8), pp. 761–765.

Jensen *et al.* (1994) ‘Protein structure of fetal antigen 1 (FA1) A novel circulating human epidermal-growth-factor-like protein expressed in neuroendocrine tumors and its relation to the gene products of dlk and pG2’, *European Journal of Biochemistry*. Wiley Online Library, 225(1), pp. 83–92.

Jensen, C. H. *et al.* (1994) ‘Protein Structure of Fetal Antigen 1 (FA1)’, *European Journal of Biochemistry*. John Wiley & Sons, Ltd, 225(1), pp. 83–92. doi: https://doi.org/10.1111/j.1432-1033.1994.00083.x.

Jensen, C. H. *et al.* (2001) ‘Neurons in the monoaminergic nuclei of the rat and human central nervous system express FA1/dlk.’, *Neuroreport*. England, 12(18), pp. 3959–3963. doi: 10.1097/00001756-200112210-00021.

Jessell, T. M. (2000) ‘Neuronal specification in the spinal cord: inductive signals and transcriptional codes’, *Nature Reviews Genetics*, 1(1), pp. 20–29. doi: 10.1038/35049541.

Jessell, T. M., Sürmeli, G. and Kelly, J. S. (2011) ‘Motor neurons and the sense of place’, *Neuron*, 72(3), pp. 419–424. doi: 10.1016/j.neuron.2011.10.021.

Jewell, U. R. *et al.* (2001) 'Induction of HIF–1α in response to hypoxia is instantaneous', *The FASEB Journal*. Wiley Online Library, 15(7), pp. 1312–1314.

Jung, H. *et al.* (2014) 'Evolving Hox Activity Profiles Govern Diversity in Locomotor Systems', *Developmental Cell*. Cell Press, 29(2), pp. 171–187. doi: 10.1016/J.DEVCEL.2014.03.008.

Kaelin Jr, W. G. (2008) 'The von Hippel–Lindau tumour suppressor protein: O2 sensing and cancer', *Nature Reviews Cancer*, 8(11), pp. 865–873. doi: 10.1038/nrc2502.

Kafer, G. R. and Cesare, A. J. (2020) 'A Survey of Essential Genome Stability Genes Reveals That Replication Stress Mitigation Is Critical for Peri-Implantation Embryogenesis ', *Frontiers in Cell and Developmental Biology* . Available at: https://www.frontiersin.org/article/10.3389/fcell.2020.00416.

Kalluri, R. (2009) 'EMT: when epithelial cells decide to become mesenchymal-like cells', *The Journal of clinical investigation*. American Society for Clinical Investigation, 119(6), pp. 1417–1419. doi: 10.1172/JCI39675.

Kandell, E. R. *et al.* (2013) *Principles of neural science*.

Kania, A. and Jessell, T. M. (2003) 'Topographic motor projections in the limb imposed by LIM homeodomain protein regulation of ephrin-A: EphA interactions', *Neuron*. Elsevier, 38(4), pp. 581–596.

Kania, A., Johnson, R. L. and Jessell, T. M. (2000) 'Coordinate roles for LIM homeobox genes in directing the dorsoventral trajectory of motor axons in the vertebrate limb', *Cell*. Elsevier, 102(2), pp. 161–173.

Kanning, K. C., Kaplan, A. and Henderson, C. E. (2010) 'Motor Neuron Diversity in Development and Disease', *Annual Review of Neuroscience*. Annual Reviews, 33(1), pp. 409–440. doi: 10.1146/annurev.neuro.051508.135722.

Kaplan, A. *et al.* (2014) 'Neuronal matrix metalloproteinase-9 is a determinant of selective neurodegeneration', *Neuron*. Elsevier, 81(2), pp. 333–348.

Karfunkel, P. (1974) 'The mechanisms of neural tube formation', *International review of cytology*. Elsevier, 38, pp. 245–271.

Kaufmann, M. H. (2005) *The Atlas of Mouse Development*.

Kawahara, R. *et al.* (2014) 'Deciphering the role of the ADAM17-dependent secretome in cell signaling', *Journal of proteome research*. ACS Publications, 13(4), pp. 2080–2093.

Keith, B., Johnson, R. S. and Simon, M. C. (2011) 'HIF1α and HIF2α: sibling rivalry in hypoxic tumour growth and progression', *Nature reviews. Cancer*, 12(1), pp. 9–22. doi: 10.1038/nrc3183.

Khan, M. N. (2018) *Regulatory mechanisms driving motor neuron functional diversification*.

Khan, M. N. *et al.* (2022) 'Orphan nuclear receptors Err2 and 3 promote a feature-specific terminal differentiation program underlying gamma motor neuron function and proprioceptive movement control', *bioRxiv*, p. 2022.01.25.477566. doi: 10.1101/2022.01.25.477566.

Kiehn, O. (2016) 'Decoding the organization of spinal circuits that control locomotion', *Nature Reviews Neuroscience*. Nature Publishing Group, 17(4), pp. 224–238.

Kim, S. H. and Yoon, J. (2019) 'Effect of serum-containing and serum-free culture medium-mediated activation of matrix metalloproteinases on embryonic developmental competence', *Czech Journal of Animal Science*, 64, pp. 473–482. doi: 10.17221/205/2019-CJAS.

Komatsu, H. *et al.* (2008) 'OSM-11 facilitates LIN-12 Notch signaling during Caenorhabditis elegans vulval development.', *PLoS biology*, 6(8), p. e196. doi: 10.1371/journal.pbio.0060196.

Kondoh, H. and Takemoto, T. (2012) 'Axial stem cells deriving both posterior neural and mesodermal tissues during gastrulation', *Current opinion in genetics & development*. Elsevier, 22(4), pp. 374–380.

Kondrychyn, I. *et al.* (2013) 'Stretching Morphogenesis of the Roof Plate and Formation of the Central Canal', *PLOS ONE*. Public Library of Science, 8(2), p. e56219. Available at: https://doi.org/10.1371/journal.pone.0056219.

Krock, B. L., Skuli, N. and Simon, M. C. (2011) 'Hypoxia-induced angiogenesis: good and evil.', *Genes & cancer*, 2(12), pp. 1117–1133. doi: 10.1177/1947601911423654.

Krupa, M. *et al.* (2014) 'Allocation of inner cells to epiblast vs primitive endoderm in the mouse embryo is biased but not determined by the round of asymmetric divisions (8→16- and 16→32-cells)', *Developmental Biology*, 385(1), pp. 136–148. doi: https://doi.org/10.1016/j.ydbio.2013.09.008.

Kuzmin, A. A. *et al.* (2019) 'Genetic tool for fate mapping of Oct4 (Pou5f1)-expressing cells and their progeny past the pluripotency stage', *Stem cell research & therapy*. BioMed Central, 10(1), p. 391. doi: 10.1186/s13287-019-1520-6.

Laborda, J. *et al.* (1993) 'dlk, a putative mammalian homeotic gene differentially expressed in small cell lung carcinoma and neuroendocrine tumor cell line.', *The Journal of biological chemistry*. United States, 268(6), pp. 3817–3820.

Lamouille, S., Xu, J. and Derynck, R. (2014) 'Molecular mechanisms of epithelial–mesenchymal transition', *Nature Reviews Molecular Cell Biology*, 15(3), pp. 178–196. doi: 10.1038/nrm3758.

Landmesser, L. T. (2001) 'The acquisition of motoneuron subtype identity and motor circuit formation', *International Journal of Developmental Neuroscience*. Pergamon, 19(2), pp. 175–182. doi: 10.1016/S0736-5748(00)00090-3.

Lee, S.-K. *et al.* (2005) 'Olig2 and Ngn2 function in opposition to modulate gene expression in motor neuron progenitor cells', *Genes & development*. Cold Spring Harbor Laboratory Press, 19(2), pp. 282–294. doi: 10.1101/gad.1257105.

Lee, S.-K. and Pfaff, S. L. (2001) 'Transcriptional networks regulating neuronal identity in the developing spinal cord', *Nature Neuroscience*, 4(11), pp. 1183–1191. doi: 10.1038/nn750.

Leksell, L. (1945) *The action potential and excitatory effects of the small ventral root fibres to skeletal muscle*. Ivar Hæggströms Boktryckeri AB.

Li, G. *et al.* (2021) 'The role of hypoxia in stem cell regulation of the central nervous system: From embryonic development to adult proliferation', *CNS Neuroscience & Therapeutics*. John Wiley & Sons, Ltd, 27(12), pp. 1446–1457. doi: https://doi.org/10.1111/cns.13754.

Li, L. *et al.* (2014) 'DLK1 promotes lung cancer cell invasion through upregulation of MMP9 expression depending on Notch signaling', *PloS one*. Public Library of Science, 9(3), p. e91509.

Lian, G. *et al.* (2019) 'Macrophage metabolic reprogramming aggravates aortic dissection through the HIF1α-ADAM17 pathway☆', *EBioMedicine*, 49, pp. 291–304. doi: https://doi.org/10.1016/j.ebiom.2019.09.041.

Liang, X. *et al.* (2011) 'Isl1 is required for multiple aspects of motor neuron development.', *Molecular and cellular neurosciences*, 47(3), pp. 215–222. doi: 10.1016/j.mcn.2011.04.007.

Liauchuk, V. (2021) *No Titlespinal motor neuron diversification and differential vulnerability in vivo and in vitro*.

Liddell, E. G. T. and Sherrington, C. S. (1925) 'Recruitment and some other features of reflex inhibition', *Proceedings of the Royal Society of London. Series B, Containing Papers of a Biological Character*. The Royal Society London, 97(686), pp. 488–518.

Lieberam, I. *et al.* (2005) 'A Cxcl12-CXCR4 chemokine signaling pathway defines the initial trajectory of mammalian motor axons', *Neuron*. Elsevier, 47(5), pp. 667–679.

Linn, J. and Brückmann, H. (2009) 'Differential diagnosis of nontraumatic intracerebral hemorrhage.', *Klinische Neuroradiologie*. Germany, 19(1), pp. 45–61. doi: 10.1007/s00062-009-8036-x.

Liu, C., Peng, G. and Jing, N. (2018) 'TGF-β signaling pathway in early mouse development and embryonic stem cells', *Acta Biochimica et Biophysica Sinica*. Oxford University Press, pp. 68–73. doi: 10.1093/abbs/gmx120.

Liu, F. *et al.* (2009) 'Changes in experimental stroke outcome across the life span', *Journal of Cerebral Blood Flow & Metabolism*. SAGE Publications Sage UK: London, England, 29(4), pp. 792–802.

Liu, S., Luo, W. and Wang, Y. (2022) 'Emerging role of PARP-1 and PARthanatos in ischemic stroke', *Journal of Neurochemistry*. John Wiley & Sons, Ltd, 160(1), pp. 74–87. doi: https://doi.org/10.1111/jnc.15464.

Lotto, R. B. *et al.* (2001) 'Target-derived neurotrophic factors regulate the death of developing forebrain neurons after a change in their trophic requirements.', *The Journal of neuroscience : the official journal of the Society for Neuroscience*, 21(11), pp. 3904–3910. doi: 10.1523/JNEUROSCI.21-11-03904.2001.

Majmundar, A. J., Wong, W. J. and Simon, M. C. (2010) 'Hypoxia-inducible factors and the response to hypoxic stress.', *Molecular cell*, 40(2), pp. 294–309. doi: 10.1016/j.molcel.2010.09.022.

Manuel, M. (2011) 'ALPHA, BETA AND GAMMA MOTONEURONS: FUNCTIONAL DIVERSITY IN THE MOTOR SYSTEM'S FINAL PATHWAY', *Journal of integrative neuroscience*, 10(3), pp. 243–276. doi: 10.1142/S0219635211002786.

Manuel, M. *et al.* (2019) 'Scaling of motor output, from mouse to humans', *Physiology*, 34(1), pp. 5–13. doi: 10.1152/physiol.00021.2018.

Manuel, M. and Zytnicki, D. (2019) 'Molecular and electrophysiological properties of mouse motoneuron and motor unit subtypes', *Current Opinion in Physiology*, 8, pp. 23–29. doi: https://doi.org/10.1016/j.cophys.2018.11.008.

Manwani, B. *et al.* (2013) 'Differential effects of aging and sex on stroke induced inflammation across the lifespan', *Experimental neurology*. Elsevier, 249, pp. 120–131.

Manwani, B. and McCullough, L. D. (2011) 'Sexual dimorphism in ischemic stroke: lessons from the laboratory.', *Women's health (London, England)*, 7(3), pp. 319–339. doi: 10.2217/whe.11.22.

De Marco Garcia, N. V and Jessell, T. M. (2008) 'Early motor neuron pool identity and muscle nerve trajectory defined by postmitotic restrictions in Nkx6.1 activity', *Neuron*, 57(2), pp. 217–231. doi: 10.1016/j.neuron.2007.11.033.

Marquardt, T. and Pfaff, S. L. (2001) 'Cracking the Transcriptional Code for Cell Specification in the Neural Tube', *Cell*. Cell Press, 106(6), pp. 651–654. doi: 10.1016/S0092-8674(01)00499-8.

Martìnez-Hernandez, G. *et al.* (2010) 'Regulation of proteinases during mouse peri-implantation development: Urokinase-type plasminogen activator expression and cross talk with matrix metalloproteinase 9', *Reproduction (Cambridge, England)*, 141, pp. 227–239. doi: 10.1530/REP-10-0334.

Mauch, T. J. and Schoenwolf, G. C. (2001) 'Developmental Biology. Sixth Edition. By Scott F. Gilbert', *American Journal of Medical Genetics*. John Wiley & Sons, Ltd, 99(2), pp. 170–171. doi: https://doi.org/10.1002/1096-8628(2000)9999:999<00::AID-AJMG1133>3.0.CO;2-G.

Maxwell, P. H. *et al.* (1999) 'The tumour suppressor protein VHL targets hypoxia-inducible factors for oxygen-dependent proteolysis', *Nature*, 399(6733), pp. 271–275. doi: 10.1038/20459.

Mazzoni, E. O. *et al.* (2013) 'Synergistic binding of transcription factors to cell-specific enhancers programs motor neuron identity', *Nature neuroscience*. 2013/07/21, 16(9), pp. 1219–1227. doi: 10.1038/nn.3467.

McDermott, A. *et al.* (2005) 'Gli2 and Gli3 have redundant and context-dependent function in skeletal muscle formation'. Oxford University Press for The Company of Biologists Limited.

Mei, B. *et al.* (2002) 'Only the large soluble form of preadipocyte factor-1 (Pref-1), but not the small soluble and membrane forms, inhibits adipocyte differentiation: role of alternative splicing.', *The Biochemical journal*, 364(Pt 1), pp. 137–144. doi: 10.1042/bj3640137.

Mendell, L. M. (2005) 'The size principle: a rule describing the recruitment of motoneurons', *Journal of neurophysiology*. American Physiological Society, 93(6), pp. 3024–3026.

Meyer, N. P. and Roelink, H. (2003) 'GH3 antagonizes the Shh response in the developing spinal cord.', in *DEVELOPMENTAL BIOLOGY*. ACADEMIC PRESS INC ELSEVIER SCIENCE 525 B ST, STE 1900, SAN DIEGO, CA 92101 …, pp. 602–603.

Miller, A. J. and Cole, S. E. (2014) 'Multiple Dlk1 splice variants are expressed during early mouse embryogenesis', *International Journal of Developmental Biology*. UPV/EHU Press, 58(1), pp. 65–70.

Mirshekar-Syahkal, B. *et al.* (2013) 'Dlk1 is a negative regulator of emerging hematopoietic stem and progenitor cells.', *Haematologica*, 98(2), pp. 163–171. doi: 10.3324/haematol.2012.070789.

Miyaoka, Y. *et al.* (2010) 'A novel regulatory mechanism for Fgf18 signaling involving cysteine-rich FGF receptor (Cfr) and delta-like protein (Dlk).', *Development (Cambridge, England)*. England, 137(1), pp. 159–167. doi: 10.1242/dev.041574.

Mohlin, S. *et al.* (2017) 'Hypoxia, pseudohypoxia and cellular differentiation.', *Experimental cell research*. United States, 356(2), pp. 192–196. doi: 10.1016/j.yexcr.2017.03.007.

Montalbán-Loro, R. *et al.* (2021) 'Dlk1 dosage regulates hippocampal neurogenesis and cognition.', *Proceedings of the National Academy of Sciences of the United States of America*, 118(11). doi: 10.1073/pnas.2015505118.

Morgana, F., Giuseppe, B. and Alberto, C. (2012) 'Spike timing plays a key role in synapse elimination at the neuromuscular junction', *Proceedings of the National Academy of Sciences*. Proceedings of the National Academy of Sciences, 109(25), pp. E1667–E1675. doi: 10.1073/pnas.1201147109.

Morisaki, Y. *et al.* (2016) 'Selective Expression of Osteopontin in ALS-resistant Motor Neurons is a Critical Determinant of Late Phase Neurodegeneration Mediated by Matrix Metalloproteinase-9', *Scientific Reports*, 6(1), p. 27354. doi: 10.1038/srep27354.

Morita, Y. *et al.* (2003) 'Critical Oxygen Delivery in Conscious Septic Rats under Stagnant or Anemic Hypoxia', *American Journal of Respiratory and Critical Care Medicine*. American Thoracic Society - AJRCCM, 167(6), pp. 868–872. doi: 10.1164/rccm.200205-490OC.

Morris, S. A. *et al.* (2012) 'Dynamics of anterior–posterior axis formation in the developing mouse embryo', *Nature communications*. Nature Publishing Group, 3(1), pp. 1–10.

Morris, S. A., Guo, Y. and Zernicka-Goetz, M. (2012) 'Developmental Plasticity Is Bound by Pluripotency and the Fgf and Wnt Signaling Pathways', *Cell Reports*, 2(4), pp. 756–765. doi: https://doi.org/10.1016/j.celrep.2012.08.029.

Moschovakis, A. K., Burke, R. E. and Fyffe, R. E. W. (1991) 'The size and dendritic structure of HRP-labeled gamma motoneurons in the cat spinal cord', *Journal of Comparative Neurology*. Wiley Online Library, 311(4), pp. 531–545.

Mullen, R. J., Buck, C. R. and Smith, A. M. (1992) 'NeuN, a neuronal specific nuclear protein in vertebrates', *Development*, 116(1), pp. 201–211. doi: 10.1242/dev.116.1.201.

Müller, D. (2012) *Identification and characterization of molecular mechanisms driving the functional specification of motor neurons The Delta like homolog 1 protein*.

Müller, D. *et al.* (2014) 'Dlk1 Promotes a Fast Motor Neuron Biophysical Signature Required for Peak Force Execution', *Science*, 343(6176), pp. 1264 LP – 1266. doi: 10.1126/science.1246448.

Murakoshi, H. and Trimmer, J. S. (1999) 'Identification of the Kv2.1 K⁺ Channel as a Major Component of the Delayed Rectifier K⁺ Current in Rat Hippocampal Neurons', *The Journal of Neuroscience*, 19(5), pp. 1728 LP – 1735. doi: 10.1523/JNEUROSCI.19-05-01728.1999.

Musumeci, G. *et al.* (2015) 'Somitogenesis: From somite to skeletal muscle', *Acta Histochemica*. Elsevier, 117(4–5), pp. 313–328.

Nagashima, H. *et al.* (2020) 'Novel concept for the epaxial/hypaxial boundary based on neuronal development.', *Journal of anatomy*, 237(3), pp. 427–438. doi: 10.1111/joa.13219.

Navarrete, F. *et al.* (2017) 'Deletion of Dlk2 increases the vulnerability to anxiety-like behaviors and impairs the anxiolytic action of alprazolam', *Psychoneuroendocrinology*. Pergamon, 85, pp. 134–141. doi: 10.1016/J.PSYNEUEN.2017.08.015.

Nguyen, A. Q. *et al.* (2020) 'Mouse embryos exposed to oxygen concentrations that mimic changes in the oviduct and uterus show improvement in blastocyst rate, blastocyst size, and accelerated cell division', *Reproductive Biology*. Elsevier Sp. z o.o., 20(2), pp. 147–153. doi: 10.1016/j.repbio.2020.03.011.

Niwa, H. (2001) 'Molecular mechanism to maintain stem cell renewal of ES cells', *Cell structure and function*. Japan Society for Cell Biology, 26(3), pp. 137–148.

Novitch, B. G., Chen, A. I. and Jessell, T. M. (2001) 'Coordinate Regulation of Motor Neuron Subtype Identity and Pan-Neuronal Properties by the bHLH Repressor Olig2', *Neuron*. Cell Press, 31(5), pp. 773–789. doi: 10.1016/S0896-6273(01)00407-X.

Nueda, M.-L. *et al.* (2007) 'The EGF-like protein dlk1 inhibits notch signaling and potentiates

adipogenesis of mesenchymal cells', *Journal of molecular biology*. Elsevier, 367(5), pp. 1281–1293.

Nueda, M.-L. *et al.* (2008) 'dlk1 specifically interacts with insulin-like growth factor binding protein 1 to modulate adipogenesis of 3T3-L1 cells.', *Journal of molecular biology*. England, 379(3), pp. 428–442. doi: 10.1016/j.jmb.2008.03.070.

Oppenheim, R. W. (1991) 'Cell Death During Development of the Nervous System', *Annual Review of Neuroscience*. Annual Reviews, 14(1), pp. 453–501. doi: 10.1146/annurev.ne.14.030191.002321.

Ortega, J. A. *et al.* (2017) 'Oxygen Levels Regulate the Development of Human Cortical Radial Glia Cells', *Cerebral Cortex*, 27(7), pp. 3736–3751. doi: 10.1093/cercor/bhw194.

Pachikara, A. *et al.* (2007) 'Activation of Class I transcription factors by low level Sonic hedgehog signaling is mediated by Gli2-dependent and independent mechanisms', *Developmental biology*. Elsevier, 305(1), pp. 52–62.

Papageorgiou, S. (2015) 'Hox Gene Collinearity: From A-P Patterning to Radially Symmetric Animals.', *Current genomics*, 17(5), pp. 444–449. doi: 10.2174/1389202917666160616082436.

Patterson, A. J. and Zhang, L. (2010) 'Hypoxia and fetal heart development.', *Current molecular medicine*, 10(7), pp. 653–666. doi: 10.2174/156652410792630643.

Perea-Gomez, A. *et al.* (2004) 'Initiation of gastrulation in the mouse embryo is preceded by an apparent shift in the orientation of the anterior-posterior axis', *Current Biology*. Elsevier, 14(3), pp. 197–207.

Persson, M. *et al.* (2002) 'Dorsal-ventral patterning of the spinal cord requires Gli3 transcriptional repressor activity', *Genes & development*. Cold Spring Harbor Lab, 16(22), pp. 2865–2878.

Philippidou, P. and Dasen, J. S. (2013) 'Hox genes: choreographers in neural development, architects of circuit organization', *Neuron*. Elsevier, 80(1), pp. 12–34.

Piehl, F. *et al.* (1993) 'Calcitonin gene-related peptide-like immunoreactivity in motoneuron pools innervating different hind limb muscles in the rat.', *Experimental brain research*. Germany, 96(2), pp. 291–303. doi: 10.1007/BF00227109.

Pittman, R. (2011) 'Regulation of Tissue Oxygenation'.

Powers, W. J. (2020) 'Acute ischemic stroke', *New England Journal of Medicine*. Mass Medical Soc, 383(3), pp. 252–260.

Proske, U. and Gandevia, S. C. (2012) 'The proprioceptive senses: their roles in signaling body shape, body position and movement, and muscle force', *Physiological reviews*. American Physiological Society Bethesda, MD.

Pyrgaki, C. *et al.* (2010) 'Dynamic imaging of mammalian neural tube closure', *Developmental Biology*, 344(2), pp. 941–947. doi: https://doi.org/10.1016/j.ydbio.2010.06.010.

Rao, A., Luo, C. and Hogan, P. G. (1997) 'Transcription factors of the NFAT family: regulation and function', *Annual review of immunology*. Annual Reviews 4139 El Camino Way, PO Box 10139, Palo Alto, CA 94303-0139, USA, 15(1), pp. 707–747.

Robertson, E. J. *et al.* (2003) 'Control of early anterior-posterior patterning in the mouse embryo by TGF-β signalling', *Philosophical Transactions of the Royal Society of London. Series B: Biological Sciences*. The Royal Society, 358(1436), pp. 1351–1358.

Rodriguez, P. *et al.* (2019) 'Deletion of delta-like 1 homologue accelerates fibroblast-myofibroblast differentiation and induces myocardial fibrosis.', *European heart journal*, 40(12), pp. 967–978. doi: 10.1093/eurheartj/ehy188.

Rodriguez, T. A. *et al.* (2005) 'Induction and migration of the anterior visceral endoderm is regulated by the extra-embryonic ectoderm'. Oxford University Press for The Company of Biologists Limited.

Roelink, H. *et al.* (1995) 'Floor plate and motor neuron induction by different concentrations of the amino-terminal cleavage product of sonic hedgehog autoproteolysis', *Cell*, 81(3), pp. 445–455. doi: https://doi.org/10.1016/0092-8674(95)90397-6.

Rogers, C. D., Moody, S. A. and Casey, E. S. (2009) 'Neural induction and factors that stabilize a neural fate', *Birth defects research. Part C, Embryo today : reviews*, 87(3), pp. 249–262. doi: 10.1002/bdrc.20157.

Romana, B. *et al.* (2019) 'HIF-1α is required for development of the sympathetic nervous system', *Proceedings of the National Academy of Sciences*. Proceedings of the National Academy of Sciences, 116(27), pp. 13414–13423. doi: 10.1073/pnas.1903510116.

Romanes, G. J. (1951) 'The motor cell columns of the lumbo-sacral spinal cord of the cat', *Journal of Comparative Neurology*. Wiley Online Library, 94(2), pp. 313–363.

Roy-O'Reilly, M. and McCullough, L. D. (2018) 'Age and Sex Are Critical Factors in Ischemic Stroke Pathology.', *Endocrinology*, 159(8), pp. 3120–3131. doi: 10.1210/en.2018-00465.

Sadri, N. and Zhang, P. J. (2013) 'Hypoxia-Inducible Factors: Mediators of Cancer Progression; Prognostic and Therapeutic Targets in Soft Tissue Sarcomas', *Cancers* . doi: 10.3390/cancers5020320.

Sagner, A. *et al.* (2018) 'Olig2 and Hes regulatory dynamics during motor neuron differentiation revealed by single cell transcriptomics', *PLOS Biology*. Public Library of Science, 16(2), p. e2003127. Available at: https://doi.org/10.1371/journal.pbio.2003127.

Sakajiri, S. *et al.* (2005) 'Dlk1 in normal and abnormal hematopoiesis', *Leukemia*, 19(8), pp. 1404–1410. doi: 10.1038/sj.leu.2403832.

Sánchez-Solana, B. *et al.* (2011) 'The EGF-like proteins DLK1 and DLK2 function as inhibitory non-canonical ligands of NOTCH1 receptor that modulate each other's activities', *Biochimica et Biophysica Acta (BBA) - Molecular Cell Research*, 1813(6), pp. 1153–1164. doi: https://doi.org/10.1016/j.bbamcr.2011.03.004.

Santilli, G. *et al.* (2010) 'Mild hypoxia enhances proliferation and multipotency of human neural stem cells.', *PloS one*, 5(1), p. e8575. doi: 10.1371/journal.pone.0008575.

Sarkar, M., Niranjan, N. and Banyal, P. K. (2017) 'Mechanisms of hypoxemia.', *Lung India : official organ of Indian Chest Society*, 34(1), pp. 47–60. doi: 10.4103/0970-2113.197116.

Sarnat, H. B., Nochlin, D. and Born, D. E. (1998) 'Neuronal nuclear antigen (NeuN): a marker of neuronal maturation in the early human fetal nervous system', *Brain and Development*. Elsevier, 20(2), pp. 88–94.

Scardigli, R. *et al.* (2001) 'Crossregulation between Neurogenin2 and Pathways Specifying Neuronal Identity in the Spinal Cord', *Neuron*. Cell Press, 31(2), pp. 203–217. doi: 10.1016/S0896-6273(01)00358-0.

Scheller, J. *et al.* (2011) 'ADAM17: a molecular switch to control inflammation and tissue regeneration', *Trends in immunology*. Elsevier, 32(8), pp. 380–387.

Schiaffino, S. and Reggiani, C. (2011) 'Fiber types in mammalian skeletal muscles', *Physiological reviews*. American Physiological Society Bethesda, MD, 91(4), pp. 1447–1531.

Schöler, H. R. *et al.* (1990) 'Oct-4: a germline-specific transcription factor mapping to the mouse t-complex.', *The EMBO journal*, 9(7), pp. 2185–2195.

Schwarz, C. *et al.* (2010) 'The head-fixed behaving rat—procedures and pitfalls', *Somatosensory & motor research*. Taylor & Francis, 27(4), pp. 131–148.

Semenza, G. L. (2007) 'Hypoxia-inducible factor 1 (HIF-1) pathway', *Science's STKE*. American Association for the Advancement of Science, 2007(407), pp. cm8–cm8.

Shi, G. and Jin, Y. (2010) 'Role of Oct4 in maintaining and regaining stem cell pluripotency', *Stem Cell Research & Therapy*, 1(5), p. 39. doi: 10.1186/scrt39.

Shinozuka, T. *et al.* (2019) 'Wnt produced by stretched roof-plate cells is required for the promotion of cell proliferation around the central canal of the spinal cord', *Development*, 146(2), p. dev159343. doi: 10.1242/dev.159343.

Shneider, N. *et al.* (2009) 'Gamma motor neurons express distinct genetic markers at birth and require muscle spindle-derived GDNF for postnatal survival', *Neural Development*, 4(1). doi: 10.1186/1749-8104-4-42.

Simon, M. C. and Keith, B. (2008) 'The role of oxygen availability in embryonic development and stem cell function', *Nature Reviews Molecular Cell Biology*. Nature Publishing Group, 9(4), pp. 285–296. doi: 10.1038/nrm2354.

Slack, R. S. *et al.* (1998) 'A critical temporal requirement for the retinoblastoma protein family during neuronal determination.', *The Journal of cell biology*, 140(6), pp. 1497–1509. doi: 10.1083/jcb.140.6.1497.

Smas, C. M., Green, D. and Sul, H. S. (1994) 'Structural characterization and alternate splicing of the gene encoding the preadipocyte EGF-like protein pref-1', *Biochemistry*. ACS Publications, 33(31), pp. 9257–9265.

Smas, C. M. and Sul, H. S. (1993) 'Pref-1, a protein containing EGF-like repeats, inhibits adipocyte differentiation', *Cell*. Elsevier, 73(4), pp. 725–734. doi: 10.1016/0092-8674(93)90252-L.

Smith, J. L., Gesteland, K. M. and Schoenwolf, G. C. (1994) 'Prospective fate map of the mouse primitive streak at 7.5 days of gestation', *Developmental Dynamics*. Wiley Online Library, 201(3), pp. 279–289.

Sokoloski, J. A. *et al.* (1991) 'Inhibition by pertussis toxin of the activation of Na+-dependent uridine transport in dimethyl-sulphoxide-induced HL-60 leukaemia cells', *Biochemical Journal*. Portland Press Ltd., 280(2), pp. 515–519.

Soula, C. *et al.* (2001) 'Distinct sites of origin of oligodendrocytes and somatic motoneurons in the chick spinal cord: oligodendrocytes arise from Nkx2. 2-expressing progenitors by a Shh-dependent mechanism', *Development*. Company of Biologists The Company of Biologists, Bidder Building, 140 Cowley …, 128(8), pp. 1369–1379.

Spiller, K. J. *et al.* (2019) 'Reduction of matrix metalloproteinase 9 (MMP-9) protects motor neurons from TDP-43-triggered death in rNLS8 mice', *Neurobiology of Disease*, 124, pp. 133–140. doi:

https://doi.org/10.1016/j.nbd.2018.11.013.

Stifani, N. (2014a) 'Motor neurons and the generation of spinal motor neuron diversity', *Frontiers in Cellular Neuroscience*, 8(OCT). doi: 10.3389/fncel.2014.00293.

Stifani, N. (2014b) 'Motor neurons and the generation of spinal motor neurons diversity ', *Frontiers in Cellular Neuroscience* , p. 293. Available at: https://www.frontiersin.org/article/10.3389/fncel.2014.00293.

Subhashini, N. (2016) 'Dlk1 membrane-to-nuclear signalling during motor neuron functional diversification'.

Sul, H. S. (2009) 'Minireview: Pref-1: role in adipogenesis and mesenchymal cell fate', *Molecular endocrinology*. Oxford University Press, 23(11), pp. 1717–1725.

Sun, Y., Chen, C. S. and Fu, J. (2012) 'Forcing Stem Cells to Behave: A Biophysical Perspective of the Cellular Microenvironment', *Annual Review of Biophysics*. Annual Reviews, 41(1), pp. 519–542. doi: 10.1146/annurev-biophys-042910-155306.

Surmacz, B. *et al.* (2012) 'DLK1 promotes neurogenesis of human and mouse pluripotent stem cell-derived neural progenitors via modulating Notch and BMP signalling', *Stem Cell Reviews and Reports*. Springer, 8(2), pp. 459–471.

Swanson, G. J. and Lewis, J. (1982) 'The timetable of innervation and its control in the chick wing bud.', *Journal of embryology and experimental morphology*. England, 71, pp. 121–137.

Takeoka, A. *et al.* (2014) 'Muscle spindle feedback directs locomotor recovery and circuit reorganization after spinal cord injury', *Cell*. Elsevier, 159(7), pp. 1626–1639.

Talbot, J. and Maves, L. (2016) 'Skeletal muscle fiber type: using insights from muscle developmental biology to dissect targets for susceptibility and resistance to muscle disease', *Wiley Interdisciplinary Reviews: Developmental Biology*. Wiley Online Library, 5(4), pp. 518–534.

Tam, P. P. L. and Loebel, D. A. F. (2007) 'Gene function in mouse embryogenesis: get set for gastrulation', *Nature Reviews Genetics*, 8(5), pp. 368–381. doi: 10.1038/nrg2084.

Thaler, J. P. *et al.* (2002) 'LIM Factor Lhx3 Contributes to the Specification of Motor Neuron and Interneuron Identity through Cell-Type-Specific Protein-Protein Interactions', *Cell*. Cell Press, 110(2), pp. 237–249. doi: 10.1016/S0092-8674(02)00823-1.

Toch, M. *et al.* (2020) 'Onecut-dependent Nkx6.2 transcription factor expression is required for proper formation and activity of spinal locomotor circuits', *Scientific Reports*, 10(1), p. 996. doi: 10.1038/s41598-020-57945-4.

Tosney, K. W. and Landmesser, L. T. (1985) 'Specificity of early motoneuron growth cone outgrowth in the chick embryo.', *The Journal of neuroscience : the official journal of the Society for Neuroscience*, 5(9), pp. 2336–2344. doi: 10.1523/JNEUROSCI.05-09-02336.1985.

Traustadóttir, G. Á. *et al.* (2016) 'Evidence of non-canonical NOTCH signaling: Delta-like 1 homolog (DLK1) directly interacts with the NOTCH1 receptor in mammals.', *Cellular signalling*. England, 28(4), pp. 246–254. doi: 10.1016/j.cellsig.2016.01.003.

Traustadóttir, G. Á. *et al.* (2017) 'The non-canonical NOTCH1 ligand Delta-like 1 homolog (DLK1) self interacts in mammals', *International journal of biological macromolecules*. Elsevier, 97, pp. 460–467.

Traustadóttir, G. Á. *et al.* (2019) 'The imprinted gene Delta like non-canonical Notch ligand 1 (Dlk1) is

conserved in mammals, and serves a growth modulatory role during tissue development and regeneration through Notch dependent and independent mechanisms', *Cytokine & Growth Factor Reviews*. Pergamon. doi: 10.1016/J.CYTOGFR.2019.03.006.

Tsao, C. W. *et al.* (2022) 'Heart Disease and Stroke Statistics—2022 Update: A Report From the American Heart Association', *Circulation*. American Heart Association, 145(8), pp. e153–e639. doi: 10.1161/CIR.0000000000001052.

Tuo, Q.-Z., Zhang, S.-T. and Lei, P. (2022) 'Mechanisms of neuronal cell death in ischemic stroke and their therapeutic implications.', *Medicinal research reviews*. United States, 42(1), pp. 259–305. doi: 10.1002/med.21817.

Vallstedt, A. *et al.* (2001) 'Different levels of repressor activity assign redundant and specific roles to Nkx6 genes in motor neuron and interneuron specification', *Neuron*. Elsevier, 31(5), pp. 743–755.

Villanueva, C., Jacquier, S. and de Roux, N. (2012) 'DLK1 Is a Somato-Dendritic Protein Expressed in Hypothalamic Arginine-Vasopressin and Oxytocin Neurons', *PLOS ONE*. Public Library of Science, 7(4), p. e36134. Available at: https://doi.org/10.1371/journal.pone.0036134.

Virani, S. S. *et al.* (2020) 'American Heart Association Council on E, Prevention Statistics C, Stroke Statistics S: Heart Disease and Stroke Statistics-2020 Update: A Report From the American Heart Association', *Circulation*, 141(9), pp. e139–e596.

Vokes, S. A. *et al.* (2007) 'Genomic characterization of Gli-activator targets in sonic hedgehog-mediated neural patterning'. Oxford University Press for The Company of Biologists Limited.

Vokes, S. A. *et al.* (2008) 'A genome-scale analysis of the cis-regulatory circuitry underlying sonic hedgehog-mediated patterning of the mammalian limb', *Genes & development*. Cold Spring Harbor Lab, 22(19), pp. 2651–2663.

Wakhloo, D. *et al.* (2021) 'Targeting carbonic anhydrase IX depletes breast cancer stem cells within the hypoxic niche', *Oncogene*. Nature Publishing Group, 11(1), pp. 5210–5219. doi: 10.1038/s41598-020-79978-5.

Wang, G. L. *et al.* (1995) 'Hypoxia-inducible factor 1 is a basic-helix-loop-helix-PAS heterodimer regulated by cellular O2 tension', *Proceedings of the National Academy of Sciences of the United States of America*, 92(12), pp. 5510–5514. doi: 10.1073/pnas.92.12.5510.

Wang, G. L. and Semenza, G. L. (1993) 'Characterization of hypoxia-inducible factor 1 and regulation of DNA binding activity by hypoxia.', *Journal of Biological Chemistry*. Elsevier, 268(29), pp. 21513–21518.

Wang, M. M. (2011) 'Notch signaling and Notch signaling modifiers', *The international journal of biochemistry & cell biology*. 2011/08/12, 43(11), pp. 1550–1562. doi: 10.1016/j.biocel.2011.08.005.

Wang, X.-J., Feng, C.-W. and Li, M. (2013) 'ADAM17 mediates hypoxia-induced drug resistance in hepatocellular carcinoma cells through activation of EGFR/PI3K/Akt pathway.', *Molecular and cellular biochemistry*. Netherlands, 380(1–2), pp. 57–66. doi: 10.1007/s11010-013-1657-z.

Wang, Y. *et al.* (2006) 'Pref-1, a preadipocyte secreted factor that inhibits adipogenesis', *The Journal of nutrition*. Oxford University Press, 136(12), pp. 2953–2956.

Wang, Y. *et al.* (2010) 'Pref-1 interacts with fibronectin to inhibit adipocyte differentiation', *Molecular and cellular biology*. 2010/05/10. American Society for Microbiology (ASM), 30(14), pp. 3480–3492. doi: 10.1128/MCB.00057-10.

Wang, Y. and Sul, H. S. (2006) 'Ectodomain shedding of preadipocyte factor 1 (Pref-1) by tumor necrosis factor alpha converting enzyme (TACE) and inhibition of adipocyte differentiation', *Molecular and cellular biology*. Am Soc Microbiol, 26(14), pp. 5421–5435.

Watson, A. J., Natale, D. R. and Barcroft, L. C. (2004) 'Molecular regulation of blastocyst formation', *Animal Reproduction Science*, 82–83, pp. 583–592. doi: https://doi.org/10.1016/j.anireprosci.2004.04.004.

Wennekamp, S. *et al.* (2013) 'A self-organization framework for symmetry breaking in the mammalian embryo', *Nature Reviews Molecular Cell Biology*, 14(7), pp. 452–459. doi: 10.1038/nrm3602.

Westbury, D. R. (1982) 'A comparison of the structures of alpha and gamma-spinal motoneurones of the cat.', *The Journal of physiology*, 325, pp. 79–91. doi: 10.1113/jphysiol.1982.sp014137.

Weyer, A. and Schilling, K. (2003) 'Developmental and cell type-specific expression of the neuronal marker NeuN in the murine cerebellum', *Journal of neuroscience research*. Wiley Online Library, 73(3), pp. 400–409.

Whalley, K. (2011) 'A niche role for DLK1', *Nature Reviews Neuroscience*, 12(9), p. 489. doi: 10.1038/nrn3092.

Wichterle, H. *et al.* (2002) 'Directed Differentiation of Embryonic Stem Cells into Motor Neurons', *Cell*. Cell Press, 110(3), pp. 385–397. doi: 10.1016/S0092-8674(02)00835-8.

Wiesener, M. S. *et al.* (2003) 'Widespread, hypoxia-inducible expression of HIF-2α in distinct cell populations of different organs', *The FASEB Journal*. Wiley Online Library, 17(2), pp. 271–273.

Wijgerde, M. *et al.* (2002) 'A direct requirement for Hedgehog signaling for normal specification of all ventral progenitor domains in the presumptive mammalian spinal cord', *Genes & development*. Cold Spring Harbor Lab, 16(22), pp. 2849–2864.

Wilkinson, K. A. (2021) 'Methodological advances for studying gamma motor neurons', *Current Opinion in Physiology*, 19, pp. 135–140. doi: https://doi.org/10.1016/j.cophys.2020.10.002.

Williams, M. *et al.* (2012) 'Mouse primitive streak forms in situ by initiation of epithelial to mesenchymal transition without migration of a cell population', *Developmental Dynamics*. John Wiley & Sons, Ltd, 241(2), pp. 270–283. doi: https://doi.org/10.1002/dvdy.23711.

Wilson, J. M., Rempel, J. and Brownstone, R. M. (2004) 'Postnatal development of cholinergic synapses on mouse spinal motoneurons.', *The Journal of comparative neurology*. United States, 474(1), pp. 13–23. doi: 10.1002/cne.20089.

Wilson, S. *et al.* (2001) 'The status of Wnt signalling regulates neural and epidermal fates in the chick embryo', *Nature*. Nature Publishing Group, 411(6835), pp. 325–330.

Wolf, H. K. *et al.* (1996) 'NeuN: a useful neuronal marker for diagnostic histopathology.', *Journal of Histochemistry & Cytochemistry*. SAGE Publications, 44(10), pp. 1167–1171.

Wolpert, L. *et al.* (2007) *Principles of Development*.

Wu, M.-Y. *et al.* (2018) 'Current Mechanistic Concepts in Ischemia and Reperfusion Injury', *Cellular Physiology and Biochemistry*, 46(4), pp. 1650–1667. doi: 10.1159/000489241.

Wylie, A. A. *et al.* (2000) 'Novel imprinted DLK1/GTL2 domain on human chromosome 14 contains motifs that mimic those implicated in IGF2/H19 regulation', *Genome research*. Cold Spring Harbor Laboratory Press, 10(11), pp. 1711–1718. doi: 10.1101/gr.161600.

Yamaguchi, Y. and Miura, M. (2015) 'Programmed cell death in neurodevelopment.', *Developmental cell*. United States, 32(4), pp. 478–490. doi: 10.1016/j.devcel.2015.01.019.

Yamanaka, Y. *et al.* (2006) 'Cell and molecular regulation of the mouse blastocyst', *Developmental dynamics: an official publication of the American Association of Anatomists*. Wiley Online Library, 235(9), pp. 2301–2314.

Yevtodiyenko, A. and Schmidt, J. (2006) 'Dlk1 expression marks developing endothelium and sites of branching morphogenesis in the mouse embryo and placenta', *Developmental dynamics : an official publication of the American Association of Anatomists*, 235, pp. 1115–1123. doi: 10.1002/dvdy.20705.

Yu, F. *et al.* (2001) 'HIF-1α binding to VHL is regulated by stimulus-sensitive proline hydroxylation', *Proceedings of the National Academy of Sciences*. National Acad Sciences, 98(17), pp. 9630–9635.

Yuan, Y. *et al.* (2012) 'Ethanol reduces expression of apoptotic proteins after hypoxia/reoxygenation in a brain slice model', *Neurological research*. Taylor & Francis, 34(4), pp. 373–378.

Zayia, L. C. and Tadi, P. (2022) 'Neuroanatomy, Motor Neuron.', in. Treasure Island (FL).

Zengel, J. E. *et al.* (1985) 'Membrane electrical properties and prediction of motor-unit type of medial gastrocnemius motoneurons in the cat.', *Journal of neurophysiology*. United States, 53(5), pp. 1323–1344. doi: 10.1152/jn.1985.53.5.1323.

Zhang, C. *et al.* (2007) 'Characteristics of neural stem cells expanded in lowered oxygen and the potential role of hypoxia-inducible factor-1Alpha.', *Neuro-Signals*. Switzerland, 15(5), pp. 259–265. doi: 10.1159/000103385.

Zhang, Y. *et al.* (2004) 'Identification and characterization of 4-[[4-(2-butynyloxy) phenyl] sulfonyl]-N-hydroxy-2, 2-dimethyl-(3S) thiomorpholinecarboxamide (TMI-1), a novel dual tumor necrosis factor-α-converting enzyme/matrix metalloprotease inhibitor for the treatment of rheu', *Journal of Pharmacology and Experimental Therapeutics*. ASPET, 309(1), pp. 348–355.

Zhou, Q., Choi, G. and Anderson, D. J. (2001) 'The bHLH transcription factor Olig2 promotes oligodendrocyte differentiation in collaboration with Nkx2. 2', *Neuron*. Elsevier, 31(5), pp. 791–807.

Zunke, F. and Rose-John, S. (2017) 'The shedding protease ADAM17: Physiology and pathophysiology', *Biochimica et Biophysica Acta (BBA) - Molecular Cell Research*, 1864(11, Part B), pp. 2059–2070. doi: https://doi.org/10.1016/j.bbamcr.2017.07.001.

Abbreviations

aCSF	Artificial cerebrospinal fluid
Adam	A disintegrin and metalloprotease
ATP	Adenosintriphosphate
BDNF	Brain-derived neurotrophic factor
bFgf	basic fibroblast growth factor
BMP	Bone morphogen protein
bp	base pair
BSA	bovine serum albumin
CCMB	Center for Cellular and Molecular Biology
cDNA	complementary DNA
CH	CH90221
ChAT	Choline Acetyltransferase
CNS	central nervous system
DAPI	4', 6 Diamidin-2-phenylindol
DBZ	Dibenzazepine
Dlk1	delta like homologue 1
Dlk2	delta like homologue 2
DMEM	Dulbecco's modified Eagle's medium
DMSO	Dimethylsulfoxid
DNA	deoxyribonucleic acid
E	embryonic day
ECD	Extracellular domain
ECL	Electrochemiluminescence
ECM	extracelluar matrix
EDTA	Ethylenediaminetetraacetic acid
EpiSCs	epiblast stem cells
ESC	embryonic stem cell
EtOH	Ethanol
FCS	fetal calf serum
FF	Fast-twitch fatigable
Fgf	fibroblast growth factor
FI	Fast-twitch fatigable intermediate
FP	Fast-fatigue resistant
FR	Fast-twitch fatigable resistance
h	hour
HA	hemagglutinin
ICC	Immunocytochemistry
ICF	Intracellular fragment
Kac	Potassium acetate
kbp	kilo base pair
KOAc	Potassium acetate
LB	lysogenic broth
LDH	lactate dehydrogenase
LIF	murine leukaemia inhibitory factor
MC	Motor column
MEF	murine embryonic fibroblast
mESC	murine embryonic stem cell

min	Minutes
MIP	maximum intensity projection
Mmp	Matrix metalloprotease
Mmp9	Matrix metalloprotease 9
MN	Motor neuron
MW	molecular weight
NaCl	Sodium chloride
NCBI	National Center for Biotechnology Information
NeuN	Neuronal nuclear protein
Ngn2	Neurogenin2
NGS	Normal goat serum
NHEJ	Non-homologous end joining
NP	Neural plate
NT	Neural tube
OGD	Oxygen Glucose Deprivation
Olig2	Oligodendrocyte transcription factor 2
OPN	Osteopontin
ORF	Open reading frame
PBS	Phosphate-buffered saline
PCR	Polymerase chain reaction
PD	PD0325901
PFA	Paraformaldehyde
pMN	Motor neuron progenitor domain
pMN	Motor neuron progenitor
PRKcd	Protein kinase C delta
qRT PCR	Quantitative real time PCR
RA	Retinoic acid
RF	Roof plate
RIPA	Radioimmunoprecipitation assay buffer
RNA	Ribonucleic acid
RPM	Revolutions per minute
RT	Room temperature
s	Slow
SAG	Smoothened agonist
SD	Standard deviation
SDS	Sodium dodecyl sulfate
sec	Seconds
Shh	Sonic hedgehog
SOB	Super optimal broth
ssODN	Single-stranded oligodeoxynucleotides
TAE	Tris, acetic EDTA
TBS	Tris-buffered saline
TE	Transformation efficiency
TM	transmembrane region
TNF	Tumor Necrosis Factor
Tris	Tris(hydroxymethyl)-aminomethane
Tubb3	Tubulin Beta 3 Class III
Tuj1	Neuron-specific Class III β-tubulin
UTR	Untranslated region

VAChT	Vesicular acetylcholine transporter
Vegf	Vascular Endothelial Growth Factor
WB	Western blot
Wnt	Wingless and Int-1
α	Alpha
β	Beta
γ	Gamma

Curriculum Vitae

Academic Education

Since 2019	Ph.D Graduate Colleague RTG2416 of the RWTH Aachen, Germany Specialisation: Neurology
2016-2019	M.Sc. Biology, RWTH Aachen, Germany Specialisation: Neurobiological information processing
2013-2016	B.Sc. Biology, University of cologne, Germany Specialisation: Neurophysiology and cell biology

Professional Experience

Since 2019	Research associated, RWTH Aachen, Germany
2016, 2018	Research assistant, RWTH Aachen, Germany

Publications

2021	Margreiter, M. A., Witzenberger, M., **Wasser, Y.**, Davydova, E., Janowski, R., Metz, J., Habib, P., Sahnoun, S., Sobisch, C., Poma, B., Palomino-Hernandez, O., Wagner, M., Carell, T., Jon Shah, N., Schulz, J. B., Niessing, D., Voigt, A., & Rossetti, G. (2021). Small-molecule modulators of TRMT2A decrease PolyQ aggregation and PolyQ-induced cell death. *Computational and structural biotechnology journal*, *20*, 443–458. https://doi.org/10.1016/j.csbj.2021.12.029
2021	Elsholz, L., **Wasser, Y**., Ziegler, P., Habib, P., & Voigt, A. (2021). CK1BP Reduces α-Synuclein Oligomerization and Aggregation Independent of Serine 129 Phosphorylation. *Cells*, *10*(11), 2830. https://doi.org/10.3390/cells10112830
2019	Prasad, V., **Wasser, Y**., Hans, F., Goswami, A., Katona, I., Outeiro, T. F., Kahle, P. J., Schulz, J. B., & Voigt, A. (2019). Monitoring α-synuclein multimerization in vivo. *FASEB journal: official publication of the Federation of American Societies for Experimental Biology*, *33*(2), 2116–2131. https://doi.org/10.1096/fj.201800148RRR

X

Yasmine Wasser
M.Sc.